

# **Membrane Modeling, Simulation and Optimization for Propylene/Propane Separation**

Dissertation by

**Ali K. Alshehri**

In Partial Fulfillment of the Requirements

For the Degree of

**Doctor of Philosophy**

King Abdullah University of Science and Technology

Thuwal, Kingdom of Saudi Arabia

© June 2015

Ali K. Alshehri

All Rights Reserved

The dissertation of Ali K. Alshehri is approved by the examination committee.

Committee Chairperson:

Prof. Dr. Zhiping Lai

Committee Members:

Prof. Dr. Zhiping Lai

Prof. Dr. Ingo Pinna

Prof. Dr. Shuyu Sun

Prof. Dr. Ali Abbas

## Abstract

### Membrane Modeling, Simulation and Optimization for Propylene/Propane Separation

*Ali Alshehri*

Energy efficiency is critical for sustainable industrial growth and the reduction of environmental impacts. Energy consumption by the industrial sector accounts for more than half of the total global energy usage and, therefore, greater attention is focused on enhancing this sector's energy efficiency. It is predicted that by 2020, more than 20% of today's energy consumption can be avoided in countries that have effectively implemented an action plan towards efficient energy utilization. Breakthroughs in material synthesis of high selective membranes have enabled the technology to be more energy efficient. Hence, high selective membranes are increasingly replacing conventional energy intensive separation processes, such as distillation and adsorption units. Moreover, the technology offers more special features (which are essential for special applications) and its small footprint makes membrane technology suitable for platform operations (e.g., nitrogen enrichment for oil and gas offshore sites). In addition, its low maintenance characteristics allow the technology to be applied to remote operations. For these reasons, amongst other, the membrane technology market is forecast to reach \$16 billion by 2017.

This thesis is concerned with the engineering aspects of membrane technology and covers modeling, simulation and optimization of membranes as a stand-alone process or as a unit operation within a hybrid system. Incorporating the membrane model into a process modeling software simplifies the simulation and optimization of the different membrane processes and hybrid configurations, since all other unit operations are pre-configured. Various parametric analyses demonstrated that only the membrane selectivity and transmembrane pressure ratio parameters define a membrane's ability to accomplish a certain separation task. Moreover, it was found that both membrane selectivity and pressure ratio exhibit a minimum value that is only defined by the feed composition, product purity and the recovery ratio. These findings were utilized to develop simple and accurate empirical correlations to predict the attainability behavior in real membranes, which showed good agreement with experimental and simulation results for various applications. Furthermore, the attainability of the most promising two and three-stage membrane systems are discussed by considering the complete well mixed assumption. The same behaviors that describe single-stage attainability are also recognized for multiple-stages. This discussion leads to a major discovery regarding the nature of the relationship between the attainability parameters in a multiple-stage membrane system with that of a single-stage system. Study of the economics of the multiple-stage membrane process for propylene/propane separation identifies the technology as a potential alternative to the conventional distillation process, even at the existing membrane performance, but conditionally at low to moderate membrane cost and sufficient durability.

To study the energy efficiency of membrane retrofitting to an existing distillation process, a shortcut method was developed to calculate the minimum practical separation energy (MPSE) of the membrane and distillation processes. It was discovered that the MPSE of the hybrid system is only determined by the membrane selectivity and the applied transmembrane pressure ratio in three stages. At the first stage, when selectivity is low, the membrane process is not competitive to the distillation process. At the second medium selectivity stage, the membrane/distillation hybrid system can help to reduce the energy consumption; the higher the membrane selectivity the lower the energy requirement. The energy conservation is further improved as the pressure ratio increases. At the third stage, when both the selectivity and pressure ratio are high, the hybrid system will change to a single-stage membrane unit, resulting in a significant reduction in energy consumption. The energy at this stage continues to slowly decrease with selectivity but increases slightly with pressure ratio. Overall, the higher the membrane selectivity, the more energy that is saved. These results should be very useful in guiding membrane research and their applications. Finally, an economic study is conducted concerning hypothetical membranes and the necessity for low cost and more durable membranes rises as the key for a viable hybrid process.

## Acknowledgements

I would like to begin by expressing my deepest and sincere gratitude to the sole of King Abdullah who was inspired to inspire all scholars in Saudi Arabia and the world.

My deep thanks to my advisor Dr. Zhiping Lai for the continuous support, guidance and mentorship over the last four years. Learning his systematic way of conducting scientific analysis will be of great importance to my future as it was during my research. My appreciation is extended to the committee members Prof. Ingo Pinna, Prof. Shuyu Sun and Prof. Ali Abbas. They have directed me during the research period and provided helpful comments and suggestions. Sincere thanks are due to my colleagues in the Advanced Membrane and Porous Material Center for their encouragement and support.

I am really indebted to Saudi Aramco Oil Company and its management who believed in my ability and provided me with the chance to continue study and achieve another milestone in my life. Special Thanks goes to my Aramco Advisors Mr. Ahmed Mohamed and Mr. Abdullah Al-Gahtani for their continuous support.

Finally, I would like to extend my gratitude to my family. They have always encouraged me and assisted me during the research. Foremost among these is my mother, wife, sisters and brothers without whose constant support and encouragement over the long months of writing, this work would not have been finished. At the end I want to thank my son Zaid and the three angles Wasan, Layan and Wajd for taking care of me during the rough times I passed through. I wish the acknowledgement page was large enough to name each and every one who has touched my life in so many meaningful ways.

## List of Symbols

A      membrane area ( $\text{m}^2$ )

$C_p$     gas specific heat  $\text{J}/(\text{mol}\cdot\text{K})$

d      hollow fiber diameter (m)

D      distillate flow (mol/s)

E      separation energy (J/mol)

F      feed flow rate (mol/s)

f      normalized feed flow rate ( $f = F/F_0$ )

G      permeate flow rate (mol/s)

g      normalized permeate flow rate ( $g = G/F_0$ )

m      number of feed streams

n      number of components

$P_0$     feed initial pressure (Pa)

$P_h$     feed side pressure (Pa)

$P_l$     permeate side pressure (Pa)

$P_{\text{out}}$  compressor outlet pressure (Pa)

Q      heat exchanger duty (J/s)

q mixture liquid fraction

R retentate flow rate (mol/s) or ideal gas constant

r molar fraction of retentate stream

Re Reynolds number

$R_{\min}$  minimum reflux ratio

$S_j$  selectivity that is defined as the permeability ratio of the most permeable component relative to component j

T feed temperature (K)

$T_{in}$  compressor inlet temperature (K)

$T_{out}$  compressor outlet temperature (K)

V vapor flow rate, mol/s

W machinery shaft work, J/s

x molar fraction of feed stream

y molar fraction of permeate stream

z number of side streams

$\alpha_i$  relative volatility of component i

- $\beta$  permeability that is defined as the flux normalized for transmembrane pressure difference and membrane thickness (mol/m·s·Pa)
- $\beta_m$  permeability of the most permeable component (mol/m·s·Pa)
- $\gamma$  feed to permeate pressure ratio ( $P_h/P_l$ )
- $\varepsilon$  target component enrichment ( $y_A/x_A$ )
- $\tau$  stage-cut defined as the flow rate ratio of permeate stream to the stage feed
- $\lambda$  latent heat/enthalpy of vaporization (J/mol)
- $\theta$  underwood polynomial root
- $\eta$  recovery ratio of the target component ( $Gy_A/Fx_A$ )
- $\psi$  ratio between recycle stream flow rate to the raw feed flow rate (Q/F)
- $\phi$  separation coefficient  $\left(\frac{y_A(1-x_A)}{x_A(1-y_A)}\right)$

## Table of Contents

<b>1. Introduction</b>	24
1.1 Background.....	24
1.2 Motivation .....	28
1.3 Research objectives .....	29
1.4 Thesis outline.....	31
1.5 References .....	31
<b>2. Membrane Background &amp; Literature Review</b>	36
2.1 History of membrane technology .....	36
2.2 Membrane separation background .....	39
2.3 Membrane module designs.....	43
2.3.1 Plate-and-Frame design .....	43
2.3.2 Spiral wound design .....	44
2.3.3 Hollow fiber design .....	45
2.4 Module flow patterns.....	48
2.5 Membrane systems for gas separations .....	49
2.5.1 Single-stage configuration.....	51
2.5.2 Multi-stage configuration .....	53
2.5.3 Membrane/distillation hybrid configurations .....	57
2.5.3.1 Pre-distillation hybrid configuration .....	59
2.5.3.2 Post-distillation hybrid configuration.....	60

2.5.3.3 Integrated-distillation hybrid configuration .....	61
2.5.4 Simulation of membrane/distillation hybrid configurations.....	62
2.6 Economic evaluation basis .....	65
2.7 References .....	31
<b>3. Membrane Mathematical Modeling and Parametric Investigation</b> .....	<b>76</b>
3.1 Introduction .....	76
3.2 Membrane mathematic model .....	78
3.3 Model solution.....	84
3.4 Model validation.....	87
3.5 Creating membrane unit operation in Aspen Plus® .....	90
3.6 Parametric investigation .....	94
3.6.2 Pressure ratio impact .....	97
3.6.3 Feed concentration impact.....	100
3.7 References .....	103
<b>4. Attainability of Single-Stage Membrane Process</b> .....	<b>105</b>
4.1 Abstract.....	105
4.2 Introduction .....	105
4.3 Attainability of single-stage membrane process.....	107
4.4 Parametric investigation .....	110
4.4.1 Influence of feed composition.....	110
4.4.2 Influence of product purity .....	111

4.4.3 Influence of recovery ratio .....	113
4.5 Empirical relationship of the minimum selectivity in hollow fiber membranes .....	114
4.6 Approximation of the attainability behavior .....	120
4.7 Case studies .....	122
4.7.1 Post-combustion carbon capture.....	122
4.7.2 Oxygen enrichment .....	126
4.8 Conclusion.....	128
4.9 References .....	130
<b>5. Attainability and Minimum Energy of Multiple-Stage Cascade Membrane Systems</b> .....	<b>131</b>
5.1 Abstract.....	131
5.2 Introduction .....	132
5.3 Analysis methodology .....	134
5.4 Mathematic models .....	137
5.4.1 Model derivation method .....	140
5.4.2 Minimum energy of multi-stage membrane systems .....	142
5.5 Results and discussion.....	144
5.5.1 Attainability of multi-stage membrane systems .....	144
5.5.2 Energy consumption of membrane systems .....	150
5.6 Conclusions .....	154

5.7 References .....	156
<b>6. Systematic Synthesis and Optimization of Membrane Networks for Gas Separation</b> .....	159
6.1 Introduction .....	159
6.2 Network superstructure modelling and optimization .....	162
6.3 Membrane network optimization .....	165
6.5 Case study description.....	169
6.6 Results discussion.....	171
6.7 Conclusion.....	178
6.8 References .....	180
<b>7. Minimum Energy of Single-Stage Membrane and Membrane/Distillation Hybrid Processes</b> .....	183
7.1 Abstract.....	183
7.2 Introduction .....	184
7.3 Membrane distillation hybrid configurations .....	189
7.4 Minimum practical energy of separation.....	192
7.4.1 Distillation process .....	193
7.4.2 Membrane process.....	195
7.4.3 Membrane/distillation hybrid configuration.....	197
7.5 Results and discussion.....	199
7.5.1 MPSE of the distillation process for propylene/propane separation .....	199

7.5.2 Effect of side stream flow rate and concentration .....	200
7.5.3 Effect of stage-cut.....	202
7.5.4 Effect of membrane selectivity and pressure ratio .....	203
7.6 Further discussions .....	207
7.7 Conclusions .....	209
7.8 References .....	210
<b>8. Optimization of Membrane/distillation Hybrid Process for Propylene/Propane Separation</b> .....	212
8.1 Abstract.....	212
8.2 Introduction .....	212
8.3 Economic evaluation basis and methods .....	215
8. 2.1 Distillation column .....	216
8.2.2 Module specification .....	218
8.3 Optimization method .....	219
8.4 Results and discussion.....	222
8.4.1 Membrane pre-distillation hybrid.....	222
8.4.2 Integrated membrane/distillation hybrid .....	229
8.5 Conclusion.....	236
8.6 References .....	238
<b>9. Conclusions and Future Recommendations</b> .....	240
9.1 General conclusions and contributions.....	240

9.1.1 Attainability of single-stage membrane.....	240
9.1.2 Attainability and minimum energy of multiple-stage cascade membrane systems.....	241
9.1.3 Systematic synthesis and optimization of membrane networks for gas separation .....	242
9.1.4 Minimum energy of single-stage membrane and membrane/ distillation Hybrid processes .....	243
9.1.5 Optimization of membrane/distillation hybrid process for propylene/propane separation.....	244
9.2 Suggestions for future work .....	244
Appendix A: Model derivation based on complete well-mixed.....	247
Appendix B: Model derivation for cascade membrane systems .....	247

## List of Tables

Table 2. 1 Pressure factor for distillation column cost .....	67
Table 2.2 Material factor for distillation column cost .....	67
Table 2.3 Tray type correction factor .....	68
Table 2. 4 Tray spacing correction factor .....	68
Table 2.5 Trays' material correction factor .....	68
Table 2.6 Material correction factor for shell and tube heat exchanger .....	69
Table 2.7 Vessel pressure correction factor .....	69
Table 2.8 Heat exchanger design correction factor .....	69
Table 3.1 Membrane module specification and operating conditions for the air separation experiment .....	89
Table 4.1 Comparison between the empirical and hollow fiber simulation results for the process shown in Fig. 4.12 .....	124
Table 4.2 Comparsion between corrolated and simulated results for oxygen enrichment to 50, 60 and 70 mol%. ....	128
Table 6.1 High performance membrane for propylene/propane separation. ....	169
Table 8. 1 Costs of chemical plant common utilities.....	218
Table 8.2 Reduction in TAC of the hybrid configuration at permeance of 50 GPU and membrane price of \$100/m <sup>2</sup> .....	225
Table 8.3 Reduction in TAC of the hybrid configuration at permeance of 100 GPU and Membrane price of \$500/m <sup>2</sup> .....	227

## List of Figures

Fig. 1.1 An overview of the different steps involved in the development of a membrane process for a specific application.....	28
Fig. 2.1 The two inventions to manufacture thin layer membranes a) Loeb- Sourirajan membrane b) multilayer composite membranes .....	38
Fig. 2.2 Schematic illustration of membrane separation process.....	40
Fig. 2.3 Illustration of the three steps involved in the solution diffusion theory .....	42
Fig. 2.4 Schematic of plate and frame design for membrane module .....	44
Fig. 2.5 Schematic illustration of spiral wound design.....	45
Fig. 2.6 Hollow fiber module with counter-current flow pattern .....	46
Fig. 2.7 The two flow patterns applicable in hollow fiber membrane modules. ....	49
Fig. 2.8 Creating driving force through the membrane module by a) feed compression b) permeate vacuum pumping.....	52
Fig. 2.9 Schematic of N-stage cascade membrane system with recycles. ....	55
Fig. 2.10 Some probable optimum configurations of membrane stages.....	56
Fig. 2.11 Schematic of a) three-stage stripping b) two/three-stage enriching systems	57
Fig. 2.12 Membrane/distillation with Pre-distillation setup. ....	59
Fig. 2.13 Membrane/distillation hybrid with post-distillation configuration .....	60

Fig. 2.14 Membrane/distillation hybrid with integrated setup.....	62
Fig. 3.1 Illustration of single-stage permeator with counter-current flow.....	79
Fig. 3. 2 Algorithm to solve counter-current membrane model. ....	86
Fig. 3.3 Model validation against experimental data for a multicomponent gas mixture. The simulation results are represented by the solid line and are in good agreement with the experimental results, which are illustrated by scattered points.....	88
Fig. 3. 4 Model validation against experimental data for air separation.....	89
Fig. 3.5 Aspen Plus interface to define the feed stream components and conditions... 92	
Fig. 3.6 Screen shot from Aspen Plus to illustrate the configured specifications for membrane design. ....	93
Fig. 3.7 Exporting the membrane design parameters to a Fortran file to generate a Dynamic Link Library (DLL). ....	94
Fig. 3.8 Impact of membrane selectivity on product purity and recovery ratio for a binary gas mixture with equimolar concentration at fixed membrane area, permeate and feed pressures. ....	96
Fig. 3.9 Influence of membrane selectivity on dimensionless membrane area to produce recovery ratios of 90, 95 and 99%. ....	97
Fig. 3.10 Impact of pressure ratio on product purity and recovery ratio (membrane area 100 m <sup>2</sup> , permeate side pressure of 1 bar, permeance of 100 GPU and selectivity of 100). ....	98
Fig. 3.11 Effect of pressure ratio on the minimum membrane area to produce a permeate stream with purity of 96% and recovery ratio of 95% using a membrane with	

selectivity of 100. The feed to the membrane is a binary gas mixture with equimolar concentration.....	99
Fig. 3.12 Importance of pressure ratio to enhance product purity while maintaining the recovery.....	100
Fig. 4.1 Attainability of a single-stage membrane in well-mixed model.....	108
Fig. 4.2 Minimum pressure ratio against selectivity for a single hollow fiber membrane module to produce permeate stream at purity of 96% and recovery ratio of 95%. ....	110
Fig. 4.3 Impact of feed composition on a) the attainability region and b) the minimum selectivity at infinite pressure ratio. ....	111
Fig. 4.4 Impact of product purity impact on a) attainability region and b) the minimum selectivity at infinite pressure ratio. ....	112
Fig. 4.5 Impact of recovery ratio on a) the attainability region and b) the minimum selectivity at infinity pressure ratio. ....	114
Fig. 4.6 Behavior of the minimum selectivity over the entire recovery ratio range: a) at different feed compositions and fixed purity of 95% b) at different product concentrations and equimolar feed. ....	115
Fig. 4.7 Regression between the non-recovered fraction ( $1-\eta$ ) of the high permeable component and the minimum selectivity to obtain the required purity at various: a) feed composition b) purity target.....	116
Fig. 5.1 Schematic of cascade membrane system with recycle streams.....	133
Fig. 5.2 Black box representation of a membrane process to perform a separation task to a binary mixture. The transmembrane pressure ratio is created by feed compression. Energy recovery is also considered to minimize the separation energy penalty. ....	134

Fig. 5.3 Different designs of two-stage cascade membrane systems. a) two-stage striping cascade; b) two-stage enriching cascade; c) a different drawing of the two-stage enriching cascade..... 136

Fig. 5.4 Three cascade designs for three-stage membrane systems. (a) feed to the first stage (only stripping stages); (b) feed to the second stage (with both enriching and stripping stages); (c) feed to the third stage (with only enriching stages). ..... 137

Fig. 5.5 Relationship between the stripping stage-cut and enriching stage-cut at different G/R ratios in three-stage membrane cascade with both enriching and stripping stages. Dotted lines shows the relationship in constant stage-cut scheme and solid line shows the relationship in constant recycle ratio scheme..... 140

Fig. 5.6 Attainability of multi-stage cascade membrane systems under the constant recycle ratio scheme for the bench separation system. (a) single-stage; (b) two-stage stripping cascade; (c) two-stage enriching cascade; (d) three-stage with feed to the first stage; (e) thee-stage with feed to the second stage; (f) three-stage with feed to the third stage. .... 147

Fig. 5.7 Attainability of multi-stage cascade membrane systems under the constant stage-cut scheme for the bench separation system. (a) single-stage; (b) two-stage stripping cascade; (c) two-stage enriching cascade; (d) three-stage with feed to the first stage; (e) thee-stage with feed to the second stage; (f) three-stage with feed to the third stage. .... 150

Fig. 5.8 Energy consumption by multi-stage cascade membrane systems for the bench separation system (a) single-stage; (b) two-stage enriching cascade; (c) three-stage with feed to the second stage. The red dotted line shows the energy consumption of the distillation process for the bench separation system..... 152

Fig. 5.9 Illustration of the minimum energy consumption at different membrane selectivity in the three-stage with feed to the second stage cascade system for the bench separation system. Blue line is the energy envelope curve generated by the

theory of “envelope of family of curves in plane”. Red dotted line shows the energy consumption of the distillation process for the bench separation system. ....	153
Fig. 6.1 Schematic of a five-stage membrane superstructure. ....	165
Fig. 6.2 Conventional distillation process for propylene/propane separation. ....	171
Fig. 6.3 The optimal membrane network corresponds to the minimum annualized cost for a membrane material with selectivity of 35 and permeance of 100 GPU at a fixed pressure ratio of 14. The membrane unit area price including installation is assumed to be 100 U\$/m <sup>2</sup> and the membrane lifetime is assumed to be 5 years.....	172
Fig. 6.4 The cost distribution for the membrane process in Fig. 6.3. ....	172
Fig. 6.5 Economic analysis of membrane superstructure for the separation of propylene/propane under uncertainty in membrane cost and lifetime. a) cost of 50 \$/m <sup>2</sup> and lifetime of 5 years b) cost of 50 \$/m <sup>2</sup> and lifetime of 2 years c) cost of 500 \$/m <sup>2</sup> and lifetime of 5 years d) cost of 500 \$/m <sup>2</sup> and lifetime of 2 years e) cost of 1000 \$/m <sup>2</sup> and lifetime of 5 years a) cost of 1000 \$/m <sup>2</sup> and lifetime of 2 years.....	177
Fig. 6.6 Relationship between the membrane material price and the breakeven permeance at membrane selectivity of 40.....	178
Fig 7.1 Possible membrane/distillation hybrid configurations for membrane material selective toward the light key component: a) pre-distillation b) parallel membrane distillation c) post-distillation. ....	191
Fig 7.2 Energy requirement for a single membrane unit considering feed compression, permeate vacuum pumping and recompression and energy recovery from the retentate stream.....	196
Fig 7.3 Impact of membrane feed composition on the hybrid MPSE ( $x_f = 0.5$ , $x_Z/x_{f0} = 0.5$ , $x_D = 0.96$ and $\gamma = 50$ ) .....	201

Fig 7.4 MPSE for parallel configuration at various selectivities and as a function of proportional side-stream flow rate ( $x_f = 0.5$ , $x_z/x_{f0} = 0.5$ , $x_D = 0.96$ and $\gamma=50$ ) .....	202
Fig 7.5 Behaviour of MPSE ( $x_f = 0.5$ , $x_D = 0.96$ and $\eta=0.95$ ) against stage-cut at fixed selectivities of 25, 50, 75 and 100, $\gamma =50$ , $F_z/F = 1$ and $x_z/x_f = 0.5$ .....	203
Fig 7.6 Behaviour of MPSE ( $x_f = 0.5$ , $x_D = 0.96$ and $\eta=0.95$ ) against membrane selectivity at variable pressure ratio (25, 50 and 100) .....	205
Fig 7.7 Behaviour of MPSE ( $x_f = 0.7$ , $x_D = 0.96$ and $\eta=0.99$ ) against membrane selectivity at variable pressure ratio (25, 50 and 100) .....	206
Fig 7.8 Behaviour of MPSE ( $x_f = 0.7$ , $x_D = 0.995$ and $\eta=0.99$ ) against membrane selectivity at variable pressure ratio (25, 50 and 100) .....	207
Fig. 8.1 Existing distillation process described by Gokhale [15] .....	217
Fig. 8.2 Optimal design of distillation process for propylene purity of 99.5% .....	217
Fig. 8.3 Membrane/distillation hybrid configurations a) pre-distillation hybrid b) parallel or integrated hybrid.....	221
Fig. 8.4 TAC of pre-distillation hybrid configuration at membrane cost of \$100/m <sup>2</sup> and lifetime of a) 5 years b) 2 years. ....	223
Fig. 8.5 TAC of pre-distillation hybrid configuration at membrane cost of \$500/m <sup>2</sup> and lifetime of a) 5 years b) 2 years. ....	227
Fig. 8.6 TAC of the pre-distillation hybrid configuration at membrane cost of \$1000/m <sup>2</sup> and lifetime of 5 years. ....	229
Fig. 8.7 TAC of the membrane/distillation parallel configuration at membrane cost of \$100/m <sup>2</sup> and lifetime of a) 5 years b) 2 years. ....	231

Fig. 8.8 The optimal design of the integrated hybrid configuration for a membrane with selectivity of 40 and permeance of 50. ....	231
Fig. 8.9 TAC of the membrane/distillation parallel configuration at membrane cost of \$500/m <sup>2</sup> and lifetime of a) 5 years b) 2 years. ....	233
Fig. 8.10 TAC of the membrane/distillation parallel configuration at membrane cost of 1000\$/m <sup>2</sup> and lifetime of 5 years. ....	234
Fig. 8.11 The minimum membrane performance (selectivity and permeability) for feasible membrane/distillation hybrid process under membrane cost of 100, 500 and 1000 \$/m <sup>2</sup> and durability of a) 2-years b) 5-years. ....	236

## 1. Introduction

### 1.1 Background

In the past few decades, the energy efficiency of separation processes have transformed from being a profit-related matter to be a global concern. This transformation resulted from realizing the environmental impact of green-house gas emission as well as the finite nature of energy resources. In 2010, the industry sector consumed more than 272 quadrillion British thermal units (Btu) [1]. This consumption is about 51% of total global energy usage [1]. The separation processes in the chemical manufacturing industry accounts for more than 50% of the sector's overall energy consumption [2]. For example, the distillation process, which is the most adopted separation method for gas and liquid separations, is estimated to account for between 40 and 70% of the overall energy consumption in olefin/paraffin split processes [3]. For these reasons, and for profitability, there are ongoing efforts to develop less energy intense separation technologies. The fact that the separation mechanism of membrane technology relies on a concentration gradient makes it very attractive to applications where the conventional separation units are thermally driven. As seen in water desalination, over the past 30 years reverse osmosis (RO) has occupied a significant fraction of the thermal desalination market. In fact, recent figures show that RO has already surpassed multi-stage flash distillation (MSF) with 52 and 25% shares of the market respectively. This has occurred for two reasons: 1) RO consumes about one third to one quarter of the energy of MSF for sea water desalination (RO consumes 2.2–6.7 kWh/m<sup>3</sup>, while MSF consumes 17–18 kWh/m<sup>3</sup>) and; 2) the recovery ratio of the

processed inlet is 3-4 times higher than the thermal recovery processes (40–60% for RO and 10–20% for MSF) [4].

Membrane technology has been mooted as a solution to many of the shortcomings of conventional separation units. Although energy efficiency is a major factor, other important factors have helped the technology to expand its share of the separation technology market, including the ease of operation and start-up, its small footprint, low maintenance cost and (most importantly) low capital investment. Membrane technology started to emerge into the field of gas purification on an industrial scale mainly after the development of stable and selective polymeric membranes. Although membranes were only introduced to gas separations in 1979, the technology has since been applied in a wide range of industrial applications, such as hydrogen recovery from ammonia synthesis flue gas, nitrogen enrichment from air and carbon dioxide removal from natural gas [5].

Membranes have two important parameters, named selectivity and permeability. The permeability is defined as the pressure and thickness normalized flux of the penetrant component [6]. The membrane selectivity is the ratio between the permeabilities of the different components in a mixture [7]. While the membrane permeability heavily controls the capital investment through inverse proportionality with the required area [8], the selectivity has a major role in reducing the operating cost related to pressure ratio [9]. Hence, permeability and selectivity are the two specifications that should be met when considering a material for membrane commercialization. The development of high flux membranes (by reducing effective thickness) transformed membrane technology from a theory- and lab-scale tool into an emerging technology. This occurred after the inventions

of asymmetric and composite membranes. The invention of asymmetric membranes enhanced membrane flux [10] while the discovery of multilayer composite membranes allowed a reduction in production costs while retaining the high flux advantage. Following these breakthroughs, a further challenge was to develop compact membrane modules with high permeation surface area to satisfy high flow rate applications capable of withstanding high pressure operations. Hollow fiber membranes were developed to overcome these challenges. Hollow fibers are self-supporting and the module has high packing density, reaching  $100 \text{ cm}^2/\text{cm}^3$ . For a material to be considered for membrane manufacturing it should exhibit the following characteristics [11]:

1. Sufficient selectivity to achieve the separation task at reasonable pressure ratio.
2. High permeability or flux to minimize the module size.
3. Mechanical and thermal stability.
4. Mechanical flexibility and strength for assembly in modules.
5. Tolerance to contaminants.
6. Manufacturing reproducibility.
7. Economical feasible production cost.

For gas separation processes, the driving force in membranes is the transmembrane partial pressure. Therefore, the pressure at the membrane feed side ( $P_h$ ) is typically larger than the permeate side pressure ( $P_l$ ). The transmembrane pressure difference can be

created in various ways. The feed stream can be compressed to a higher pressure, which is typically the case for liquid separations such as seawater desalination, with the pressure of the retentate stream then returned to the initial pressure through energy recovery systems. Alternatively, the permeate side can be evacuated by a vacuum pump, which is often the case for gas separations, and the product stream then compressed back to the initial pressure for delivery. A combination of the above approaches is also possible. However, the operating cost required to create a driving force form a challenge to membranes that can meet the product purity and recovery requirements are often too high, e.g., in the separation of ethylene/ethane in chemical industry. This is worsened when a diluted feed mixture is involved, such as in carbon dioxide capture from coal fired power plant's flue gas.

Although single membrane configuration corresponds to the lowest capital investment, in most cases this approach cannot achieve high product recovery and purity unless high pressure ratio is applied to maximize the driving force. Thus, single-stage membrane systems have the highest energy consumption. In order to maximize product recovery together with high enrichment, a multi-stage membrane network is normally used. In addition, partial product recycle is typically applied to maximize product purity. When a high performance membrane is not available for a specific application and the product value is extremely high, techno-economically hybrid systems will outperform any membrane configuration.

An overview of the various steps involved in designing a membrane system for a specific application is shown in Figure 1.1. The process begins with gathering knowledge

about the separation task. A process simulation is then required to exemplify the real process conditions and define the minimum separation performance for feasible operation. Moreover, the simulation and optimization should be repeated based on the actual performance of the developed membrane before installation, thus allowing optimization of the operating conditions.

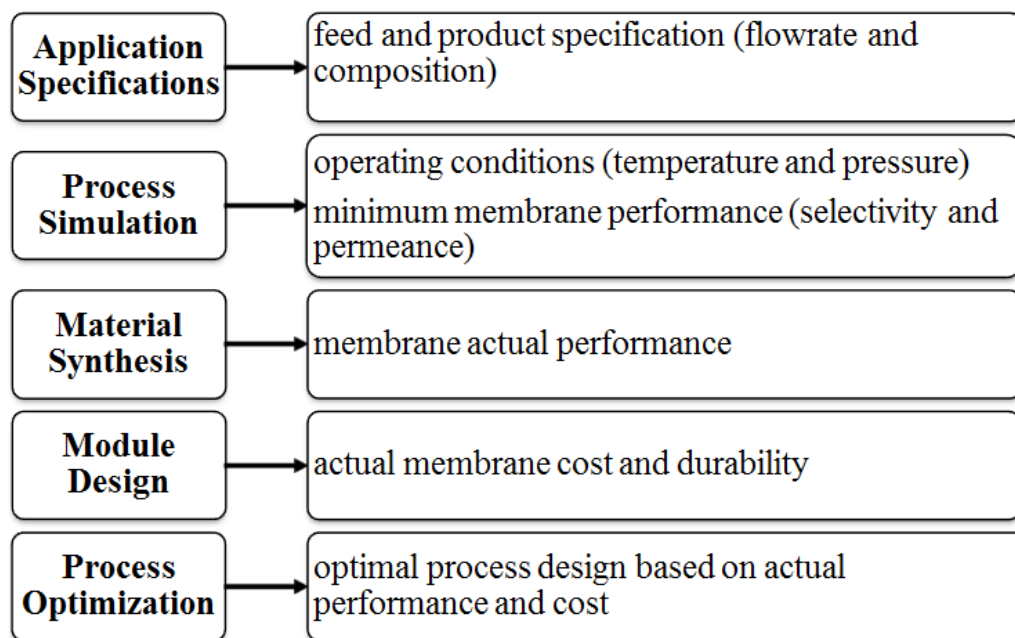


**Fig. 1.1** An overview of the different steps involved in the development of a membrane process for a specific application.

## 1.2 Motivation

This thesis is motivated by the industry need for developing novel energy efficient and environmental friendly separation processes for the separation of close volatility gas components. Membrane technology is a proven alternative to some of the conventional high energy consuming separation processes, such as sea water desalination, air

separation and hydrogen recovery from ammonia production flue gas. Therefore, membrane technology has become an attractive option for many industrial applications. In order to investigate the applicability of a certain membrane to replace or hybridize with an existing separation unit, process simulation of possible configurations is needed. The simulation results, when put together, are expected to help with generating guidelines useful for designing other separation processes and correct concepts that are misinterpreted due to the complexity of membrane mathematical modelling.

### **1.3 Research objectives**

**1) Develop an accurate mathematical model for gas separation in a counter-current hollow fiber module. The model will be incorporated into Aspen Plus® software to simulate the membrane process under various membrane/distillation configurations.**

The previously developed mathematical models available from the literature for membrane gas separation will be evaluated and the most suitable and accurate will be selected. The selected model should be applicable to both binary and multicomponent gas mixtures. The model governing equations are in the form of ordinary differential equations, therefore, the solution algorithm requires the use of an approximation method. The backward Gear's method with adaptive step size is selected as an integral approximation method.

The algorithm developed for resolving the mathematical membrane model will be solved in a FORTRAN subroutine and a dynamic linking library (DLL) will be

generated. The DLL will be incorporated into a user custom model within Aspen Plus®. This setup enables Aspen Plus® to solve the simulation case without the need for linking with external computational software, which enhances the calculation processing time.

**2) Studying the attainability of membrane systems to meet the separation task.**

Defining the minimum requirements for a membrane process to accomplish a certain separation task is one of the most important questions of the field, however, this issue has yet to be clearly resolved. The attainability of a single-stage and the most promising two and three-stage designs will be investigated to obtain important guidelines for system design.

**3) Formulating an optimization case to be used in Aspen Plus® built-in optimizer to determine the most profitable configuration, design and operating conditions.**

The efficiency of an optimization case depends on the selection of a descriptive objective function and accurate setting of constraints. In this work, both energy and economic analyses will be conducted to investigate the technology potential in a stand-alone or hybrid setup. The objective function for energy analysis is the minimum practical separation energy. For economic analysis, the objective function is to minimize the system total annualized cost. The optimization constraints are the product purity and recovery ratio for all the membrane/distillation hybrid configurations, which includes the: 1) single-stage membrane unit; 2) multi-stage membrane network; 3) pre-distillation hybrid system and 4) integrated-distillation hybrid system.

The optimization case will be carried out at different membrane separation parameters (selectivity and permeance) and membrane cost per unit area. Moreover, the impact of membrane durability on the separation economics will be investigated.

**4) Investigating the optimal operating conditions, system design and the corresponding membrane performance parameters in order to discover general guidelines to design membrane multi-stage and membrane/distillation hybrid systems.**

The optimization results will be analyzed to understand the impact of the membrane performance parameters (selectivity and permeance) on the system feasibility. The role of pressure ratio on process attainability and system feasibility will be thoroughly investigated. In order to generalize this work outcome to other gas processes, the results will be presented in general forms and will discuss the behavior rather than the specific values.

## **1.4 Thesis outline**

**Chapter 1** presents an overview of the study background and clearly states the study objectives.

**Chapter 2** introduces membrane technology for gas separation, the different designs of membrane modules and flow patterns. A review of the literature covering membrane network and membrane hybrid processes is also included.

**Chapter 3** discusses mathematical modeling of gas permeation in hollow fiber modules, the solution algorithm and the interface of model to commercial process simulation software. Afterward, the chapter brings a comprehensive parametric investigation of membrane performance and process variables.

**Chapter 4** investigates the attainability of membrane technology to meet certain separation tasks considering the complete well mixed and counter-current flow patterns. The attainability behavior is investigated and simple empirical correlations are obtained. This allows simplification of the calculation used to predict the required attainability parameters for accomplishing a given separation task in a counter-current membrane module.

**Chapter 5** investigates and compares the attainability of membrane cascade systems to single-stage membrane process. Furthermore, the potential of the cascade systems to reduce energy consumption is explored over a wide range in membrane selectivity.

**Chapter 6** proposes a simplified superstructure to optimize a membrane network without the need to consider all possible stream connections, as seen in the literature. The proposed arrangement combines the conceptual network design knowledge drawn from literature studies with the superstructure optimization methodology to minimize the calculation time without impacting accuracy.

**Chapter 7** introduces a thermodynamic analysis of single-stage membrane and membrane distillation hybrid processes. The role of pressure ratio and membrane selectivity is thoroughly investigated and some guidelines are proposed.

**Chapter 8** provides a comprehensive optimization and economic analysis of membrane distillation hybrid configuration for membranes subjected to different costs and lifetimes.

**Chapter 9** summarizes the major conclusions drawn from this study and highlights the study's contribution to research. The chapter also provided recommendations for future work to be considered.

## 1.5 References

- [1] A. Sieminski, International energy outlook 2013, US Energy Information Administration (EIA) Report Number: DOE/EIA-0484, (2013).
- [2] G.J. Ruiz, S.B. Kim, J. Moon, L.B. Zhang, A.A. Linninger, Design and optimization of energy efficient complex separation networks, *Comput Chem Eng*, 34 (2010) 1556-1563.
- [3] I.L. Chien, Opportunities for Energy Savings in Azeotropic Separation Processes, *Comput-Aided Chem En*, 31 (2012) 75-82.
- [4] M.G. Buonomenna, Membrane processes for a sustainable industrial growth, *Rsc Adv*, 3 (2013) 5694-5740.
- [5] R.W. Baker, Future directions of membrane gas separation technology, *Ind Eng Chem Res*, 41 (2002) 1393-1411.
- [6] I.C. Omole, Crosslinked polyimide hollow fiber membranes for aggressive natural gas feed streams, ProQuest, 2008.
- [7] A. Motelica, O.S. Bruinsma, R. Kreiter, M. den Exter, J.F. Vente, Membrane Retrofit Option for Paraffin/Olefin Separation • A Technoeconomic Evaluation, *Ind Eng Chem Res*, 51 (2012) 6977-6986.
- [8] T.C. Merkel, H.Q. Lin, X.T. Wei, R. Baker, Power plant post-combustion carbon dioxide capture: An opportunity for membranes, *J Membrane Sci*, 359 (2010) 126-139.
- [9] Y. Huang, T.C. Merkel, R.W. Baker, Pressure ratio and its impact on membrane gas separation processes, *J Membrane Sci*, 463 (2014) 33-40.
- [10] H. Strathmann, K. Kock, P. Amar, R. Baker, The formation mechanism of asymmetric membranes, *Desalination*, 16 (1975) 179-203.

- [11] I. Pinna, Recent advances in the formation of ultrathin polymeric membranes for gas separations, *Polymers for Advanced Technologies*, 5 (1994) 733-744.

## 2. Membrane Background & Literature Review

### 2.1 History of membrane technology

The history of membrane technology recorded the discovery of membrane separation to the middle of the eighteenth century. At that time, Nollet [1] studied animal's bladders and found it passes preferentially ethanol from a water-ethanol mixture to the other side which is in direct contact with pure water. Later, Thomas Graham investigated the diffusivity of different gases through rubber and found them to exhibit different permeabilities [2]. In 1866, Graham proposed the concept of the solution-diffusion mechanism. Since the discovery of membrane separation until the middle of the twentieth century, technology studies were based on scientific interests while industry interest and support were absent.

More attention is given to the membrane technology since 1950 due to the rapid industrial interest and the development in polymer synthesis. After recognizing the impact of adopting membrane technology on the reduction of processing cost, the transport mechanism was studied by many scientists (Van Amerongen (1950) [3], Barrer (1951) [4], Meares (1954) [5], Stern (1966) [6, 7] and others). These studies lead to the discovery of the solution diffusion mechanism for gas permeation in membranes [8]. The interest in technology was drastically increased after the development of high-flux asymmetric membranes and large-surface-area membrane modules for reverse osmosis applications followed by discovering the theory of composite membranes.

In the early 1960s, Sourirajan and Loeb discovered that annealing cellulose acetate under certain conditions produces a thin skin layer of smaller pore size making the material more selective without impacting its permeation flux. The skin layer had a dense structure with a thickness of 0.1-1.0  $\mu\text{m}$  on top of highly porous with connected open channel structure as illustrated in Fig. 2.1a [9]. The invention of high-flux asymmetric membranes was the main driver toward creating large surface area membrane modules with defect free material. After that and in the mid of 1970s, a new breakthrough is achieved in membrane material synthesis when the composite membranes are developed by combining polysulfone with polyamide [10]. Fig. 2.1b is a schematic illustration of the multilayer composite membranes. The invention of high-flux asymmetric membranes resulted in a less use of the selective material to create a membrane without significant loss in mechanical strength. Actually, it was found that 50 g of the selective layer material can produce one square meter of membrane by Loeb- Sourirajan technique while only 1 to 2 g are enough to prepare one square meter of a multilayer composite membranes [11].

a)

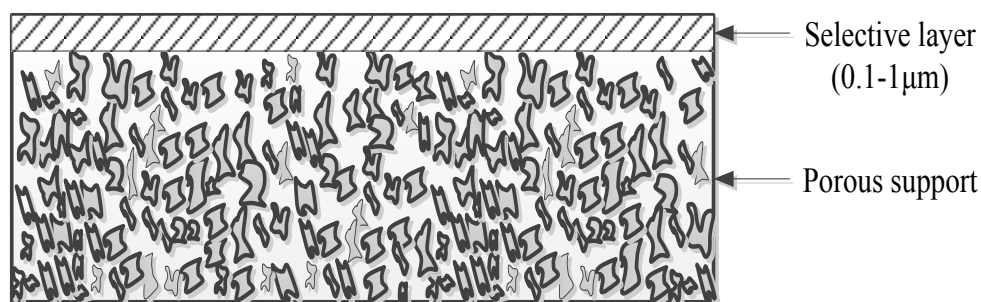




**Fig. 2.1** The two inventions to manufacture thin layer membranes a) Loeb- Sourirajan membrane b) multilayer composite membranes.

These developments were exploited to scale up the technology. The success of water treatment through RO membranes at lower cost than the conventional thermal separation started a new era in the history of membrane technology. The huge energy consumption to separate gaseous mixtures by conventional technologies makes the membrane technology more attractive for these applications.

Though the employment of membranes for gas separations started as early as 1963, these membranes were not viable to replace the conventional unit operations such as pressure swing adsorption, cryogenic distillation or absorption. In 1979, Monsanto introduced its hydrogen-separating Prism membrane to recover hydrogen from ammonia purge gas. Henis and Tripodi discovered that coating a highly permeable polymer on the surface of asymmetric hollow fibers seal the defects without significant impact on the selective layer “caulk” separation performance [12]. This success encourages companies such as Cynara, Separex, and Grace to develop membranes for carbon dioxide removal

from natural gas. Later, the first membrane based process for air separation was introduced by Dow. For the past three decades, the implementation of membranes in gas separation applications is expanding covering wide variety of applications ranging from air dehydration to carbon dioxide removal from natural [13].

In 1998, the market for membrane technology was about US\$4.4 billion. The share of gas separation applications from the membrane sales was less than 10% [14]. It is anticipated the technology share of the market for gas separations will reach to US\$760 million in 2020 [15]. The technology has emerged with different extents in applications such as hydrogen recovery, air separation and carbon dioxide removal from natural gas. The high potential separation processes for membrane technology are carbon capture from coal fired power plants' flue gas and olefin/paraffin in petrochemical industry. Other potential applications exists but with less impact on technology future market.

## 2.2 Membrane separation background

Separation in a membrane unit occurs due to fluid (gas or liquid) penetration through a layer which is preferentially permeable to mixture molecules. Thus, the membrane separation process functions by selective split of the feed mixture into two product streams. Those two streams are commonly named as permeate and retentate. The permeate stream consists of material that has penetrated through the membrane selective layer while the retentate stream is formed from material rejected by the selective layer. A simple membrane process can be schematically represented as shown in Fig. 2.2.

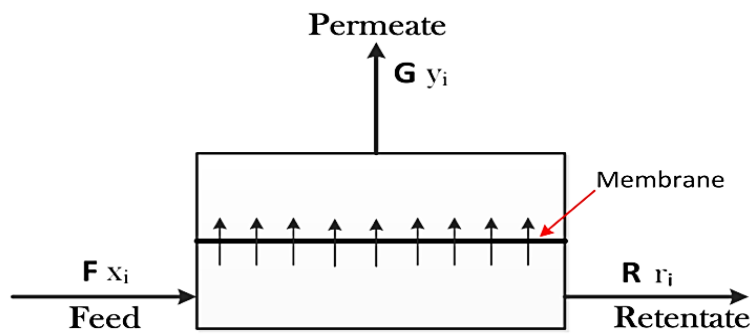


**Fig. 2.2** Schematic illustration of membrane separation process.

Membranes performance is usually characterized by two important parameters named selectivity ( $S$ ) and permeability ( $\beta$ ). The permeability (sometimes described as permeability coefficient) is the ability of the material to permeate a specific component. The permeability is only dependent on the material of the selective layer and it is measured in laboratories and reported in Barrer ( $1 \text{ Barrer} = 10^{-10} \text{cm}^3(\text{STP}) \cdot \text{cm}/\text{cm}^2 \cdot \text{s} \cdot \text{cmHg}$ ). The membrane selectivity is the ratio of the components' permeabilities and can be written as:

$$S_{A/B} = \frac{\beta_A}{\beta_B} \quad (2.1)$$

For most gas and liquid separation processes, the driving force of transport is the transmembrane pressure drop. Therefore, the pressure at the membrane feed side  $P_h$  is typically larger than the pressure at the permeate side  $P_l$ . The transmembrane pressure difference can be created in different ways. The first method is feed compression which is typically the case for liquid separations such as seawater desalination, and then the pressure of the retentate stream can be recovered back to the initial pressure through an energy recovery system. The second way is vacuum pumping of the permeate side. This

method is often applied in gas separations, and then the product stream is compressed back to the initial pressure for delivery. The third method of creating the transmembrane pressure difference is to use both compression and vacuum pumping due to equipment limitation. The ratio of  $P_h$  to  $P_l$  is defined as pressure ratio  $\gamma = P_h/P_l$ .

The gas transport in membranes is strongly dependent on the selective layer structure, characteristics of gas molecules and the interaction between the gas molecules and the membrane material. While the solution diffusion is the most accepted transport mechanism in dense membranes, Convective flow, Knudsen diffusion, and molecular sieving are the three accepted mechanisms for porous membranes [16]. The convective flow is found to take place when the pores of the microporous layer are larger than 0.1  $\mu\text{m}$ . As the pore becomes smaller and the ratio between the pore radius to the gas mean free path is less than one, the dominant transport mechanism is the Knudsen diffusion. The molecular sieving mechanism requires smaller pore diameter in the range of 5-10 Å. Though, porous materials are very attractive from conceptual point of view but making these materials as defect-free membranes is limiting their opportunity for scale-up.

The solution diffusion transport mechanism involves three steps as explained by Graham, as schematically illustrated in Fig. 2.3. The hypothesis here is that the fluid molecule dissolves into the polymer surface then it diffuses through the membrane layer till it reaches the low pressure side. At the low pressure side, the molecule desorb from membrane material. The sorption and desorption steps (first and last steps) occurs at faster rate than the diffusion rate in the polymer. Therefore, the fluid diffusion through the membrane is the rate determining step. Hence, the fluid components are separated due

to the difference in their solubility and diffusivity in and through the membrane selective layer.

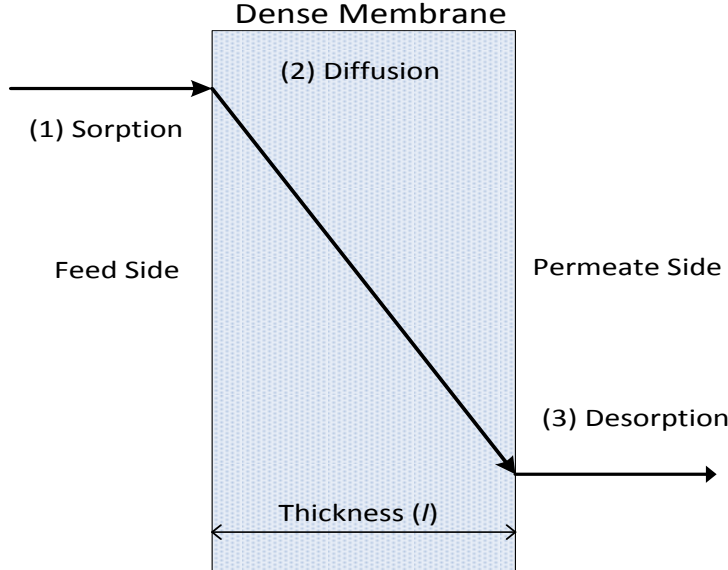


**Fig. 2.3** Illustration of the three steps involved in the solution diffusion theory.

Fluid diffusion through the membrane material obeys Fick's law which describes the diffusion flux ( $J$ ) as a function of concentration gradient as:

$$J_A = -D_A \frac{dc_A}{dx} \quad (2.2)$$

The gas concentration of component  $A$  at the feed side interface of the membrane can be expressed in terms of its solubility by the Henry's law as following:

$$c_A = S_A \cdot P_h^A \quad (2.3)$$

Similarly, the permeate side concentration can be written as:

$$c_A = S_A \cdot P_l^A \quad (2.4)$$

Substituting equation equations (2.3) and (2.4) into equation (2.2), the permeation flux becomes:

$$J_A = -S_A \cdot D_A \frac{(P_h^A - P_l^A)}{l} \quad (2.5)$$

Where;  $l$  is the membrane selective layer thickness. Defining the product of solubility and diffusivity as the membrane permeability coefficient ( $\beta_A$ ), then the flux relationship becomes:

$$J_A = -\beta_A \frac{(P_h^A - P_l^A)}{l} \quad (2.6)$$

## 2.3 Membrane module designs

In order to make a membrane module for industrial applications, the selective layer may take different configurations inside a housing compartment. The major configurations normally considered to prepare membrane modules are plate-and-frame, spiral wound and hollow fiber. The discussion below provides sufficiently enough information about these three designs.

### 2.3.1 Plate-and-Frame design

The configuration in a plate-and-frame module is formed by placing two membrane sheets facing each other and separated by a spacer. In order to maintain constant flow bath for permeate and feed streams, spacers are used. An illustration of this design is shown in Fig. 2.4. Moreover, to meet the product purity and recovery ratio required by a

specific separation process, the membrane area is adjusted by changing the number of plates hosted by the housing vessel. The major disadvantages of this configuration are low packing density ( $100\text{--}400 \text{ m}^2/\text{m}^3$ ), high pressure loss and use of many seals. This configuration is very practical for pervaporation separation processes but not efficient for gas separation applications. [17]

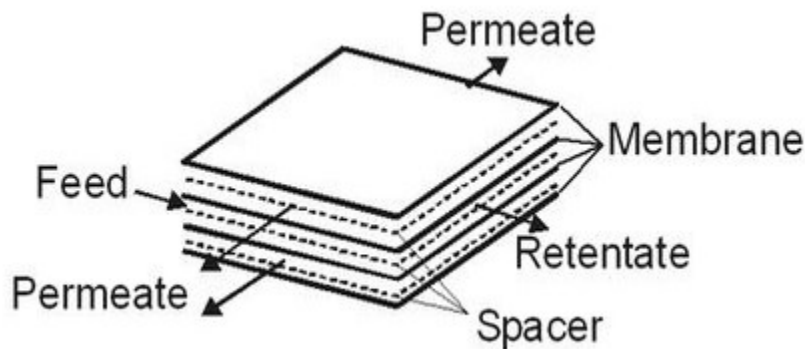


**Fig. 2.4** Schematic of plate and frame design for membrane module.

### 2.3.2 Spiral wound design

The spiral wound configuration is formed from many plate-and-frame systems rolled around a central collection pipe from which the permeate stream is extracted. Suitable spacers are used between the membrane sheets to maintain open flow channels for permeate even at high pressure. The permeate-side spacer is glued to the three free edges of membrane sheets to form what's called a membrane envelope. Moreover, feed- side spacers are used to allow uniform feed flow to the entire membrane surface and act as turbulence promoter. The details of this design are illustrated in Fig. 2.5. The feed stream moves in an axial direction over the envelopes formed from two membrane stacks. This configuration has a moderate packing density ( $300\text{--}1000 \text{ m}^2/\text{m}^3$ ) but the major

disadvantage of spiral wound configuration is the hardness of cleaning to remove fouling objects. [18]

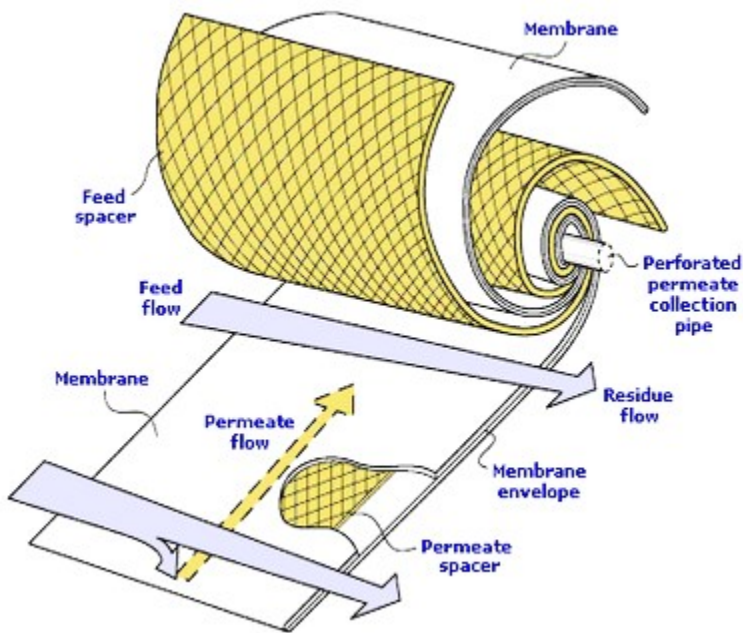


**Fig. 2.5** Schematic illustration of spiral wound design.

### 2.3.3 Hollow fiber design

The assembly in a hollow fiber module is identical to that of a shell and tube heat exchanger, as illustrated in Fig. 2.6. The fiber is hollow from inside and the selective layer is coated on the fiber inner surface for inside fiber feed flow and on the outer surface for shell side feed flow. Hollow fibers consist of a porous, non-selective support layer (about 40-200  $\mu\text{m}$ ), and an active layer (about 40 nm). The active layer is the actual membrane, but due to its small thickness it must be supported by a thicker layer in order to provide mechanical strength, to withstand the applied pressure difference across the membrane. It consists of a large number of hollow fibers assembled in a module to maximize the membrane surface area which is required for high product recovery.

Based on the side at which the feed stream flows, there are two types of hollow fiber modules which are known as shell-side feed modules and lumen-side feed module. The shell-side module is more practical for high pressure applications. On the other hand, the lumen-side module is more preferred when the separated mixture shows tendency to foul on the selective layer surface since maintaining good flow reduces accumulation. Also, the good flow maintained by the lumen-side feed reduces the effect of concentration polarization.

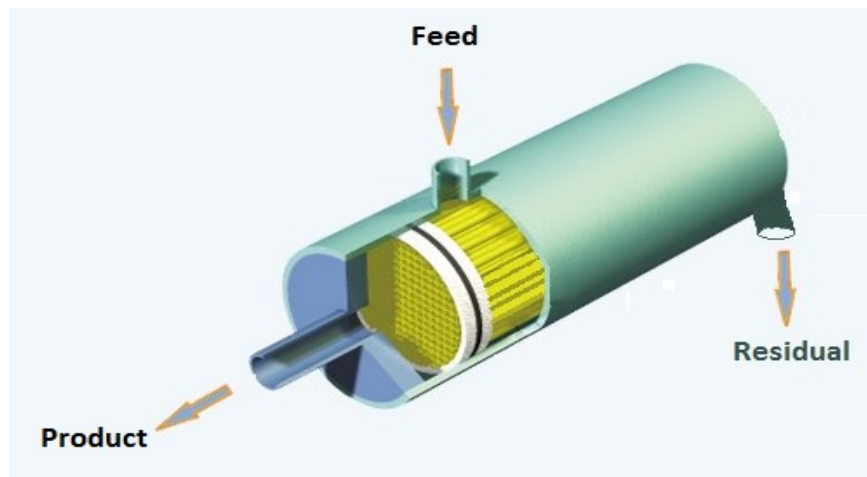


**Fig. 2.6** Hollow fiber module with counter-current flow pattern.

The advantages of the hollow fiber design can be summarized in the following points [19]:

- 1- The membrane material is self-supported. Therefore, no mechanical supports are needed such as spacers or any other hardware. Also, the module can withstand high feed pressure and low permeate pressure.

2- High packing area or membrane active surface area to module volume ratio.

Hollow fiber module of  $0.04 \text{ m}^3$  can accommodate an active surface area of  $575 \text{ m}^2$  while the same volume of a spiral wound design can only accommodate  $30 \text{ m}^2$ .

The major disadvantage of the hollow fiber design is that it requires feed stream pretreatment facility to remove large size particles which could plug the module fibers and severely reduce its efficiency. Furthermore, the module processing time per unit area is very high compared to other designs.

The membrane module design and its operating conditions have to be chosen carefully for each separation process. In order to fully exploit the maximum separation ability of the membrane, the following general requirements need to be fulfilled: [18]

- Practical packing density.
- Resistance to mechanical, thermal and chemical effects.
- High flow distribution to prevent the presence of dead zones and channeling.
- Low pressure loss.
- Resistance to fouling and ease of cleaning.
- Low cost of modules manufacturing and operation.
- Ease of membrane replacement.

The importance of these elements varies based on the process setup and the specific application. In gas separation processes, the most important factors are high packing density and low pressure drop of product streams. Permeate/retentate pressure loss becomes of no importance if the stream has no value and will not be processed any further like retentate stream vented from oxygen enrichment unit.

## 2.4 Module flow patterns

Based on the flow direction of feed and permeate streams, there are five different configurations. The type of flow configuration has a direct impact on module's performance especially when the feed concentration varies at high rate along the membrane length and the porous supporting layer has minimal impact on separation (high flux membranes). The possible flow patterns in a membrane module are:

- Co-current
- Counter-current
- Cross-flow
- Free flow permeate (One Side Mixing)
- Ideal mixed feed and permeate side (Perfect Mixing)

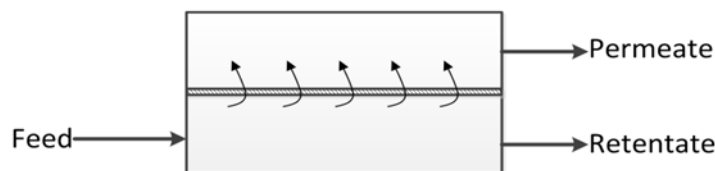
All of the mentioned five configurations are applicable to spiral wound configuration while in hollow fiber configuration only co-current and counter-current are possible [20]. Therefore, only the two flow patterns applicable for hollow fiber configuration are discussed below.

As illustrated in Fig. 2.7a, in co-current configuration both the feed and the permeate streams flow parallel to each other and in the same direction. The driving force decreases along the membrane length since the partial pressure of the high permeable component decreases on the feed side and at the same time increases on the permeate side. [17]

In counter-current configuration, the permeate stream flows in the barrel but opposite direction to the feed stream as schematically represented in Fig. 2.7b. In this flow mode,

the permeation driving force generated from the concentration gradient between the two sides of the membrane is high compared to co-current. Thus, in most applications and in particular those with retentate products, counter current flow is advantageous. [17]

### a) co-current flow



### b) counter-current flow

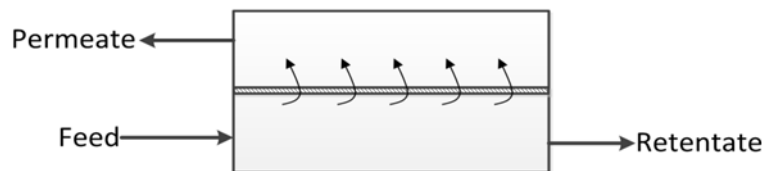


**Fig. 2.7** The two flow patterns applicable in hollow fiber membrane modules.

## 2.5 Membrane systems for gas separations

Membrane technology is proven as an alternative to some of the high energy consuming separation processes like seawater desalination, air separation and ammonia production. Adopting membrane technology is attractive to industrial applications for many reasons such as simple operation, low maintenance cost as it does not have moving parts, relatively low capital cost, small physical footprint which makes it favorable for platform operations and low energy consumption operations. In order to recommend a membrane system for a specific gas separation process it should be proven that it can

perform better separation or has better economics than other competing separation processes. Absorption, adsorption, and cryogenic distillation are widely adopted processes for large scale gas production when high purity and high recovery are required [21]. Nevertheless, these processes are high energy consuming giving room for membrane systems to compete with them on an economical basis. The membrane unit can be used as a single-stage, membrane network or hybridize with other separation process.

There is general consensus that membranes can perform better for bulk separation. Separation processes can be categorized into two major groups that most industrial applications fall into. The first one is when the concentration of target component (TC) in the inlet feed is high. In such case membranes can perform very well compared to other separation processes, resulting in high purity permeate. But they fail in satisfying retentate with low TC concentration. As an example, the discussion of natural gas sweetening is introduced. Traditionally, the sweetening was carried out with amine-based absorption/desorption processes. In the 1980s, the application of membranes to this process was introduced for the cases where the sour gas concentration is high. Later, it was realized that though membranes are economical for separation of bulk of sour gas, it was not capable of treating natural gas (retentate) with sour gas concentration less than 2% (enforced by pipeline specifications). Therefore, an amine-membrane hybrid system was introduced; so that the membrane's role is in the bulk separation while the amine-system further reduces the sour concentration of retentate to the target concentration.

The second category is when the concentration of TC in the inlet feed is comparatively low where a membrane unit cannot neither satisfy high purity in permeate stream nor low concentration in retentate stream through a single-stage membrane. Therefore, the optimal design that satisfies both recovery and purity will be at higher membrane areas and appropriate pressure. Such arrangements result in higher CAPEX (due to high membrane area) and OPEX (due to high compression costs) making the performance of membranes debatable for such conditions of low concentration feed. In such scenarios, industry has not considered membranes as best available technology (BAT) and therefore has continued to use other separation processes. The selection of appropriate separation options requires detailed techno-economical investigations. The solution for such cases has been a combination of membrane systems consisting of a few stages arranged in parallel or in series to reach higher qualities. The success and adoption of membrane systems will be, thus, very much dependent on membrane systems engineering.

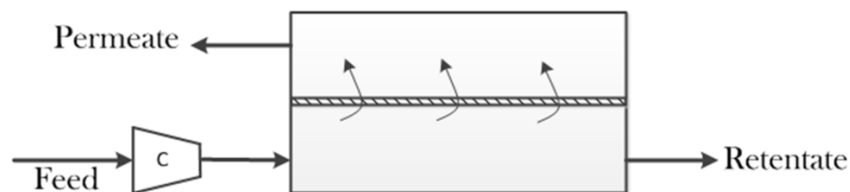
In order to build a new process flowsheet to perform a certain separation task and correspond to optimal system economics then process system synthesis appears as the only systematic method to achieve such goals. The different configurations which will be later evaluated are briefly described below.

### **2.5.1 Single-stage configuration**

A single-stage membrane configuration consists of one permeation unit or more than one unit but all are arranged in a barrel setup and has the same feed composition. This configuration is the simplest and corresponds to the lowest capital investment. The

single-stage configuration is schematically shown in Fig. 2.8. The driving force across the membrane can be created by feed compression or vacuum pumping the permeate side.

a) driving force by **compressor**



b) driving force by **vacuum pump**

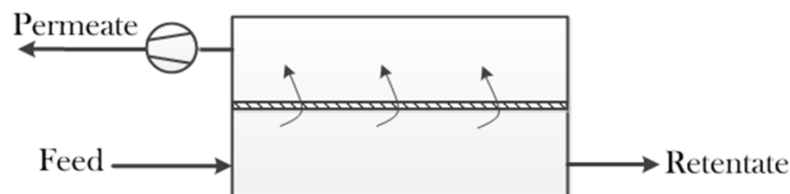


**Fig. 2.8** Creating driving force through the membrane module by a) feed compression b) permeate vacuum pumping.

The performance of a membrane unit is usually represented by the permeance of the highest permeable component and its selectivity compared to other components in the mixture. At relatively high inlet concentration of target component ( $X_{TC} > 0.2$ ), moderate product purity and recovery, considering a highly efficient membrane (if exist) can outperform the conventional gas separation processes like pressure swing adsorption (PSA) and cryogenic distillation. Criteria upon which a membrane can be considered as high performance membrane are material and process dependent. The material used for the synthesis of the membrane selective layer controls the permeation flux and product

purity. The dependence of membrane performance on the process can be summarized in the feed concentration, product purity and recovery ratio. The applicability of a membrane process to a specific process is normally evaluated techno-economically with respect to a base process adopted for the same process and at the same feed and product specifications.

### **2.5.2 Multi-stage configuration**

As seen in many industrial applications, the single-stage membrane separation has limitation in achieving high quality permeate or retentate while typically the objective of separation is either of these. The reason is due to the permeation requiring a driving force between the two membrane sides, i.e.  $x_i P_h - y_i P_l > 0$ , resulting in:

$$y_i < \frac{x_i P_h}{P_l} = \frac{x_i}{\gamma} \quad (2.7)$$

Therefore, when the target component concentration in the feed stream ( $x_i$ ) is low, even high pressure ratio ( $\gamma$ ) may not achieve high permeate purity ( $y_i$ ). As such, more stages are required in order to accomplish the desired product quality and recovery ratio. The first solution, to the best of our knowledge, was a patent by Pfefferle [22] who presented a two stage system with permeate recycle in order to reach high purity permeate. Following the two-stage presentation, a cascade of membrane systems was introduced for a binary gas mixture separation [23, 24]. Gruzdev et al. [25] proposed a method for calculation of a cascade system when there is a multicomponent gas mixture. Some studies have moreover proposed using different membrane materials in the cascade system [26]. The cascade model shown in Fig. 2.9 is the most general multistage

membrane design. This design idea is borrowed from conventional mass transfer operation designs such as multi-stage distillation or extraction systems. The downstream membranes enrich permeate to higher purities of the target components (TCs) while upstream membranes strip remaining traces of TCs to desired values. In many processes either of the enriching or stripping sections is required. For instance in the case of oxygen separation from air in an Air Separation Unit (ASU), the downstream enriching section is not required. In the case of natural gas sweetening, the objective is to minimize concentration of sour gas ( $\text{CO}_2$  and  $\text{H}_2\text{S}$ ) in the stream retentate. Therefore the upstream stripping section is required. Moreover, low concentration of natural gas in the permeate stream is also required to minimize natural gas loss. Therefore, the downstream section is also needed.

It is however discussed that, except at very low feed concentration or low-efficient membrane [27], membrane systems consisting of two- [23] or three stages [28] are the most techno-economically optimal configurations. Though the introduction of more stage results in slightly less membrane areas and compression energy, the increase in number of compressors ultimately neutralizes this advantage [28].

In literature, there have been numerous studies which discussed the optimal configurations of two and three stage membrane systems. Kao et al. [29] compared two different membrane systems. One was the so-called continuous column membrane, CCM [22] and the other one was two strippers in series permeator, TSSP. They reported sweet-spot operating condition for each configuration. According to them, TSSP is superior to CMC configuration unless the objective is to minimize membrane area or to have high

purity permeate. A similar conclusion was reported by Qiu et al. [30] as a result of economic evaluation stating that TSSP is the most efficient configuration when the objective is high quality retentate while for the case of high quality permeate CMC is more efficient.

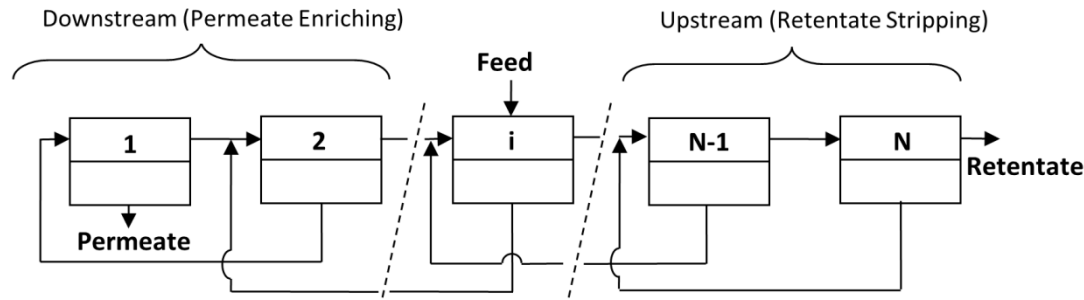


**Fig. 2.9** Schematic of N-stage cascade membrane system with recycles.

Bhide and Stern [31] studied seven different one, two and three-stage configurations with respect to minimum costs. They found that a three stage system with a single permeation stage in series with a two-stage permeation cascade with recycle was the best. Pettersen and Lien [28] studied the intrinsic behavior of several single-stage and multi-stage permeator systems. They also divided the multi-stage system into enriching and stripping cascades which could be two or three-stages. According to them, if the objective is to have retentate product with minimum concentration of the high permeable component, then the upstream section of the cascade system (stripping) will be chosen while for high purity permeate product, the downstream section (enriching) is the best choice.

Datta and Sen [32] techno-economically reviewed ten different one-, two- and three-stage configurations, shown in Fig. 2.10, for natural gas sweetening. They reported that the selection of the best configuration is highly related to feed concentration, separation objectives and products market value. For example in case the natural gas price is low, high permeate (mainly carbon dioxide) enrichment is not desired while at high natural gas prices, the objective is to minimize natural gas loss in permeate stream by adding enriching stages. According to them, the optimum configuration is unique in certain range of feed quality, separation policy and market price.

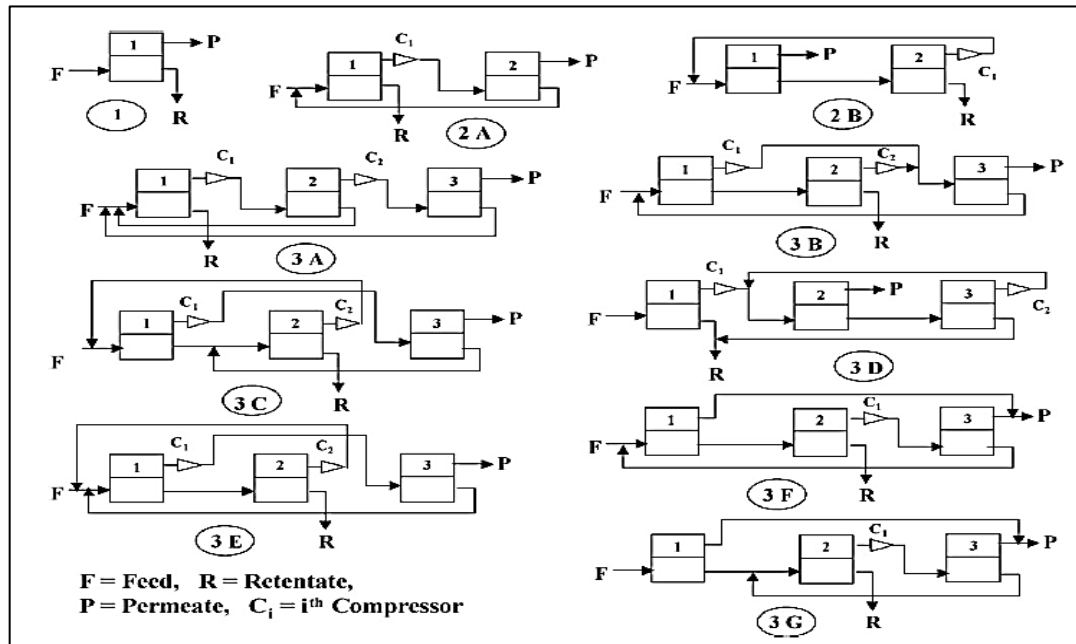


**Fig. 2.10** Some probable optimum configurations of membrane stages.

Therefore, it can be concluded that the selection of the proper multi-stage system is highly dependent on the separation policy which is mostly affected by the economical inputs. When the retentate stream is the target product and its partial loss with the

permeate stream is not economically important, the policy will be mere stripping. For mere stripping objectives, two-stage (Figure 2.11a) or three-stage stripper would be selected. However, when the objective is high purity permeate, the policy will be enriching for which two or three-stage enriching system will be the choice (Fig. 2.11b).

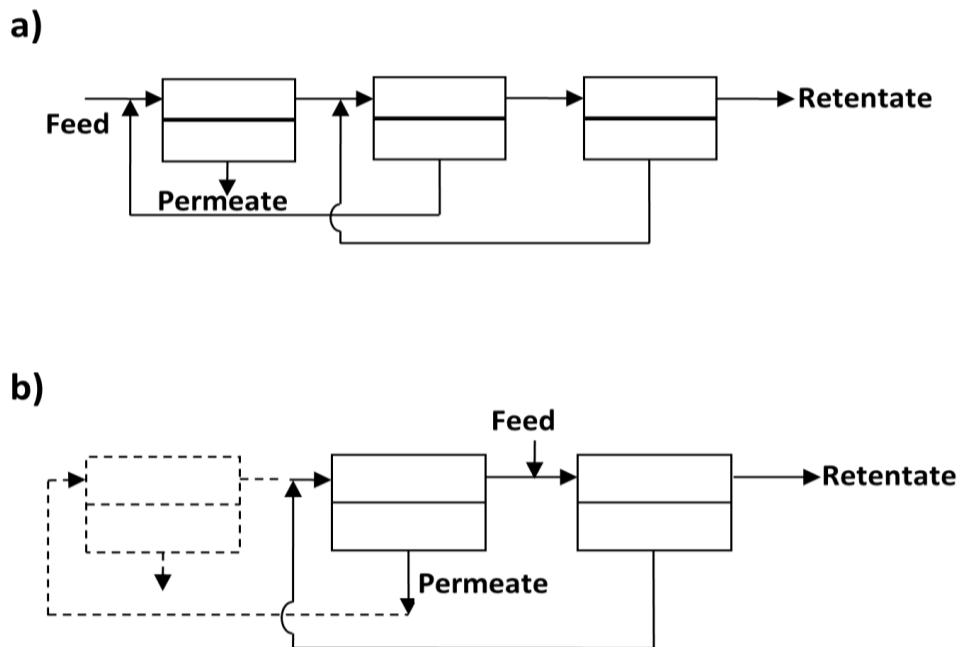


**Fig. 2.11** Schematic of a) three-stage stripping b) two/three-stage enriching systems.

### 2.5.3 Membrane/distillation hybrid configurations

Even though single membrane configuration corresponds to the lowest capital investment, in most cases it cannot meet high product purity and recovery unless high pressure ratio is applied to maximize the driving force. Thus, single-stage membrane corresponds to high energy consumption. In order to maximize product recovery, multi-stage membrane network is normally used. Also, product recycle is mostly used to

maximize product purity. When high performance membrane is not available for a specific application and the product market value is high then techno-economically a hybrid system outperforms any membrane configuration.

Membrane/distillation hybrid systems are normally needed to shift the azeotrope limit which exists between the mixture constituents at certain temperature, pressure and composition. Also, the hybrid system is effective to separate gases of close relative volatilities in order to achieve high purity products. In such cases, the separation of hydrocarbon constitutes is performed by cryogenic distillation. Even though cryogenic distillation provides high purity products, it is one of the most high energy separation processes. This is due to the fact that the condenser cooling duty is the dominant cost element which is normally order of magnitude higher than the other costs in the distillation unit.[33]

Membrane/distillation hybrid separation is a promising alternative to the conventional separation techniques in gas separation processes. The hybrid system is advantageous since it minimizes the energy consumption and maximizes product recovery. Based on the most permeable component, the different possible configurations of membrane/distillation hybrid system can be identified. Therefore, the hybrid system can have membranes in series with the distillation column or integrated with distillation. The series hybrid system can be categorized based on distillation column location. When the distillation unit is upstream of the membrane unit, the configuration is called post-distillation hybrid otherwise it is called pre-distillation hybrid.

### 2.5.3.1 Pre-distillation hybrid configuration

In the pre-distillation configuration, the membrane unit is placed upstream the distillation column. The function of the membrane unit in such setup is to minimize the separation load on the distillation especially when the qualities of either one of permeate and retentate streams meet the separation requirement. In case the permeate stream purity is lower than the product specification then it should be fed to the column rectifying section. Likewise, if the retentate stream purity is lower than the process requirement then it should be fed to the stripping section. The pre-distillation configuration is illustrated in Fig. 2.12.

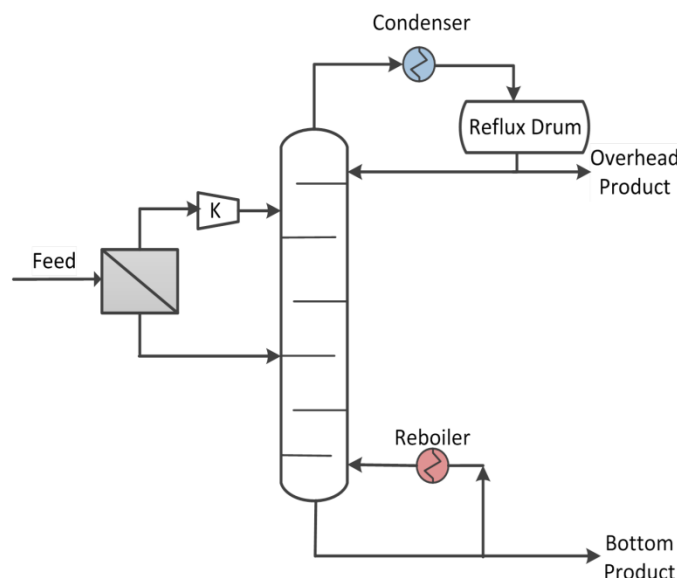


**Fig. 2.12** Membrane/distillation hybrid with pre-distillation configuration.

### 2.5.3.2 Post-distillation hybrid configuration

In this configuration, the membrane unit is installed after the distillation unit to further purify the overhead or the bottom product. In case the membrane is selective to the light key component then the permeate stream or part of it is produced while the retentate stream is recycled to the distillation column as illustrated in Fig. 2.13. Also, in case the adopted membrane is only sufficient for gas mixture separation, then the condensate should be reheated to regenerate gaseous mixture. On the other hand, when the adopted membrane is selective for the heavy component, the permeate stream is compressed and recycled to distillation while retentate stream or part of it is the final product.

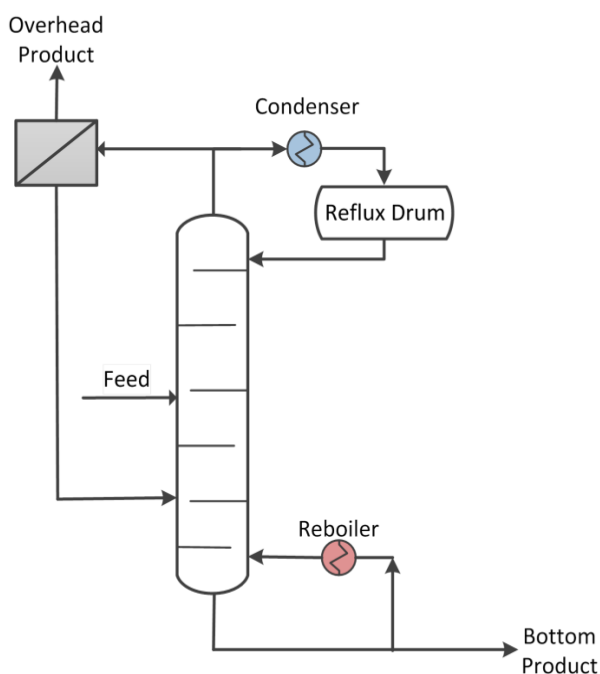


**Fig. 2.13** Membrane/distillation hybrid with post-distillation configuration.

### 2.5.3.3 Integrated-distillation hybrid configuration

In this configuration, the membrane unit and the distillation column are in parallel position. The feed enters to the distillation column and after certain number of stages a side stream is withdrawn from either the rectifying section or the stripping section to feed the membrane unit. Based on permeate and retentate purities, they can be produced or recycled back to the distillation column. Once the permeate stream is to be recycled then it should be compressed and returned to a stage higher than the side stream if the membrane is selective for the light key component or the opposite if membrane is selective for the heavy key component. Also, the retentate stream if not satisfying the product quality then it should be recycled to a lower stage than the side stream feeding the same membrane unit in case the membrane is selective for the light key component and the opposite in case the membrane is selective for the heavy key component.

Recycling both product streams from the membrane unit to the column results in a fully integrated hybrid configuration. This setup is potentially advantageous to assist the distillation column in separating binary or multicomponent gas mixtures where the column is least effective, i. e. near the feed stream. Fig. 2.14 is an illustration of the fully integrated hybrid system.

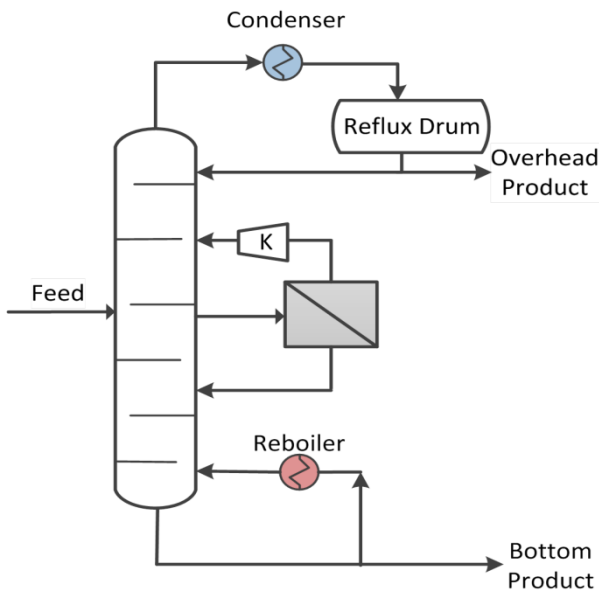


**Fig. 2.14** Membrane/distillation hybrid with integrated configuration.

#### 2.5.4 Simulation of membrane/distillation hybrid configurations

The designs of membrane/distillation hybrid system have been discussed in many studies. Pettersen and Lien [33] presented a design model for vapor permeation systems. The method considered McCabe diagrams to solve the distillation part while the gas permeation part is solved through a mathematical model which is only valid for binary mixtures. Pressly and Ng [34] developed a screening procedure to calculate the breakeven point above which the hybrid system becomes not economically feasible compared to the only distillation case. Bausa and Marquardt [35] calculated the minimum energy required for the separation of a multicomponent mixture in order to estimate the minimum required membrane area and identify the optimal side stream location. This method can be applied to multicomponent non-ideal mixtures. Szitkai et al. [36] applied the superstructure mathematical modeling to the separation of water-ethanol mixture to

produce pure ethanol using a pervaporation unit. The mathematical model was solved using the quadratic and exponential regression to simplify the integral approximation. Steinigeweg and Gmehling [37] showed through simulation and experimental results that a hybrid system of reactive distillation tower and pervaporation unit is economically favorable. Simulating the membrane separation in a process simulator will avoid assumptions normally made to simplify the mathematical modeling of the hybrid system. Marquardt et al [38] proposed a framework for the design of membrane/distillation hybrid systems following a systematic procedure of three steps: 1. Generation of flow-sheet alternatives. 2. Developing a shortcut evaluation method of these alternatives. 3. Conducting a rigorous MINLP optimization of the most promising alternatives to obtain the optimal flow-sheet design. Caballero et al. [39] proposed a mathematical approach to investigate the applicability of a membrane unit to retrofit an existing distillation column considering the parallel hybrid configuration. In this paper, the rigorous MINLP optimization was carried out in a process simulator for the distillation column and the auxiliary equipment while the membrane model was solved in MATLAB. Eliceche et al [40] conducted a study to optimize the operating conditions of a hybrid membrane/distillation system using a process simulator but the location of the feeds and withdrawn streams was carried out by a trial and error procedure.

Kookos [41] proposed a methodology for the structural and parametric optimization of continuous hybrid separation systems. He described the superstructure of the hybrid process using a simplified steady-state mathematical model where it was assumed that all streams taken from, or returned to, the distillation column were vapor streams.

Furthermore, it was outlined that the hybrid system can potentially reduce the operating cost by 22% if the system is operated at the optimum conditions.

Verhoef et al. [42] simulated a hybrid pervaporation membrane process where the distillation process is performed in Aspen Plus® simulator while the prevaporation membrane calculation is done in Excel Visual Basic for Applications (EVB) and results are linked to Aspen Plus®. The simulation was run to optimize the hybrid system for dehydration and recycling of ethanol and purification of acetic acid.

Davis [43] implemented a hollow fiber membrane model in Aspen HYSYS with the assumption of negligible pressure drop without external custom programming. Chowdhury et al. [44] presented a numerical solution approach to incorporate the membrane mathematical model presented by Pan in Aspen Plus® for both co-current and counter-current membrane configurations. In addition, Hussain and Hagg [45] implemented a one-dimensional isothermal model in Aspen HYSYS to study the impact of the different process parameters on the feasibility of adopting a facilitated transport membrane for CO<sub>2</sub> capture from flue gas. Faizan et al. [46] created a user defined membrane unit in Aspen HYSYS and simulated the different configurations of a two dimensional cross flow hollow fiber membrane for the separation of CO<sub>2</sub> from natural gas. The used mathematical model is only valid for a binary mixture and assumes no pressure drop inside the fiber lumen.

Most of the above mentioned membrane models which are implemented in commercial process simulators are only applicable to binary mixtures separation processes but cannot be used for multi-component mixtures. In addition, some models

considered negligible pressure drop in the hollow fiber lumen. Moreover, all simulation work are performed to investigate the applicability of a specific membrane to a certain separation process instead of evaluating the membrane performance over a wide range of permeance and selectivity. The proposed analysis will help to understand the challenges that the research groups need to overcome when designing a new material for a specific application. In order to make the simulation results more effective the following guidelines should be followed:

- 1- The performance parameters of a membrane unit should be evaluated over wide range to consider the future development in membranes.
- 2- Results should be reported in fixed indicators such as membrane surface area, machinery horsepower and heat exchanger duty.

## **2.6 Economic evaluation basis**

Demonstrating the potential of a technology to perform a certain separation is usually done by conducting an energy assessment study or techno-economic analysis. The energy assessment is a preliminary tool to measure the technology attractiveness while the economic analysis is a high level tool upon which a decision can be made. The mostly used indicator to compare the economic significance of the proposed technology is the Total Annualized Cost (TAC). Hence, this indicator is to be used in this dissertation to compare the membrane technology to the conventional distillation process and also to compare the different process alternatives. The annualized system cost consists of the equipment annual depreciation and the process annual operating expenses. The equipment annual depreciation is the product of the annual depreciation rate and the

equipment installation cost. The operating cost is the sum of utilities, maintenance and labor expenses. In most of chemical and petrochemical plants the utilities accounts for more than 95% of the operating expenses and hence the other expenses can be ignored. Therefore, the operating cost reduces to the energy cost. The cost elements will be considered in the economic evaluation are:

- 1- The capital equipment cost is calculated based on the Marshall and swift index of 2013.
- 2- The electric power cost is considered to be fixed at 0.06 \$/kWh.
- 3- The cost of cooling water is 0.2 \$/GJ.
- 4- The cost of moderate pressure steam used in the reboiler is 8.0 \$/GJ
- 5- The membrane module cost considered is in the range of 100- 1000 \$/m<sup>2</sup>.
- 6- The membrane depreciation time is assumed to be 2 or 5 years.

In literature, there are different correlations to estimate equipment's installation cost. The materials used for equipment construction are subjected to inflation or deflation and therefore the cost correlations are made as a function of cost indices. These indices adjust for the cost change over the time period since the correlation is made till the evaluation date. These cost indices are frequently updated and published in chemical engineering journals. The most popular indices are the Chemical Engineering Plant Cost Index (CEPCI), Marshall and Swift (M&S) and Intratec Chemical Plant Construction Index (IC). These correlations are based on operating conditions and material of construction. The equipment cost correlations developed by Guthrie in 1969 is still mostly used for

project preliminary cost estimation. Guthrie's cost correlations for equipment that will be used in this study are discussed below:

### **Cost of Distillation Column ( $C_{DC}$ )**

$$C_{DC} = \left( \frac{M \& S}{280} \right) 101.9 \times D^{1.066} \times H^{0.802} \times (2.18 + F) \quad (2.8)$$

Where D is the column diameter (ft), H is the column height (ft) and F is a correction factor to adjust for the operating pressure and material of construction.

$$F = F_p F_M \quad (2.9)$$

**Table 2.1** Pressure factor for distillation column cost.

P (psig)	50	100	200	300	400	500	900	1000
F <sub>p</sub>	1.00	1.05	1.15	1.20	1.35	1.45	2.3	2.5

**Table 2.2** Material factor for distillation column cost.

Material	F <sub>m</sub>
Carbon Steel	1.0
316 Stainless Steel	1.3
304 Stainless Steel	1.3
Monel	1.65

### **Cost of Column Trays and Internals ( $C_{CI}$ )**

$$C_{CI} = \left( \frac{M \& S}{280} \right) 4.7 \times D^{1.55} H \times F \quad (2.10)$$

The correction factor  $F$  is calculated from the following formula:

$$F = F_{TS} + F_{TT} + F_M \quad (2.11)$$

**Table 2.3** Tray type correction factor.

Tray Type	F <sub>TT</sub>
Sieve type	0
valve type	0.4
Bubble Cap type	1.8

**Table 2.4** Tray spacing correction factor.

Tray Spacing (inch)	24	18	12
F <sub>s</sub>	1.0	1.4	2.2

**Table 2.5** Trays' material correction factor.

Material	F <sub>m</sub>
Carbon Steel	0
316 Stainless Steel	1.7
Monel	8.9

### Cost of Heat Exchanger (C<sub>HE</sub>)

$$C_{HE} = \left( \frac{M \& S}{280} \right) 101.3 \times A^{0.65} \times (2.29 + F) \quad (2.12)$$

Where, F is a correction factor that accounts for the differences in operating pressure, design type and material used and A is the heat transfer area in  $\text{ft}^2$ .

$$F = (F_D + F_P)F_M \quad (2.13)$$

**Table 2.6** Material correction factor for shell and tube heat exchanger.

Surface Area ( $\text{ft}^2$ )	CS/CS	SS/SS	Monel/Monel
Up to 100	1.0	2.5	3.2
100-500	1.0	3.1	3.5
500-1000	1.0	3.26	3.65
1000-5000	1.0	3.75	4.25

**Table 2.7** Vessel pressure correction factor.

Pressure (psig)	150	300	400	800	1000
$F_P$	0	0.1	0.25	0.52	0.55

**Table 2.8** Heat exchanger design correction factor.

Design Type	$F_D$
Kettle Reboiler	1.35
Floating Head	1.00
Fixed tube sheet	0.80
U Tube	0.85

### Gas Compressors ( $C_{\text{Comp}}$ )

$$C_{Comp} = \left( \frac{M \& S}{280} \right) 517.5 \times 3.11 bhp^{0.82} \quad (2.14)$$

Where  $bhp$  is the compressor break horsepower which can be calculated from the horsepower ( $hp$ ) and efficiency ( $eff$ ) as following:

$$bhp = \frac{hp}{eff} \quad (2.15)$$

## 2.7 References

- [1] J.A. Nollet, Investigations on the Causes for the Ebullition of Liquids (Reprinted from Histoire De L'Academie Royale Des Sciences 1748, Pg 57-104, 1752), *J Membrane Sci.*, 100 (1995) 1-3.
- [2] T. Graham, On the molecular mobility of gases, *Philosophical Transactions of the Royal Society of London*, 153 (1863) 385-405.
- [3] G. Van Amerongen, Influence of structure of elastomers on their permeability to gases, *Journal of polymer science*, 5 (1950) 307-332.
- [4] R.M. Barrer, *Diffusion in and through solids*, Cambridge University Press, London, 1951.
- [5] P. Meares, The Diffusion of Gases Through Polyvinyl Acetate1, *Journal of the American Chemical Society*, 76 (1954) 3415-3422.
- [6] S.A. Stern, Industrial applications of membrane processes: the separation of gas mixtures, in *Membrane Processes for Industry*, Proceedings of the Symposium, Southern Research Institute, Birmingham, (1966).
- [7] Walawend.Wp, S.A. Stern, Analysis of Membrane Separation Parameters .2. Countercurrent and Cocurrent Flow in a Single Permeation Stage, *Separ Sci.*, 7 (1972) 553-584.
- [8] R.W. Baker, *Membrane technology*, Wiley Online Library, 2000.
- [9] A.Y. Tamime, *Membrane Processing: Dairy and Beverage Applications*, John Wiley & Sons, 2012.
- [10] J. Cadotte, R. Petersen, R. Larson, E. Erickson, A new thin-film composite seawater reverse osmosis membrane, *Desalination*, 32 (1980) 25-31.
- [11] R.W. Baker, B.T. Low, Gas Separation Membrane Materials: A Perspective, *Macromolecules*, 47 (2014) 6999-7013.

- [12] J.M. Henis, M.K. Tripodi, A novel approach to gas separations using composite hollow fiber membranes, *Separ Sci Technol*, 15 (1980) 1059-1068.
- [13] P. Bernardo, E. Drioli, Membrane gas separation progresses for process intensification strategy in the petrochemical industry, *Petrol Chem+*, 50 (2010) 271-282.
- [14] S.P. Nunes, K.V. Peinemann, *Membrane technology in the chemical industry*, Wiley-VCH, Weinheim ; New York, 2006.
- [15] R.W. Baker, Future directions of membrane gas separation technology, *Ind Eng Chem Res*, 41 (2002) 1393-1411.
- [16] B. Bettens, S. Dekeyzer, B. Van der Bruggen, J. Degreve, C. Vandecasteele, Transport of pure components in pervaporation through a microporous silica membrane, *J Phys Chem B*, 109 (2005) 5216-5222.
- [17] E. Drioli, G. Barbieri, *Membrane engineering for the treatment of gases*, Royal Society Chemistry, 2011.
- [18] M. Mulder, *Basic Principles of Membrane Technology*, Springer, 1996.
- [19] G. Zhang, X. Song, S. Ji, N. Wang, Z. Liu, Self-assembly of inner skin hollow fiber polyelectrolyte multilayer membranes by a dynamic negative pressure layer-by-layer technique, *J Membrane Sci*, 325 (2008) 109-116.
- [20] P.K. Kundu, A. Chakma, X.S. Feng, Simulation of binary gas separation with asymmetric hollow fibre membranes and case studies of air separation, *Can J Chem Eng*, 90 (2012) 1253-1268.
- [21] R.W. Spillman, Economics of Gas Separation Membranes, *Chem Eng Prog*, 85 (1989) 41-62.
- [22] W.C. Pfefferle, An early version of the continuous membrane column was described by Diffusion purification of gases, (111964) U.S. Pat. 3,144,313.

- [23] M. Ohno, T. Morisue, O. Ozaki, T. Miyauchi, Gas Separation Performance of Tapered Cascade with Membrane, *J Nucl Sci Technol*, 15 (1978) 411-420.
- [24] M. Ohno, T. Morisue, O. Ozaki, T. Miyauchi, Comparison of gas membrane separation cascades using conventional separation cell and two-unit separation cells, *J Nucl Sci Technol*, 15 (1978) 376-386.
- [25] E. Gruzdev, N. Laguntsov, B. Nikolaev, A. Todosiev, G. Sulaberidze, A method of calculating membrane-element cascades for separating multicomponent mixtures, *Atomic Energy*, 57 (1984) 553-557.
- [26] S.A. Stern, J.E. Perrin, E.J. Naimon, Recycle and Multimembrane Permeators for Gas Separations, *J Membrane Sci*, 20 (1984) 25-43.
- [27] M.S. Avgidou, S.P. Kaldis, G.P. Sakellaropoulos, Membrane cascade schemes for the separation of LPG olefins and paraffins, *Journal of Membrane Science*, 233 (2004) 21-37.
- [28] T. Pettersen, K.M. Lien, Design Studies of Membrane Permeator Processes for Gas Separation, *Gas Sep Purif*, 9 (1995) 151-169.
- [29] Y.K. Kao, M.M. Qiu, S.T. Hwang, Critical evaluations of two membrane gas-permeator designs: continuous membrane column and two strippers in series, *Ind Eng Chem Res*, 28 (1989) 1514-1520.
- [30] M.M. Qiu, S.T. Hwang, Y.K. Kao, Economic-Evaluation of Gas Membrane Separator Designs, *Ind Eng Chem Res*, 28 (1989) 1670-1677.
- [31] B.D. Bhide, S.A. Stern, Membrane Processes for the Removal of Acid Gases from Natural-Gas .2. Effects of Operating-Conditions, Economic-Parameters, and Membrane-Properties, *J Membrane Sci*, 81 (1993) 239-252.
- [32] A.K. Datta, P.K. Sen, Optimization of membrane unit for removing carbon dioxide from natural gas, *J Membrane Sci*, 283 (2006) 291-300.

- [33] T. Pettersen, K.M. Lien, Design of Hybrid Distillation and Vapor Permeation Processes, *J Membrane Sci*, 102 (1995) 21-30.
- [34] T.G. Pressly, K.M. Ng, A break-even analysis of distillation – membrane hybrids, *AIChE journal*, 44 (1998) 93-105.
- [35] J. Bausa, W. Marquardt, Shortcut design methods for hybrid membrane/distillation processes for the separation of nonideal multicomponent mixtures, *Ind Eng Chem Res*, 39 (2000) 1658-1672.
- [36] Z. Szitkai, Z. Lelkes, E. Rev, Z. Fonyo, Optimization of hybrid ethanol dehydration systems, *Chem Eng Process*, 41 (2002) 631-646.
- [37] S. Steinigeweg, J. Gmehling, Transesterification processes by combination of reactive distillation and pervaporation, *Chem Eng Process*, 43 (2004) 447-456.
- [38] W. Marquardt, S. Kossack, K. Kraemer, A framework for the systematic design of hybrid separation processes, *Chinese J Chem Eng*, 16 (2008) 333-342.
- [39] J.A. Caballero, I.E. Grossmann, M. Keyvani, E.S. Lenz, Design of Hybrid Distillation– Vapor Membrane Separation Systems, *Ind Eng Chem Res*, 48 (2009) 9151-9162.
- [40] A.M. Eliceche, M.C. Daviou, P.M. Hoch, I.O. Uribe, Optimisation of azeotropic distillation columns combined with pervaporation membranes, *Comput Chem Eng*, 26 (2002) 563-573.
- [41] I.K. Kookos, Optimal design of membrane/distillation column hybrid processes, *Ind Eng Chem Res*, 42 (2003) 1731-1738.
- [42] A. Verhoef, J. Degreve, B. Huybrechs, H. van Veen, P. Pex, B. Van der Bruggen, Simulation of a hybrid pervaporation-distillation process, *Comput Chem Eng*, 32 (2008) 1135-1146.
- [43] R.A. Davis, Simple gas permeation and pervaporation membrane unit operation models for process simulators, *Chem Eng Technol*, 25 (2002) 717-722.

- [44] M.H.M. Chowdhury, X.S. Feng, P. Douglas, E. Croiset, A new numerical approach for a detailed multicomponent gas separation membrane model and AspenPlus simulation, *Chem Eng Technol*, 28 (2005) 773-782.
- [45] A. Hussain, M.B. Hagg, A feasibility study of CO<sub>2</sub> capture from flue gas by a facilitated transport membrane, *J Membrane Sci*, 359 (2010) 140-148.
- [46] A. Faizan, K.L. Kok, S.A. Mohd, M. Ghulam, CO<sub>2</sub> Capture from Natural Gas using Membrane Separation System: Process Simulation, Parametric Analysis and Joule Thompson Effect, *Res J Chem Environ*, 15 (2011) 238-244.

### 3. Membrane Mathematical Modeling and Parametric Investigation

#### 3.1 Introduction

Membrane modeling started in 1950 when Weller and Steiner [1] proposed the first mathematical representation of membrane separation. Since then, a number of models and calculation techniques have been suggested for the different flow patterns and module configurations. Most of these models have focused on binary gas mixtures [2-7] and only a few considered the separation of multicomponent mixtures [8-10]. Mathematical models are a platform for simulating membrane processes, and selecting the most accurate and appropriate model for a gas separation process thus determines the accuracy of the results.

Many mathematical models have been reported to describe the gas permeation of binary gas mixtures. However, most industrial separation applications involve multicomponent separation. Hence, deriving a mathematical model based on a multicomponent mixture is highly important. PAN [11] proposed that the gas permeation in an asymmetric high flux membrane can be estimated by cross-flow pattern calculations, regardless of the actual flow direction. This implies that the local driving force is influenced by the local permeate composition instead of the bulk composition. Based on this assumption, mathematical models for hollow fiber and spiral wound configurations were derived for binary [12] and multi-component mixture [11]. The multicomponent model showed good agreement with experimental data, especially at low stage cut. The

binary mixture model was later corrected to consider the pressure change on the lumen side [13].

Shindo et al. [9] developed a method to approximate multicomponent gas separations in five flow patterns: one-side mixing, complete mixing, cross flow, counter-current flow, and co-current flow. The model is applicable to both spiral wound and hollow fiber configurations since it was generated by assuming negligible pressure drop on both sides of the permeator. The model predictions showed good agreement with experimental data. This model also has no limitations on the type of barrier, but the mechanism of transport through the barrier should predominantly be solution diffusion. Also, the model is applicable to both high and low permeation flux.

Tessendorf et al. [14] generated mathematical models for co-current and counter-current flow patterns in a single-stage membrane system. The models are applicable for binary and multicomponent mixtures. They also accounted for the pressure drop effect. The models' ordinary differential equations (ODEs) were integrated using the Runge-Kutta method over the membrane length. Coker et al. [15] developed a multicomponent gas separation model for co-current, counter-current, and cross-flow configurations in a hollow fiber module with permeate sweep. The model was used to explore the effect of permeate purging on the separation performance for an air separation unit. Later, they modified the model to incorporate heat effects [16].

Hinchliffe and Porter [17] proposed a simplified cross-current model for binary mixtures. The model was used for economic evaluation of one- and two-unit configurations for carbon monoxide production in an acetic acid production process.

Marriott and Sorensen [18] presented an approach for modeling membrane modules. The proposed model is applicable for gas permeation, gas-liquid, and liquid-liquid processes. The mathematical model was applied to gas permeation with different module designs, and variations in pressure and temperature were considered. The models were simulated and validated by parameter estimation using gPROMS linked with Multiflash to provide fluid properties. Scholz et al. [19] presented a comprehensive modeling study in which the mathematical model considered non-ideal effects such as concentration polarization, the Joule-Thomson effect, pressure losses, and real gas behavior. However, when simulating the process of carbon dioxide removal from a methane stream, notable error was observed when ideality was assumed.

The literature on modeling and simulation to compare different flow patterns in a membrane module indicates that the cross-flow and counter-current flow patterns are the most efficient in terms of separating highly permeating gas. The model by Pan (1983) [3] has been considered most often in research on binary systems, although the model developed by Shindo et al. is highly preferred for multicomponent gas mixtures.

### **3.2 Membrane mathematic model**

As mentioned earlier, Shindo et al. model is applicable for both hollow fiber and flat sheet configurations since it is derived for the change in feed flow rate and components' mole fraction over the change in membrane area then converted to the change in dimensionless area. Also, it is more conservative in mathematical derivation as we will see later during the model derivation. Hence, the mathematical model that will be used in this work was originally derived by Shindo et al. [9] for counter-current flow scheme but

in addition the permeate pressure change in the fiber lumen side is considered. In order to formulate the model the following assumptions were taken in consideration:

- 1- Fick's Law controls gas permeation.
- 2- Permeability of pure gas component is a good approximation for the same gas permeability in the mixture.
- 3- The membrane effective thickness is uniform over the porous substrate.
- 4- The behavior of permeate and feed streams obey plug flow situation.
- 5- No concentration gradient in the direction of permeation.
- 6- Concentration polarization effect is negligible.

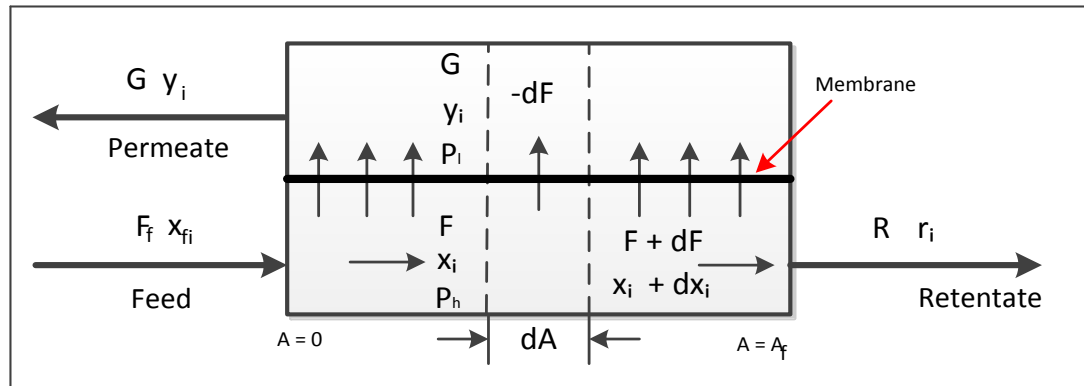


**Fig. 3.1** Illustration of single-stage permeator with counter-current flow.

The mathematic model is to be derived based on the notations used in Fig. 3.1. Therefore, the overall mass balance over a segment of the membrane which has a differential area of  $dA$  yields:

$$-dF = dG \quad (3.1)$$

From Fick's Law, the permeation rate can be described as follows:

$$dG = dA \sum_{k=1}^n \frac{\beta_k}{l} (P_h x_k - P_l y_k) \quad (3.2)$$

Material balance for component i yield:

$$-d(x_i F) = d(y_i G) \quad (3.3)$$

Solving the right hand side of equation (3.3) using the product rule of differentiation as shown in equation (3.4) is what makes this model more mathematically accurate than other models. The multicomponent model proposed by Pan in 1986 simplified the model derivation by considering that the right hand side of equation (3.3) can be approximated by  $y_i dG$ . Such assumption introduces an error to the model. The error magnitude becomes significant as the stage cut increases since the feed side molar fraction change becomes non-ignorable.

$$d(x_i F) = x_i dF + F dx_i \quad (3.4)$$

$$-d(x_i F) = dA \frac{\beta_k}{l} (P_h x_k - P_l y_k) \quad (3.5)$$

$$\sum_{k=1}^n x_i = 1 \quad (3.6)$$

$$\sum_{k=1}^n y_i = 1 \quad (3.7)$$

Substituting equation (3.5) and (3.2) into equation (3.4) and solving for  $dx_i$  gives:

$$dx_i = -\frac{dA}{F} \left[ \frac{\beta_i}{l} (P_h x_i - P_l y_i) - x_i \sum_{k=1}^n \frac{\beta_k}{l} (P_h x_k - P_l y_k) \right] \quad (3.8)$$

By integrating equations (3.1) and (3.3) from  $A=0$  to  $A=A_f$ :

$$G = F_f - F \quad (3.9)$$

$$y_i = \frac{x_{fi} F_f - x_i R}{(F_f - R)} \quad \text{if } G \neq 0 \quad (3.10)$$

if  $G=0$ , the permeate mole fraction of component  $i$  can be derived by L'Hospital rule as  $F \rightarrow F_f$

$$y_i = \frac{\frac{\beta_i}{l} (P_h x_i - P_l y_i)}{\sum_{k=1}^n \frac{\beta_k}{l} (P_h x_k - P_l y_k)} \quad \text{if } G = 0 \quad (3.11)$$

From this step ahead  $i$  denotes component  $i$  which will be considered as reference component in order to generate a simplified model. Now, the ratio of permeate mole fraction for components  $i$  and  $j$  is explained in equation (3.12):

$$\frac{y_i}{y_j} = \frac{\beta_i (P_h x_i - P_l y_i)}{\beta_j (P_h x_j - P_l y_j)} \quad (3.12)$$

Solving for  $y_j$  leads to:

$$y_j = \frac{x_j \frac{\beta_j}{\beta_i}}{\frac{P_l}{P_h} \left[ \left( \frac{\beta_j}{\beta_i} \right) - 1 \right] + \left( \frac{x_i}{y_i} \right)} \quad (3.13)$$

Substituting equation (3.13) into equation (3.7) gives:

$$\sum_{k=1}^n \frac{x_j \frac{\beta_j}{\beta_i}}{\frac{P_l}{P_h} \left[ \left( \frac{\beta_j}{\beta_i} \right) - 1 \right] + \left( \frac{x_i}{y_i} \right)} = 1 \quad (3.14)$$

In order to normalize the model, the following dimensionless variables are defined:

$$\omega = A \frac{\beta_m P_h}{F_f l} \quad \omega_t = A_t \frac{\beta_m P_h}{F_f l} \quad (3.15)$$

$$\tau = \frac{(F_f - R)}{F_f} \quad (3.16)$$

$$g = \frac{G}{F_f} \quad (3.17)$$

$$S_i = \frac{\beta_m}{\beta_i} \quad (3.18)$$

Thus from equations (3.2), (3.6) through (3.10), (3.13) and (3.14) the counter-current model can be obtained as in the following equations:

$$\frac{df}{d\omega} = - \sum_{k=1}^n \frac{1}{S_k} \left( x_k - \frac{y_k}{\gamma} \right) \quad (3.19)$$

$$\frac{dx_i}{d\omega} = -\frac{1}{fS_i} \left( x_i - \frac{y_i}{\gamma} \right) + \frac{x_i}{f} \sum_{k=1}^n \frac{1}{S_k} \left( x_k - \frac{y_k}{\gamma} \right), \quad i = 1, \dots, n-1 \quad (3.20)$$

$$x_n = 1 - \sum_{i=1}^{n-1} x_i \quad (3.21)$$

$$g = f - (1 - \tau) \quad (3.22)$$

The following initial conditions are used to solve equations 3.19 through 3.22.

If  $g \neq 0$ ,

$$y_i = \frac{x_i f - r_i(1 - \tau)}{f - (1 - \tau)}, \quad i = 1, \dots, n-1 \quad (3.23)$$

$$y_n = 1 - \sum_{j=1}^{n-1} y_j \quad (3.24)$$

If  $g = 0$ ,

$$\sum_{k=1}^n \frac{x_i (S_i/S_k)}{\gamma^{-1}(S_i/S_k - 1) + (x_i/y_i)} = 1 \quad (3.25)$$

$$y_j = \frac{x_i S_i/S_j}{\gamma^{-1}(S_i/S_j - 1) + (x_i/y_i)}, \quad (j \neq i, n) \quad (3.26)$$

Considering a hollow fiber membrane module in which the feed is introduced at the shell side while the permeate is collected at the bore side and assuming low velocity of permeate. Then, at low permeate velocity the friction factor ( $\xi$ ) is only a function of Reynolds number (Re) and can be expressed as:

$$\xi = \frac{64}{Re} \quad (3.27)$$

Therefore, the pressure change in fiber lumen under counter-current flow scheme can be calculated by:

$$\frac{d(\gamma^{-1})}{d\omega} = -Kg\gamma \quad (3.28)$$

Where,

$$K = \frac{128 \mu R^G T R^2 L^2}{A_t^3 d^3 P_h^3} \frac{l}{\beta_m} \quad (3.29)$$

### 3.3 Model solution

The input data for the model include the feed composition and flow rate, process conditions such as pressure and temperature and membrane characteristics such as the membrane thickness, hollow fibers inner and outer diameters and components' permeability. Equations (3.20) to (3.27) with equation (3.29) can be solved using FORTRAN subroutine. The code solves the first order differential equations through

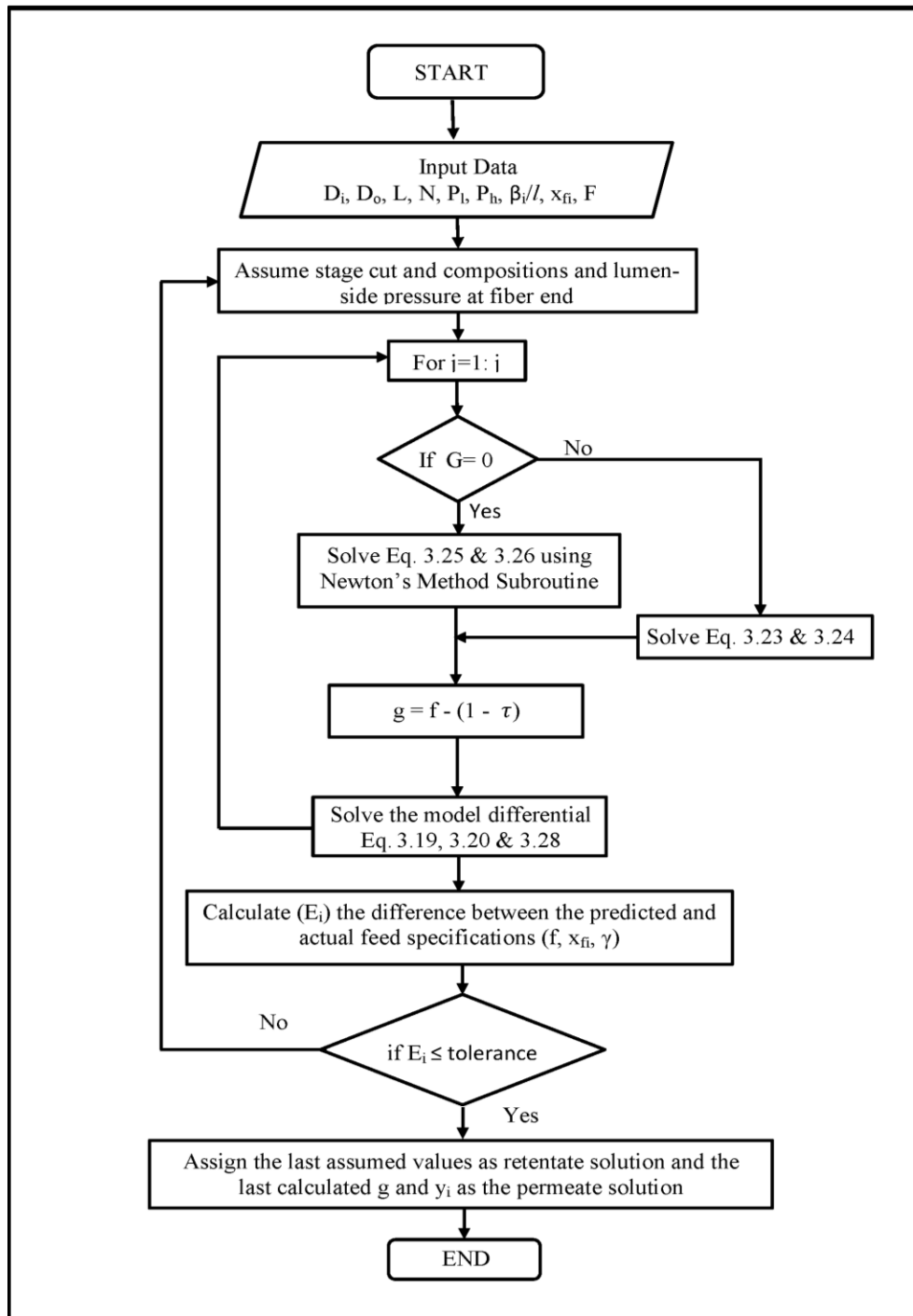
backward-difference scheme using Gear's method with adaptive step size while equation (3.24) is solved using Newton-Raphson method.

For the counter-current flow pattern, the model is solved using the shooting method utilizing the solution algorithm described in Fig 3.2. The model is solved in a backward manner starting from the module end ( $\omega = \omega_f$ ) toward the module inlet ( $\omega = 0$ ). Therefore, the components' composition, retentate flow rate and permeate pressure should be guessed. The error between the solution and feed condition is then used to generate a new but more accurate guess for each parameter.

In this study, complex and iterative optimizations will be intensively used to obtain the optimal design of membrane systems and membrane/distillation hybrids for the different separation processes, which will be discussed. Moreover, the different process designs will be investigated over wide ranges of the impacting parameters such as the feed and products compositions, the applied pressure ratio, selectivity and permeability. Therefore, the solution time is very critical. The solution time can be minimized without impacting the solution accuracy by supplying closer guess for the differential equations variables. Since the model solution in the case of co-current flow pattern and constant pressure on lumen side is non-iterative, the initial guess for the counter-current case can be generated by solving for co-current flow pattern design. The co-current model is identical to the counter-current except equations (3.22) and (3.23) should be replaced by equations (3.30) and (3.31), respectively.

$$g = 1 - f \quad (3.30)$$

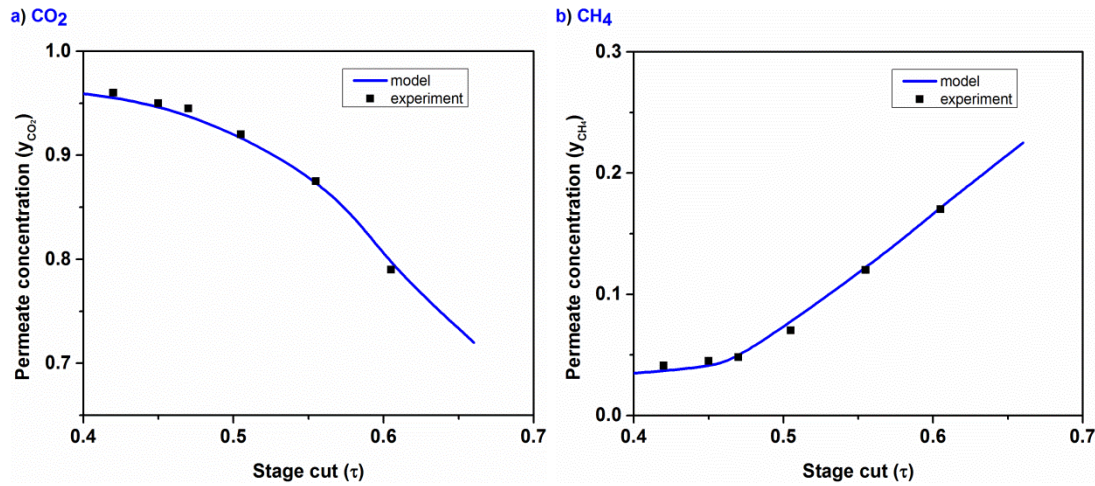
$$y_i = \frac{x_{fi} - fx_i}{1 - f} \quad (3.31)$$



**Fig. 3. 2** Algorithm to solve counter-current membrane model.

### 3.4 Model validation

To investigate the accuracy of the mathematical model and the proposed solution algorithm, simulation predictions were validated against experimental data reported by Pan in 1986 [10]. The feed mixture consists of carbon dioxide, methane, ethane, and propane with concentrations of 48.5, 27.4, 16.26, and 7.34%, respectively. The permeances of the pure components are 134, 3.72, 1.02, and 0.2 ( $10^{-10}$  mole/s.m<sup>2</sup>.Pa) for CO<sub>2</sub>, CH<sub>4</sub>, C<sub>2</sub>H<sub>6</sub>, and C<sub>3</sub>H<sub>8</sub>, respectively. The feed enters the shell side at a pressure of 3,528 kPa, while the permeate stream is collected from the fiber side at a pressure of 92.8 kPa. These experimental conditions were used to investigate the membrane performance at high feed composition, pressure ratio, and target component selectivity. The experiment was carried out for both co-current and counter-current flow patterns. The model results are plotted against the experimental results in Fig. 3.3 for the counter-current flow pattern. The model shows good agreement with experimental data over the tested range of stage cut.



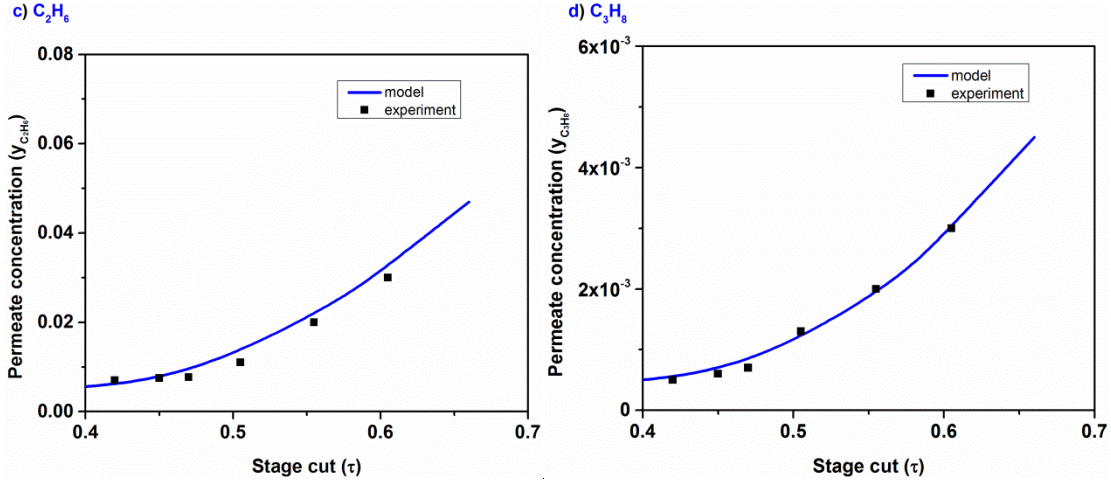


**Fig. 3.3** Model validation against experimental data for a multicomponent gas mixture.

The simulation results are represented by the solid line and are in good agreement with the experimental results, which are illustrated by scattered points.

The model was also validated against the membrane air separation experiment reported by Feng et al. in 1999 [6]. The conditions of this experiment are different from those of the previous experiment. This experiment investigated the membrane performance at low feed concentration and oxygen-to-nitrogen selectivity. The feed conditions, operating conditions, and membrane module specifications are listed in Table 3.1. The reported experimental data includes the oxygen concentration in the permeate stream and the nitrogen concentration in the retentate stream at different product stage cut. The simulation results are represented against the reported experimental data in Fig. 3.4. These simulation results are also in good agreement with the experimental results over the experimental range of stage cut.

**Table 3.1** Membrane module specifications and operating conditions for the air separation experiment.

Specification	Value
Material	Asymmetric cellulose acetate
Number of fibers	368
Inner diameter ( $\mu\text{m}$ )	80
Outer diameter ( $\mu\text{m}$ )	160
Active length (m)	0.25
Feed composition (mol %)	79.5 N <sub>2</sub>
	20.5 O <sub>2</sub>
Temperature (°K)	296.15
Feed pressure (kPa)	790.8
Permeate Pressure (kPa)	101.3
Permeance ( $10^{-10}$ mol/s m <sup>2</sup> Pa)	O <sub>2</sub> : 30.78
	N <sub>2</sub> : 5.7

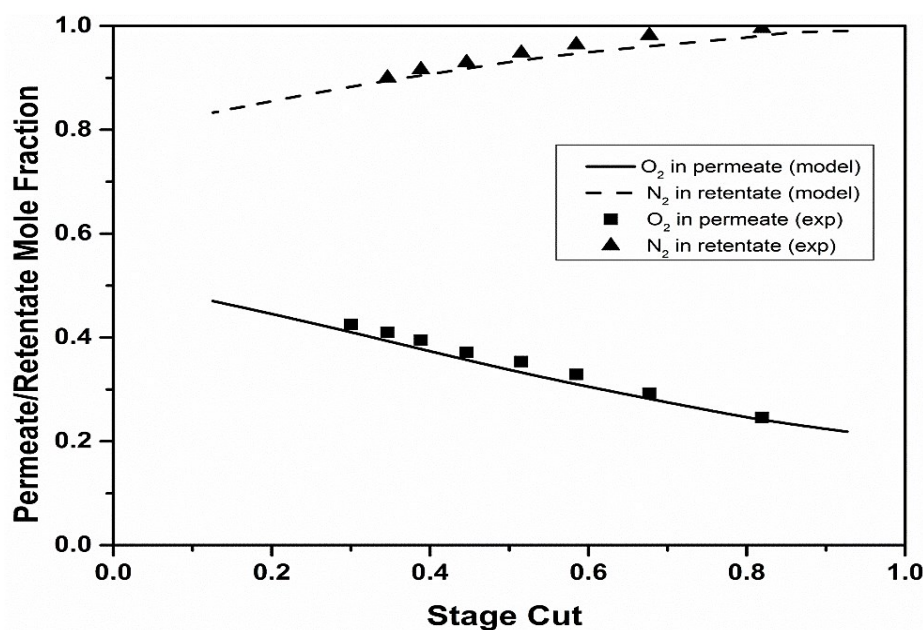


**Fig. 3.4** Model validation against experimental data for air separation.

### **3.5 Creating membrane unit operation in Aspen Plus®**

The need for creating a membrane unit operation in a process simulator such as Aspen Plus® or Aspen HYSYS is very important when the performance of the membrane unit in a hybrid system must be evaluated. Process simulation and optimization with commercial software offers accuracy and time savings through the following:

- 1- Most unit operations such as compressors, pumps, heat exchangers, and distillation columns have built-in models in Aspen Plus software
- 2- Optimization toolboxes are available, and it is easy to build the optimization case
- 3- Material and energy balances can be calculated, and physical and thermodynamic properties can be estimated accurately
- 4- Process constraints for unit operations are specified in software

In Aspen Plus, three custom user models (USER, USER2 and USER3) are available in the software unit operations library. The user model design step includes:

- 1- Designing the unit operation icon to better represent the equipment
- 2- Determining the number of feed and product streams
- 3- Defining the configuration variables such as the membrane selectivity, permeance, number of hollow fibers, fiber length, and permeate pressure

The custom user models can be linked with Microsoft Excel, Fortran, or both to create a custom model in the model library of Aspen Plus. The USER model can only be

linked to a user-supplied Fortran subroutine and cannot process more than four inlet and outlet streams. The USER2 model can be linked to a user-supplied Fortran subroutine or an Excel spreadsheet and can handle any number of inlet and outlet streams. The USER3 model is an equation-oriented unit operation model defined by a user-supplied Fortran subroutine or a pre-compiled model from the PML library.

Aspen Plus software is supported by some utilities that are customized for convenient read and write access to the user-defined variables defined in the Fortran user model routine. This simplifies mapping of the user-defined parameters into the external user routine. The defined parameters in the user-defined routine can be in scalar or vector form. The parameter quantities can be integer, real, or character values. The dimension of vector data can be assigned based on one of nine standard lengths, such as the number of components or the number of conventional inlet streams. The vector can also be a user-defined integer variable.

The data configured as input to the Fortran subroutine are basically the feed conditions and the membrane module design parameters. The feed condition parameters are:

- The number of components in the feed stream
- Feed molar flow rate of each component
- Feed temperature
- Feed pressure

These parameters are defined by the user in Aspen Plus through the user interface illustrated in Fig. 3.5. The mixture component formulas and the thermodynamics package

should also be specified by the user to allow the system to estimate the physical properties of the product streams (permeate and retentate).

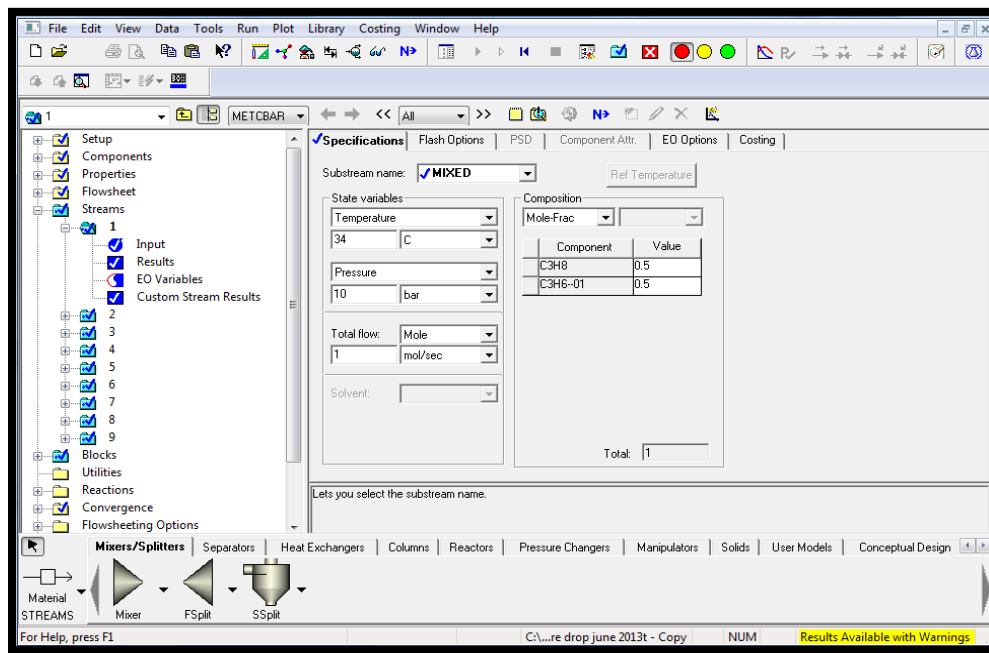


**Fig. 3.5** Aspen Plus interface to define the feed stream components and conditions.

The membrane design parameters read by the subroutine are:

- Membrane permeance or permeability and thickness of the selective layer
- Membrane ideal selectivity
- Inner and outer diameter of the fiber
- Number of hollow fibers
- Length of hollow fibers

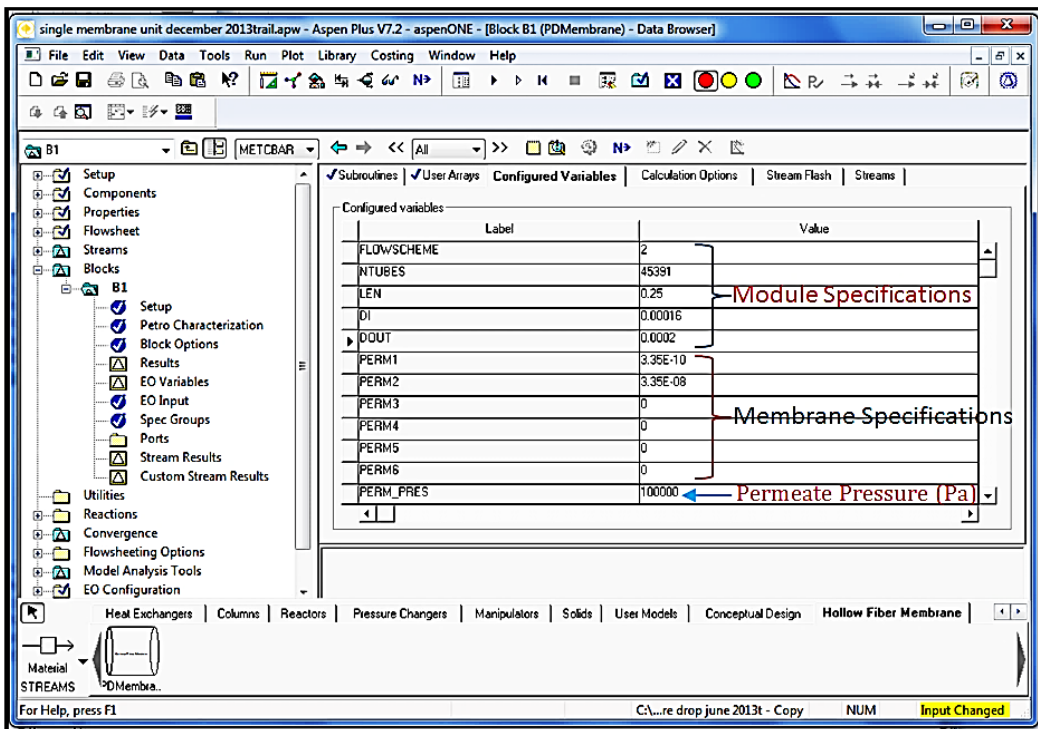


**Fig. 3.6** Screen shot from Aspen Plus to illustrate the configured specifications for membrane design.

These design parameters are defined in Aspen Plus® and exported to a Fortran subroutine, which is compiled using Intel Fortran Compiler software. Then, the source file that contains the solution subroutine is compiled, and both files are linked through the Aspen Plus Simulation Engine to generate a Dynamic Link Library (DLL). The generated DLL should be saved in the same directory of the simulation flowsheet. After this step is completed, the flowsheet can be run. To ensure proper integration of the user model subroutine with the Aspen Plus flowsheet, the integrated membrane unit was used in the same conditions of Pan's experiment [10], and the results were identical to those obtained earlier and shown in Fig. 3.3.

```

UVARS.f - Microsoft Visual Studio
File Edit View Debug Team Data Tools Test Window Help
UVARS.f (Global Scope) UVARS(NVARS, ICOL, IROW)
INTEGER FUNCTION UVARS(NVARS,ICOL,IROW)
PARAMETER (IPARAM_NVARS=12)
INTEGER IVARIABLES(8,IPARAM_NVARS), IVRSN
DATA IVARIABLES/
1 4HFLOW, 4HSCHE, 4HME , 4H      , 0, -1, 0, 1,
1 4HTUB, 4HES , 4H      , 4H      , 1, -1, 0, 1,
1 4HLEN , 4H      , 4H      , 4H      , 1, -1, 0, 1,
1 4HDI , 4H      , 4H      , 4H      , 1, -1, 0, 1,
1 4HDOUT, 4H      , 4H      , 4H      , 1, -1, 0, 1,
1 4HPERM, 4H1 , 4H      , 4H      , 1, -1, 0, 1,
1 4HPERM, 4H2 , 4H      , 4H      , 1, -1, 0, 1,
1 4HPERM, 4H3 , 4H      , 4H      , 1, -1, 0, 1,
1 4HPERM, 4H4 , 4H      , 4H      , 1, -1, 0, 1,
1 4HPERM, 4H5 , 4H      , 4H      , 1, -1, 0, 1,
1 4HPERM, 4H6 , 4H      , 4H      , 1, -1, 0, 1,
1 4HPERM, 4H_PRE, 4HS , 4H      , 1, -1, 0, 1/
DATA IVRSN/1372088810/
NVARS = IPARAM_NVARS
IF(IROW .EQ. 0) THEN
  UVARS=IVRSN
ELSE IF(IROW .LE. NVARS) THEN
  UVARS=IVARIABLES(ICOL,IROW)
ENDIF
RETURN
END

```

**Fig. 3.7** Exporting the membrane design parameters to a Fortran file to generate a Dynamic Link Library (DLL).

### 3.6 Parametric investigation

The parametric investigation in this section focuses on the impact of membrane permeability, selectivity, and applied pressure ratio across the membrane. The case study application is a split process of propylene/propane to obtain product purity that meets the requirements for polymer grade ( $y_A > 99.5\%$ ) or chemical grade ( $y_A > 96\%$ ). Product recovery ( $\eta$ ) is discussed as a product but not as a controlling parameter.

### 3.6.1 Selectivity impact

As shown by the mathematical model (Eq. 3.19), the permeation flux of the mixture components depends on their permeability, their feed-side and permeate-side concentrations, and the applied pressure difference across the membrane. The permeate side concentration is a resultant, while all other parameters are controllable parameters. The relationship between the selectivity and the product concentration is proportional, meaning that higher selectivity correlates with lower driving force at a fixed pressure ratio and membrane area. This results in lower product recovery, which has a tradeoff relationship with purity. The tradeoff behavior is illustrated in Fig. 3.8 for an equimolar binary feed mixture entering the feed side of a membrane module, which has a permeance of 100 GPU ( $3.35 \times 10^{-8}$  mol/m<sup>2</sup> s Pa) and an available permeation area of 100 m<sup>2</sup>. The feed stream has a pressure of 20 bar, while the permeate stream leaves the membrane at a pressure of 1.0 bar. Fig. 3.8 also demonstrates the negative impact of high selectivity on product recovery.

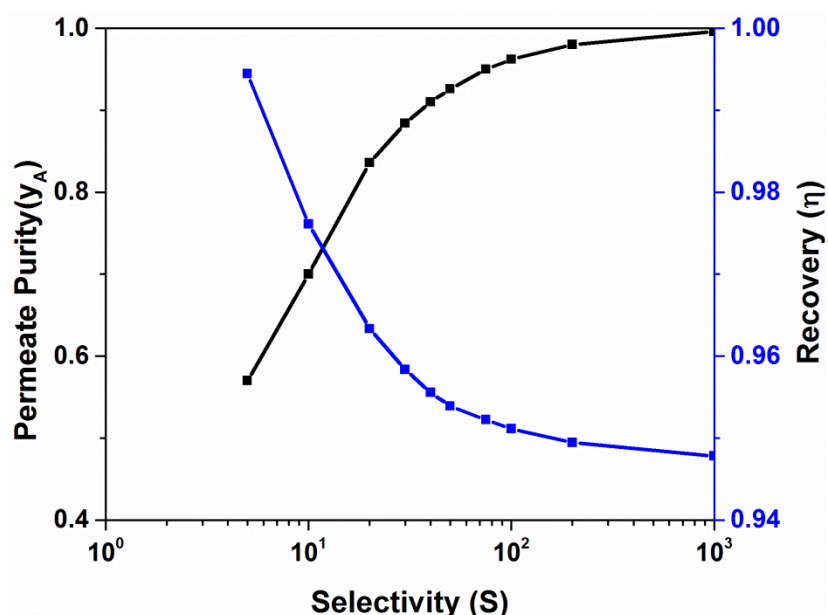


**Fig. 3.8** Impact of membrane selectivity on product purity and recovery ratio for a binary gas mixture with equimolar concentration at fixed membrane area, permeate and feed pressures.

To investigate the impact of selectivity on the dimensionless membrane area required to accomplish a certain recovery ratio, a simulation was run at fixed permeance ( $3.35 \times 10^{-8} \text{ mol/m}^2 \text{ s Pa}$ ), pressure ratio (10), and feed flow rate (1 mol/s). An optimization problem was formulated to minimize the required dimensionless membrane area subjected to a product recovery of 95%. The solution was obtained at various membrane selectivities ranging between 10 and 300. The generated results are illustrated in Fig. 3.9.

A larger dimensionless membrane area is the absolute resultant from increasing the membrane selectivity to achieve a certain recovery ratio. The dimensionless membrane area showed a steady but slow increase for a recovery ratio of 90%. As the recovery ratio was increased to 95%, the dimensionless membrane area showed a strong and proportional dependence on selectivity. The dependence further increased when the recovery ratio was increased to 99%, where the required dimensionless membrane area at a selectivity of 200 was about 15 times more than what is needed when the selectivity is only 10, as shown in Fig. 3.9. Therefore, it is recommended that a membrane be used with the lowest selectivity that can meet the purity and recovery requirements while the pressure ratio is within practical and economical limits.

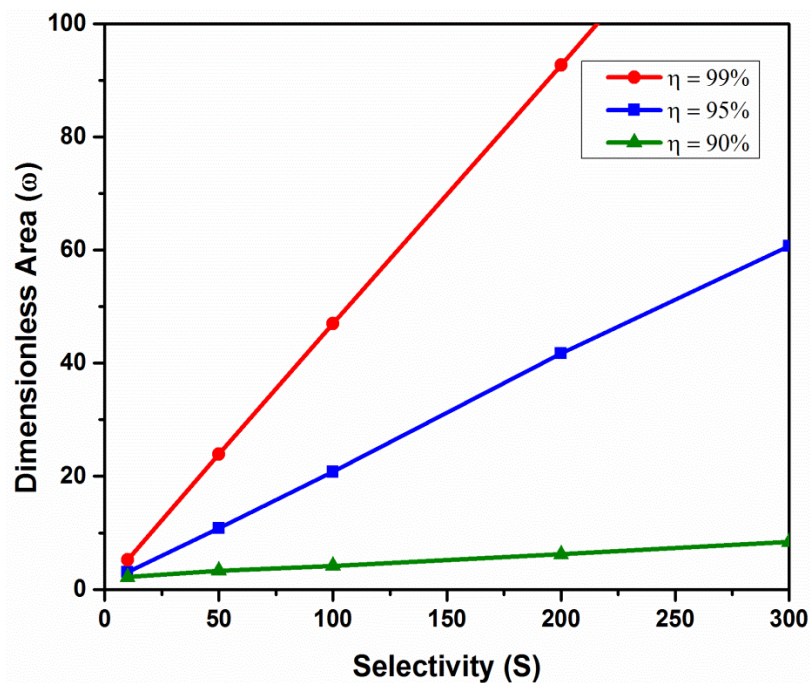


**Fig. 3.9** Influence of membrane selectivity on dimensionless membrane area to produce recovery ratios of 90, 95 and 99%.

### 3.6.2 Pressure ratio impact

To demonstrate the role of the applied pressures on both sides of the membrane, the permeate pressure was kept constant while the feed-side pressure was varied. This allows for investigation of the impact of the pressure ratio on the product purity and recovery ratio. Fig. 3.10 shows the simulation results for the example considered earlier with a fixed membrane area, permeate side pressure of 1 bar, permeance of 100 GPU, and selectivity of 100. Increasing the pressure ratio always increased the membrane area and thus enhanced the product recovery, but the target component concentration in the permeate stream was reduced.

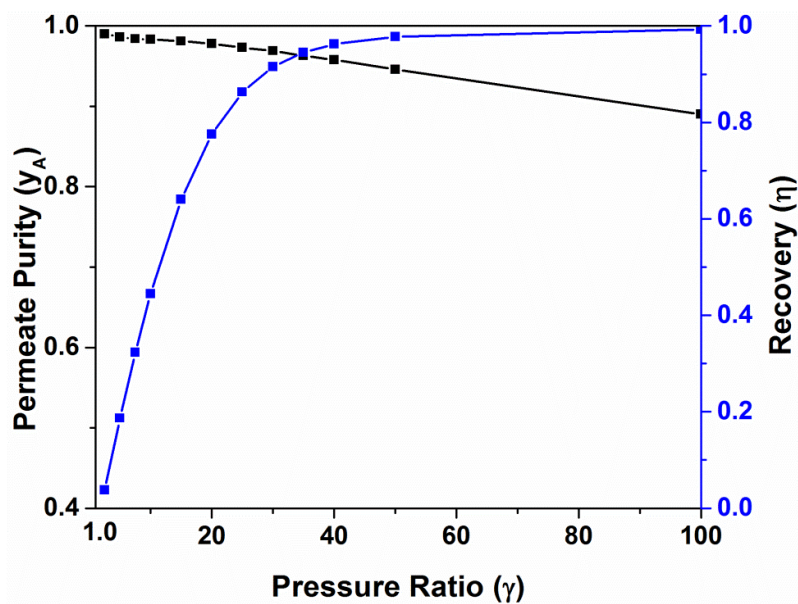


**Fig. 3.10** Impact of pressure ratio on product purity and recovery ratio (membrane area  $100 \text{ m}^2$ , permeate side pressure of 1 bar, permeance of 100 GPU and selectivity of 100).

In practice, the transmembrane pressure ratio is usually created by feed compression or permeate vacuum pumping. Feed compression helps to enhance the pressure ratio and to increase the dimensionless membrane area, resulting in a lower membrane area. However, using a vacuum pump on the permeate stream is efficient for applications with low target component concentration, such as oxygen enrichment from air and carbon capture from the flue gas of coal-fired power plants.

For the production of a permeate stream with a purity of 96% and a recovery ratio of 95%, an optimization problem can be formulated to minimize the membrane area subjected to the separation task requirements. The minimum required membrane area is plotted against the applied pressure ratio in Fig. 3.11. The minimum pressure ratio is 33, and there is no way to accomplish the required separation unless this boundary is met.

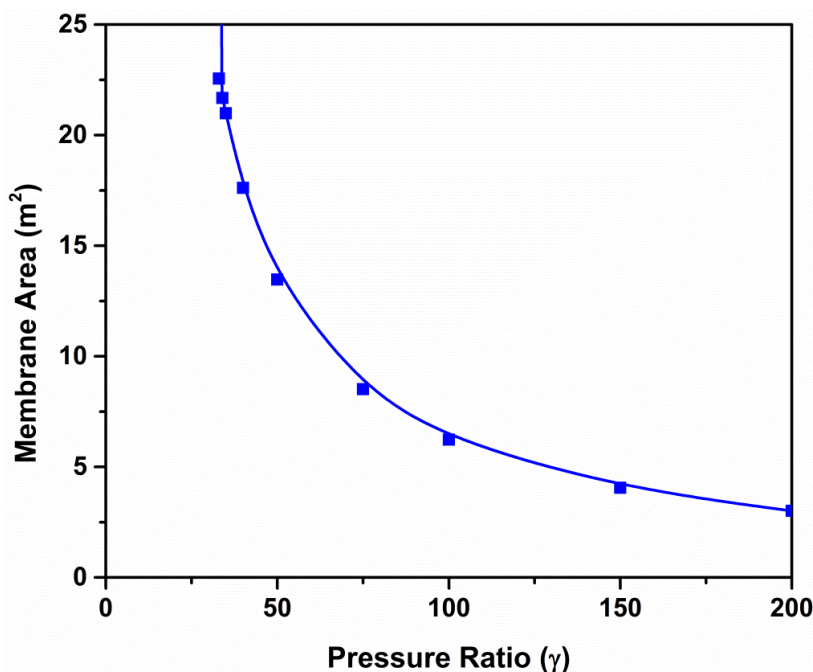


**Fig. 3.11** Effect of pressure ratio on the minimum membrane area to produce a permeate stream with purity of 96% and recovery ratio of 95% using a membrane with selectivity of 100. The feed to the membrane is a binary gas mixture with equimolar concentration.

Increasing the targeted recovery to 99% while maintain all other conditions as in the previous case, the single-stage setup requires selectivity higher than 200, whereas only 80 is needed for a recovery of 95%. These minimum selectivities appear when the applied pressure ratio is extremely high. This is due to the low driving force that occurs at the module end where the pressure ratio is insufficient and the product purity is severely impacted. When the separation task becomes more challenging with very high purity and recovery requirements, as in actual practice for the olefin/paraffin split processes, the minimum selectivity to perform the separation by a single stage is at least 10 times higher than the maximum value reported.

Fig. 3.12 shows the obtained product purity as a function of membrane selectivity and pressure ratio to recover 99% of the target component in the permeate stream from a binary gas mixture with equimolar concentration. The figure clearly shows that increasing the membrane selectivity is ineffective unless combined with sufficiently high pressure ratio. Only at a membrane selectivity of 1000 and a pressure ratio of 100 can a product purity of 99% be produced at this high recovery ratio.

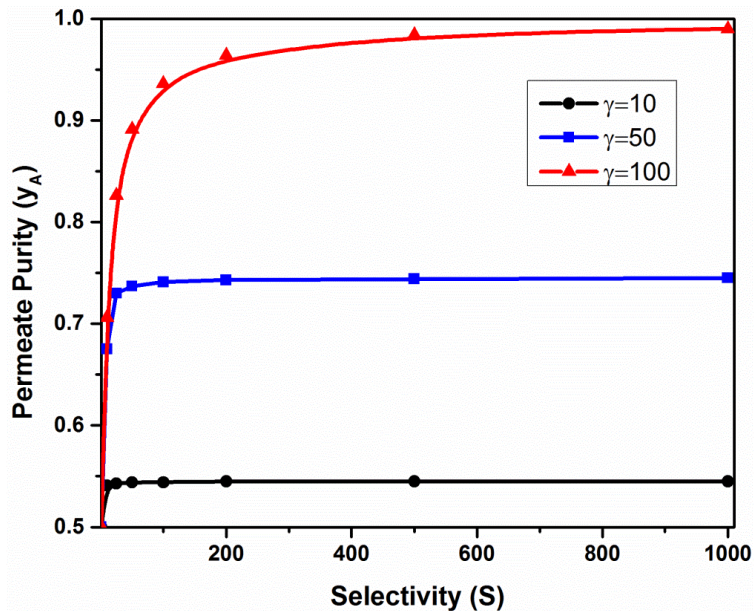


**Fig. 3.12** Importance of pressure ratio to enhance product purity while maintaining the recovery

### 3.6.3 Feed concentration impact

As seen in the selectivity impact investigation, the required membrane selectivity to produce high purity with high recovery ratio is much higher than the maximum reported for olefin/paraffin separation (less than 100). The feed concentration of the desired component is directly involved in defining the magnitude of the separation driving force.

Hence, it is expected that the membrane process can achieve the same separation task at lower selectivity as the feed concentration increases. To investigate this impact, the separation task was fixed in terms of purity and recovery ratio (0.96 and 0.95, respectively) while the pressure ratio was set to three different values of 10, 20, and 30. The results are shown in Fig. 3.13.

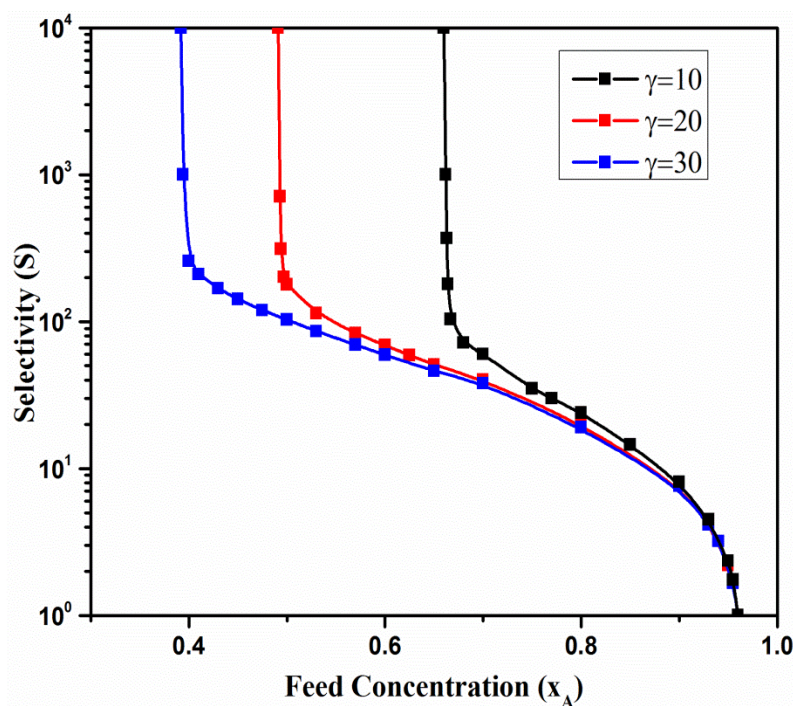


**Fig 3.13** Feed concentration impact on the required minimum selectivity to accomplish the separation task at different operating pressure ratios.

Although the recovery ratio was fixed, the required selectivity showed a sharp decrease with increasing feed-side concentration. This can be explained by calculating the available driving force at the membrane end. When the feed compositions are 50 and 80 mol%, the feed-side concentrations at the module end are 5.0 and 19.2 mol%. Hence, the module-end driving forces for a pressure ratio of 20 are  $1.48 \times 10^{-3}$  and  $1.44 \times 10^{-1}$ ,

respectively. Therefore, the driving force for a feed concentration of 80 mol% is about 100 times higher than that for a feed concentration of 50 mol%. This also explains the lower pressure ratio required to accomplish the separation task at higher feed concentrations. These results support the need for partially recycling the permeate stream to enhance the permeation driving force, as shown in previous studies.

### 3.7 References

- [1] S. Weller, W.A. Steiner, Separation of gases by fractional permeation through membranes, *Journal of Applied Physics*, 21 (2004) 279-283.
- [2] C.Y. Pan, H. Habgood, Gas separation by permeation Part I. Calculation methods and parametric analysis, *The Canadian journal of Chemical Engineering*, 56 (1978) 197-209.
- [3] C. Pan, Gas separation by permeators with high-flux asymmetric membranes, *AIChE journal*, 29 (1983) 545-552.
- [4] M. Sidhoum, A. Sengupta, K. Sirkar, Asymmetric cellulose acetate hollow fibers: studies in gas permeation, *AIChE journal*, 34 (1988) 417-425.
- [5] S. Kaldis, G. Kapantaidakis, G. Sakellaropoulos, Simulation of multicomponent gas separation in a hollow fiber membrane by orthogonal collocation—hydrogen recovery from refinery gases, *Journal of Membrane Science*, 173 (2000) 61-71.
- [6] X. Feng, J. Ivory, V.S. Rajan, Air separation by integrally asymmetric hollow-fiber membranes, *AIChE journal*, 45 (1999) 2142-2152.
- [7] P.K. Kundu, A. Chakma, X. Feng, Simulation of binary gas separation with asymmetric hollow fibre membranes and case studies of air separation, *The Canadian Journal of Chemical Engineering*, 90 (2012) 1253-1268.
- [8] R. Khalilpour, A. Abbas, Z. Lai, I. Pinna, Analysis of hollow fibre membrane systems for multicomponent gas separation, *Chemical Engineering Research and Design*, 91 (2013) 332-347.
- [9] Y. Shindo, T. Hakuta, H. Yoshitome, H. Inoue, Calculation methods for multicomponent gas separation by permeation, *Separation science and technology*, 20 (1985) 445-459.

- [10] C. Pan, Gas separation by high-flux, asymmetric hollow-fiber membrane, AIChE journal, 32 (1986) 2020-2027.
- [11] C.Y. Pan, Gas Separation by High-Flux, Asymmetric Hollow-Fiber Membrane, Aiche Journal, 32 (1986) 2020-2027.
- [12] C.Y. Pan, Gas Separation by Permeators with High-Flux Asymmetric Membranes, Aiche Journal, 29 (1983) 545-555.
- [13] P.K. Kundu, A. Chakma, X.S. Feng, Simulation of binary gas separation with asymmetric hollow fibre membranes and case studies of air separation, Can J Chem Eng, 90 (2012) 1253-1268.
- [14] S. Tessendorf, R. Gani, M.L. Michelsen, Modeling, simulation and optimization of membrane-based gas separation systems, Chem Eng Sci, 54 (1999) 943-955.
- [15] D.T. Coker, B.D. Freeman, G.K. Fleming, Modeling multicomponent gas separation using hollow-fiber membrane contactors, Aiche Journal, 44 (1998) 1289-1302.
- [16] D.T. Coker, T. Allen, B.D. Freeman, G.K. Fleming, Nonisothermal model for gas separation hollow-fiber membranes, Aiche Journal, 45 (1999) 1451-1468.
- [17] A.B. Hinchliffe, K.E. Porter, Gas separation using membranes .1. Optimization of the separation process using new cost parameters, Ind Eng Chem Res, 36 (1997) 821-829.
- [18] J. Marriott, E. Sorensen, A general approach to modelling membrane modules, Chem Eng Sci, 58 (2003) 4975-4990.
- [19] M. Scholz, T. Harlacher, T. Melin, M. Wessling, Modeling Gas Permeation by Linking Nonideal Effects, Ind Eng Chem Res, 52 (2013) 1079-1088.

## 4. Attainability of Single-Stage Membrane Process

### 4.1 Abstract

The attainability of membranes to perform a separation task is investigated by considering the simple well-mixed model and the hollow fiber model. Both analyses revealed that membrane selectivity and the applied pressure ratio are the only two controlling parameters. The behavior of those two parameters is monotonic and therefore, a minimum selectivity and a minimum pressure ratio exist. While the minimum pressure ratio is found independent of the membrane configuration, the minimum selectivity is strongly dependent. Conducting a comprehensive parametric analysis over the impacting parameters i.e. feed composition, product purity and recovery ratio, the minimum selectivity is found to be a power function of the recovery ratio. This observation was expanded to formulate simple correlations to define the attainability region in a single-stage membrane process.

### 4.2 Introduction

The membrane process is a simple unit operation to the extent that it can be described by only two parameters for a binary mixture. These parameters named selectivity ( $S$ ) and permeability ( $\beta$ ). Permeability is defined as the pressure and thickness normalized flux of the penetrant component [1]. Selectivity is the ratio between the permeabilities of different components in the mixture [2]. At ideal conditions, these parameters depend only on the intrinsic properties of the membrane material and are not a function of the operation conditions [3]. For most gas and liquid separation processes, the driving force

of transport is the transmembrane pressure drop. Regardless of the membrane process simplicity, no simple and accurate empirical or short-cut method is reported to estimate the membrane properties to accomplish a defined separation task.

The objective of this chapter is to identify the parameters that define the attainability curve of single-stage membrane processes for a given separation task. The simulation started from a simple well-mixed membrane model followed by a more complicated hollow fiber membrane model. The well-mixed model can be solved analytically, so a simple relationship can be obtained for the attainability curve. This will allow us to understand clearly the influence of different membrane parameters. The results of the hollow fiber model are much more accurate than the well-mixed model and therefore, should be more useful for real membrane process designs. However, the hollow fiber model involves non-linear differential equations which require numerical solutions and hence the results are not so straightforward. Chemical engineers often use short-cut methods or empirical relations in conceptual design of actual processes such as distillation, chemical reactor and heat exchange networks, etc. This approach is also adapted here for design of hollow fiber membrane processes. An empirical equation was explored for the attainability curves at different separation tasks. Error analysis was performed to confirm equation accuracy and validity region. Furthermore, the power of the short-cut method was demonstrated by two gas separation processes. One is for CO<sub>2</sub> capture and the other for air separation.

### 4.3 Attainability of single-stage membrane process

For a single-stage membrane process, the simplest model is to assume that both the feed stream and the permeate stream are well mixed, as shown in Fig. 4.1. The following relationship can be derived from the mass balance (as derived in Appendix-A).

$$\frac{y_A}{1-x_A} = S \frac{\gamma r_A - y_A}{\gamma(1-r_A) - (1-y_A)} \quad (4.1)$$

This formula can be also written as:

$$S = \frac{(\varphi - \eta)\gamma - (\varepsilon - \eta)}{(1-\eta)\gamma - (\varepsilon - \eta)} \quad (4.2)$$

Where,  $\varepsilon$  is the target component enrichment factor ( $\varepsilon = y_A/x_A$ ),  $\eta$  is the target component recovery ratio in the permeate stream ( $\eta = Gy_A/Fx_A$ ) and the  $\varphi$  is the separation coefficient or the separation factor at zero recovery ratio ( $\varphi = \frac{y_A(1-x_A)}{x_A(1-y_A)}$ ).

Equation (4.2) indicates that both selectivity and pressure ratio exhibit a minimum value. The minimum selectivity  $S_{min}$  can be obtained at infinite pressure ratio, and similarly the minimum pressure ratio  $\gamma_{min}$  can be obtained at infinite selectivity.

$$S \geq S_{min} = \frac{\varphi - \eta}{1 - \eta} \quad (4.3)$$

$$\gamma \geq \gamma_{min} = \frac{\varepsilon - \eta}{1 - \eta} \quad (4.4)$$

Plotting equation (4.2) for  $\gamma$  vs.  $S$  at ( $x_A = 0.5, y_A = 0.96, \eta = 0.95$ ) gives Fig. 4.1. The plotted data showed four interesting regions. The first region exists at low membrane selectivity. When membrane selectivity is less than  $S_{min}$ , the selectivity is not enough to reach the purity requirement, regardless of how permeable a membrane is or the value of

any other operation conditions. The second region is when pressure ratio is less than  $\gamma_{\min}$ , the transport driving force is not enough to reach the recovery ratio requirement, which is again regardless of the value of any other parameters. The third region is when membrane selectivity is less than the minimum selectivity and pressure ratio is smaller than the minimum pressure ratio, then neither the targeted purity nor the targeted recovery ratio can be achieved. To meet the separation task in both purity and recovery ratio, membrane must operate in the region above the curve, which is region 4.

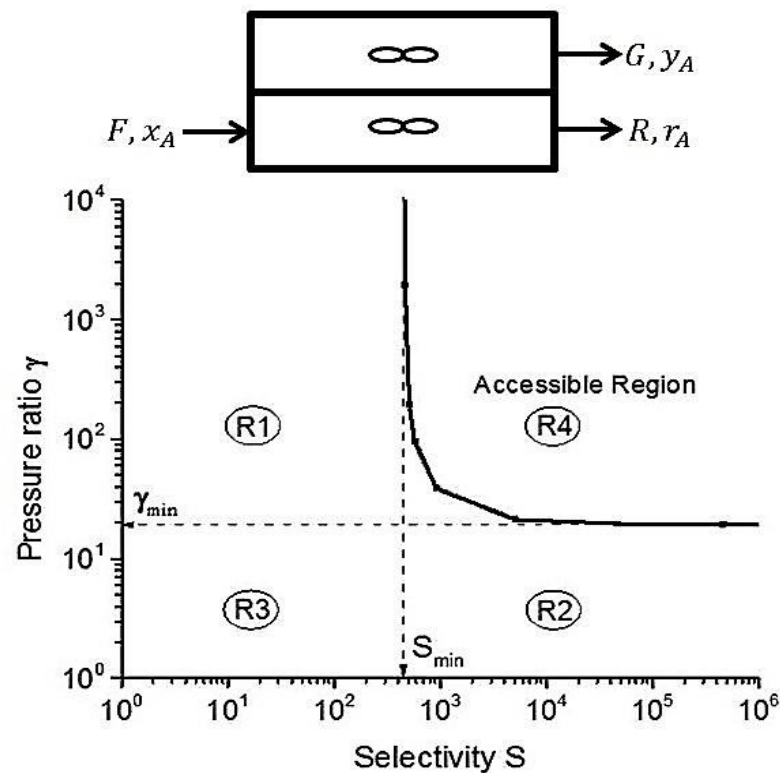


**Fig. 4.1** Attainability of a single-stage membrane in well-mixed model.

The well-mixed model simplifies the mass balance derivation, so an analytical solution for the relationship between selectivity and pressure ratio can be easily obtained, but it is not applicable for real membrane processes. Therefore, in the next discussion the

hollow fiber membrane design is considered. Hollow fiber is one of the most important membrane modules mainly due to its high packing density. A mathematical model described in chapter 3 was developed to simulate the hollow fiber membrane process in counter-current flow pattern. In our simulation, each fiber has a diameter of 200  $\mu\text{m}$  and a length of 0.5 m. The total number of fibers is determined by the total membrane area. From the numeric solution the relationship between pressure ratio and membrane selectivity was obtained and plotted in Fig. 4.2 at the same operation conditions as the previous case. The curve is similar to that shown in Fig. 4.1. Again, membrane selectivity and pressure ratio exhibit minimum thresholds to meet the requirements in purity and in recovery ratio, respectively. The minimum pressure ratio in this case is still defined by Equation (4.4); hence it has the same value as the previous case. However, the minimum selectivity is much smaller. In the previous case the minimum selectivity is about 460, but it decreased to about 70 in the hollow fiber module. This is because the hollow fiber module can provide higher average driving force compared to the well-mixed model. Nevertheless, to meet the separation task in both purity and recovery ratio, the hollow fiber membrane module should also be operated in the region above the curve in Fig. 4.2, that is, the membrane selectivity must be higher than the minimum selectivity, and the pressure ratio higher than the minimum pressure ratio.

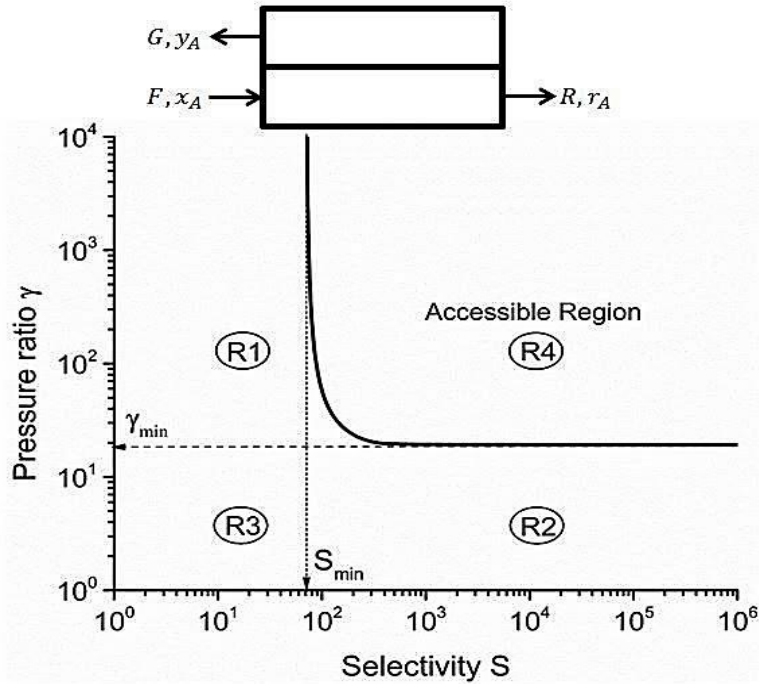


**Fig. 4.2** Minimum pressure ratio against selectivity for a single hollow fiber membrane module to produce permeate stream at purity of 96% and recovery ratio of 95%.

#### 4.4 Parametric investigation

Equation (4.2) indicates that the attainability curve is determined by the separation task parameters only, which include enrichment factor  $\varepsilon$ , recovery ratio  $\eta$  and separation coefficient  $\varphi$ . The effects of these three parameters in the hollow fiber membrane model are studied in more details below.

##### 4.4.1 Influence of feed composition

Fig. 4.3a shows the attainability curves at feed compositions of 0.3, 0.5 and 0.7 when the product purity and recycle ratio are fixed at 0.96 and 0.95, respectively. Lower feed composition results in a smaller attainability region. The impact of the feed composition

on the minimum selectivity is illustrated in Fig. 4.3b. The lower the feed composition the higher is the required selectivity in order to meet the separation task. At the two extreme composition boundaries where the feed composition approaches 0 or 1, the curve can be fitted by a linear relationship.

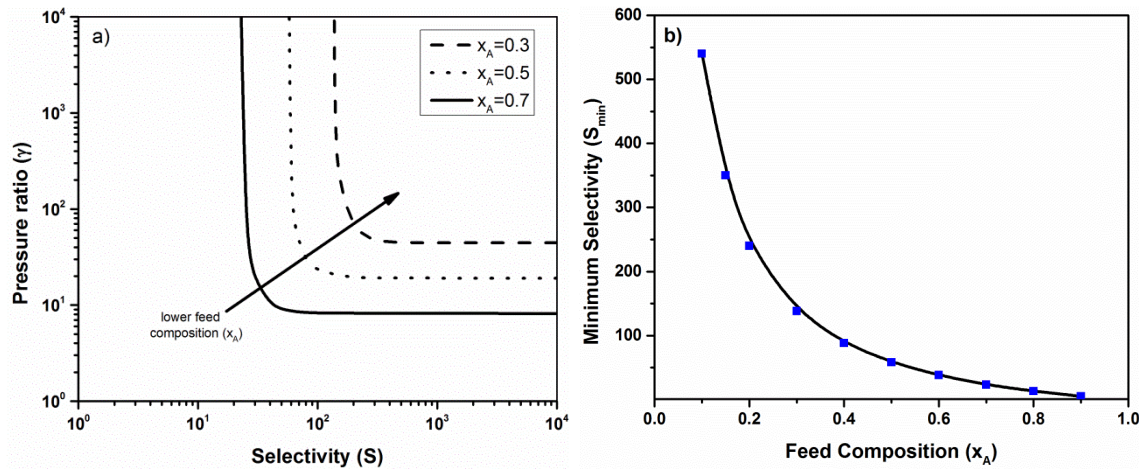


**Fig. 4.3** Impact of feed composition on a) the attainability region and b) the minimum selectivity at infinite pressure ratio.

#### 4.4.2 Influence of product purity

Fig. 4.4a illustrates the impact of the product purity. It shows the product purity has a strong impact on selectivity but a weak influence on pressure ratio. The week influence of purity on pressure ratio can be explained by referring back to equation (4.3) and (4.4). The product purity affects the pressure ratio through the enrichment factor, which is a linear function of product purity, the product purity affects the selectivity through the separation coefficient  $\varphi$ . Dividing the separation coefficient by the enrichment factor, the obtained ratio ( $\frac{(1-x_A)}{(1-y_A)}$ ) can approximate the relative impact of the product purity on

selectivity to pressure ratio (For the case study discussed in Fig. 4.2, this ratio is 24).

Hence, the impact of the product purity on membrane selectivity is stronger than its impact on pressure ratio. The behavior of the required minimum selectivity against the product purity is illustrated in Fig. 4.4b. The minimum selectivity is small and increases slowly when product purity is less than 0.9. Afterwards, the selectivity increases dramatically to infinity when the product purity approaches 1.

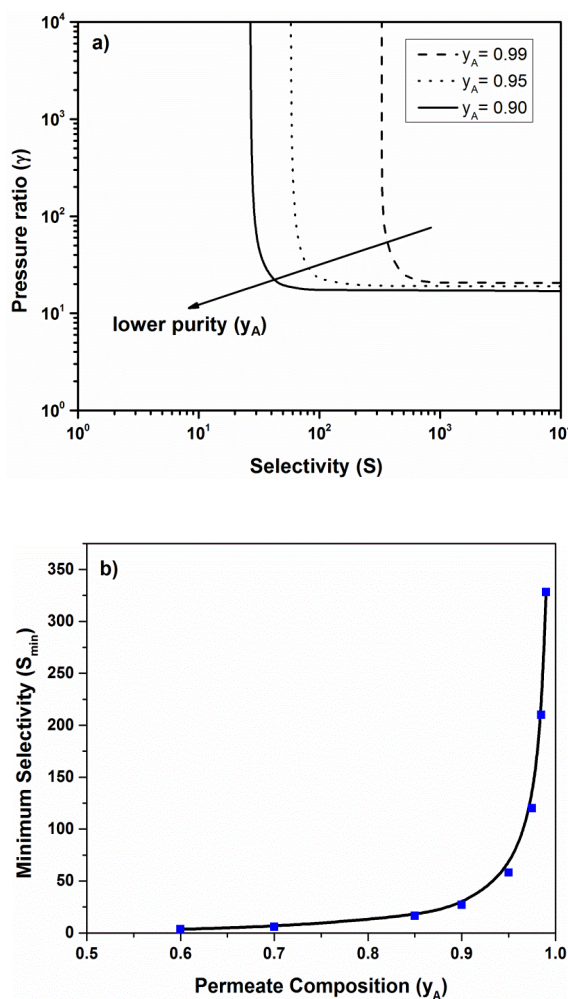
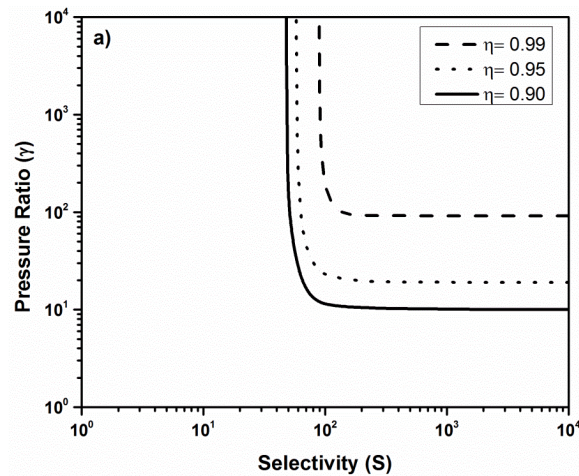


**Fig. 4.4** Impact of product purity impact on a) attainability region and b) the minimum selectivity at infinite pressure ratio.

#### 4.4.3 Influence of recovery ratio

The impact of the recovery ratio on the required selectivity is found to be weaker than the impacts of feed composition and product purity, as can be concluded by comparing the results in Fig. 4.5a to the previously obtained ones. It is noted from the attainability diagram that the recovery ratio has more contribution in defining the pressure ratio than the product purity. Fixing the feed composition and the product purity the relationship between recovery ratio and the minimum selectivity can be obtained and illustrated in Fig. 4.5b. Similar to Fig. 4.4b, the minimum selectivity increases slowly when recovery ratio is less than 0.9, but dramatically increases to infinity when recovery ratio approaches 1. At zero recovery, the minimum selectivity equals to the separation coefficient  $\varphi$ , which can be derived from the well-mixed model as:

$$S_{min}(\eta = 0) = \lim_{\gamma \rightarrow \infty} \frac{(\varphi - \eta)\gamma - (\varepsilon - \eta)}{(1 - \eta)\gamma - (\varepsilon - \eta)} = \varphi \quad (4.5)$$



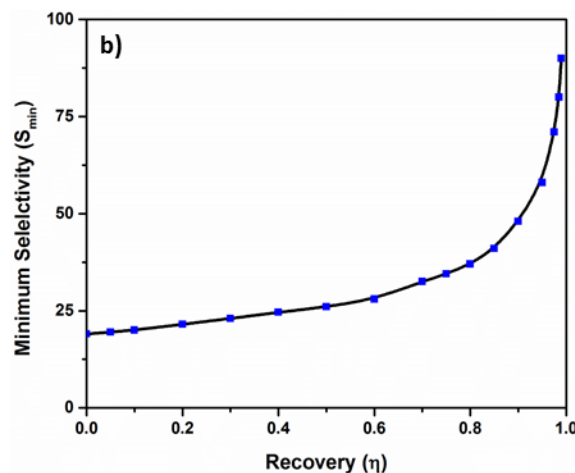


**Fig. 4.5** Impact of recovery ratio on a) the attainability region and b) the minimum selectivity at infinity pressure ratio.

#### 4.5 Empirical relationship of the minimum selectivity in hollow fiber membranes

The relationship in Fig. 4.5b can be used to develop a regression relationship between the separation task parameters and the minimum selectivity. To analyze the impact of feed composition, the membrane process is simulated at various feed compositions while the product concentration is kept constant as 95%. Fig. 6 illustrates the minimum selectivity behavior over the recovery ratio range. While the minimum selectivity function maintained the exponential behavior over the recovery range, it is noticed that the feed composition defines the minimum selectivity at the zero recovery ratio. Then, the impact of product concentration is analyzed in Fig. 6b at fixed feed concentration of 50%.

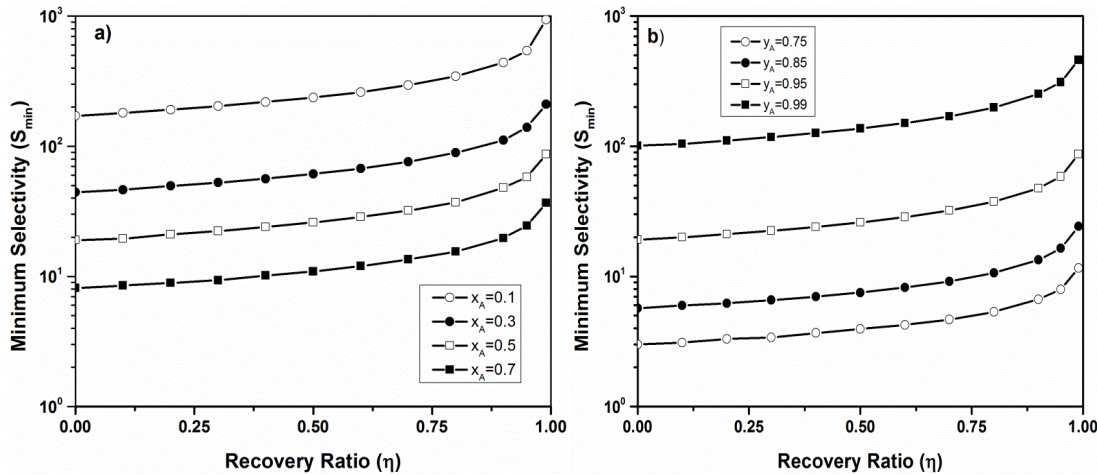


**Fig. 4.6** Behavior of the minimum selectivity over the entire recovery ratio range: a) at different feed compositions and fixed purity of 95% b) at different product concentrations and equimolar feed.

The impact of the three parameters on the minimum selectivity is studied over the range between 0 and 1 for each parameter. It is found that the minimum selectivity at a given recovery ratio  $\eta$  is a function of the minimum selectivity at zero recovery. Based on the simulation data, a relationship of the form in Eq. (4.6) is found to accurately estimate the minimum selectivity as verified in Fig. 5.

$$S_{\min} = \varphi(1 - \eta)^{-\kappa} \quad (4.6)$$

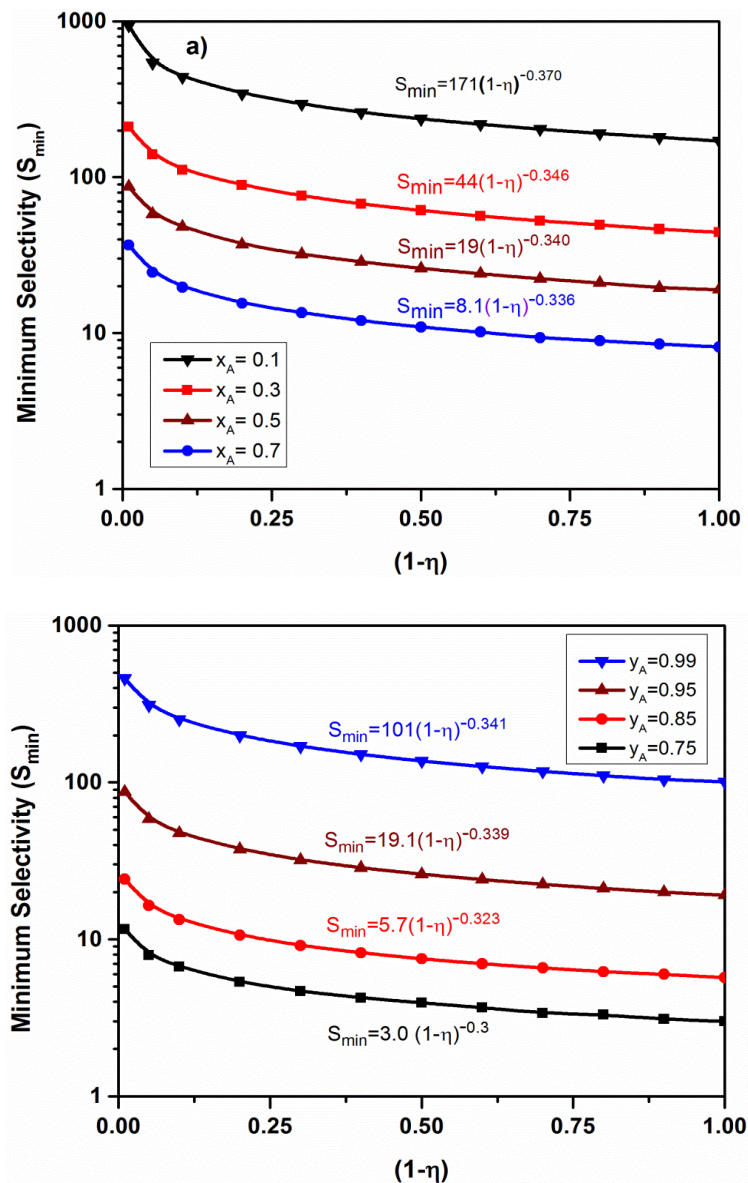


**Fig. 4.7** Regression between the non-recovered fraction  $(1-\eta)$  of the high permeable component and the minimum selectivity to obtain the required purity at various: a) feed composition b) purity target.

The power coefficient  $\kappa$  is found to be strongly dependent on the feed composition and product purity. The data sample showed a power coefficient between 2 and 4 for

most of the cases but no simple correlation is obtained due to the strong nonlinearity of the relation. Following a trial and error procedure to adjust the weight of the impact parameters, the following relationship is formulated.

$$\kappa = \frac{1}{\frac{1}{2} \left[ \sqrt{y_A} \exp(y_A) + \frac{\exp(y_A)}{y_A} - \frac{1}{2} \ln(1-x_A) \right] + \vartheta} \quad (4.7)$$

Where,  $\vartheta$  is a correction factor introduced to enhance the power coefficient accuracy. This coefficient is a decision dependent since it depends on whether the separation is limited by the product purity or instead by the recovery ratio. When the purity is higher than the recovery ratio the correction factor is given by:

$$\vartheta = -\frac{e^{y_A}}{10} \quad (4.8)$$

Otherwise,

$$\vartheta = \frac{e}{10} \quad (4.9)$$

Using these correlations, the minimum selectivity required for the cases discussed in Fig. 5 and Fig. 6 are calculated and compared to the simulation results in Fig. 8. The obtained results are in good agreement with simulation. The maximum deviation occurs at extremely high recovery ratio but with an error of less than 5%.

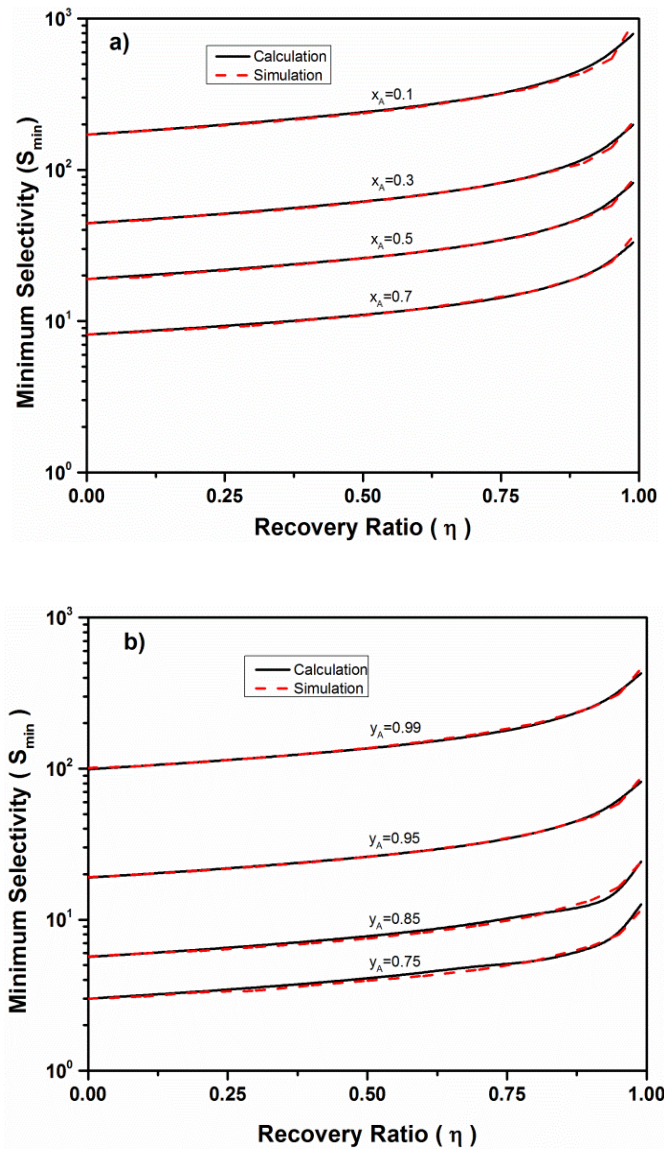


**Fig. 4.8** validation of correlations estimate of the minimum selectivity against the simulation results at: a) various feed compositions b) various product purities

In order to verify the accuracy of the formulated correlations over the range between 1 and 0 for all the impacting parameters, a set of representative data is used. The data covers the entire range of the impacting parameters. Fig. 4.8 shows the data distribution over the impacting parameters. The distribution of data shows less data points at low product purity but this is due to the fact the purity is always higher than the feed

composition. As seen previously in Fig. 4.8, the correlated results for the minimum selectivity are expected to deviate more at extremely high recovery ratios. Therefore, more data points should present at high recovery ratio.

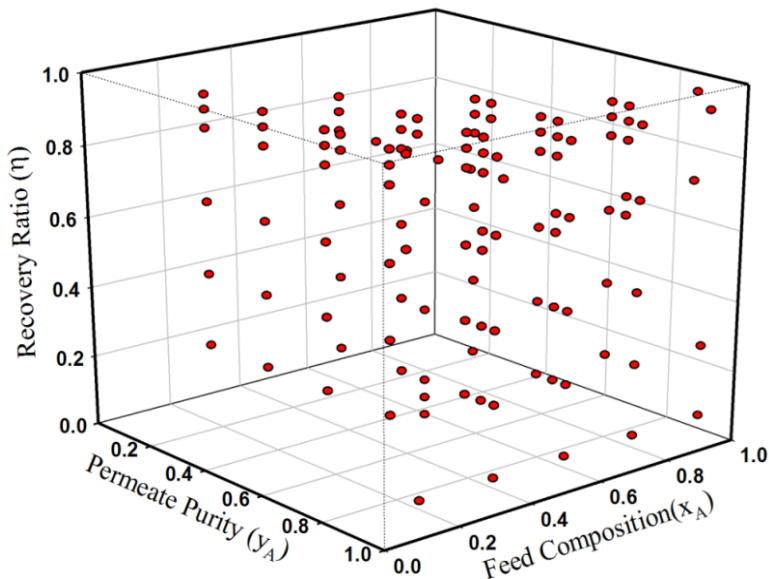


**Fig. 4.9** Distribution of data sample over the impacting variables (feed composition, product purity and the recovery ratio)

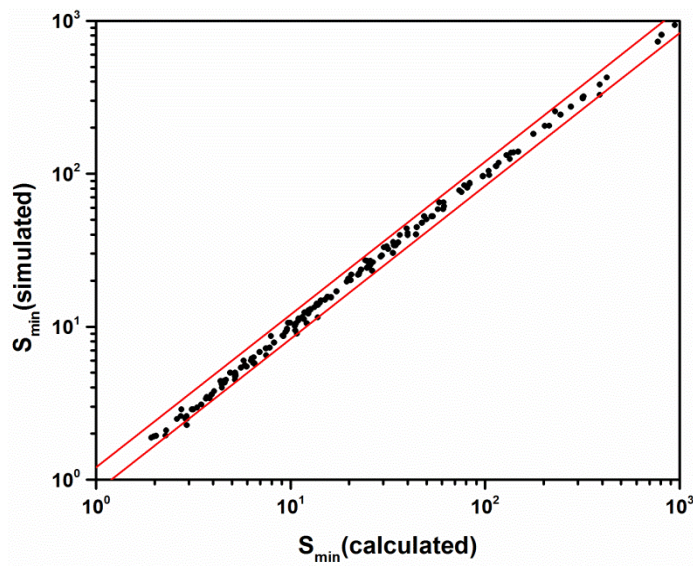


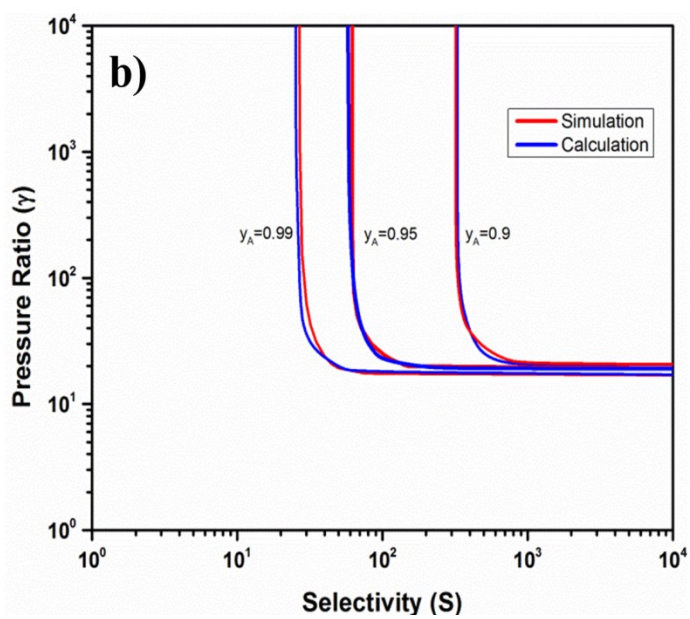
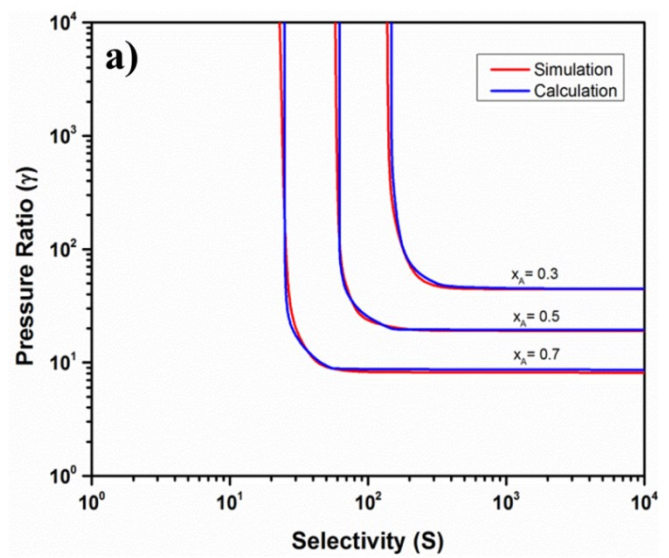
**Fig. 4.10** Accuracy of the calculated minimum selectivity for the data sample discussed in Fig 4.8. The red lines represent the 20% deviation limits.

## 4.6 Approximation of the attainability behavior

As can be concluded from the attainability charts in Fig. 4.4a, 4.5a and 4.6a, the relationship between the required selectivity and pressure has a decay nature. Hence, the required pressure decreases exponentially when selectivity increases. Therefore, it is found that the minimum required selectivity at a fix pressure ratio ( $\gamma$ ) can be approximated by the following relationship:

$$S(\gamma) = S_{\min} \exp \left( \frac{\gamma_{\min}}{\gamma} \right)^{\kappa} + \exp (\gamma - \gamma_{\min})^{-\kappa} \quad (4.10)$$

This formula provides an approximation of the attainability behavior in the hollow fiber membrane module. As seen in many membranes modelling studies that the module design has a minor impact on both stage-cut and purity. Some other studies generalized this finding and approximated the membrane separation in the counter-current modules by assuming cross flow. The simulated attainability charts presented earlier in Fig. 4.3, 4.4 and 4.5 are generated using formula 4.10 as illustrated in Fig. 4.11. The correlated attainability chart shows good agreement with simulation results.



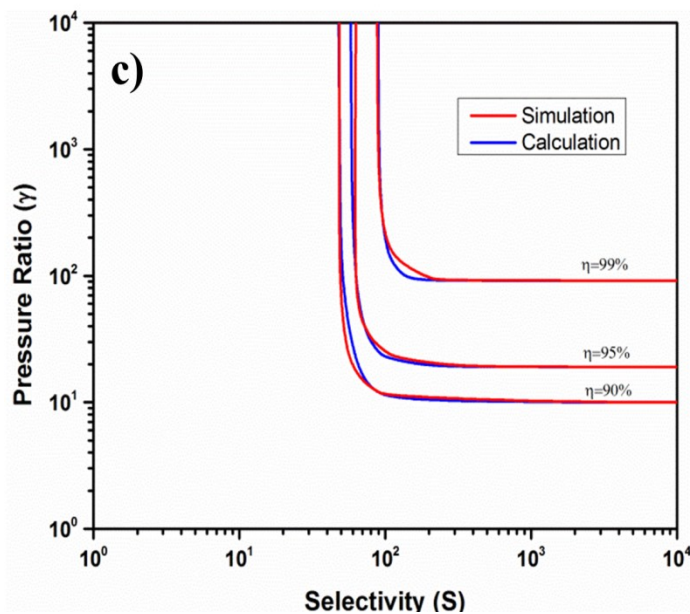


**Fig. 4.11** Comparision between the calculated and simulated membrane attainability region for the separation at: (a) variable feed composition ( $y_A=0.95$ ,  $\eta=0.95$ ) (b) variable permeate purity ( $x_A=0.5$ ,  $\eta=0.95$ ) (c) variable product recovery ratio ( $x_A=0.5$ ,  $y_A=0.95$ )

## 4.7 Case studies

### 4.7.1 Post-combustion carbon capture

Carbon dioxide capture from coal fired power plants flue gas is one of the most studied processes for membrane adequacy. This is due to the environmental impact caused by carbon dioxide emission and the lack of an energy efficient separation method. The major challenges to membrane technology in this application are the large flow rate of flue gas, low feed pressure, dilution of carbon dioxide in mainly nitrogen and the high quality and recovery requirements for the captured CO<sub>2</sub>. The flue gas contains CO<sub>2</sub> at concentrations between 5 and 15 mol% while the capture requirement is to concentrate

$\text{CO}_2$  to 90% at high recovery ratio. The recovery ratio goal set by the US department of energy (DOE) is 90% [4]. These requirements from such diluted feed are proven to be not economically viable by a single-stage membrane unit due to the high pressure ratio needed. Therefore, in this example we will simulate the performance of the first stage in a multiple-stage setup. The example will be considered for this application is schematically illustrated in Fig. 4.12. This process is also simulated in two recently published articles [5, 6].

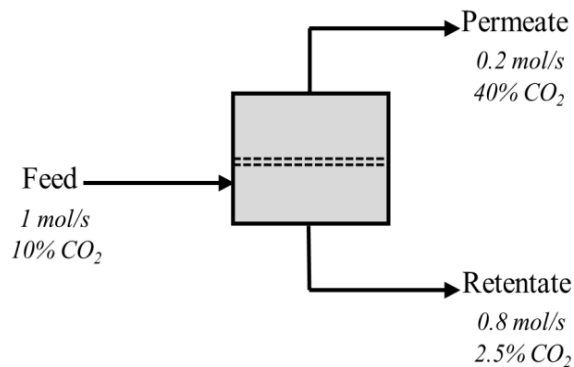


**Fig. 4.12** First stage in a membrane system for carbon capture application.

The minimum pressure ratio is calculated using formula (4.4) which gives a value of 16 ( $\epsilon=4$  and  $\eta=0.8$ ). Using equation (4.5), the minimum selectivity that can meet the product purity at zero recovery ratio is 6.0. Now, the minimum selectivity at zero recovery ratio can be used in equation (4.7) and using the correction factor presented in equation (4.9), the minimum selectivity at the process recovery ratio can be obtained. Performing this calculation a value of 12.8 is obtained. Therefore, in order to produce a permeate stream at  $\text{CO}_2$  concentration of 40%, both the selectivity and pressure ratio should be higher than 16.7 and 12.8, respectively. Regardless of how high is the

membrane selectivity the pressure ratio should be maintained above 16 to meet the separation task. Likewise, regardless of the applied pressure ratio, the minimum selectivity to achieve the permeate purity is 12.8. To operate the process close to the minimum pressure ratio where the operation expense is only 10% higher than the minimum then the selectivity ( $S^*_{\min}$ ) should be least 68. All the calculated results are in good agreement with those obtained from process simulation. Table 4.1 compares the correlated and the simulated values of the minimum selectivity ( $S_{\min}$ ), the minimum pressure ratio ( $\gamma_{\min}$ ) and the minimum selectivity ( $S^*_{\min}$ ) at an operating pressure of 10% higher than the minimum pressure ratio.

**Table 4.1** Comparison between the empirical and hollow fiber simulation results for the process shown in Fig. 4.12.

Parameter	Calculated	Simulation	Error (%)
$S_{\min}$	10.2	11.3	10.6
$\gamma_{\min}$	16	16	0
$S^*_{\min}$	73	68	6.8

As CO<sub>2</sub> recovery ratio is reduced to 70%, the minimum pressure ratio reduces to 11 while the required selectivity reduces to 9. In contrast, increasing the recovery target to 90% increases the minimum pressure ratio to 31 which is two times higher than that required for 80% recovery while the minimum selectivity increases to 13. The permeation of 80% of CO<sub>2</sub> while maintaining its concentration higher than 55% in a single-stage membrane process requires minimum selectivity of 20 at infinitely pressure ratio. On the other hand, the minimum pressure ratio required in the presence of highly

selective membrane is 23.5. In order to operate the membrane process at a pressure ratio of 10% higher than the minimum then the selectivity should be at least 40.

Now based on the obtained results which can be considered as the first stage in a two stage membrane system for carbon capture, the requirements for the second stage can be calculated. Fig. 4.13 graphically illustrates the two-stage membrane system which will be considered in this discussion. The task of the second stage is to recover 95% of CO<sub>2</sub> from the first stage permeate stream with purity of 90%. Using the empirical approximation the attainability of the second stage is limited by minimum selectivity of 36 and minimum pressure ratio of 26. As found in many techno-economical assessment studies for membrane utilization in carbon capture, the compression cost is the most critical parameter to design a competitive process. Therefore, the pressure ratio is adjusted to be only 10% higher than the minimum value. This makes the pressure ratio becomes 28.6. Hence, the objective here is to identify the minimum membrane selectivity that can accomplish the stage task at this pressure ratio. Using equation 4.10 the selectivity is identified to be 75.

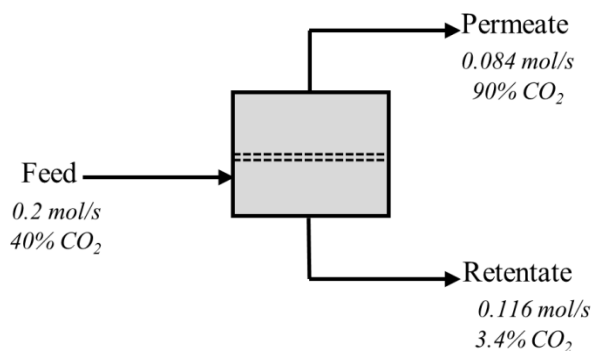


**Fig 4. 13** The separation task in the second stage of a two-stage membrane process for carbon capture process

#### 4.7.2 Oxygen enrichment

Traditionally the air separation is performed using cryogenic distillation or pressure swing adsorption. Though these processes are adequate for high purity product yet they are highly energy-intensive [7]. Membrane technology is seen as the most promising alternative but unfortunately up to date, the application of membranes in this field is limited to oxygen enriched air. This is due to the low selectivity of the commercially available membranes.

The most selective polymer reported in literature has a selectivity of 7 [8, 9]. Theoretically the highest purity that can be achieved with a membrane having a selectivity of 7 is 65% at zero stage cut and infinite pressure ratio. Using the empirical approximation then when the recovery ratio of oxygen is 50% and infinite pressure ratio, the maximum purity that can be achieved is 0.55. Reducing the recovery ratio to 40% will result in oxygen purity of 0.53 if the applied pressure ratio is more than 3.6.

The feed air to a single membrane module is considered to contain 20.5 mol% O<sub>2</sub> with the balance fraction of nitrogen. The separation task is to enrich oxygen to concentrations of 50, 60 and 70 mol% along with recovery ratio of 50%. The impact of oxygen enrichment and recovery on the attainability parameters (pressure ratio and selectivity) is to be studied. The attainability charts obtained from equation 4.10 and process simulator for oxygen enrichment to 50 mol% is illustrated in Fig. 4.14.

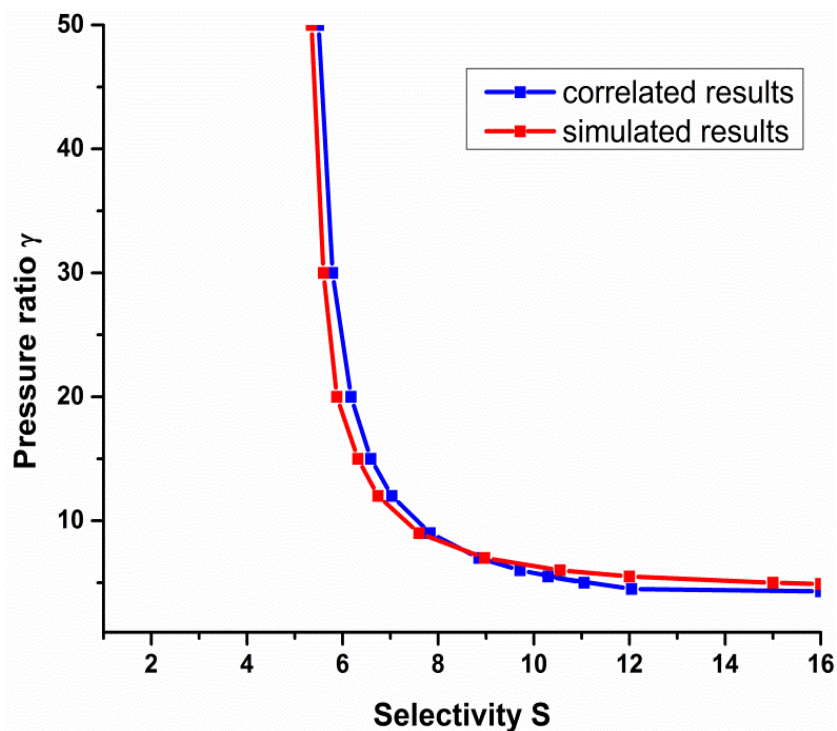


**Fig. 4.14** Attainability chart generated by the developed empirical and process simulation for oxygen enrichment to 50 mol% in a single-stage membrane process.

The objective of simulating the membrane process for oxygen enriched air application is to calculate the minimum pressure ( $\gamma_{\min}$ ) at which a membrane with certain selectivity can meet the separation task. Table 4.2 compares the minimum selectivity and pressure ratio obtained by the developed correlations and model simulation. At such low selectivity and pressure ratio, the short cut method showed high accuracy in estimating both the minimum selectivity and pressure ratio. The maximum error in predicting the minimum selectivity is found to be less than 8.6%.

**Table 4.2** Comparsion between corrolated and simulated results for oxygen enrichment to 50, 60 and 70 mol%.

Product Purity	Correlations			Simulation			$S_{\min}$ error (%)
	$S_{\min}$	$\gamma_{\min}$	$\gamma^*_{\min} (S=1.5S_{\min})$	$S_{\min}$	$\gamma_{\min}$	$\gamma^*_{\min} (S=1.5S_{\min})$	
0.5	5.1	3.88	9.7	5.2	3.88	9.6	2.0
0.6	7.6	4.85	12	7.9	4.85	12	3.8
0.7	11.7	5.83	14.4	12.8	5.83	14.33	8.6

## 4.8 Conclusion

Investigating the separation in a single-stage membrane using the complete well mixed model, the membrane selectivity and the transmembrane pressure ratio are identified to be the only parameters defining the process attainability region to accomplish a certain separation task. The relationship between these parameters is monotonic. Hence, both membrane selectivity and pressure ratio exhibit minimum thresholds that are independent of the value of any other parameters. Hence the minimum selectivity and the minimum pressure ratio define the attainability region of a single-stage membrane process. The hollow fiber model presented the same behavior but at lower minimum selectivity due to the higher overall driving force.

In order to turn these findings into correlations to approximate the attainability behavior, a parametric investigation is conducted. Plotting the simulated minimum selectivity in a hollow fiber module against the non-recovered fraction of the high permeable component, a power relationship is found to accurately fit all data points. The function intercept is equivalent to the separation factor while the power coefficient is a nonlinear function of product purity and feed composition. Adjusting the impact weight

of these two parameters, a simple representation of the power factor is obtained. Correlations showed a maximum error of 20% when validation is conducted over a large data sample. Using the minimum selectivity a relationship is obtained to generate the attainability behavior. Studying the attainability of membrane process for two case studies, accurate results are obtained.

## 4.9 References

- [1] I.C. Omole, Crosslinked polyimide hollow fiber membranes for aggressive natural gas feed streams, ProQuest, 2008.
- [2] A. Motelica, O.S. Bruinsma, R. Kreiter, M. den Exter, J.F. Vente, Membrane Retrofit Option for Paraffin/Olefin Separation • A Technoeconomic Evaluation, Ind Eng Chem Res, 51 (2012) 6977-6986.
- [3] R.W. Baker, J. Wijmans, Y. Huang, Permeability, permeance and selectivity: a preferred way of reporting pervaporation performance data, J Membrane Sci, 348 (2010) 346-352.
- [4] T.F. J.D. Figueroa, S. Plasynski, H. McIlvried, R.D. Srivastava, Advances in CO<sub>2</sub> capture technology – the U.S. Department of Energy's Carbon Sequestration Program, International Journal of Greenhouse Gas Control 2(2008) 9-20.
- [5] A. Brunetti, E. Drioli, Y.M. Lee, G. Barbieri, Engineering evaluation of CO<sub>2</sub> separation by membrane gas separation systems, Journal of Membrane Science, 454 (2014) 305-315.
- [6] Y. Huang, T.C. Merkel, R.W. Baker, Pressure ratio and its impact on membrane gas separation processes, Journal of Membrane Science, 463 (2014) 33-40.
- [7] F.G. Kerry, Industrial gas handbook: gas separation and purification, CRC Press, 2010.
- [8] R.W. Baker, Future directions of membrane gas separation technology, Industrial & Engineering Chemistry Research, 41 (2002) 1393-1411.
- [9] X.S. Feng, J. Ivory, V.S.V. Rajan, Air separation by integrally asymmetric hollow-fiber membranes, Aiche Journal, 45 (1999) 2142-2152.

## **5. Attainability and Minimum Energy of Multiple-Stage Cascade Membrane Systems**

### **5.1 Abstract**

The attainability and energy consumption of multi-stage membrane cascade systems are studied using the complete well-mixed membrane model. It was found that the attainability curve of multi-stage systems is defined by pressure ratio and membrane selectivity. At the constant recycle ratio scheme, the recycle ratio can shift the attainability behavior between single-stage and multi-stage membrane systems. When recycle ratio is zero, all multi-stage membrane process will decay to single-stage membrane process. When recycle ratio approach infinity, the required selectivity and pressure ratio reach the absolute minimum selectivity and pressure ratio which have a simple relationship with that of single-stage membrane process:  $S_n = \sqrt[n]{S_1}$ ,  $\gamma_n = \sqrt[n]{\gamma_1}$ , where n is the number of stages. Similar trends were find in the constant stage-cut scheme. When the enriching stage-cut is 1, all enriching stages will disappear and the system will decay to the membrane system which has the stripping stages only. When the enriching stage-cut approaches 0, the required selectivity and pressure ratio will again reach the absolute minimum selectivity and the absolute minimum pressure ratio. The energy consumption of multi-stage membrane process is mainly determined by membrane selectivity and recycle ratio. A small recycle ratio can significantly reduce the required membrane selectivity without much energy penalty. The energy envelope curve

can provide a guideline from the energy point of view to determine the minimum required membrane selectivity in membrane process designs in order to compete with conventional separation processes such as distillation.

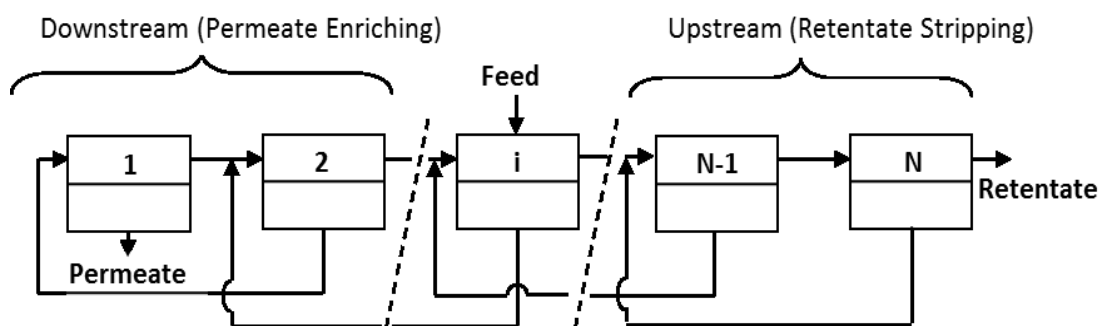
## 5.2 Introduction

Membrane process has played a more and more important role in many challenging gas separation systems such as CO<sub>2</sub> capture and nature gas separation, etc.[1] Our previous study on the attainability of a single-stage membrane process revealed that selectivity S and pressure ratio  $\gamma$  are the only two controlling parameters [2]. Each of them exhibits a minimum value in order to meet a certain separation task that is defined by the recovery ratio ( $\eta$ ) and the enrichment factor ( $\varepsilon$ ). This finding is consistent with many other studies in the literature [3, 4]. In real cases these two parameters are often limited by many factors including material properties, equipment limitations and economic feasibility, etc. One solution to overcome these limits is to use multiple membrane separation stages [5-8].

In a multiple-stage membrane design, the retentate stream may feed to the next stage to extract more permeate in order to increase the recovery ratio, while the permeate stream may recycle back to the downstream stages in order to further purify the product. The stages to further purify the permeate streams are commonly named as the enriching section while the other stages the stripping section. The entire structure is called membrane cascade that is analogous to the flow cascade in distillation processes. Fig. 5.1 illustrates the most common membrane cascade design where the permeate streams recycle one stage back to the previous stage. The concentration of the recycled streams

normally will not be equal to the streams that they are mixing with, but if their concentrations are designed to be equal, this is called the non-mixing or ideal design. Studies on the separation performance, particularly the possible impact on the membrane area as well as the power consumption of the ideal and non-ideal cascade designs have been discussed in literature [9-11]. The process simulation of ideal and non-ideal membrane cascade designs are also well covered in literature [7, 12]. However, the attainability as well as the minimum energy consumption of multi-stage cascade membrane systems have not been studied yet.

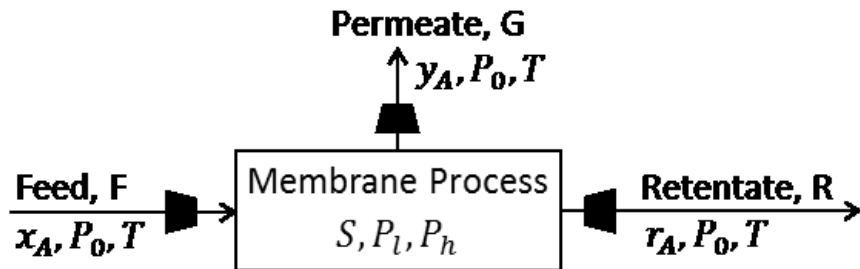
In this study we aim to investigate the behavior of the attainability parameters in the most promising two and three-stage membrane cascade systems. The complete well-mixed model is used to allow for obtaining simple mathematic models defining the system limiting parameters. This will serve the study objective in producing conceptual design basis. The separation of propylene/propane that is important in petrochemical industry is used as a bench system to study the energy consumption and the results are compared with the standard distillation process.



**Fig. 5.1** Schematic of cascade membrane system with recycle streams.

### 5.3 Analysis methodology

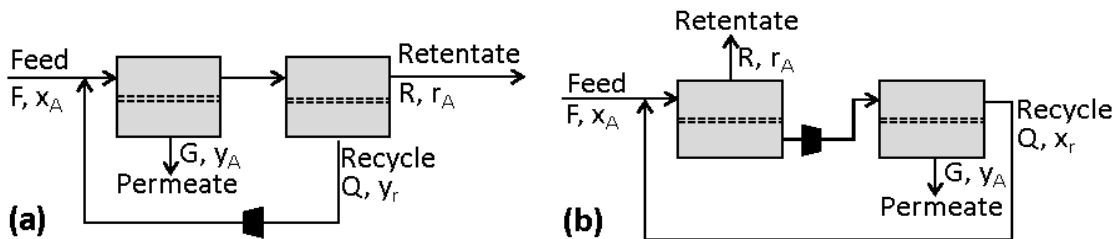
All the analyses followed in this study are based on a general membrane separation process schematically presented in Fig. 5.2. A binary gas mixture ( $x_A$ , T,  $P_0$ ) is fed into a membrane unit and preferentially split into a permeate stream as a product and a retentate stream as a by-product. The permeate stream is enriched in the high permeable component. The separation task is that the product should meet certain purity ( $y_A$ ) and certain recovery ratio ( $\eta$ ). To get a well-defined energy consumption equation, we assume both permeate and retentate streams leave the system at the same pressure and temperature as the feed stream ( $P_0$ , T).

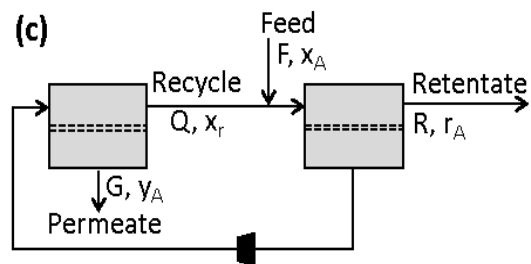


**Fig. 5.2** Black box representation of a membrane process to perform a separation task to a binary mixture. The transmembrane pressure ratio is created by feed compression. Energy recovery is also considered to minimize the separation energy penalty.

The two most common designs in two-stage systems are shown in Fig. 5.3a and 5.3b, which is often named as two-stage stripping cascade and two-stage enriching cascade, respectively[13, 14]. The stripping cascade is also referred to as two strippers in series permeator system (TSSP) in literature[15]. This design is found to be the most economically feasible design for highly diluted target component in the feed mixture

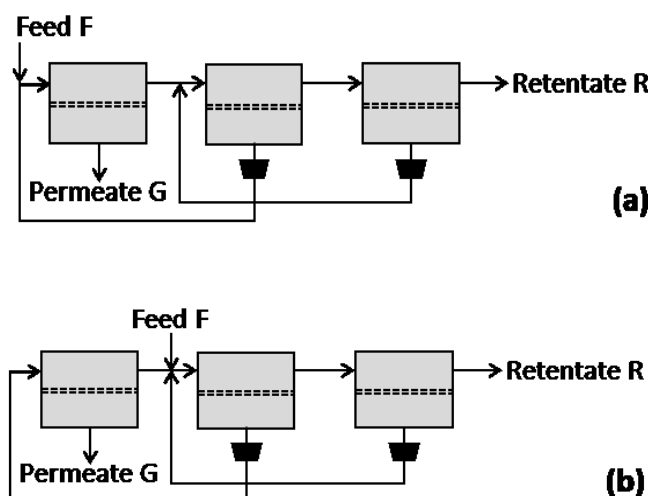
[16], while the enriching cascaded system is reported as more efficient for the production of high purity of the less permeable component [17, 18]. In the two-stage stripping cascade, the retentate of the first stage feeds to the second stage, while the permeate of the second stage recycles back to the feed of the first stage in order to achieve better recovery ratio. The recycle stream in this case is the permeate stream, whose flow rate is defined as  $Q$  and the concentration as  $y_r$ . Controlling the amount of  $Q$  is equivalent to control the stage-cut  $\tau$ . The higher the amount of  $Q$ , the higher is the stage-cut as well as the recovery ratio. In the two-stage enriching cascade, the permeate of the first stage feeds to the second stage, while the retentate of the second stage recycles back to the feed of the first stage in order to achieve better product purity. The recycle stream in this case is the retentate stream, and the higher the amount of the recycle stream, the lower is the stage-cut but the higher the product purity. The design in Fig. 5.3b seems not to follow the cascade design, but if redrawing it as Fig. 5.3c, one can clearly see that this design is indeed a cascade design but the feed position shifts to the second stage. However, the recycle streams are different in these two cases. From the above discussions we can make a general definition for recycle streams as follows. For stages in the enriching section, the recycle streams are the retentate streams, while for stages in the stripping stages the recycle streams are the permeate streams.





**Fig. 5.3** Different designs of two-stage cascade membrane systems. a) two-stage stripping cascade; b) two-stage enriching cascade; c) a different drawing of the two-stage enriching cascade.

Following the same idea the three-stage cascade membrane system will have three different designs, as shown in Fig. 5.4. It was found that the design in Fig. 5.4b is the most efficient to accomplish high enrichment from a moderate feed molar fraction (30 to 70%) [19]. This is because this design consists of both stripping and enriching stages and hence it is expected to combine the advantages of the two-stage stripping and enriching cascades.



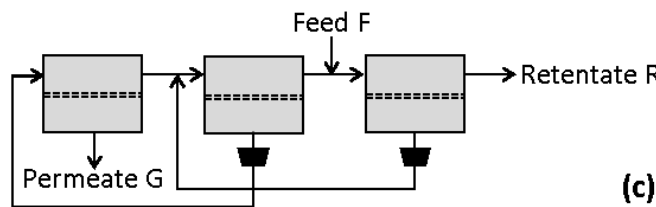


**Fig. 5. 4** Three cascade designs for three-stage membrane systems. (a) feed to the first stage (only stripping stages); (b) feed to the second stage (with both enriching and stripping stages); (c) feed to the third stage (with only enriching stages).

#### 5.4 Mathematic models

Membrane selectivity ( $S$ ) is defined as the permeability ratio of the most permeable component to other components in the multi-component mixture. The pressure ratio ( $\gamma$ ) of each stage is defined as the ratio between its feed and permeate pressures. We also define the recycle ratio ( $\psi$ ) as the normalized flow rate of a recycle stream to the flow rate of the feed stream of the system. Referring to the cascade membrane design in Fig. 5.1, the retentate streams flow upward and the by-product is taken out from the last stage, while the permeate streams of the upper stages flow one stage back to the down stages except the last one which is taken out as the product.

The attainability analysis and the minimum energy consumption calculations will be performed under the following three assumptions. First, the completely well-mixed mode is to be used to simplify the mathematical derivation of mass transport in a membrane module. So it is assumed that the membrane feed side has a homogenous concentration equivalent to the retentate stream concentration. Similarly, the permeate side of the membrane is considered to have a homogenous concentration equivalent to that of the

permeate stream. Combining the mass balance formula for a binary gas mixture with the Fick's diffusion law for gas permeation the following formula can be obtained to describe the mass transport in each stage of a membrane system (as derived in Appendix-A).

$$\frac{y_A}{1 - y_A} = S \frac{\gamma r_A - y_A}{\gamma(1 - r_A) - (1 - y_A)} \quad (5.1)$$

Second, all stages are assumed to have the same membrane selectivity and the same pressure ratio. Membrane selectivity is usually an intrinsic property related to membrane material and microstructure. If the same type of membrane used in all stages, then a constant membrane selectivity can be a good assumption. If the pressure in the retentate doesn't loss much from the feed pressure, then it is possible to maintain the same pressure ratio in all stages with the minimum number of compression units. For the third assumption, two cases are considered here. The first case is to assume a constant stage-cut. This assumption has been commonly used in literature [20, 21]. The second case is to assume a constant recycle ratio that is defined here for all stages. To the best of our knowledge this is the first time to make such an assumption in cascade designs, so it requires more explanations as follows. In the constant stage-cut assumption, all enriching stages have the same stage-cut  $\tau_E$  and all stripping stages have the same stage-cut  $\tau_S$ . The feed stage has the same stage-cut as the stripping stages, so a relationship between  $\tau_E$  and  $\tau_S$  can be established from mass balance. A detailed derivation can be found in reference [22]. Hence, when  $\tau_E$  is used as a design variable then the entire cascade can be designed accordingly. However, it can be found easily from Fig. 5.1 that the flow patterns are different for the following stages, the first stage, the rest of enriching stages, the feed stage, the last stage, and the rest stripping stages. Using the constant recycle ratio

assumption can improve this situation. In this case the above five kinds of stages will have different stage-cut. Fig. 5.5 shows the relationship between the stripping and enriching stage-cuts in the constant stage-cut scheme and the relationship between the first and last stage-cut in the constant recycle ratio scheme for a three-stage membrane cascade where the second stage is the feed stage. In both scheme, when increasing the enriching stage-cut, the stripping stage-cut will reduce. When the ratio G/R is less than one, there is not much difference between the two schemes. However, when G/R is larger than one, the difference is more significant. Particularly when the enriching stage-cut is close to 1, the stripping stage-cut reduces to 0 in the constant recycle ratio scheme, but in the constant stage-cut scheme the stripping stage-cut will remain a substantial value. Apparently, the constant recycle ratio scheme in this case is more reasonable since it means most of the product in the enriching stages will go to the permeate stream, hence there is no need to have a large permeate stream in the stripping stages. The main reason why the stripping stage-cut cannot reduce to 0 in the constant stage-cut scheme is because it is limited by the stage-cut of the feed stage, which is close to G/F.

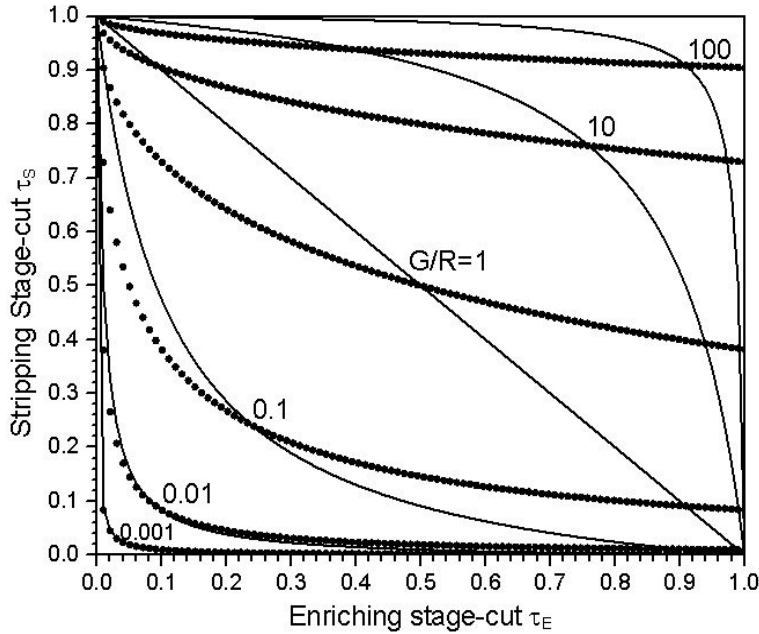


**Fig. 5.5** Relationship between the stripping stage-cut and enriching stage-cut at different G/R ratios in three-stage membrane cascade with both enriching and stripping stages. Dotted lines shows the relationship in constant stage-cut scheme and solid line shows the relationship in constant recycle ratio scheme.

#### 5.4.1 Model derivation method

As an illustration of the model derivation procedure, the two-stage stripping cascade is presented here while the derivation of other configurations is presented in Appendix-B. Carrying mass balance over the first stage and then solving the complete well-mixed solution- diffusion model gives the following relationship between selectivity S, pressure ratio  $\gamma$ , feed concentration  $x_A$ , enrichment factor  $\varepsilon$ , recovery ratio  $\eta$  and recycle stream concentration  $y_r$  and ratio  $\psi$ :

$$S = \frac{x_A(\varepsilon\eta x_A - \gamma\psi\varepsilon - \gamma\varepsilon + \gamma\eta + \gamma\varepsilon x_A + \gamma\varepsilon\psi y_r - \gamma\eta\varepsilon x_A + \psi\varepsilon + \varepsilon - \eta - \varepsilon^2\psi x_A - \varepsilon^2 x_A + \eta\varepsilon x_A)}{(\gamma x_A + \gamma\psi y_r - \gamma\eta x_A - \varepsilon\psi x_A - \varepsilon x_A + \eta x_A)(\varepsilon x_A - 1)} \quad (5.2)$$

Similarly, the mass balance over the second stage yields:

$$S = \frac{y_r(\gamma\varepsilon - \gamma\eta - \gamma\varepsilon x_A + \gamma\eta\varepsilon x_A - \varepsilon + \eta + \varepsilon y_r - \eta y_r)}{(\gamma\eta\varepsilon x_A + \varepsilon y_r - \eta y_r - \gamma\varepsilon x_A)(y_r - 1)} \quad (5.3)$$

If selectivity and pressure ratio are assumed the same for both stages then Eq. (5.2) equals to Eq. (5.3) and therefore, the recycle stream concentration ( $y_r$ ) can be calculated when the recycle ratio  $\psi$  is specified for a given feed and defined separation task. Hence, the behavior of selectivity as a function of the applied pressure ratio can be generated. The minimum selectivity ( $S_{min}$ ) can be obtained at infinite pressure ratio. Hence, taking the limits of Eq. (5.2) and (5.3) in terms of infinity pressure ratio gives:

$$S_{min} = \frac{y_r(\varepsilon - \eta - \varepsilon x_A + \eta\varepsilon x_A)}{\varepsilon x_A(1 - \eta)(1 - y_r)} \quad (5.4)$$

$$S_{min} = \frac{x_A(\psi\varepsilon + \varepsilon - \eta - \varepsilon x_A - \psi\varepsilon y_r + \varepsilon x_A\eta)}{(\psi y_r + x_A - x_A\eta)(\varepsilon x_A - 1)} \quad (5.5)$$

Eq. (5.4) and (5.5) indicate that the minimum required selectivity  $S_{min}$  is determined not only by the separation task ( $x_A$ ,  $\varepsilon$ ,  $\eta$ ), but also by the recycle ratio  $\psi$ . The higher the recycle ratio, the lower is  $S_{min}$ . When the recycle ratio goes to infinity, the required selectivity is the absolute minimum below which the two-stage system can never meet the separation task. The absolute minimum selectivity of two-stage membrane system is given by Eq. (5.6). The term in the square root is the same to calculate the minimum selectivity of single-stage membrane system, as derived in our previous report [2]. Hence, the absolute minimum selectivity of two-stage systems is the square root of the single-stage minimum selectivity.

$$S_{min} = \sqrt{\frac{\phi - \eta}{1 - \eta}} = \sqrt{s_1} \quad (5.6)$$

From the other hand, the minimum pressure ratio as a function of the recycle ratio can also be obtained from Eq. (5.2) and (5.3) by taking the limit at infinity selectivity. This resulted in the following relations:

$$\gamma_{min} = \frac{y_r(\eta - \varepsilon)}{\varepsilon x_A(\eta - 1)} \quad (5.7)$$

$$\gamma_{min} = \frac{x_A(\varepsilon\psi + \varepsilon - \eta)}{x_A + \psi y_r - x_A \eta} \quad (5.8)$$

The minimum required pressure ratio at a defined recycle ratio can be calculated by solving equations (5.7) and (5.8). The absolute minimum pressure ratio is obtained when the recycle ratio goes to infinity. This gives the following simple form. Again, the term inside the square root is found equal to the minimum pressure ratio of a single-stage membrane system, so the absolute minimum pressure ratio of a two-stage membrane system is also the square root of a single-stage minimum pressure ratio.

$$\gamma_{min} = \sqrt{\frac{\varepsilon - \eta}{1 - \eta}} = \sqrt{\gamma_1} \quad (5.9)$$

#### 5.4.2 Minimum energy of multi-stage membrane systems

Comparing the minimum work required by the membrane systems to that consumed by the conventional separation process for a specific application is of great importance to evaluate the technology potential from an energy efficiency view point. The comparison

will also help to understand the technology limitations. In this discussion, it is assumed that the membrane process is equipped with an energy recovery system and all work equipment (compressors, vacuum pumps and energy recovery system) are 100% efficient. Therefore, the energy consumption by a membrane system is the same regardless if the driving force is created either by feed compression and/or permeate vacuum pumping. Hence, the required work for the two-stage with stripping cascade, two-stage with enriching cascade and the three-stage with permeate and retentate recycle is derived in Eq. (5.10), (5.11) and (5.12), respectively.

$$E_{min}^{2SC} = F \left[ \psi + \frac{\eta}{\varepsilon} \right] C_p T \left( \gamma^{\frac{R}{C_p}} - 1 \right) \quad (5.10)$$

$$E_{min}^{2EC} = F \left[ \psi + 2 \frac{\eta}{\varepsilon} \right] C_p T \left( \gamma^{\frac{R}{C_p}} - 1 \right) \quad (5.11)$$

$$E_{min}^{3S} = 2F \left[ \psi + \frac{\eta}{\varepsilon} \right] C_p T \left( \gamma^{\frac{R}{C_p}} - 1 \right) \quad (5.12)$$

In this study the membrane technology is to be evaluated against the conventional distillation process for the separation of propylene/propane mixture. The bench system has a feed mixture at equimolar concentration and available at atmospheric pressure and ambient temperature. The separation objective is to produce propylene at a concentration of 96% with recovery ratio of 95%. The minimum energy of a distillation column is the minimum heat that needs to be supplied in the reboiler to maintain the minimum vapor at the topmost tray. The minimum vapor flow rate can be calculated from mass balance as:

$$V_{min} = D(1 + RR) \quad (5.13)$$

Therefore, the minimum energy of a conventional distillation column is:

$$E_{min}^D = \lambda D(1 + RR) \quad (5.14)$$

The minimum reflux ratio (RR) can be estimated from the underwood formula as:

$$RR = \left[ \sum_{i=1}^c \frac{\alpha_i x_{D_i}}{\alpha_i - \phi} \right] - 1 \quad (5.15)$$

where,  $\phi$  is the root of the following equation:

$$1 - q = \sum_{i=1}^c \frac{\alpha_i x_{F_i}}{\alpha_i - \phi} \quad (5.16)$$

A detail derivation of the above equations can be found in our previous report [2] or in reference [23].

## 5.5 Results and discussion

### 5.5.1 Attainability of multi-stage membrane systems

Our previous studies showed that for a single-stage membrane system, there is a boundary defined by membrane selectivity  $S$  and pressure ratio  $\gamma$  where below this boundary, as shown in the shade area in Fig. 5a, the separation task cannot be achieved. Accordingly, the curve defining the boundary is called  $S\text{-}\gamma$  attainability curve. For multi-stage cascade membrane systems, such a relationship between  $S$  and  $\gamma$  is also found exist here. For example, for two-stage stripping cascade an equation between  $S$  and  $\gamma$  can be obtained by combining Eq. (5.2) and (5.3). The equation parameters include separation

task parameters ( $x_A$ ,  $\varepsilon$ ,  $\eta$ ) and also the recycle ratio  $\psi$ . In the constant recycle ratio scheme, the recycle ratio  $\psi$  is assumed to be the same for all stages, while in the constant stage-cut scheme, the recycle ratio of each stage can be calculated from the enriching stage-cut value  $\tau_E$ . A detail derivation is shown in appendix B.

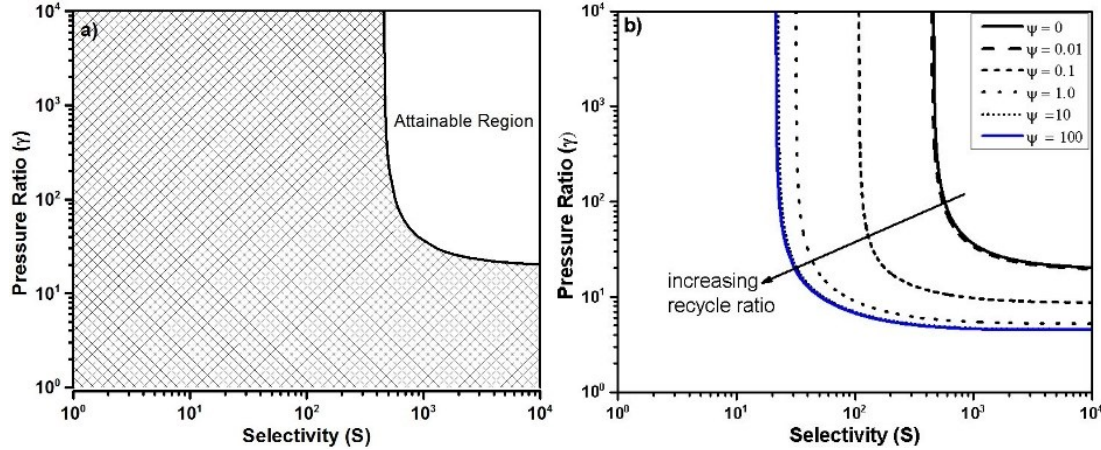
Fig. 5.6b-f show the  $S-\gamma$  attainability curves under the constant recycle ratio assumption for the bench separation system by the two-stage stripping cascade, two-stage enriching cascade, and three-stage cascades with feed to the first, second and third stages, respectively. In all these diagrams, the attainability curves move towards lower selectivity and lower pressure ratio when the recycle ratio  $\psi$  increases, indicating that the required selectivity and pressure ratio decrease when the recycle ratio increases. It is interesting to find in each diagram the attainability curves are located within two boundaries. The high-end boundary is when the recycle ratio is 0. This boundary was found identical in all diagrams and also identical to the attainability curve of the single-stage membrane system. This result indicates that when the recycle ratio decreases to 0, all multi-stage membrane systems decay to single-stage membrane system. The low-end boundary is when the recycle ratio is infinity. Although in Fig. 5.6 the recycle ratio is studied only up to 100, while from the trend of different recycle ratios the curve at infinity recycle ratio should be very close. This boundary is found identical for the same number of stages regardless of the feed position. Since this is the low-end boundary, so it can be defined as the absolute minimum selectivity and pressure ratio attainability curve. The diagrams in Fig. 5.6 show that the absolute minimum selectivity and pressure ratio for single-stage are 461 and 19.4, for two-stages are 21.5 and 4.4, and for three-stages are

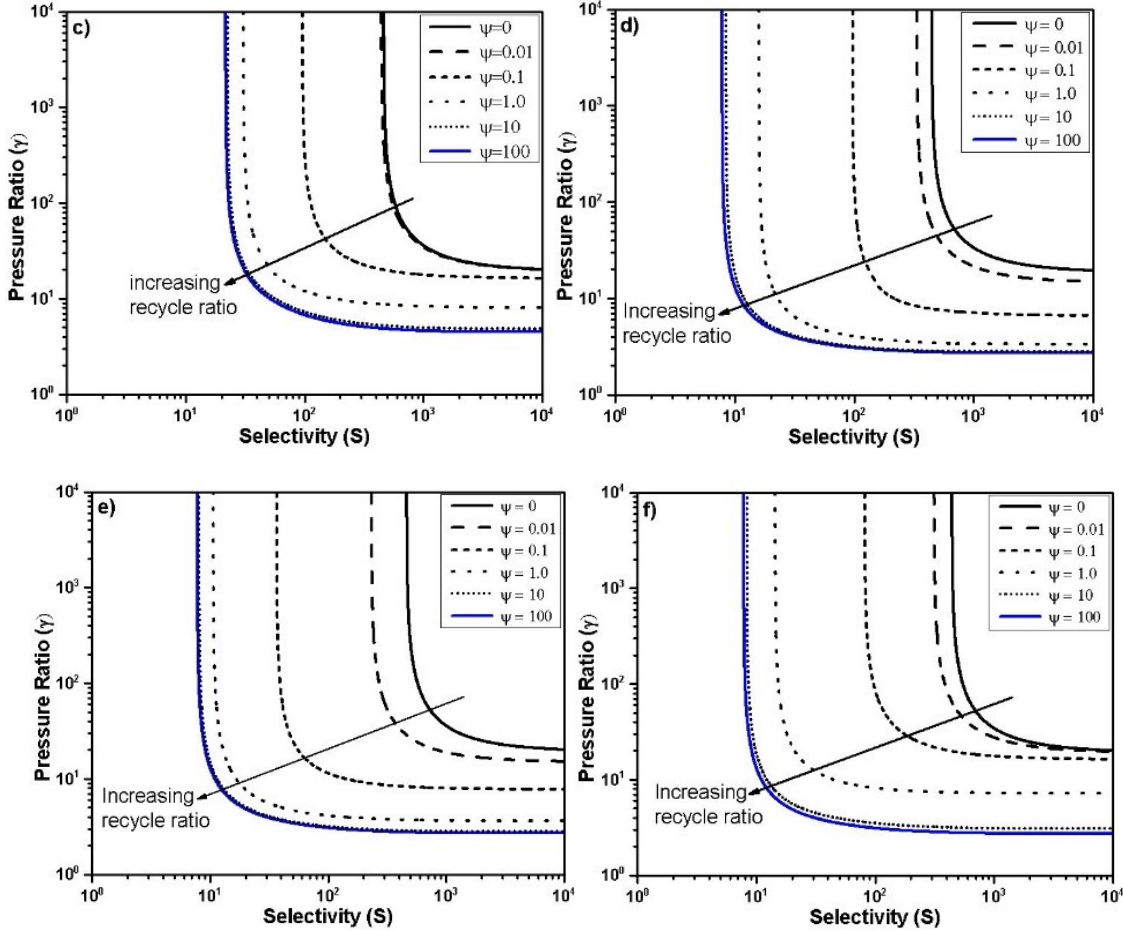
8.5 and 2.9, respectively. Hence, a square root relationship is realized between the absolute minimum selectivity and pressure ratio of the two-stage systems to the single-stage system, and a cubic root relationship is realized between the three-stage systems to the single-stage system. The square root and cubic root relationships are also derived mathematically in eq. (5.6) and (5.9) and also in Appendix B. This relationship can be further extended to any multi-stage membrane systems as below:

$$S_n = \sqrt[n]{S_1} \quad (5.17)$$

$$\gamma_n = \sqrt[n]{\gamma_1} \quad (5.18)$$

Where  $S_n$ ,  $\gamma_n$ ,  $S_1$  and  $\gamma_1$  are the absolute minimum selectivity and the absolute minimum pressure ratio of n-stage and single-stage membrane systems, respectively.



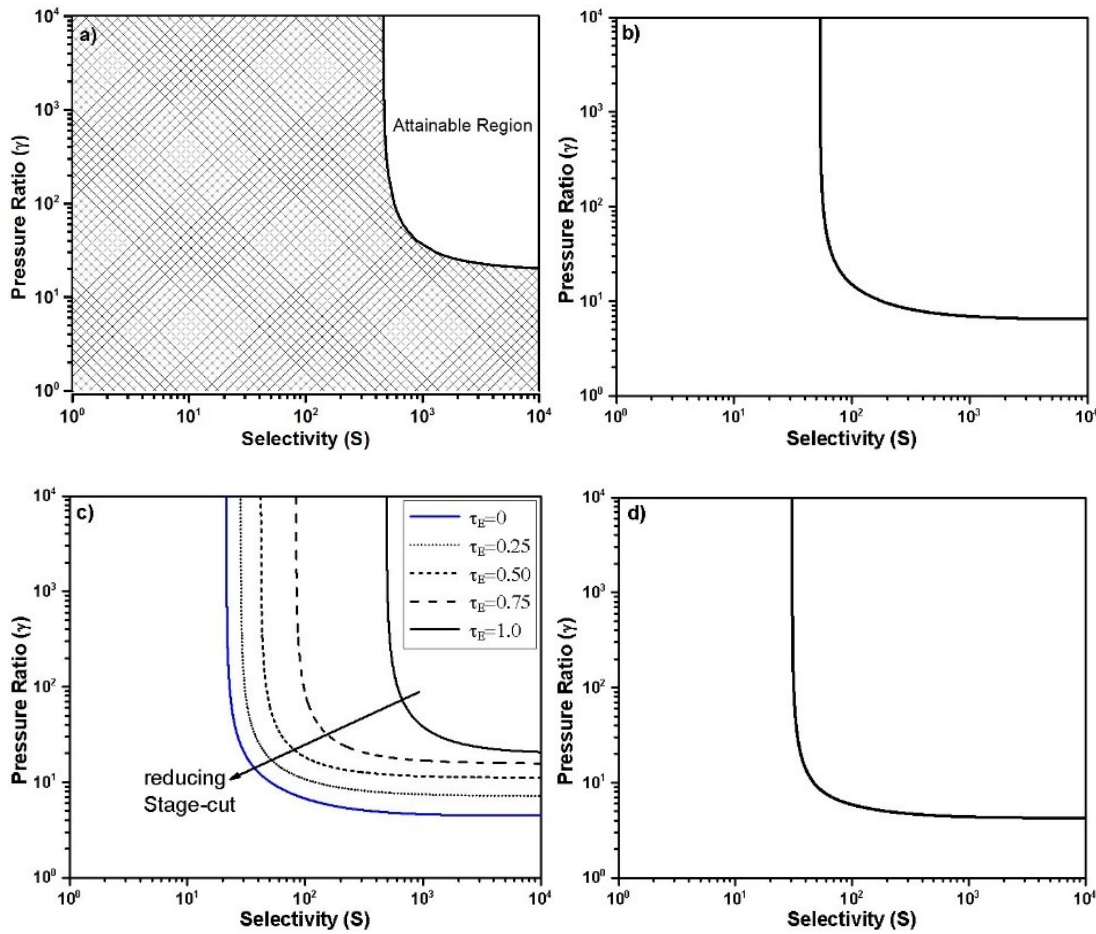


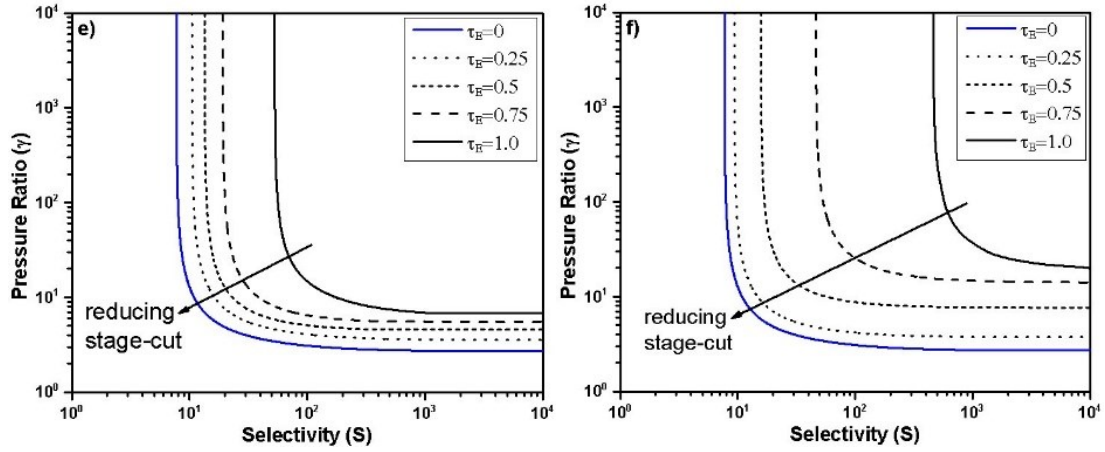
**Fig. 5.6** Attainability of multi-stage cascade membrane systems under the constant recycle ratio scheme for the bench separation system. (a) single-stage; (b) two-stage stripping cascade; (c) two-stage enriching cascade; (d) three-stage with feed to the first stage; (e) three-stage with feed to the second stage; (f) three-stage with feed to the third stage.

Fig. 5.7 shows the attainability curves at constant stage-cut scheme for two and three stage membrane systems. The separation task is the same as that in Fig. 5.6. For comparison purpose, Fig. 5.7a shows again the attainability curve of the single-stage membrane system. The two-stage system in Fig. 7b and the three-stage system in Fig.

5.7d have no enriching section. In this case the stripping stages will have a fixed stage-cut value and therefore, there is only one curve shown in each diagram. Fig. 5.7c shows the attainability curves of the two-stage enriching cascade at different enriching stage-cut values. When the enriching stage-cut decreases, the attainability curve will move towards the direction of lower selectivity and lower pressure ratio. The enriching stage-cut value of 1 and 0 define the two boundaries of these curves. When the enriching stage-cut is 1, the attainability curve is identical to the single-stage membrane system in Fig. 5.7a. This is because in this case the entire feed in the enriching stage will go to the permeate and therefore, there is no flow in the retentate stream. Since this can be achieved simply by a membrane stage with zero membrane area, so it is equivalent to the case where the enriching stage is disappeared and only the stripping stage is left in the system. This explanation can also be used to understand the diagrams in Fig. 5.7e and 5.7f for three-stage membrane systems with feed to the second and third stages, respectively. In Fig. 5.7e, when the enriching stage-cut is 1, the attainability curve is identical to the two-stage stripping cascade shown in Fig. 5.7b, while in Fig. 5.7f, the attainability curve is identical to the single-stage membrane system. The reason is because the enriching stages in this case are disappeared, so two stages in Fig. 5.7e and one stage in Fig. 5.7f is left in the stripping section. When the enriching stage-cut becomes 0, the attainability curve in Fig. 5.7c is identical to the absolute minimum attainability curves for two-stage systems in Fig. 5.6b and 5.6c, while the attainability curves in Fig. 5.7e and 5.7f are identical to the absolute minimum attainability curves for three-stage systems in Fig. 5.6e and 5.6f. This can be explained by considering the flows in the first enriching stage where the product is extracted from the permeate stream. To reach stage-cut of 0, the feed flow must be

infinity, and so is the retentate flow and the recycle ratio. It can be easily derived that the recycle ratio in the stripping stages will also be infinity. Hence, in this case the attainability behaviors of Fig. 5.7c is equivalent to Fig. 5.6b and 5.6c, and the attainability behaviors of Fig. 5.7e and 5.7f are equivalent to Fig. 5.6e and 5.6f. From the above discussions, a generalized conclusion can be drawn as follows for all multi-stage membrane systems in constant stage-cut scheme. When enriching stage-cut is 1, the attainability behaviors of multi-stage membrane systems will decay to only stripping stages, while when the enriching stage-cut is 0, the attainability behavior reaches the absolute minimum attainability curve of the same number of stages.





**Fig. 5.7** Attainability of multi-stage cascade membrane systems under the constant stage-cut scheme for the bench separation system. (a) single-stage; (b) two-stage stripping cascade; (c) two-stage enriching cascade; (d) three-stage with feed to the first stage; (e) three-stage with feed to the second stage; (f) three-stage with feed to the third stage.

### 5.5.2 Energy consumption of membrane systems

The energy consumption in multi-stage cascade systems is mainly used to drive the inter-stage pumps to provide the required pressure ratio in each stage. The energy consumption is a function of selectivity and pressure ratio. However, the energy consumption is an optimal function over pressure ratio. Equations (5.10-5.12) are derived to calculate the minimum energy at optimal pressure ratio for single-stage, two-stage and three-stage membrane systems, respectively. The separation of propylene/propane is used as a bench system where 96% purity of propylene in the permeate stream and 95% recovery ratio should be achieved from an equimolar feed. For comparison purpose, the energy consumption by a conventional distillation process to achieve the same separation task is calculated from equation (5.14). The physical properties used in calculation are the following:  $\alpha = 1.3$  (relative volatility of propylene to propane),  $C_p = 56$  J/mol K

(mixture specific heat capacity) and  $\lambda = 18.8 \text{ kJ/mol}$  (propane latent heat of vaporization).

The minimum distillation energy is reached at the reflux ratio around 7.0, where the energy consumption is about 78 kJ/mol.

Fig. 5.8a-5.8c shows the energy consumption of the bench system under optimal pressure ratios in single-stage, two-stage enriching cascade and three-stage cascade with feed entering to the second stage, respectively. For single-stage membrane system, the energy increases sharply when the selectivity is less than a certain value and this value is actually the minimum selectivity at the optimal pressure ratio. This result indicates that a single-stage membrane system is able to achieve much lower energy consumption, but the required selectivity is very high. For multi-stage membrane systems, when recycle ratio is zero, the energy curves are equal to the single-stage membrane system. However, slightly increasing the recycle ratio, for example, a recycle ratio of 0.1 in all three multi-stage membrane systems, leads to slightly reduction in energy consumption, but significant reduction in the required membrane selectivity. Three-stage membrane system requires much lower selectivity than that of the two-stage membrane systems, indicating that the higher the number of stages, the more reduction is in the required membrane selectivity. However, further increasing the recycle ratio will increase the energy consumption. When the recycle ratio is 100, the energy consumptions in multi-stage membrane systems are too high to compete with the existing distillation process. The reason is obviously since too much energy will be required to drive inter-stage streams.

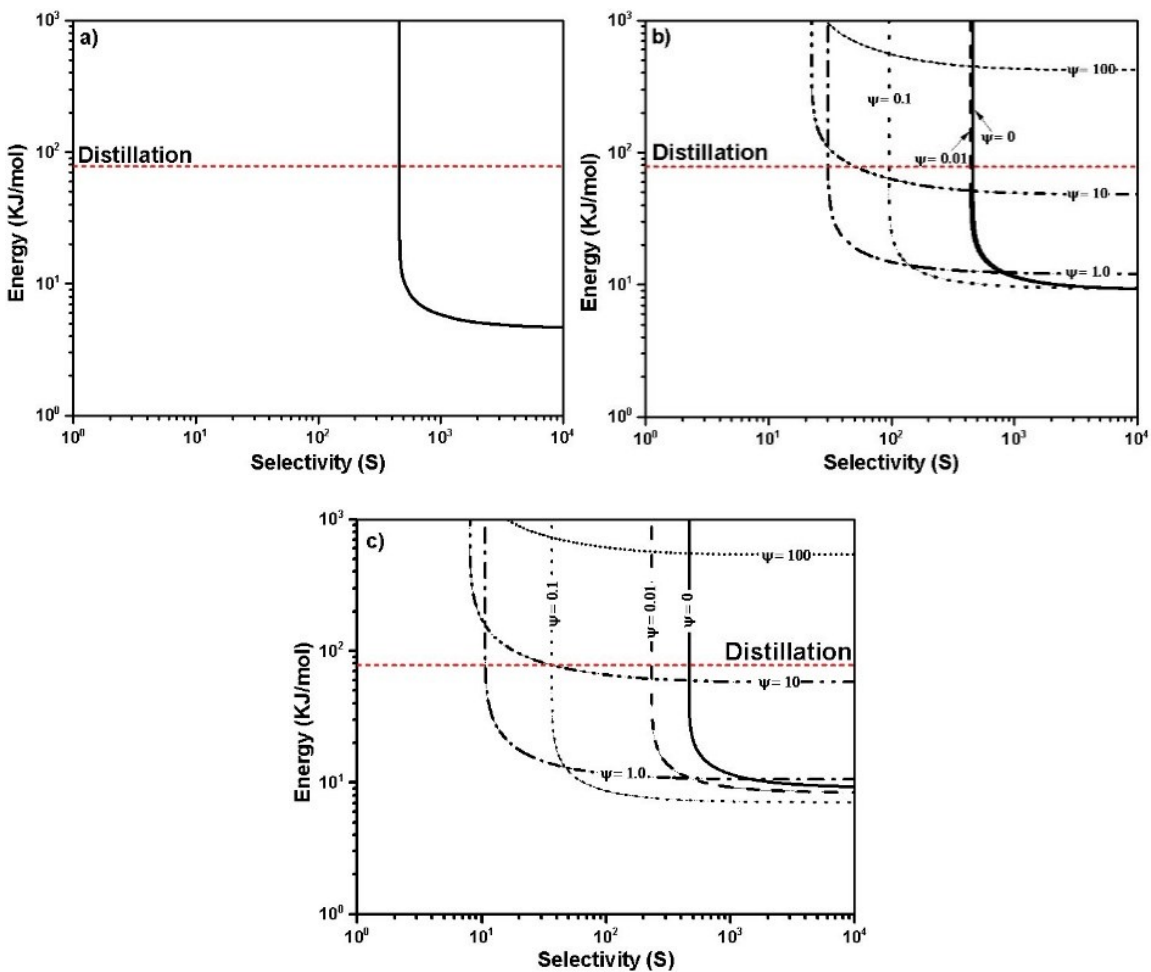


**Fig. 5.8** Energy consumption by multi-stage cascade membrane systems for the bench separation system (a) single-stage; (b) two-stage enriching cascade; (c) three-stage with feed to the second stage. The red dotted line shows the energy consumption of the distillation process for the bench separation system.

To demonstrate the effect of the recycle ratio, we can further use the mathematical technique known as “envelope of family of curves in plane” [24] to plot the tangent line to the lowest energy points at various recycling ratios as illustrated in Fig. 5.9 for three-stage cascade with feed entering to the second stage. Each point on this curve tells the minimum energy that can be achieved by the three-stage cascade at that membrane

selectivity. For example, the envelope curve meets the distillation energy curve at selectivity around 10. This means when a membrane with selectivity of 10 is used in each stage, the minimum energy that can be achieved by a three-stage cascade will be equal to the distillation process. In another word, to compete with the distillation process by a three-stage membrane cascade, the minimum required membrane selectivity is around 10. Therefore, this curve will provide a guideline for selectivity in multi-stage membrane cascade designs.

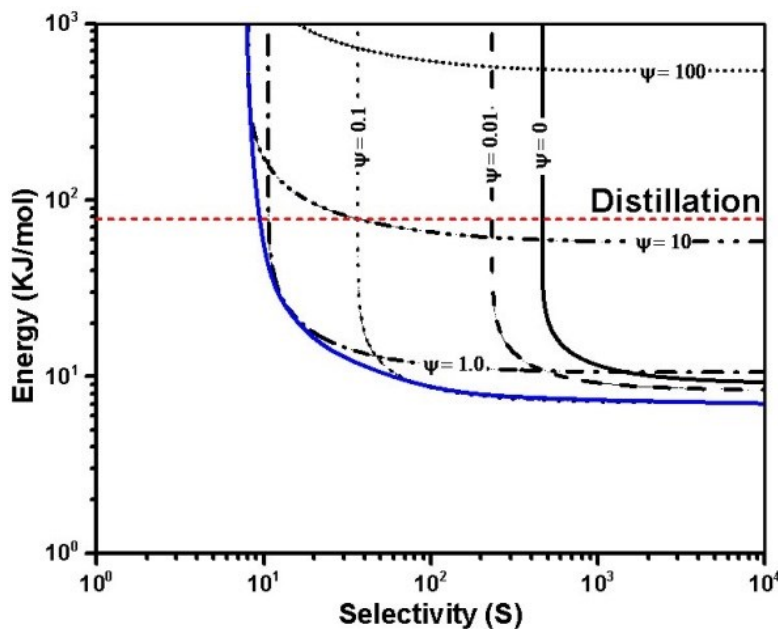


**Fig. 5.9** Illustration of the minimum energy consumption at different membrane selectivity in the three-stage with feed to the second stage cascade system for the bench separation system. Blue line is the energy envelope curve generated by the theory of “envelope of family of curves in plane”. Red dotted line shows the energy consumption of the distillation process for the bench separation system.

## 5.6 Conclusions

In summary, the attainability curves and the minimum energy consumption of multi-stage membrane cascade systems are studies using the simplest well-mixed membrane model under two schemes: constant recycle ratio and constant stage-cut. The following useful guidelines are obtained in both schemes. First, to meet a certain separation task that is defined by feed concentration  $x_A$ , product purity enrichment  $\varepsilon$  and recover ratio  $\eta$ , the attainability curves of multi-stage membrane cascade systems are defined by membrane selectivity  $S$  and pressure ratio  $\gamma$ . Recycle ratio or enriching stage-cut will shift the attainability curve. When increasing the recycle ratio from 0 to infinity or decreasing the enriching stage-cut from 1 to 0, the attainability curve will move towards lower selectivity and lower pressure ratio. In the constant recycle ratio scheme, when recycle ratio is 0, the attainability behaviour of any multi-stage membrane cascade systems will decay to that of a single-stage membrane process. When recycle ratio approaches to infinity, the selectivity and pressure ratio will reach to the absolute minimum selectivity and absolute minimum pressure ratio which have the following simple relationships with the minimum selectivity and pressure ratio of a single-stage membrane system:  $S_n = \sqrt[n]{S_1}$ ,  $\gamma_n = \sqrt[n]{\gamma_1}$ . In the constant stage-cut scheme, when the enriching stage-cut is 1, the attainability behavior of multi-stage membrane cascade systems will decay to the membrane system that contains only the stripping stages. When the enriching stage-cut approaches 0, then it is equivalent to the infinity recycle ratio scheme and the selectivity and pressure ratio will reach to the absolute minimum selectivity and absolute minimum pressure ratio.

Second, the energy consumption of multi-stage membrane systems is found primary determined by membrane selectivity. In general the higher the membrane selectivity, the lower is the energy consumption. Using a small recycle ratio will not change the energy consumption much, but can significantly reduce the required membrane selectivity. This indicates the benefit of using recycle streams in the membrane cascade designs. However, using a large recycle ratio will cause a big energy penalty, although it may further reduce the required membrane selectivity and pressure ratio and such benefit will become more and more marginal at larger recycle ratio. The minimum energy consumption at different membrane selectivity can be found by the energy envelope. This envelope curve can provide a simple way to find the minimum required membrane selectivity for multi-stage membrane designs in order to compete with conventional separation techniques from the energy point of view.

## 5.7 References

- [1] M.B. Hagg, Membranes in chemical processing - A review of applications and novel developments, *Separ. Purif. Method.*, 27 (1998) 51-168.
- [2] A. Alshehri, Z.P. Lai, Attainability and minimum energy of single-stage membrane and membrane/distillation hybrid processes, *J. Membr. Sci.*, 472 (2014) 272-280.
- [3] J. Wilcox, Carbon capture, Springer, New York, 2012.
- [4] R.W. Baker, Membrane technology and applications, 2nd ed., J. Wiley, Chichester ; New York, 2004.
- [5] I. Song, H. Ahn, H. Jeon, H.K. Jeong, Y. Lee, S.H. Choi, J.H. Kim, S.B. Lee, Optimal design of multiple stage membrane process for carbon dioxide separation, *Desalination*, 234 (2008) 307-315.
- [6] A. Brunetti, E. Drioli, Y.M. Lee, G. Barbieri, Engineering evaluation of CO<sub>2</sub> separation by membrane gas separation systems, *J. Membr. Sci.*, 454 (2014) 305-315.
- [7] R.H. Qi, M.A. Henson, Membrane system design for multicomponent gas mixtures via mixed-integer nonlinear programming, *Comput. Chem. Eng.*, 24 (2000) 2719-2737.
- [8] F. Ahmad, K.K. Lau, A.M. Shariff, G. Murshid, Process simulation and optimal design of membrane separation system for CO<sub>2</sub> capture from natural gas, *Comput. Chem. Eng.*, 36 (2012) 119-128.
- [9] R. Pathare, R. Agrawal, Design of membrane cascades for gas separation, *J. Membr. Sci.*, 364 (2010) 263-277.
- [10] J.G. Xu, R. Agrawal, Membrane separation process analysis and design strategies based on thermodynamic efficiency of permeation, *Chem. Eng. Sci.*, 51 (1996) 365-385.

- [11] R. Agrawal, J.G. Xu, Gas separation membrane cascades .2. Two-compressor cascades, *J. Membr. Sci.*, 112 (1996) 129-146.
- [12] S. Kheawhom, M. Hirao, Decision support tools for environmentally benign process design under uncertainty, *Comput. Chem. Eng.*, 28 (2004) 1715-1723.
- [13] L.K. Wang, *Membrane and desalination technologies*, Humana Press, New York, NY, 2011.
- [14] R. Smith, *Chemical process design and integration*, Wiley, Chichester, West Sussex, England ; Hoboken, NJ, 2005.
- [15] R. Khalilpour, K. Mumford, H. Zhai, A. Abbas, G. Stevens, E.S. Rubin, Membrane-based carbon capture from flue gas: a review, *J. Cleaner Prod.*, (2014).
- [16] M.M. Qiu, S.T. Hwang, Y.K. Kao, Economic-Evaluation of Gas Membrane Separator Designs, *Ind. Eng. Chem. Res.*, 28 (1989) 1670-1677.
- [17] A.K. Datta, P.K. Sen, Optimization of membrane unit for removing carbon dioxide from natural gas, *J. Membr. Sci.*, 283 (2006) 291-300.
- [18] J.G. Xu, R. Agrawal, Gas separation membrane cascades .1. One-compressor cascades with minimal exergy losses due to mixing, *J. Membr. Sci.*, 112 (1996) 115-128.
- [19] R.H. Qi, M.A. Henson, Optimal design of spiral-wound membrane networks for gas separations, *J. Membr. Sci.*, 148 (1998) 71-89.
- [20] K. Hattenbach, A New-Work Diagram Suitable for Pervaporation and Gas Separation under Cross Flow, *J. Membr. Sci.*, 36 (1988) 405-412.
- [21] S.A. Stern, S.C. Wang, Permeation Cascades for the Separation of Krypton and Xenon from Nuclear-Reactor Atmospheres, *AIChE J.*, 26 (1980) 891-901.
- [22] M.S. Avgidou, S.P. Kaldis, G.P. Sakellaropoulos, Membrane cascade schemes for the separation of LPG olefins and paraffins, *J. Membr. Sci.*, 233 (2004) 21-37.

- [23] I.J. Halvorsen, S. Skogestad, Minimum energy consumption in multicomponent distillation. 1. V-min diagram for a two-product column, Ind. Eng. Chem. Res., 42 (2003) 596-604.
- [24] G.A. Anastassiou, I.F. Iatan, Differential Geometry of Curves and Surfaces, in: Intelligent Routines II, Springer, 2014, pp. 197-234.

## 6. Systematic Synthesis and Optimization of Membrane Networks for Gas Separation

### 6.1 Introduction

The distillation process is the conventional method for separating most gas mixtures in the chemical and petrochemical industry. However, the technology suffers from low efficiency as the boiling points of the components approach each other. Thus, the distillation column consists of large number of trays and operates at high reflux ratio which results in high capital investment and energy consumption. The high cost of the distillation process has motivated the industry to explore alternative processes. In order to recommend a membrane system for a specific separation process, it should be proven that it can perform better separation, or has better economics compared with the competing separation processes. Studying the energy consumption by the membrane cascade systems in Chapter 5 motivated us to conduct a comprehensive economic analysis.

Membrane technology can be adopted in the form of a single or multi-stage network based on separation requirements, product price and energy penalty. As seen in many industrial applications, single-stage membrane separation has limitations in achieving high quality permeate or retentate while typically the objective of separation is either of these. The situation becomes even more challenging for membrane technology when the two products are valuable, as in the application of olefin/paraffin split process. Thus, the separation objective is to produce high purity and recovery ratio. As such, more stages are required and their setup is crucial to performance and viability. The first solution, to

the best of our knowledge, was a patent by Pfefferle who presented a two-stage system with permeate recycle in order to reach high purity permeate. Following the two-stage presentation, a cascade of membrane systems was introduced for a binary gas mixture separation [1, 2]. Gruzdev et al. [3] proposed a method for calculation of a cascade system when there is a multicomponent gas mixture. Some studies have moreover proposed using different membrane materials in the cascade system [4].

It is however discussed that, except at very low concentration of the target component in the feed gas or having low-efficiency membrane [5], membrane systems consisting of two [1] or three stages [6] are the most techno-economically optimal configurations. It is also proven that introducing more stages, though resulting in slightly less membrane areas and compression energy, the increase in number of compressors ultimately neutralizes these advantages [6]. Hence, a number of studies for optimal configurations focused on two/three-stage membrane systems. Kao et al. [7] compared two systems. One was the so-called continuous membrane column (CMC) and the other one was two strippers in series permeator (TSSP). They reported sweet-spot operating condition for each configuration. According to them, TSSP is superior to CMC configuration unless the objective is to minimize the membrane area or to accomplish high permeate purity. A similar conclusion was reported by Qiu et al. [8] as a result of economic evaluation stating that TSSP is the most efficient configuration when the objective is high quality retentate, while for the case of high quality permeate, CMC is more efficient.

Bhide and Stern [9] studied seven different one-, two-, and three-stage configurations with respect to minimum costs. They found that a three-stage system with a single permeation stage in series with a two-stage permeation cascade with recycle was the most efficient design. Pettersen and Lien [6] studied the intrinsic behavior of several single-stage and multi-stage permeator systems. They also divided the multi-stage system into enriching and stripping cascades which could be two or three-stages. According to them, if the objective is to have retentate with minimum concentration of the high permeable component, then the upstream section of cascade (stripping) will be chosen while for high purity permeate product, downstream section (enriching) is the best choice.

Datta and Sen [10] techno-economically reviewed ten different one-, two-, and three-stage configurations for natural gas sweetening. They reported that the selection of the best configuration is highly related to the feed quality, separation objectives and market values. Also, the optimum configuration was found unique in a certain range of feed quality, separation policy and market price.

In general, there are two approaches followed in literature for membrane network synthesis. The first one, which is heavily considered, focuses on studying all the possible network configurations or the most promising ones from the knowledge gained from the open literature [9]. The most considered designs of the network are the Continuous Membrane Column (CMC) and the Recycle Membrane Cascades (RMC). This approach eliminates many network designs from which the optimal design could be. The other approach synthesizes the membrane network through the superstructure optimization technique [6, 10]. In this technique any stage product stream is a potential candidate feed

to any membrane stage in the network including the stage from which this stream was produced. Therefore, the number of process setup alternatives increases exponentially with the number of stages. This makes this analysis method unfavorable for membrane network investigation especially when the adopted membrane model requires an iterative algorithm as the one to be used in this study.

This chapter provides a systematic procedure for membrane network flowsheet optimization which relies on the concept of superstructure technique and membrane network conceptual design knowledge gained from literature studies. This produces a simplified membrane superstructure which makes the optimization problem size manageable and can be implemented in process simulation software. The network economics and product specifications are used to identify the optimal structure subjected to the specific membrane properties (permeance and selectivity) and cost parameters (membrane area price and membrane lifetime). Economic evaluation of the optimal membrane network in comparison to the conventional separation process can be of great importance to membrane synthesis researchers as discussed in this paper for the separation of propylene/propane mixture.

## **6.2 Network superstructure modelling and optimization**

The superstructure optimization is a technique aiming to define the optimal flowsheet design. It determines equipment locations and stream interconnections corresponding to the optimal objective function and within the specified constraints. The superstructure optimization problem can be simplified by excluding the non-practical alternatives and

considering conceptual design knowledge gained from literature studies and industry best practices.

The separation policy for processes producing high market value products such as olefin/paraffin split processes imposes high purity and high product recovery ratio. Achieving high purity of permeate stream mandates the use of an enriching section while the requirement of high recovery ratio mandates the use of a stripping section. In literature, it was concluded that the use of one or two stripping stages after the feed stage was optimal to produce high purity retentate stream [6, 9]. Also, the optimal design was found to consist of one or two stages upstream of the feed stage to produce high purity of the high permeable component [5]. Thus the membrane network considered in this study consists of a feed stage, two enriching stages and two stripping stages.

Superstructure optimization of a multi-stage membrane network in a process simulator produces a complicated flowsheet as the number of network stages increase. Moreover, the solution iterations exponentially increase. Consequently, considering a superstructure optimization of more than four stages becomes relatively impossible as the number of optimization parameters increase. The proposed simplified superstructure helps to keep the problem size manageable without decomposition and thus possible for implementation in process simulation software. Superstructure optimization in a process simulator such as ASPEN PLUS® or Aspen HYSYS® offers an accurate and time saving means to simulate the entire process since:

1. Most of unit operations such as compressors, pumps, mixers, splitters and heat exchangers have built-in models.

2. Optimization toolbox is available and made easy to formulate an optimization problem.
3. It has the capability to calculate material and energy balances and provide accurate estimation of physical and thermodynamic properties.
4. Process constraints for unit operations are software specified.

The building blocks used to create the membrane network for the superstructure optimization are hollow fiber membrane modules, mixers, splitters, compressors and heat exchangers as shown in Fig. 6.1. A membrane stage exists only if its area is greater than zero while a mixer block defines an expected stream connection point. The stream connection point is only confirmed if the stream split ratio is greater than zero. Compression and cooling are applied to all permeate streams to meet the temperature and pressure requirements for the specific mixing point.

The upstream section of the network enriches the concentration of the least permeable component and at the same time enhances the recovery of the high permeable component. On the other hand, the downstream section enriches the high permeable component concentration and maximizes the recovery of the least permeable component. Therefore, any connection of a retentate stream in the upstream section to the downstream section breaks the logical sequence of permeate enriching. Likewise, any connection of a permeate stream in the downstream section to the upstream section increases the system entropy and lowers the separation efficiency. Thus, such connections should be avoided. To enrich the purity of the least permeable component, any retentate stream in the upstream section can be recycled to any stage not in permeate enriching section

(downstream section) including the feed stage. This also applies to recycle of a permeate stream in the downstream section so, permeate stream recycle should be to the same stage, upstream stages in the same section or the feed stage.

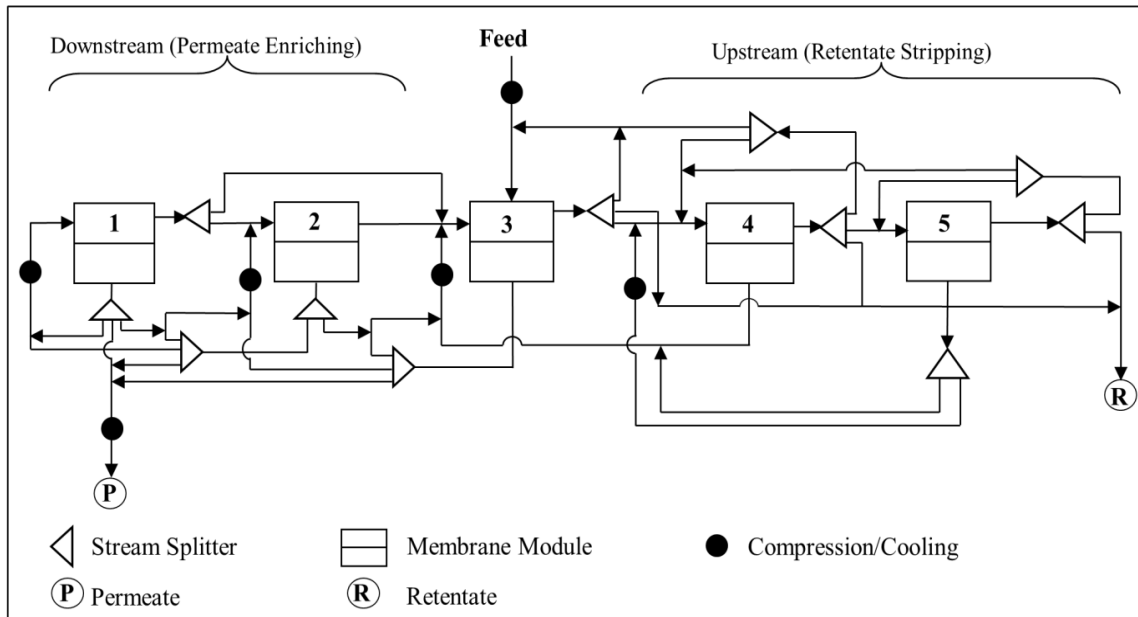


**Fig. 6.1** Schematic of a five-stage membrane superstructure.

### 6.3 Membrane network optimization

The efficiency of a multi-stage membrane network depends on the performance of each permeation unit besides that of the network due to the presence of recycle streams. Thus, optimizing each stage separately does not necessarily lead to the optimal design of the network. Also, designing a multi-stage membrane network without considering an optimization technique is a very difficult and time-consuming task as it requires consideration of all possible configurations at different operating conditions, split ratios and location of recycle streams.

The Total Annualized Cost (TAC) of the process is selected as an indicator to assess the economic attractiveness of investment in membrane technology to minimize the separation cost. The total annual cost is the sum of capital investment, utilities, maintenance, eventual replacement costs, and labor salaries. In the case of membrane gas separation plant the maintenance and labor costs are very low compared to power bill [11]. Therefore, these costs can be either ignored or just added as a fraction of the capital cost. Then, the network annualized cost is simplified to the sum of the annual cost of capitals and operating cost. Equipment annual cost is calculated by multiplying the equipment capital expenditure (CAPEX) by the depreciation factor ( $r$ ) [12]. Therefore, the optimization objective function can be written as:

$$\text{Minimize } \mathbf{TAC} = (\mathbf{OPEX} + r \times \mathbf{CAPEX}) \quad (6.1)$$

The membrane network capital expenditure includes the capital investment of membrane modules ( $\text{CAPEX}_{\text{memb}}$ ), compressors ( $\text{CAPEX}_{\text{comp}}$ ) and heat exchangers ( $\text{CAPEX}_{\text{HX}}$ ). Therefore, it can be described as:

$$\text{CAPEX}_{\text{memb}} = \text{CAPEX}_{\text{memb}} + \text{CAPEX}_{\text{comp}} + \text{CAPEX}_{\text{HX}} \quad (6.2)$$

The membrane module cost is calculated using the following formula:

$$\text{CAPEX}_{\text{memb}} = r (\text{Area} \times \text{Unit Area Price} \times \text{Membrane Lifetime}) \quad (6.3)$$

The compressor capital investment is calculated from its breaking horsepower (bhp) and the heat exchanger capital investment is calculated as a function of surface area ( $A_{\text{HX}}$ ) using Guthrie [13] economic model. The model cost functions are timely updated using the Marshal and Swift index (M&S) as per the following two equations:

$$CAPEX_{comp} = \left(\frac{M \& S}{280}\right) 1610 bhp^{0.82} \quad (6.4)$$

$$CAPEX_{HX} = \left(\frac{M \& S}{280}\right) 378.9 A_{HX}^{0.65} \quad (6.5)$$

The cost elements considered in the economic evaluation are:

- 1- The capital equipment cost is calculated based on the Marshall and Swift index of 2013.
- 2- The electric power cost is considered to be fixed at 0.06 \$/kWh [14].
- 3- The cost of cooling water is 0.354 \$/GJ [14].
- 4- The cost of steam used in the reboiler is 8.0 \$/GJ [15].
- 5- The membrane lifetime span is assumed to be 2 and 5 years.

The membrane network operating expenditure (OPEX) is calculated based on equipment duties and the corresponding utility costs as described earlier and defined by Eq. (6.6) assuming a total operating time of 8000 hours annually.

$$\begin{aligned} OPEX &= OPEX_{comp} + OPEX_{HX} \\ &= 8000(0.06 D_{comp} + 0.354 D_{HX}) \end{aligned} \quad (6.6)$$

Where,  $D_{comp}$ , and  $D_{HX}$  are the compressor and heat exchanger duties per hour (GJ/h), respectively. In order to control products quality then permeate and retentate purities should be specified as optimization constraints. Providing the optimization constraints in the form of single purity and recovery, the following two constraints are considered:

$$\frac{\sum_{k=1}^{stages} M_j^i}{\sum_{k=1}^{stages} M_j} \geq Purity \ Target \quad (6.7)$$

$$\frac{\sum_{k=1}^{stages} M_j^i}{M_f^i} \geq Recovery \ Target \quad (6.8)$$

Where,  $M_k^i$  is component  $i$  molar flow rate of stage  $k$  product,  $M_k$  is total molar flow rate of stage  $k$  product and  $M_f^i$  is component  $i$  molar flow rate in feed stream.

The optimization variables for each stage are the membrane area and the split ratio of permeate and retentate streams. The feed pressure to all network stages is fixed with also fixed pressure ratio across the membrane. In this study, the membrane network performance will be evaluated over wide ranges of membrane separation parameters (permeance and selectivity) to cover the existing membranes as well as the potential high performance future membranes. The promising membranes for the separation of propylene/propane (case study) are polymeric membranes, carbon molecular sieve membranes (CMS), mixed matrix membranes and facilitated transport membranes. Table 6.1 lists some of the reported high performance membranes for this application and shows their selectivity. The membrane synthesis cost per unit area differs significantly from one membrane category to another. Polymeric membranes cost is in the range of 50 to 100 US\$/m<sup>2</sup> [16]. The cost of CMS membranes is at least ten times higher than polymeric membranes. The cost of mixed matrix membrane depends mostly on loading

ratio and cost of CMS. For the most practical loading ratios between 20 to 40%, the membrane cost is estimated to be in the range of 400-500 US\$/m<sup>2</sup>. Therefore, membrane performance is just part of the story in the selection of the optimal process and membrane cost also plays a significant role. Thus, the membrane network techno-economical evaluation will be carried out over a price range that covers all discussed membrane categories.

**Table 6.2:** High performance membrane for propylene/propane separation.

Membrane	Permeance (GPU)	Selectivity	Reference
ZIF-8/6FDA-DAM Mixed Matrix	40	25	[17]
ZIF-8	100	35	[18]
Asymmetric Polyimide	50	13	[19]
PU/AgCF <sub>3</sub> SO <sub>3</sub>	188	10	[20]

## 6.5 Case study description

The application of polypropylene in the manufacture of plastics, makes propylene the second most used raw material in petrochemical industry after ethylene. Propylene is also used as feedstock for many chemical products [6]. Therefore, the demand for the propylene is forecasted to increase with an average annual rate of 5.7% [21]. Propylene production was 77 million tonnes in year 2011 and the production is anticipated to reach 132 million tonnes by year 2025 [22]. Propylene is mainly produced as a by-product from either Steam Cracking Unit (SCU) or Fluid Catalytic Cracking (FCC). These two processes account for about 89% of worldwide propylene production [22]. The remaining fraction is produced through dehydrogenation of light olefins, metathesis of ethylene and

butylene as well as other low production processes. The concentration of propylene produced from refinery FCC unit or ethylene production process is about 70% while the polymerization feed stream should be uniform and relatively pure to produce high quality polypropylene. Thus, the separation objective for propylene/propane split unit is to produce polymer grade propylene at a purity of 99.5% and a recovery ratio higher than 99%.

The existing distillation column described by Gokhale [23] and further optimized by Kokos [24], will be used as a comparison benchmark for the network economic evaluation. Thus the same feed will be fed to the membrane network. The feed stream consists of 70% propylene and 30% propane at flow rate of 0.3 kmol/s (0.45 tonne/yr). This feed is available as pressurized gas mixture at 14.55 bars and 34°C.

The distillation column consists of 248 trays including the condenser and reboiler. The Peng-Robinson equation of state is used to model vapor-liquid equilibrium. Design of the optimal distillation column to achieve the separation objectives is schematically described in Fig. 3. Considering the Guthrie economic model [13] for equipment cost estimation and utilities cost described earlier, the distillation process was found to correspond to a total annualized cost of M\$12.3.

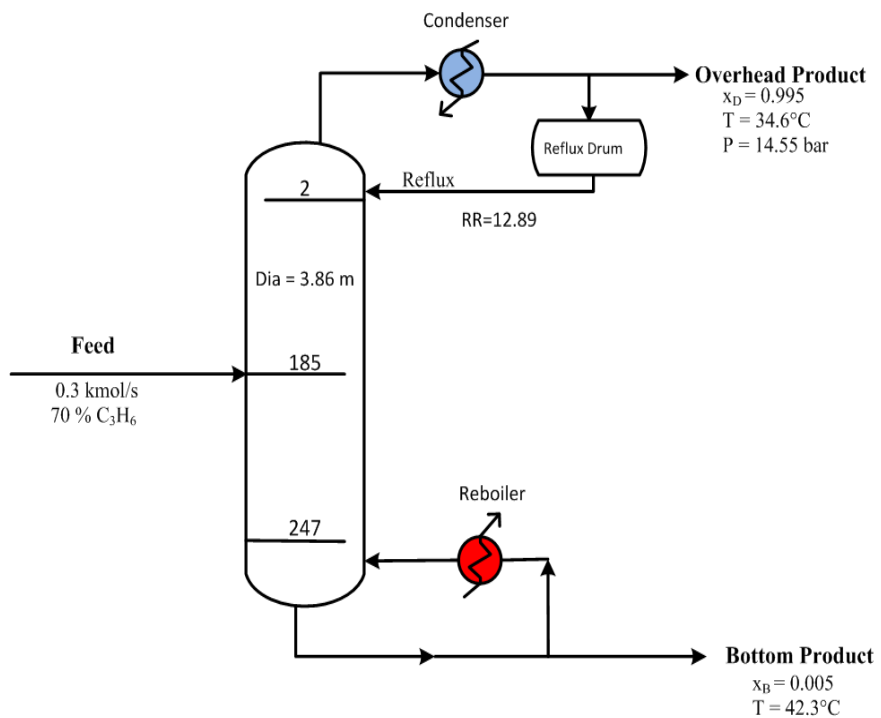


**Fig. 6.2** Conventional distillation process for propylene/propane separation.

## 6.6 Results discussion

To illustrate, the analysis method will be followed; the superstructure discussed earlier in Fig.6.1 is used to synthesis a membrane network that can meet the separation task requirements and corresponding to the minimum TAC for a specific membrane performance. The membrane selectivity and permeance in all stages are adjusted to 35 and 100 GPU, respectively. These values of selectivity and permeance are reported for ZIF-8 material in reference 29. The design of the optimal network is illustrated in Fig. 6.3. The network TAC is calculated to be 5.1 M\$/year. The contribution of the different cost elements is shown in Fig. 6.4. Hence, a membrane system with such performance, 5 years lifetime and membrane area cost of \$100/m<sup>2</sup> can reduce the separation cost by 58% compared to the conventional distillation process.

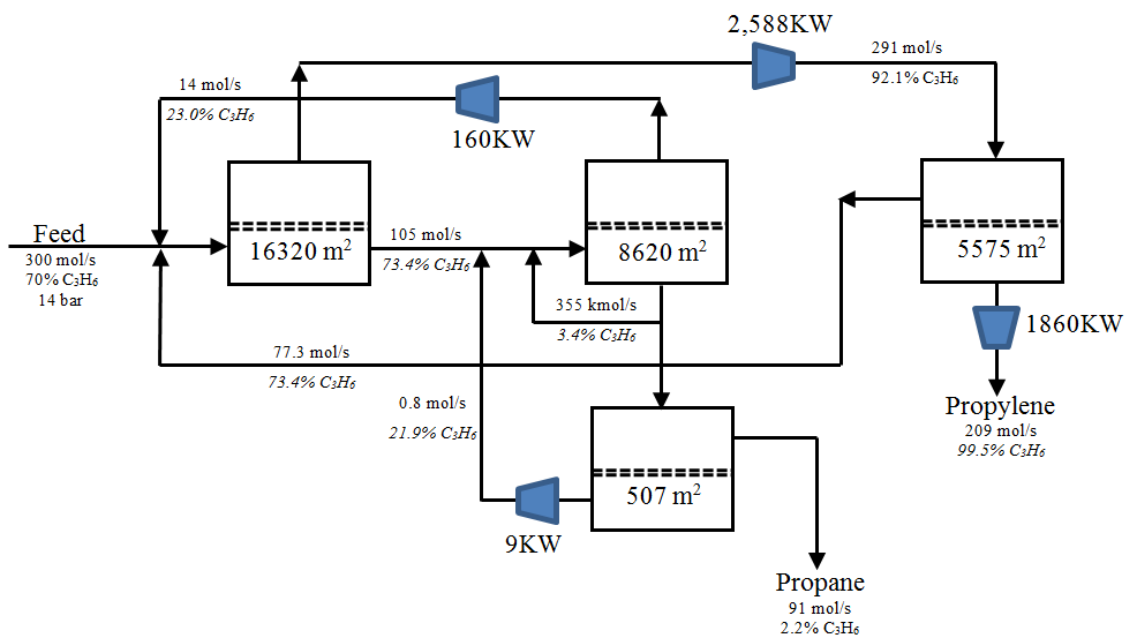


**Fig. 6.3** The optimal membrane network corresponds to the minimum annualized cost for a membrane material with selectivity of 35 and permeance of 100 GPU at a fixed pressure ratio of 14. The membrane unit area price including installation is assumed to be 100 U\$/ $m^2$  and the membrane lifetime is assumed to be 5 years.

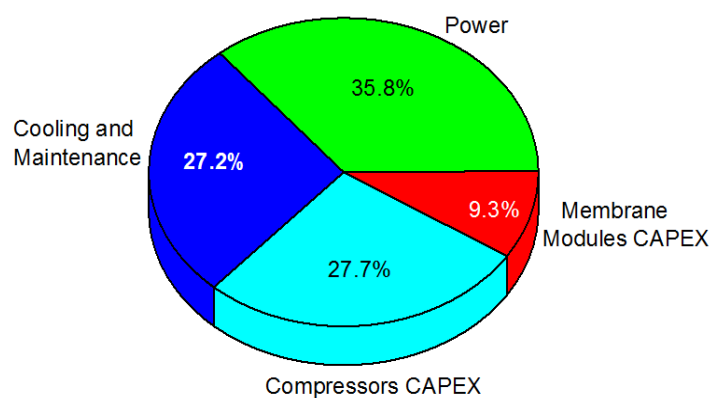


**Fig. 6.4** The cost distribution for the membrane process in Fig. 6.3.

Now, the same analysis will be followed for each of the three different membrane costs (100, 500 and 1000 \$/ $m^2$ ) and at membrane lifetimes of 5 and 2 years. For all

combinations of the cost elements, the analysis is to be conducted over wide ranges of selectivity and permeance. Fig. 6.5a illustrates the network optimal cost against membrane selectivity and permeance at membrane price of 100 \$/m<sup>2</sup> and lifetime of 5 years. At such low membrane price, the optimal network design shows higher feasibility than the conventional distillation process at selectivity and permeance higher than 9 and 10 GPU, respectively. At a fixed membrane permeance and as the selectivity increases, the cost of the optimal design sharply decreases till the selectivity reaches a value of 40. After this selectivity, the process annual cost turns out to be less dependent on the membrane selectivity. Also, the annualized cost of the membrane network at its optimal configuration is less than 6.8 M\$ if the membrane selectivity is at least 40 along with permeance higher than 20 GPU. This is because the membrane cost becomes in a lower order of magnitude than to the overall annual cost.

As the membrane durability is reduced, the membrane network requires higher membrane performance (selectivity and permeance) to breakeven with the distillation process. Fig. 6.5b illustrates the scenario with membrane durability of 2 years. At the same membrane price per unit area, the minimum membrane performance for feasible membrane network is found at permeance of 20 GPU and selectivity of 14. The network cost decreases as the permeance increases but at a slower rate as the selectivity increases. As the selectivity exceeds 40, the system cost behaves independently from selectivity. At selectivity of 40 and permeance of 40 GPU, the membrane network cost is reduced to 6.8 M\$/year. Therefore, the decrease in membrane durability from 5 to 2 years and at membrane selectivity of 40, the permeance at which the network cost is less than 6.8 M\$/year increases from 20 to 40 GPU.

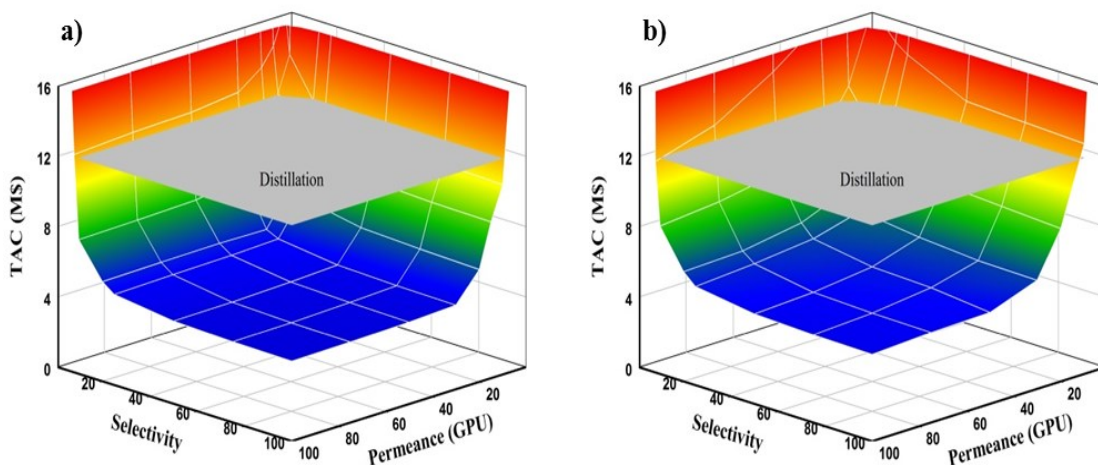
Fig. 6.5c illustrated the results of a scenario with relatively high membrane price of 500 \$/m<sup>2</sup> when the lifetime is 5 years. The membrane network starts to be more feasible only at permeance values above 50 GPU with minimum selectivity of 20. As the permeance increases, the required selectivity becomes lower. Thus, at membrane permeance of 70 GPU the minimum selectivity required to make the network at a break-even point with distillation is 10. When permeance is higher than 80 GPU and selectivity is higher than 40, the cost function becomes less sensitive to selectivity change. Over the considered range of permeance and selectivity, the optimal network design shows system cost of less than 6.7 M\$/year at permeance of 90 GPU and selectivity of 70. As the membrane durability decreases from 5 to 2 years, the challenge to membrane separation becomes more as shown in Fig. 6.5d. The multi-stage network shows feasibility only at permeance higher than 75 and selectivity of at least 50. As the membrane permeance increases to 150 GPU, the minimum selectivity required to meet the break-even point with distillation process is reduced to 17.

Fig. 6.5e illustrates the results of the scenario with extremely high membrane price of 1000 \$/m<sup>2</sup> and lifetime of 5 years. It is evident from the obtained network cost function, even at such a high membrane price; the membrane process is still competitive with distillation process though at higher permeance and selectivity. Under this scenario, membrane network starts to outperform distillation process at permeance of 75 GPU with minimum selectivity of 30. As the permeance increases to 150 GPU the minimum selectivity required to make the network at a break-even point with distillation is 15. It is also noticed that at membrane permeance and selectivity higher than 130 GPU and 70 respectively, the membrane cost becomes a stronger function of the permeance than the

selectivity. According to Fig. 6e, if at the given conditions, if a membrane has permeance of 150 and selectivity of 70 materialize, it can result in separation cost of about 6.5 M\$/year which is almost half that of the distillation process. As the membrane durability decreases from 5 to 2 years, the separation becomes more challenging and it is only viable at extremely high membrane permeance as shown in Fig. 8f. The multi-stage network shows break-even with the base case distillation process only at permeance higher than 150 and selectivity of at least 40. Even at such a high membrane price and low durability, and given the existence of a membrane with permeance of 300 GPU and selectivity of 100, the multi-stage membrane network total annualized cost becomes 7.86 M\$ which is 36% less than that for distillation process.

At membrane price of 100, 500 and 1000 \$/m<sup>2</sup> and selectivity lower than 50, the optimal design consists of a feed stage, a single enriching stage and two stripping stages. This is due to the fact that at low membrane selectivity (as the propylene partial pressure decreases) more than one stripping stage is needed to achieve high recovery and recycle permeate to increase propylene partial pressure. The increase in membrane selectivity is expected to enhance the product recovery even at lower partial pressure. Thus, the membrane network shows optimal design with only one stripping stage at high membrane selectivity regardless of permeance. Hence, it can be concluded that the membrane total area is controlled by permeance while the network design is controlled by selectivity. Also, it is noticed that as the membrane price increases or its durability is reduced, the superstructure total membrane area is reduced in conjunction with higher rates of recycle streams. This indicates that as membrane material cost increases, the compression cost becomes more favorable to minimize the optimization objective function.

It can be concluded from the model results that, at a specific membrane area cost and durability, there is a minimum sufficient permeance after which the membrane network economics becomes less sensitive to selectivity if it is higher than 40. This result implies that the research on membrane synthesis might be better directed towards synthesizing high permeable and durable materials with minimum selectivity of 40 rather than searching for high-selective membranes. At this specific selectivity, an efficient membrane network design could deliver a process competitive to conventional distillation process separation for separation of propylene and propane.



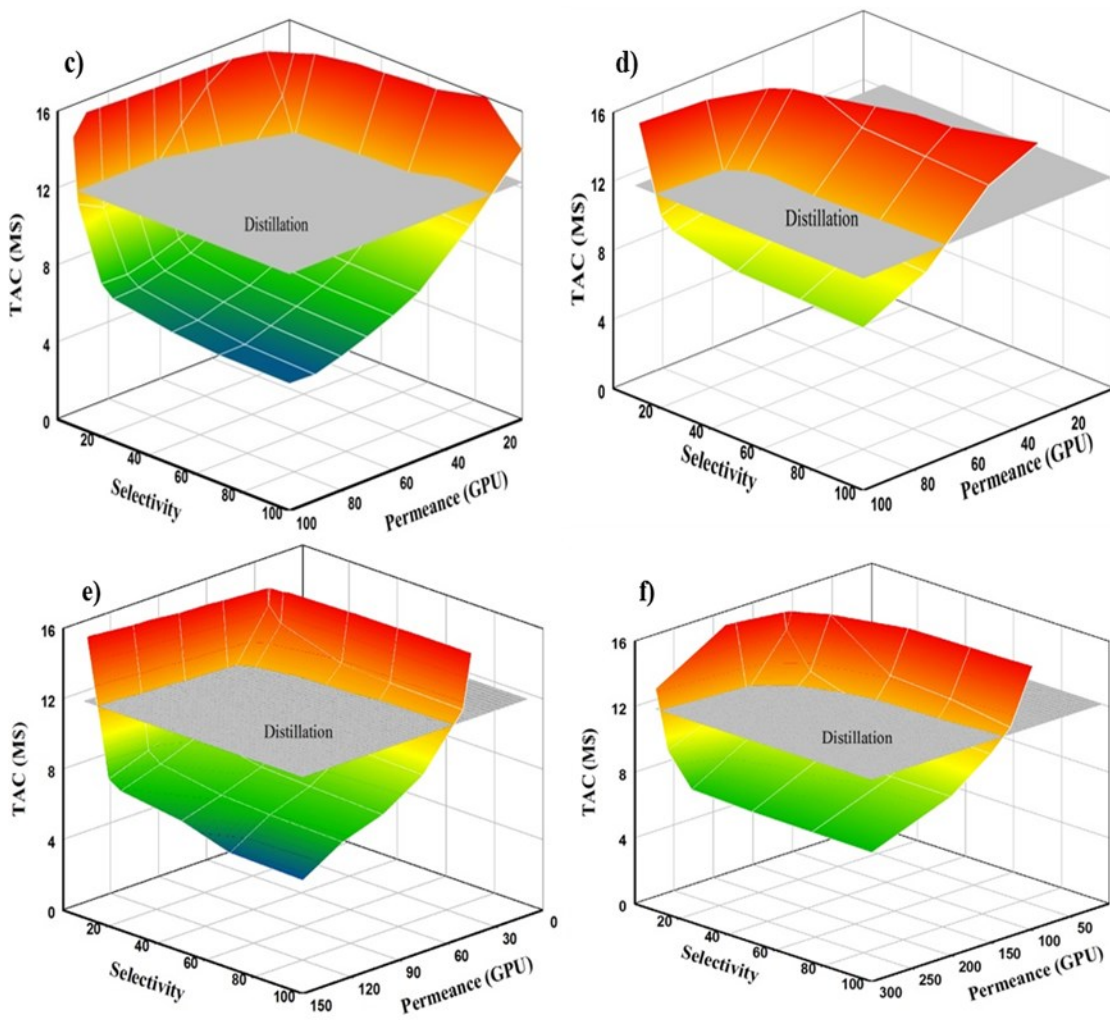


**Fig. 6.5** Economic analysis of membrane superstructure for the separation of propylene/propane under uncertainty in membrane cost and lifetime. a) cost of 50 \$/m<sup>2</sup> and lifetime of 5 years b) cost of 50 \$/m<sup>2</sup> and lifetime of 2 years c) cost of 500 \$/m<sup>2</sup> and lifetime of 5 years d) cost of 500 \$/m<sup>2</sup> and lifetime of 2 years e) cost of 1000 \$/m<sup>2</sup> and lifetime of 5 years a) cost of 1000 \$/m<sup>2</sup> and lifetime of 2 years.

For specific demonstration, the previously mentioned network optimization is carried out at fixed membrane selectivity of 40 while the permeance is varied to locate the permeance which corresponds to the break-even with distillation process. The

optimization case is evaluated at different membrane prices per unit area and for membrane lifetime of 2 and 5 years. The simulation results are plotted in Fig. 6.6. The correlation between the break-even permeance ( $P_{BE}$ ), membrane price per unit area ( $MP$ ) and membrane lifetimes ( $LT$ ) is found to be nonlinear and can be approximated by the following equation:

$$P_{BE} = (100 - 2 LT + 36.2 MP - 1.8 LT^2 - 3 LT MP)^{0.455-0.005 LT} \quad (6.9)$$

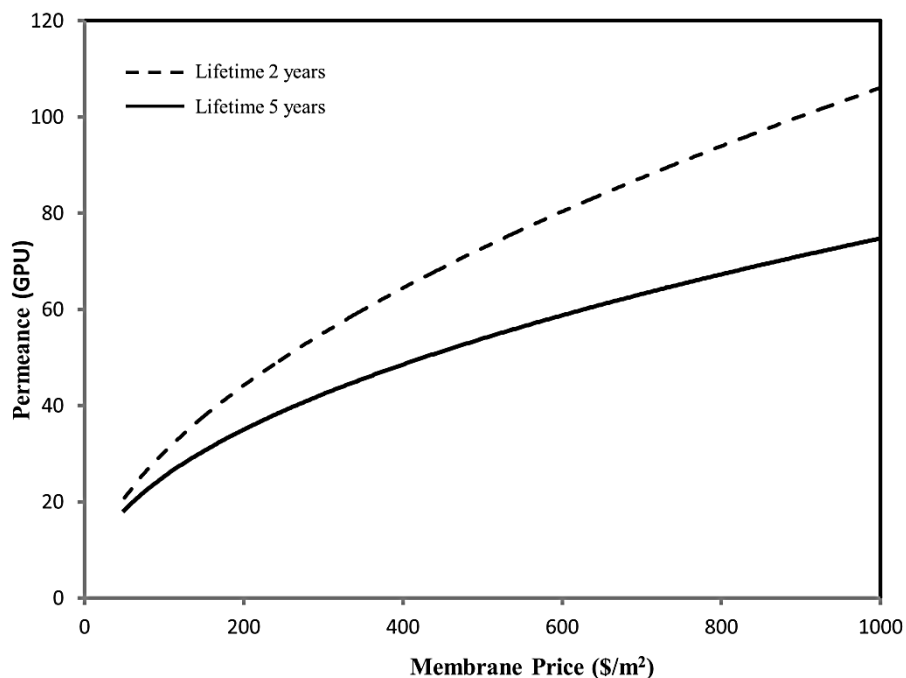


**Fig. 6.6** Relationship between the membrane material price and the breakeven permeance at membrane selectivity of 40.

## 6.7 Conclusion

The optimization of an existing propylene/propane splitting distillation column, which handles a feed with 70% propylene at a rate of 0.45 Mt/yr and produces 99.5% propylene

at a recovery rate of 99%, resulted in a total annualized cost of M\$12.3. This total cost of the distillation process was used as a threshold for the membrane network economic evaluation. By carrying out a superstructure optimization of a multi-stage membrane network (feed stage, two enriching stages and two stripping stages) at different membrane performances and under uncertainty in membrane material cost and lifetime, major guidelines are obtained. At membrane selectivity less than 50, the optimal membrane network consists of a feed stage, an enriching stage and two stripping stages. It is also noticed that the separation cost turn to be independent from the membrane selectivity after certain selectivity is reached. This selectivity is being identified to be impacted by the membrane material price and its durability. The necessity for high permeable and durable material is realized for high membrane material cost.

## 6.8 References

- [1] M. Ohno, T. Morisue, O. Ozaki, T. Miyauchi, Gas Separation Performance of Tapered Cascade with Membrane, *J Nucl Sci Technol*, 15 (1978) 411-420.
- [2] M. Ohno, T. Morisue, O. Ozaki, T. Miyauchi, Comparison of Gas Membrane Separation Cascades Using Conventional Separation Cell and 2-Unit Separation Cells, *J Nucl Sci Technol*, 15 (1978) 376-386.
- [3] E.B. Gruzdev, N.I. Laguntsov, B.I. Nikolaev, A.P. Todosiev, G.A. Sulaberidze, A Method of Calculating Membrane-Element Cascades for Separating Multicomponent Mixtures, *Sov Atom Energy+*, 57 (1984) 553-557.
- [4] S.A. Stern, J.E. Perrin, E.J. Naimon, Recycle and Multimembrane Permeators for Gas Separations, *J Membrane Sci*, 20 (1984) 25-43.
- [5] M.S. Avgidou, S.P. Kaldis, G.P. Sakellaropoulos, Membrane cascade schemes for the separation of LPG olefins and paraffins, *J Membrane Sci*, 233 (2004) 21-37.
- [6] T. Pettersen, K.M. Lien, Design Studies of Membrane Permeator Processes for Gas Separation, *Gas Sep Purif*, 9 (1995) 151-169.
- [7] Y.K. Kao, M.M. Qiu, S.T. Hwang, Critical Evaluations of 2 Membrane Gas Permeator Designs - Continuous Membrane Column and 2 Strippers in Series, *Industrial & Engineering Chemistry Research*, 28 (1989) 1514-1520.
- [8] M.M. Qiu, S.T. Hwang, Y.K. Kao, Economic-Evaluation of Gas Membrane Separator Designs, *Industrial & Engineering Chemistry Research*, 28 (1989) 1670-1677.
- [9] B.D. Bhide, S.A. Stern, Membrane Processes for the Removal of Acid Gases from Natural-Gas .2. Effects of Operating-Conditions, Economic-Parameters, and Membrane-Properties, *J Membrane Sci*, 81 (1993) 239-252.
- [10] A.K. Datta, P.K. Sen, Optimization of membrane unit for removing carbon dioxide from natural gas, *J Membrane Sci*, 283 (2006) 291-300.

- [11] T.C. Merkel, H.Q. Lin, X.T. Wei, R. Baker, Power plant post-combustion carbon dioxide capture: An opportunity for membranes, *J Membrane Sci*, 359 (2010) 126-139.
- [12] W.L. Luyben, American Institute of Chemical Engineers., *Distillation design and control using Aspen simulation*, Wiley-Interscience, Hoboken, N.J., 2006.
- [13] J.M. Douglas, *Conceptual design of chemical processes*, McGraw-Hill, New York, 1988.
- [14] J. Ploegmakers, A.R.T. Jelsma, A.G.J. van der Ham, K. Nijmeijer, Economic Evaluation of Membrane Potential for Ethylene/Ethane Separation in a Retrofitted Hybrid Membrane/distillation Plant Using Unisim Design, *Industrial & Engineering Chemistry Research*, 52 (2013) 6524-6539.
- [15] N. Ramzan, W. Witt, Multi-objective optimization in distillation unit: a case study, *Can J Chem Eng*, 84 (2006) 604-613.
- [16] M.T. Ho, G.W. Allinson, D.E. Wiley, Reducing the cost of CO<sub>2</sub> capture from flue gases using membrane technology, *Industrial & Engineering Chemistry Research*, 47 (2008) 1562-1568.
- [17] C. Zhang, Y. Dai, J.R. Johnson, O. Karvan, W.J. Koros, High performance ZIF-8/6FDA-DAM mixed matrix membrane for propylene/propane separations, *J Membrane Sci*, 389 (2012) 34-42.
- [18] Y.C. Pan, T. Li, G. Lestari, Z.P. Lai, Effective separation of propylene/propane binary mixtures by ZIF-8 membranes, *J Membrane Sci*, 390 (2012) 93-98.
- [19] K. Okamoto, S. Kawamura, M. Yoshino, H. Kita, Y. Hirayama, N. Tanihara, Y. Kusuki, Olefin/paraffin separation through carbonized membranes derived from an asymmetric polyimide hollow fiber membrane, *Industrial & Engineering Chemistry Research*, 38 (1999) 4424-4432.

- [20] L.D. Pollo, L.T. Duarte, M. Anacleto, A.C. Habert, C.P. Borges, Polymeric Membranes Containing Silver Salts for Propylene/Propane Separation, *Braz J Chem Eng*, 29 (2012) 307-314.
- [21] G. Wang, C.M. Xu, J.S. Gao, Study of cracking FCC naphtha in a secondary riser of the FCC unit for maximum propylene production, *Fuel Process Technol*, 89 (2008) 864-873.
- [22] ChemSystems®, Evolving Propylene Sources Solution to Supply Shortages, 2012, [www.chemsystems.com](http://www.chemsystems.com).
- [23] V. Gokhale, S. Hurowitz, J.B. Riggs, A Comparison of Advanced Distillation Control Techniques for a Propylene/Propane Splitter, *Industrial & Engineering Chemistry Research*, 34 (1995) 4413-4419.
- [24] I.K. Kookos, Optimal design of membrane/distillation column hybrid processes, *Industrial & Engineering Chemistry Research*, 42 (2003) 1731-1738.

## **7. Minimum Energy of Single-Stage Membrane and Membrane/Distillation Hybrid Processes**

### **7.1 Abstract**

The membrane/distillation hybrid system was used to study the energy consumption. A shortcut method was developed to calculate the minimum practical separation energy (MPSE) of the membrane process and the distillation process. It was found that the MPSE of the hybrid system is only determined by the membrane selectivity and the applied transmembrane pressure ratio in three stages. At the first stage when selectivity is low, the membrane process is not competitive to the distillation process. Adding a membrane unit to a distillation tower will not help in reducing energy. At the second medium selectivity stage, the membrane/distillation hybrid system can help reduce the energy consumption, and the higher the membrane selectivity, the lower is the energy. The energy conservation is further improved as pressure ratio increases. At the third stage when both selectivity and pressure ratio are high, the hybrid system will change to a single-stage membrane unit and this change will cause significant reduction in energy consumption. The energy at this stage keeps decreasing with selectivity at slow rate, but slightly increases with pressure ratio. Overall, the higher the membrane selectivity, the more the energy is saved. Therefore, the two fundamental questions are answered in a simple and clear manner. These results should be very useful to guide membrane research and their applications.

## 7.2 Introduction

In chemical and petroleum industries, the energy used to drive the separation processes accounts for approximately sixty percent of the plant total energy. In these industries, distillation is the conventional separation process for large scale applications. This is due to the fact that it can produce high purity products. However, the separation policy of distillation relies on temperature gradient generated by recycle of cooled reflux and heated boil-up. Therefore the amount of energy consumed by all separation processes in the sector is much lower than that consumed by distillation processes. The recent rise in energy cost and strict limitations on carbon emission accelerates researches to enhance the separation energy efficiency. Thus, distillation processes gained special attention and different alternative were evaluated such as membrane technology, adsorption and vapour recompression distillation. It is very common to evaluate the process alternatives based on profitability through economic analysis. Even though, the economic analysis is the most trusted evaluation technique to compare the different separation processes, it is very sensitive to time, geographic location and economic evaluation basis. Moreover, the economic analysis indicators are normally used to optimize the chemical process setup or operating conditions but it does not provide energy efficiency solutions.

The sever need for better understanding of energy destruction in a process generated a thermodynamic analysis tool named exergy. Recently, the exergy analysis gained more importance in separation processes since it can help to identify which processes destroy more energy. The system exergy is the maximum theoretical useful work can be obtained if the system is brought into thermodynamic equilibrium with the environment. Not like

energy, exergy has the characteristic that it is only conserved when only reversible processes occur in the system and its environment. Thus, exergy is a measure of irreversibility or thermodynamic imperfections which represent losses in energy usefulness. This simply means when energy loses its quality then exergy is destroyed. Exergy analysis is the first step to identify the weak points of an existing process conditionally that enough information about feed and product streams are available. Therefore, the exergy analysis is recognized as a powerful diagnostic tool to enhance or improve process operation. Exergetic analysis has been used to evaluate or compare the efficiency of industrial processes.

Ayotte-Sauve et al. most recently presented a thermodynamic shortcut method to determine the minimum separation energy of a binary mixture. This study evaluated retrofitting the distillation process with membrane module in a parallel setup. The energy of permeate recompression is assumed to be negligible compared to reboiler heat energy. Optimizing the generated energy function was compared to a referenced superstructure optimization case study.

The concept of minimum energy to separate mixture components from thermodynamic point of view is well covered but unfortunately the real separation unit operations operate far from the minimum energy. This fact is normally quantified from thermodynamic second law efficiency. Thus the minimum energy of separation cannot be used as screening tool to compare separation alternatives. Felbab et al. applied fundamental thermodynamic principles to conventional and vapour recompression distillation unit operations. Assuming that binary feed mixture is split into pure

components where the light key component is totally recovered at the distillate stream while the heavy key component is totally recovered as bottom product. Moreover, the minimum practical energy supplied to the distillation process equals the heat of vaporization supplied at the reboiler considering no heat recovery achieved at the condenser. This assumption is practical if the distillation column is operated at temperature range close to the ambient temperature. Economic studies for energy intensive gas separation processes showed that the contribution of energy cost to the total annualized cost is huge compared to capital and other operating expenditures. Therefore, the energy consumption for such separation processes can be used as a screening tool to compare the different flowsheet alternatives. The energy function can be also used as an objective function to optimization the process operating conditions and design parameters.

In this chapter, the concept of minimum practical energy of separation is developed for both membrane and distillation unit operations to study their performance as a function of feed stream composition and product specifications. The energy function will be then used to evaluate the different membrane/distillation hybrid configurations for an energy intensive separation process as case study. The minimum practical energy is used to locate the minimum selectivity for energetic viable hybrid and to highlight some guidelines for hybrid design. Moreover, the impact of membrane selectivity to energy consumption is thoroughly investigated.

From the attainability studies it was found that a single-stage membrane process cannot meet the separation task under certain conditions, hence a membrane/distillation hybrid system was used as the benchmark model to evaluate the minimum energy consumption. This approach has the following benefits. Firstly, the membrane/distillation hybrid system can meet the separation task at any membrane conditions. Hence, optimization of the membrane properties becomes possible when minimizing the energy. Secondly, the hybrid configuration is relatively simple. A superstructure can be found to cover most possible combinations between a membrane unit and a distillation tower. It can also cover a pure membrane unit and a pure distillation unit. Therefore, the true minimum energy consumption can be identified irrespective to specific configurations. Thirdly, the membrane/distillation hybrid system can retrofit to existing distillation processes. Hence, the results are practically valuable.

Ayotte-Sauve et al. recently proposed a thermodynamic exergy method to find the minimum energy of a membrane/distillation hybrid system[9]. In this method they first used exergy analysis to determine the optimal conditions for the membrane unit, and then the minimum energy of the membrane/distillation system was found at fixed number of trays. However, this method is hard to be used here. Firstly, the membrane properties cannot be changed because they are not involved in the optimization function. Secondly, at fixed number of trays the energy consumption of the distillation tower may not be the minimum. Thirdly, the exergy analysis is valid when the process is under thermodynamic equilibrium. Practical processes always deviate from the thermodynamic equilibrium state. Hence in this

work, the concept of minimum practical energy of separation is adopted for both membrane and distillation unit operations to study their performance as a function of membrane properties. From there the most important membrane parameters are identified.

The separation of propylene/propane was used in this report as a case study. This process is industrially important. The worldwide production rate of propylene was 77 million tonnes in year 2011 and the production rate is anticipated to reach 132 million tonnes by year 2025. The separation is currently achieved by distillation and the process requires more than 230 trays. The energy consumption is one of the highest in petrochemical processes [10]. To reduce energy, many alternative processes, particularly the membrane distillation hybrid system, have been widely discussed in literature [3, 11, 12]. Recently, our group developed a ZIF-8 type of metal-organic framework membrane which could efficiently separate propylene from propane with selectivity more than 35 and permeance of propylene more than 100 GPU [13]. Hence, using this system as a case study can help understand the feasibility of the ZIF-8 membrane in practical applications.

The production of propylene is mainly by steam cracking unit (SCU) or fluid catalytic cracking (FCC). These two processes account for about 89% of worldwide propylene production. The concentration of propylene produced from refinery FCC unit or ethylene production process is about 70 mol% while the applications of propylene such as production of polypropylene require high purity. In market, propylene is provided in three grades: polymer grade (>99.5%),

chemical grade (92-96%), and refinery grade (>60%) [14]. Both propylene and propane have a high market price which mandate high products recovery. Therefore, in this study we used the following conditions for the case study: the feed composition is 50 mol%, and the separation task is to meet the chemical grade purity requirement (96 mol%) and a recovery ratio of 95%. The analysis methodology will be then generalized to study the minimum energy of the hybrid system to recover 99% of propylene at distillate concentrations meeting the purity requirements for chemical and polymer grades from stream with 70% propylene.

### **7.3 Membrane distillation hybrid configurations**

If a single-stage membrane unit is combined with a distillation unit, then in principle this hybrid system can meet the separation task at any membrane properties. As described in the literature, the membrane unit can be combined with the distillation unit in three ways [15, 16]. The first one is shown in Fig. 7.1a and named as pre-distillation configuration, where a feed is firstly fed into a membrane unit and then the permeate stream and the retentate stream are fed into the distillation column at certain positions. To minimize the disturbance to the operation of the distillation column, the pressure and the temperature of the permeate stream should be adjusted equal to what are inside the column. The second configuration (Fig. 7.1b) is called parallel configuration where a side-stream is taken out of the distillation column and fed into the membrane unit. The permeate and retentate streams are then fed back to the column but in different positions. The third configuration is called post-distillation configuration

illustrated in Fig. 7.1c where a membrane unit is located at downstream of the distillation column. The distillate is fed into the membrane unit to be further enriched to the desired purity while the retentate stream is recycled back to the column.

The aim of this study is to find the minimum energy consumption at certain membrane properties when the distillation process is operated at optimum conditions. From Fig. 7.1, parameters of the distillation process that need to be optimized may include the reflux ratio, the positions of the feed, the permeate stream and the retentate stream, and position and flow rate of the side-stream, etc. For challenging separation systems, the boiling point of different components is close to each other. Hence to simplify the analyses, the temperature and pressure of all feed streams are set to be the same as the distillation column and assumed constant. Of course the pressure at the permeate side of the membrane unit will be lower, but as illustrated in Fig. 7.1 the permeate stream will be recompressed back to the initial pressure after the membrane unit.

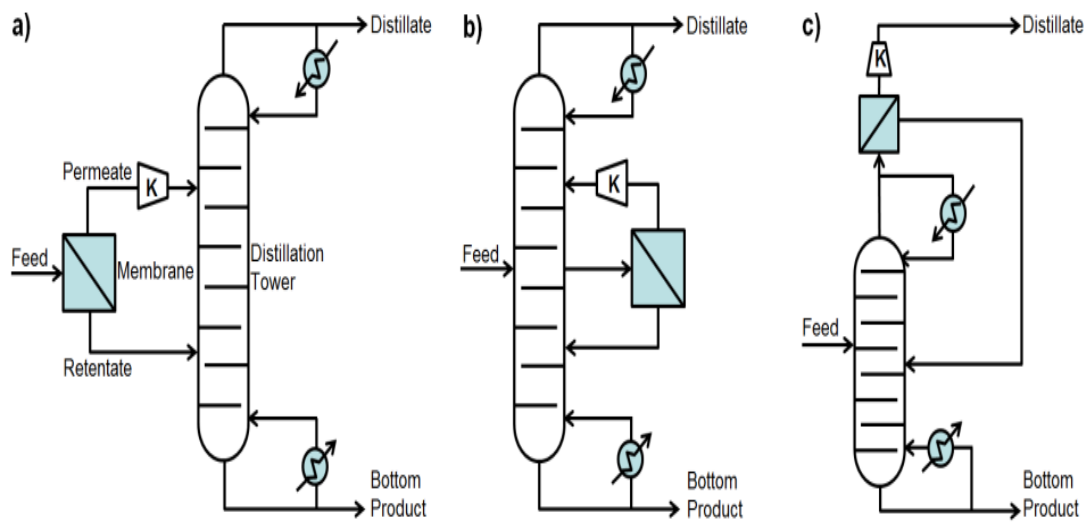


**Fig 7.1** Possible membrane/distillation hybrid configurations for membrane material selective toward the light key component: a) pre-distillation b) parallel membrane distillation c) post-distillation.

After analyses of the flow conditions in each hybrid configuration, we realized that the parallel configuration shown in Fig. 7.1b can be considered as the superstructure of the membrane/distillation hybrid system. First, if the side-stream in the parallel configuration is taken at the same position and the same flow rate as the feed, then the parallel configuration is mathematically equivalent to the pre-distillation configuration. If the position of the side-stream is moved to the topmost stage and the permeate stream becomes the distillate product while the retentate stream is recycled back to the distillation tower, then the parallel configuration is equivalent to the post-distillation configuration. In the case the feed position of the permeate stream is moved directly to the product stream and the position of the retentate stream is moved directly to the bottom stream, then essentially nothing

will feed into the distillation tower. So in this case the parallel configuration will reduce to a single-stage membrane unit. Lastly, if the membrane area is set to zero, or the membrane has no selectivity ( $S=1$ , also in this case the permeate stream and the retentate stream should be combined after the membrane unit and fed back to the same position where the side-stream is taken), then the membrane unit essentially plays no role in the separation, hence the parallel configuration simply reduces to a pure distillation unit. Therefore, analyses based on the parallel configuration are able to cover all the other configurations and find the true minimum energy consumption of the membrane/distillation hybrid systems.

In the normalized membrane model in chapter 3, the membrane properties include selectivity ( $S$ ), stage-cut ( $\tau$ ) and pressure ratio ( $\gamma$ ). Membrane permeability and membrane area are not shown in the equations because they have combined together and been represented by the parameter dimensionless membrane area ( $\omega$ ).

#### **7.4 Minimum practical energy of separation**

Due to irreversible losses of energy in real separation systems, they operate far from the thermodynamic minimum separation energy. Thus a more realistic approach to estimate the energy requirement of a separation process is needed to compare the different separation processes or flowsheets. The suggested approach relies on good knowledge of separation technique in the unit operation. This approach is usually followed for equipment design and sizing. The accuracy of such approach is expected to be higher than any other thermodynamic analytical approach. The minimum practical energy of separation for a unit operation is

estimated from the difference between the energy input and energy recovery.

Therefore, the minimum practical energy can be written as:

$$E_{min} = E_{in} - E_{out} \quad (7.1)$$

The input/output energy is in the form of heat or shaft work. Therefore, equation (7.1) can be written as:

$$E_{min} = Q_{in} + W_{in} - Q_{out} - W_{out} \quad (7.2)$$

The input heat ( $Q_{in}$ ) is usually supplied through a heat exchanger or a reboiler while heat recovery ( $Q_{out}$ ) is done by a heat exchanger or a condenser. The input work to a stream is performed by a compressor or a pump while work recovery ( $W_{out}$ ) is done by a turbine or a pressure exchanger.

#### 7.4.1 Distillation process

The energy input to a conventional distillation unit is in the form of heat supplied through a reboiler. In an ideal distillation process the same amount of energy is expelled at the top of the distillation column through a total condenser. In reality the energy recovery is lower than the supplied amount and also, in many industrial applications distillation columns operate at relatively low temperature. Thus, heat recovery is not feasible due to thermodynamic limitation (the produced cooling stream has a temperature close to the dead state temperature  $T_0$ ). The C<sub>3</sub> splitter is a good example to clarify this concept which is very critical to the thermodynamic analysis. The splitter reboiler heats the boil-up stream to a temperature of 39°C while the condenser uses cooling water to cool the reflux

stream to about 33.75°C. Thus the heat energy is transferred to the cooling water which now has a temperature of less than 29 °C. Recovering this energy from the cooling water requires huge capital investment compared to the price of the recovered energy. Therefore, in this study heat recovery will be ignored just like in real practice. Moreover the assumption made earlier that the feed stream and the distillation products are at the same pressure of the distillation column, eliminates the work recovery term ( $W_{out}$ ). These facts reduce equation (7.2) for distillation process to the following form:

$$E_{min}^D = Q_{in} \quad (7.3)$$

The column input energy supplied through the reboiler can be estimated from vapour flow through the distillation column to achieve certain distillate purity ( $x_D$ ) and recovery ( $\eta$ ). Assuming constant molar overflow (CMO) and carrying mass balance over the column stages, the vapour flow can be expressed in terms of distillate stream molar flow rate (D) and minimum molar reflux ratio ( $R_{min}$ ) as:

$$V_{min} = D(R_{min} + 1) \quad (7.4)$$

The minimum reflux ratio of a distillation column processing a binary mixture with light key component composition in feed stream of  $x_f$  to produce a distillate stream at a purity of  $x_D$  can be estimated based on feed conditions using the Underwood equation [17]. For a liquid feed at bubble point the Underwood equation takes the following form:

$$R_{min} = \frac{1}{(\alpha - 1)} \left[ \frac{x_D}{x_f} - \frac{\alpha(1 - x_D)}{(1 - x_f)} \right] \quad (7.5)$$

Where  $\alpha$  is the relative volatility. If the feed is vapour at its dew point, the Underwood equation takes the following form:

$$R_{min} = \frac{1}{(\alpha - 1)} \left[ \alpha \frac{x_D}{x_f} - \frac{(1 - x_D)}{(1 - x_f)} \right] \quad (7.6)$$

Therefore, the minimum input heat ( $Q_{min}$ ) equals the minimum heat required to evaporate the minimum vapour flow rate ( $V_{min}$ ) which can be approximated from the latent heat ( $\lambda$ ) of the light key component as following:

$$E_{min}^D = \lambda D (R_{min} + 1) \quad (7.7)$$

#### 7.4.2 Membrane process

As mentioned earlier, the driving force for gas permeation in a membrane module is the partial pressure difference between the feed and permeate side. In order to generate sufficient partial pressure difference either or both of feed side compression and permeate stream vacuum pumping should be applied. Based on the downstream process requirement, compression or pressure recovery could be applied to the membrane product streams. It is worth to note that the modern pressure recovery systems can reach almost up to 100% efficiency. Therefore, the minimum energy consumption by a membrane unit is in the form of shaft work for feed ( $W_{s,f}$ ) and permeate ( $W_{s,p}$ ) streams compression or vacuum pumping minus the recovered work ( $W_R$ ) as shown in Fig. 7.2.

$$E_{min}^M = W_{s,f} + W_{s,p} - W_R \quad (7.8)$$

In the parallel hybrid configuration the feed stream is withdrawn directly from the distillation column as a saturated vapour, therefore the transmembrane pressure difference should be created by vacuum pumping of the permeate side to avoid feed condensation if compression is applied to it. The permeate stream should be again recompressed to the same pressure of the distillation stage at which it will be fed. This makes the general energy balance of membrane process reduces to the following form:

$$E_{min}^M = W_{s,p} \quad (7.9)$$

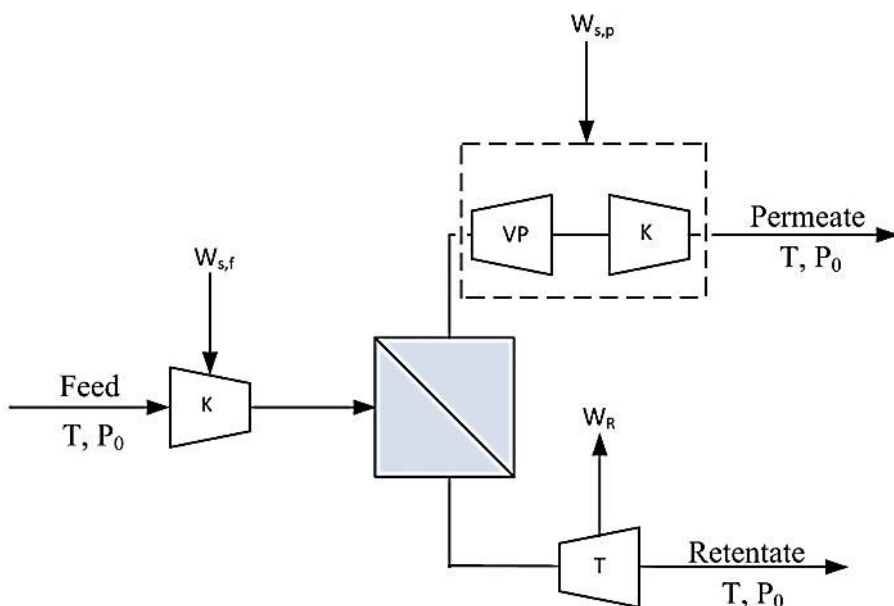


**Fig 7.2** Energy requirement for a single membrane unit considering feed compression, permeate vacuum pumping and recompression and energy recovery from the retentate stream.

The shaft work can be estimated from energy balance around the equipment. Therefore, for an inlet flow rate  $F$  the shaft work can be calculated from the

temperature difference between the inlet and outlet streams and gas specific heat ( $C_p$ ) as following:

$$W_s = FC_p(T_{out} - T_{in}) \quad (7.10)$$

Considering an ideal gas and isentropic compression/expanding then the temperature of compressor/vacuum pump outlet stream ( $T_{out}$ ) can be estimated as:

$$T_{out} = T_{in} \left[ \frac{P_{out}}{P_{in}} \right]^{\frac{R}{C_p}} \quad (7.11)$$

#### 7.4.3 Membrane/distillation hybrid configuration

As shown earlier in Fig. 7.1b, the distillation part in this configuration can be treated as a distillation column with multiple feed streams and multiple removing side-streams. Nikolaides and Malone [18] developed a shortcut method to calculate the minimum reflux ratio for a distillation column containing  $m$  number of feed streams (here  $m = 3$ ) and  $z$  number of side streams (here  $z = 1$ ).

$$R_{min} = \max[R_{M,k}], \quad k = 1, 2, \dots, m \quad (7.12)$$

$$\begin{aligned} R_{M,k} &= R_{M,k}^0 + \sum_{j=1}^{k-1} (1 - q_j) \frac{F_j}{D} - \sum_{l=1}^{z_m} (1 - q_l) \frac{Z_l}{D} \\ &\quad + \sum_{i=1}^n \frac{\alpha_i}{\alpha_i - \theta_k} \left[ \sum_{l=1}^{z_m} \frac{Z_l x_{zl,i}}{D} - \sum_{j=1}^{k-1} \frac{F_j x_{fj,i}}{D} \right] \end{aligned} \quad (7.13)$$

Where  $R_{M,k}$  is the minimum reflux ratio of the  $k^{th}$  feed,  $R_{M,k}^0$  is the reflux ratio of the  $k^{th}$  feed in the absence of all other feeds,  $n$  is the number of components in

mixture,  $z_m$  is the number of side streams above the  $k^{\text{th}}$  feed,  $\alpha_i$  is the relative volatility of component  $i$ ,  $q$  is the liquid fraction (1 for saturated liquid and 0 for saturated vapour feed stream),  $F_j$  is the molar flow rate of feed  $j$  and  $x_{fj,i}$  is the molar fraction of component  $i$  in feed  $j$ ,  $Z_l$  is the molar flow rate of the  $l^{\text{th}}$  side-stream and  $x_{zl,i}$  is the molar fraction of component  $i$  in the  $l^{\text{th}}$  side-stream.  $\theta_k$  is defined as the root of the Underwood polynomial of the  $k^{\text{th}}$  feed:

$$\sum_{i=1}^n \frac{\alpha_i x_{fk,i}}{\alpha_i - \theta_k} = 1 - q \quad (7.14)$$

Nikolaides and Malone [18] approximated  $R_{M,k}^0$  for any feed liquid-vapour fraction as a function of the saturated liquid reflux ratio ( $R_M$ ) as per the following formula:

$$\begin{aligned} R_{M,k}^0 = & R_M - (q - 1) \frac{R_M}{R_M + 1} (R_M(\emptyset - 1) - 1) \\ & + 2(q - 1)^2 \frac{R_M^2}{(R_M + 1)^3} \emptyset (R_M(\emptyset - 1) - 1) \end{aligned} \quad (7.15)$$

$R_M$  can be calculated by equation (10) and  $\emptyset$  is volatility ratio of the light key component (LK) to the heavy key component (HK),  $\alpha_{\text{LK}}/\alpha_{\text{HK}}$ . Equations (7.2-7.15) and (7.6) can be solved together to determine the minimum reflux ratio of the distillation column which then when substituted in equation (7.3) the minimum energy for the distillation part  $E_{min}^D$  can be estimated. The minimum practical energy of the hybrid system is the sum of distillation and membrane minimum practical separation energy defined as:

$$MPSE = E_{min} = E_{min}^D + E_{min}^M \quad (7.16)$$

The shortcut method can significantly reduce the degree of freedom of the optimization system. By combining Eq. 7.7, 7.10, and 7.13, it can be seen that for binary mixture when the separation task is fixed ( $\varepsilon$ ,  $\eta$ ), the minimum practical separation energy is a function of membrane selectivity, pressure ratio, stage-cut, and normalized side stream flow rate and concentration, as shown in the following formula:

$$MPSE = f\left(S, \gamma, \tau, \frac{F_z}{F_0}, \frac{x_z}{x_{f0}}\right) \quad (7.17)$$

## 7.5 Results and discussion

### 7.5.1 MPSE of the distillation process for propylene/propane separation

The values of the physical proprieties needed to perform the minimum energy calculations for the separation of propylene/propane are 1.3, 56 J/mol·K and 18.8 KJ/mol for  $\alpha$  (relative volatility of propylene to propane),  $C_p$  (mixture specific heat capacity) and  $\lambda$  (propane latent heat of vaporization), respectively. To produce chemical-grade propylene ( $x_D = 0.96$  and  $\eta = 0.95$ ) from a feed mixture of 0.50 propylene molar fraction, the MPSE of the conventional distillation process is approximately 78 KJ/mol. This minimum energy corresponds to a minimum reflux ratio of 7.0.

### 7.5.2 Effect of side stream flow rate and concentration

For the membrane/distillation hybrid system, the hollow fiber membrane model in chapter 3 was used for the membrane part, while the shortcut equations 7.12-7.15 were used for the distillation part. The simulation was first carried out to investigate the effect of the normalized side stream flow rate ( $F_z^* = F_z/F_0$ ) and concentration ( $x_z^* = x_z/x_{f0}$ ). To avoid the situation where the withdrawn side-stream is more than the available vapour, the lowest value of the minimum reflux ratio should be constraint by the following relationship:

$$F_z \leq D(R_{min} + 1) \quad (7.18)$$

For challenging separation systems like propylene/propane, this relationship is always valid because of large reflux ratio. Fig. 7.3 shows the MPSE values at different normalized side flow rate  $F_z^*$  and side concentration  $x_z^*$ . MPSE shows a minimum relationship when  $F_z^*$  varies from 0 to 3.0 and the optimum  $F_z^*$  value roughly increases when the value of  $x_z^*$  increases from 0.2 to 1.25. At different  $x_z^*$  values, the optimum MPSE also shows a minimum relationship because the optimum MPSE first decreases when  $x_z^*$  increases from 0.2 to 0.5, but then becomes increasing when  $x_z^*$  further increases from 0.5 to 1.25. The star in Fig. 7.3 marks the conditions when the normalize side flow rate and concentration both equal to 1. As mentioned earlier, the parallel configuration in this case is equivalent to the pre-distillation configuration. By calculating the MPSE of the pre-distillation configuration at the same conditions, the value is confirmed to be

the same as what obtained here. Obviously, at this condition MPSE is not the global minimum. Hence, the parallel configuration is indeed advantageous to find the true minimum.

Fig. 7.4 shows the value of MPSE at different  $F_z^*$  and different membrane selectivity when the normalized side concentration  $x_z^*$  is fixed at 0.5. The optimum  $F_z^*$  is around 1.25 and doesn't change much with the membrane selectivity. The MPSE value at the optimum condition keeps decreasing when the membrane selectivity increases and there is no reverse trend identified.

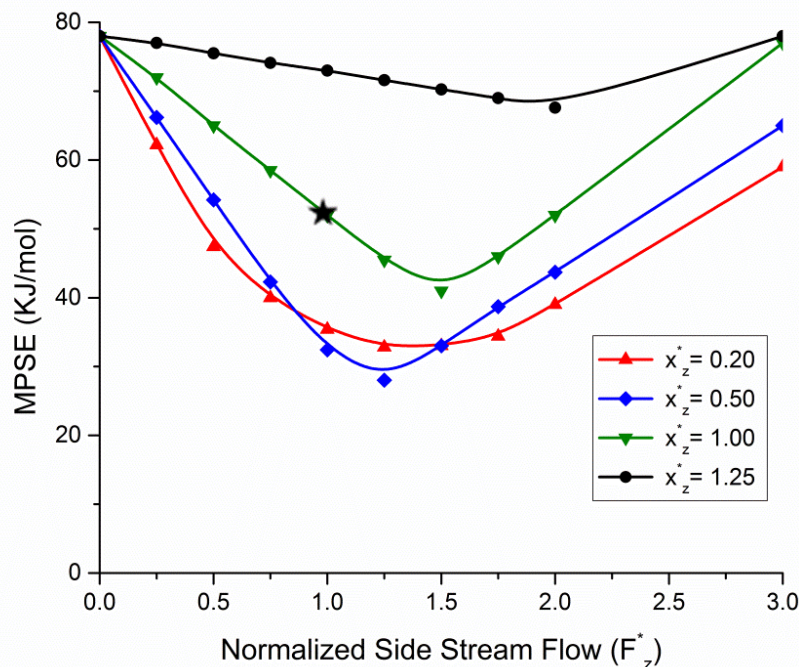


**Fig 7.3** Impact of membrane feed composition on the hybrid MPSE ( $x_f = 0.5$ ,  $x_z/x_{f0} = 0.5$ ,  $x_D=0.96$  and  $\gamma=50$ )

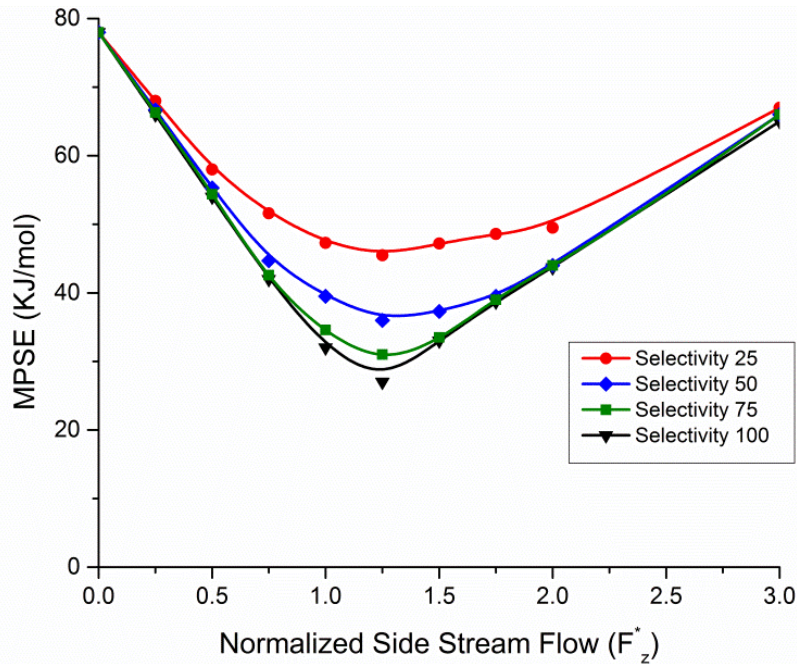


**Fig 7.4** MPSE for parallel configuration at various selectivities and as a function of proportional side-stream flow rate ( $x_f = 0.5$ ,  $x_z/x_{f0} = 0.5$ ,  $x_D=0.96$  and  $\gamma=50$ )

### 7.5.3 Effect of stage-cut

The behaviour of MPSE against the stage-cut is obtained as illustrated in Fig. 7.5. MPSE has almost no change when the stage-cut is lower than 0.2, but then it shows a sharp minimum around 0.25. The optimal stage-cut slightly increases as selectivity decreases. It is also noticed that the optimal stage-cut occurs when the minimum reflux ratio for the permeate stream equals to that for the feed stream. Based on this conclusion the following relationship is derived from equation (7.13).

$$R_{M,k} = R_{M,k}^0 + \frac{\tau F_z}{D} \left( 1 - \left[ \frac{\alpha x_f}{\alpha - \theta_f} + \frac{1 - x_f}{1 - \theta_f} \right] \right) \quad (7.19)$$

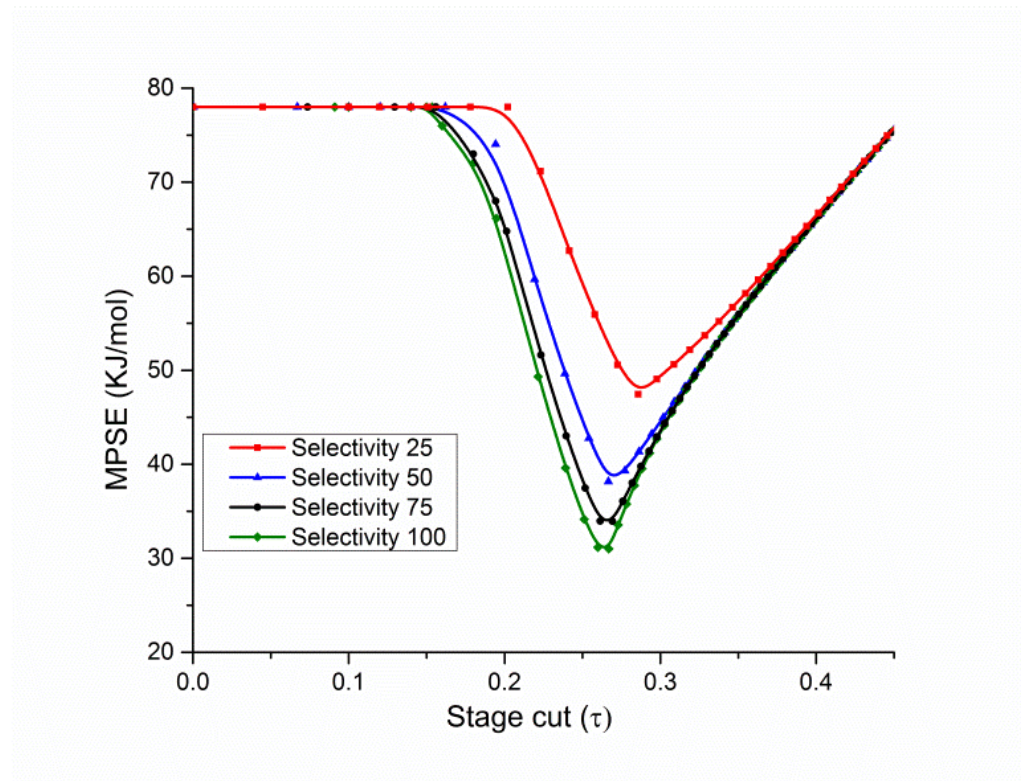


**Fig 7.5** Behaviour of MPSE ( $x_f = 0.5$ ,  $x_D = 0.96$  and  $\eta=0.95$ ) against stage-cut at fixed selectivities of 25, 50, 75 and 100,  $\gamma=50$ ,  $F_z/F = 1$  and  $x_z/x_f = 0.5$ .

#### 7.5.4 Effect of membrane selectivity and pressure ratio

The MPSE value showed a minimum relationship with the normalized side flow rate and concentration, and also the stage-cut, which means that the MPSE function can be optimized over all these parameters. The MPSE of the hybrid process at these optimal conditions is plotted in Fig. 7.6 against the membrane selectivity and pressure ratio. On Fig. 7.6 the MPSE of the pure distillation process and the thermodynamic minimum energy (Gibbs energy) of the separation are also shown as guide lines. Three stages can be clearly identified in Fig. 7.6. The first stage is when membrane selectivity is less than approx. 10. The MPSE of the

hybrid system has almost the same MPSE as the pure distillation process, which mean adding a membrane unit doesn't help to reduce the energy. In the second stage when the selectivity is higher than 10, the MPSE value starts to decrease monotonically, which means that the membrane unit now can help reduce the energy consumption. The MPSE value reduces sharply initially but slows down until approaching a constant value when increasing the membrane selectivity. MPSE also strongly depends on the applied pressure ratio. MPSE is significantly lower at higher pressure ratio. At the conditions when the applied pressure ratio is 50 or 100, an energy jump was observed at high selectivity, which differentiates the third stage from the second stage. The reason for the energy jump is because at this condition the hybrid system changed to a single-stage membrane unit. This result is consistent with the attainability studies. The pressure ratios in these two cases are higher than the minimum pressure ratio, so when the selectivity is also higher than the minimum selectivity, then a single-stage membrane process becomes possible to meet the requirements. The MPSE value of a single-stage membrane is significantly low and almost close to the Gibbs minimum energy limit. The MPSE value again decreases with selectivity, but at a very slow rate. However, the results in Fig. 7.6 shows that the energy at pressure ratio of 100 is slightly higher than that at pressure ratio of 50, indicating that increasing pressure ratio in this stage will increase the energy consumption. This is because higher pressure ratio will require more energy to reach higher vacuum in the permeate side of the membrane unit; while in the hybrid system, the energy of the membrane unit will also increase with pressure ratio, but it will be over compensated by the

energy saved in the distillation unit. From Fig. 7.6, it can also be seen that for the propylene/propane system, a membrane with selectivity of 35 will not be able to achieve the separation task through a single-stage membrane process. However, if it combines with the existing distillation process, it has potential to save up to approx. 50% energy.

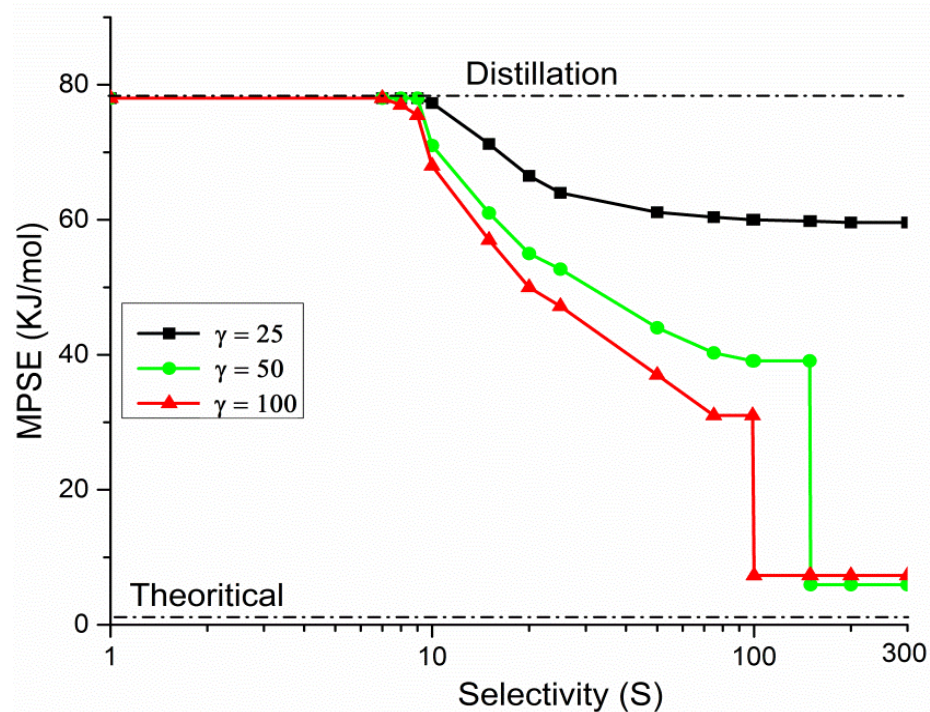


**Fig 7.6** Behaviour of MPSE ( $x_f = 0.5$ ,  $x_D = 0.96$  and  $\eta=0.95$ ) against membrane selectivity at variable pressure ratio (25, 50 and 100)

Following the same analysis, the minimum energy of the membrane/distillation hybrid is investigated to produce both chemical and polymer grade propylene but the recovery ratio this time is adjusted to the industrial specification (99%). Fig. 7.7 demonstrates the minimum energy for chemical grade production from feed mixture with 70% propylene. As seen from the attainability discussion, the

minimum pressure ratio for a single-stage membrane to accomplish the separation task is 38. Hence, beyond this pressure ratio there should be a minimum selectivity after which the single-stage setup is attainable. At pressure ratio of 50, this selectivity is found to be 65 while as the pressure ratio increases to 100 the minimum selectivity is 55.

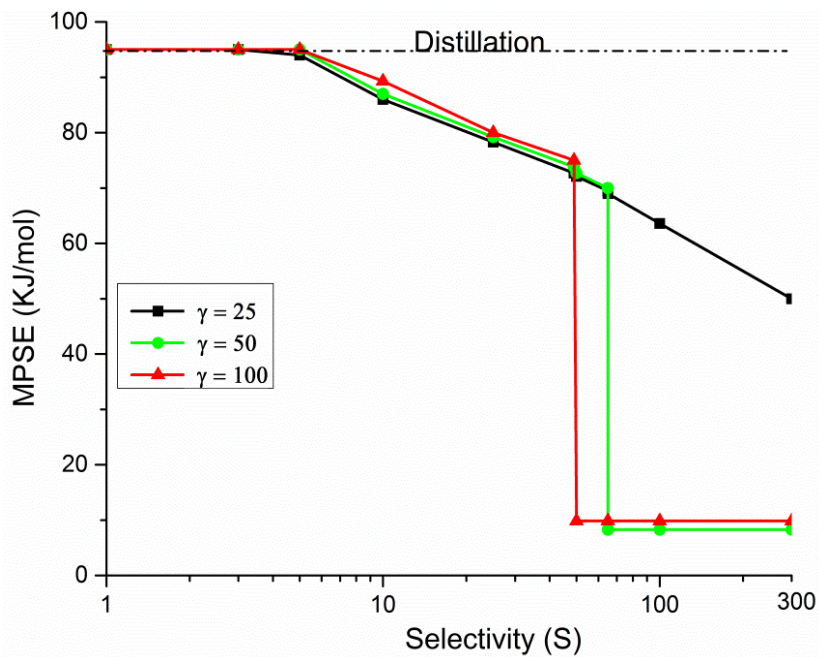


**Fig 7.7** Behaviour of MPSE ( $x_f = 0.7$ ,  $x_D = 0.96$  and  $\eta=0.99$ ) against membrane selectivity at variable pressure ratio (25, 50 and 100)

When the separation requirements are to produce distillate with the polymer grade quality ( $x_D > 0.995$ ) and 99% recovery ratio of propylene. The hybrid system minimum energy is illustrated as a function of the membrane selectivity at the three pressure ratios (25, 50 and 100). Fig. 7.8 exemplifies the potential of the membrane technology to hybridize with distillation for high energy efficient process. Though the minimum pressure ratio to perform the separation task by only

a single-stage membrane is 43 yet the minimum selectivity is beyond the tested range. When the membrane has a selectivity of 40, the hybrid system can reduce the minimum separation energy by 30%.

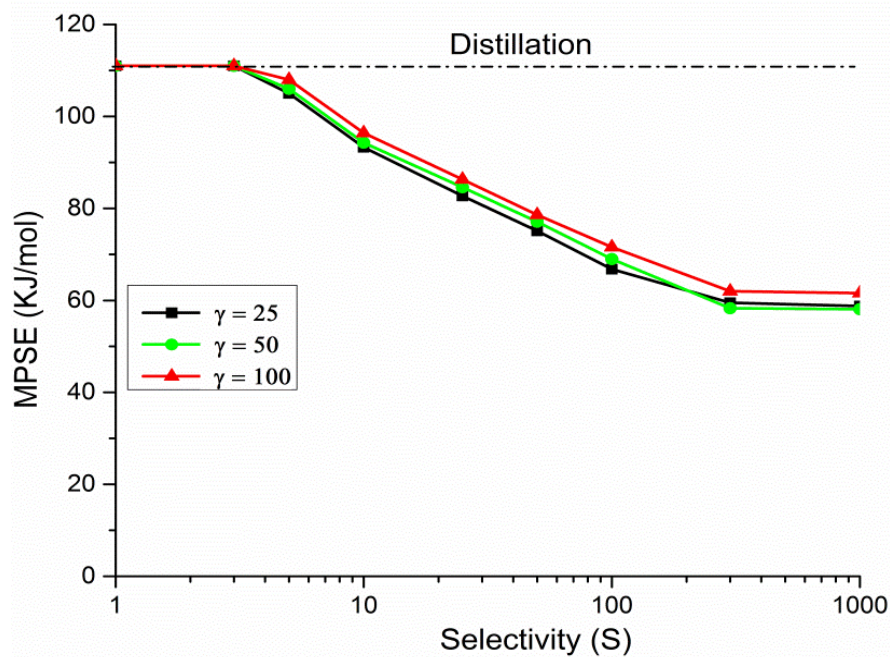


**Fig 7. 8** Behaviour of MPSE ( $x_f = 0.7$ ,  $x_D = 0.995$  and  $\eta=0.99$ ) against membrane selectivity at variable pressure ratio (25, 50 and 100)

## 7.6 Further discussions

Purity and recovery ratio are required in almost all separation processes. Even for CO<sub>2</sub> capture where CO<sub>2</sub> is a low value product, a purity of 0.9 and recovery ratio of 90% are recommended by the U.S. Department of Energy (DOE) [19]. For more valuable products the recovery ratio is very critical and its value often determines the economic feasibility of the separation process. To meet with these two separation targets both membrane selectivity and pressure ratio have minimum

threshold, and the threshold value is independent of any other parameters including the membrane permeability. In liquid separations, the minimum pressure ratio is equivalent to the osmotic pressure. To break these limitations another common approach is to use multi-stage membrane processes, which is the topic of many membrane modelling studies particularly for those systems that highly selective membranes are not available from the existing technology. The minimum membrane selectivity and the minimum pressure ratio derived in this study can also be used to guide the design of multi-stage membrane processes because the overall selectivity and the overall pressure ratio of the process will need to meet with these thresholds.

The minimum energy consumption is mainly determined by the membrane selectivity. This result can be interpreted in another way, that is, membranes with higher selectivity should be able to achieve lower energy consumption if the process is optimized. This simple conclusion can provide a useful guideline for practical membrane applications and also for membrane research. For example, in reverse osmosis seawater desalination process, the existing membranes can achieve salt rejection rate of more than 99.8%, which means the selectivity is more than 500. Hence, it is not surprising that the energy consumption of the current RO process is close to the thermodynamic minimum energy [20]. However, increasing the membrane flux will not help decrease the energy consumption. This is consistent to the conclusions made by several recent studies [20]. Of course, increasing the membrane flux will reduce the overall cost since high flux will reduce the membrane area and eventually the capital cost. Such kind of membrane

economic analysis has been well studied in literature and it is out of the current study scope.

In this study the hybrid system between membrane and distillation was considered. In principle the membrane unit can be combined with any other separation processes such as adsorption or absorption. For these systems we expect that the relationship between the minimum practical separation energy and the membrane selectivity will be similar to that depicted in the current study.

## 7.7 Conclusions

Studying the minimum practical separation energy of the membrane/distillation hybrid systems showed that the energy consumption is solely determined by the membrane selectivity and the applied transmembrane pressure ratio. At low selectivity, the membrane process is not competitive to the distillation process. Adding a membrane unit to the distillation tower will not help in reducing the energy. At medium selectivity, the membrane/distillation hybrid system will reduce the energy and the higher the membrane selectivity, the lower the energy. The pressure ratio will also significantly affect the energy. Increasing pressure ratio will further reduce energy. At high selectivity a single-stage membrane is able to achieve the separation tasks and significantly reduce the energy consumption once the applied pressure ratio is higher than the threshold limit shown in the attainability chart (Fig. 3). In general, the higher the selectivity, the lower the energy consumption is.

## 7.8 References

- [1] Y. Demirel, Sustainable Operations for Distillation Columns, Chemical Engineering & Process Techniques, (2013).
- [2] I.C. Omole, Crosslinked polyimide hollow fiber membranes for aggressive natural gas feed streams, ProQuest, 2008.
- [3] A. Motelica, O.S. Bruinsma, R. Kreiter, M. den Exter, J.F. Vente, Membrane Retrofit Option for Paraffin/Olefin Separation • A Technoeconomic Evaluation, Ind Eng Chem Res, 51 (2012) 6977-6986.
- [4] R.W. Baker, J. Wijmans, Y. Huang, Permeability, permeance and selectivity: a preferred way of reporting pervaporation performance data, J Membrane Sci, 348 (2010) 346-352.
- [5] A. Alshehri, R. Khalilpour, A. Abbas, Z. Lai, Membrane Systems Engineering for Post-combustion Carbon Capture, Energy Procedia, 37 (2013) 976-985.
- [6] A. Brunetti, E. Drioli, Y.M. Lee, G. Barbieri, Engineering evaluation of CO<sub>2</sub> separation by membrane gas separation systems, J Membrane Sci, 454 (2014) 305-315.
- [7] A. Mivechian, M. Pakizeh, Performance Comparison of Different Separation Systems for H<sub>2</sub> Recovery from Catalytic Reforming Unit Off-Gas Streams, Chemical Engineering & Technology, 36 (2013) 519-527.
- [8] Y. Huang, T.C. Merkel, R.W. Baker, Pressure Ratio and Its Impact on Membrane Gas Separation Processes, J Membrane Sci, (2014).
- [9] E. Ayotte-Sauve, M. Sorin, F. Rheault, Energy Requirement of a Distillation/Membrane Parallel Hybrid: A Thermodynamic Approach, Ind Eng Chem Res, 49 (2010) 2295-2305.

- [10] H. Jarvelin, J.R. Fair, Adsorptive Separation of Propylene Propane Mixtures, *Ind Eng Chem Res*, 32 (1993) 2201-2207.
- [11] I.K. Kookos, Optimal design of membrane/distillation column hybrid processes, *Ind Eng Chem Res*, 42 (2003) 1731-1738.
- [12] M. Benali, B. Aydin, Ethane/ethylene and propane/propylene separation in hybrid membrane distillation systems: Optimization and economic analysis, *Separation and Purification Technology*, 73 (2010) 377-390.
- [13] Y. Pan, T. Li, G. Lestari, Z. Lai, Effective separation of propylene/propane binary mixtures by ZIF-8 membranes, *J Membrane Sci*, 390 (2012) 93-98.
- [14] M. Plaza, A. Ferreira, J. Santos, A. Ribeiro, U. Müller, N. Trukhan, J. Loureiro, A. Rodrigues, Propane/propylene separation by adsorption using shaped copper trimesate MOF, *Microporous and Mesoporous Materials*, 157 (2012) 101-111.
- [15] W. Stephan, R.D. Noble, C.A. Koval, Design methodology for a membrane/distillation column hybrid process, *J Membrane Sci*, 99 (1995) 259-272.
- [16] S. Moganti, R.D. Noble, C.A. Koval, Analysis of a membrane/distillation column hydrid process, *J Membrane Sci*, 93 (1994) 31-44.
- [17] S. Hall, *Rules of Thumb for Chemical Engineers*, Butterworth-Heinemann, 2012.
- [18] I.P. Nikolaides, M.F. Malone, Approximate Design of Multiple-Feed Side-Stream Distillation Systems, *Ind Eng Chem Res*, 26 (1987) 1839-1845.
- [19] J.D. Figueroa, T. Fout, S. Plasynski, H. McIlvried, R.D. Srivastava, Advances in CO<sub>2</sub> capture technology—The US Department of Energy's Carbon Sequestration Program, *International Journal of Greenhouse Gas Control*, 2 (2008) 9-20.
- [20] M. Elimelech, W.A. Phillip, The future of seawater desalination: energy, technology and the environment, *Science*, 333 (2011) 712-717.

## **8. Optimization of Membrane/distillation Hybrid Process for Propylene/Propane Separation**

### **8.1 Abstract**

This chapter studies the economic impact of adding a membrane unit to an existing distillation process for the separation of propylene/propane. The evaluation is carried out over membrane permeance ranging from 10 to 100 GPU and propylene/propane selectivity in the range of 1.0 to 300. In order to study the economic feasibility of the hybrid configuration under uncertainty in membrane price and lifetime, three prices are selected to reflect the cost of the different membrane categories. Also, the economic evaluation is carried out at membrane lifetime of 2 and 5 years. An optimization problem is formulated to identify the optimal process design. The integrated (parallel) setup will always outperform the pre-distillation (series) setup due to the flexibility in adjusting the membrane feed flow rate and composition. It is found that membrane hybridization could notably improve the overall process economics. For instance, cost savings of 45%, 37.5%, and 32% are obtained for membrane unit area prices of 100, 500 and 1000 \$/m<sup>2</sup>, respectively, considering membrane lifetime of 5 years. Even at low membrane lifetime of 2 years, the savings are still notable at low membrane cost per unit area (39%, 28% and 8%, respectively).

### **8.2 Introduction**

The design of distillation membrane hybrid system has been discussed in many studies. Pettersen and Lien [1] presented a design model for vapor permeation systems.

The method considered McCabe diagrams to solve the distillation part while the gas permeation part is solved through a mathematical model which is only valid for binary mixture. Pressly and Ng [2] developed a screening procedure to identify membrane performance which corresponds to the breakeven point above which the hybrid system becomes un-economically feasible compared to only distillation case. Bausa and Marquardt [3] calculated the minimum energy required for the separation of multicomponent mixture in order to estimate the minimum required membrane area and identify the location of side stream. This method can be applied to multicomponent non-ideal mixtures. Szitkai et al. [4] applied membrane superstructure mathematical model to the separation of water-ethanol mixture to produce pure ethanol using pervaporation unit. The mathematical model was solved using the quadratic and exponential regression to simplify the integral approximation. Steinigeweg and Gmehling [5] showed through simulation and experimental results, that a hybrid process of a reactive distillation tower and a pervaporation unit is economically favorable. Simulating membrane technology in a process simulator will avoid assumptions normally made to simplify the mathematical modeling of the hybrid system. Marquardt et al [6] proposed a framework for the design of hybrid distillation separation processes based on three main stages: 1. Generation of flow-sheet alternatives. 2. Shortcut evaluation of the alternatives. 3. Rigorous MINLP optimization of the most promising alternatives to obtain the best flowsheet. Caballero [7] proposed a mathematical approach to investigate the applicability of a membrane unit to retrofit an existing distillation column considering parallel setup of the two units. The rigorous MINLP optimization was carried out in a process simulator for the distillation column and auxiliary equipment, while the membrane model was solved in MATLAB.

Eliceche et al [8] conducted a study to optimize the operating conditions of a hybrid membrane/distillation system using a process simulator but, identifying the tray number of feeds and withdrawn streams was carried out by a trial and error procedure.

Kookos [9] proposed a methodology for the structural and parametric optimization of continuous hybrid separation systems. He described the superstructure of the hybrid process using a simplified steady-state mathematical model where it was assumed that all streams taken from or returned to the distillation column were vapor streams. Also, it was outlined that the hybrid systems can potentially reduce the operating cost by 22% if operated at optimum conditions.

Verhoef et al. [10] simulated a hybrid pervaporation membrane process where distillation is performed in Aspen Plus® simulator while the pervaporation membrane calculation is done in Excel Visual Basic for Applications (EVB) and results are linked to Aspen Plus®. The simulation was run to optimize the hybrid system for dehydration of ethanol and purification of acetic acid.

Davis [11] implemented a hollow fiber membrane model in Aspen HYSYS with the assumption of negligible pressure drop without external custom programming. Chowdhury et al. [12] presented a numerical solution approach to incorporate the membrane mathematical model presented by Pan in Aspen Plus® for both co-current and counter-current membrane configurations. In addition, Hussain and Hagg [13] implemented a one-dimensional isothermal model in Aspen HYSYS to study the impact of process parameters on the feasibility of adopting a facilitated transport membrane for CO<sub>2</sub> capture from flue gas. Faizan et al. [14] created a user defined membrane unit in

Aspen HYSYS and simulated the different configurations of a two dimensional cross flow hollow fiber membrane for the separation of CO<sub>2</sub> from natural gas. The mathematical model used is only valid for binary mixture and assumes no pressure drop in fiber lumen.

Most of the above mentioned membrane models, which are implemented in commercial process simulators, are applicable for binary mixtures separation and cannot be used for multi-component mixture. In addition, some of them considered negligible pressure change in hollow fiber lumen which could mislead the economic evaluation. In this study, we aim to utilize a model which is applicable for multi-components gas mixture and accounts for pressure change inside fibers. The potential of membrane retrofit to an existing distillation tower will be discussed over ranges of membrane permeance and selectivity which covers most of literature reported materials for the separation of propylene/propane. The hybrid process economics will be also evaluated at different membrane unit area prices and material durability.

### **8.3 Economic evaluation basis and methods**

Process simulation and optimization is carried out using Aspen Plus® flowsheet modeling package (V7.2). The steps followed for systematic evaluation of membrane potential to retrofit the conventional distillation unit are:

- 1- Design and optimize a distillation tower for the separation of propylene/propane for the existing process described by Gokhale [15] but considering distillate purity of 99.5%.

- 2- Customize a membrane unit operation in Aspen Plus® software using User Custom Model 2.
- 3- Create a process flowsheet for membrane pre-distillation hybrid configuration.
- 4- Build an optimization case to determine the optimal design specifications at the specified membrane performance.

### **8. 2.1 Distillation column**

The existing process for propylene/propane separation which was described by Gokhale [15] and optimized by Kookos [9] is chosen as a case study. The distillation column setup and streams specifications are shown in Fig. 8.1. Propylene purity and recovery in the overhead product are modified to be 99.5% and 99% instead of 99.7% and 98% considered originally. Also, feed and product stream conditions (pressure and temperature) are fixed in all simulation scenarios, in order to avoid disturbing downstream processes.

The existing distillation column consists of 248 trays including the condenser and reboiler. The feed stream is available as pressurized gas mixture at 14.55 bar and 34°C. The optimal distillation column design considering the new separation objective (distillate purity of 99.5% and bottom product purity of 1.0%), is schematically described in Fig. 8.2. The Peng-Robinson equation of state is used to model vapor-liquid equilibrium. Considering Guthrie model [16] for equipment cost estimation and utilities cost shown in Table 1, the distillation process was found to correspond to a total annualized cost of 12.3 M\$/year. The energy cost at the reboiler is about 90% of the system operating cost and more than 70% of the total annualized cost.

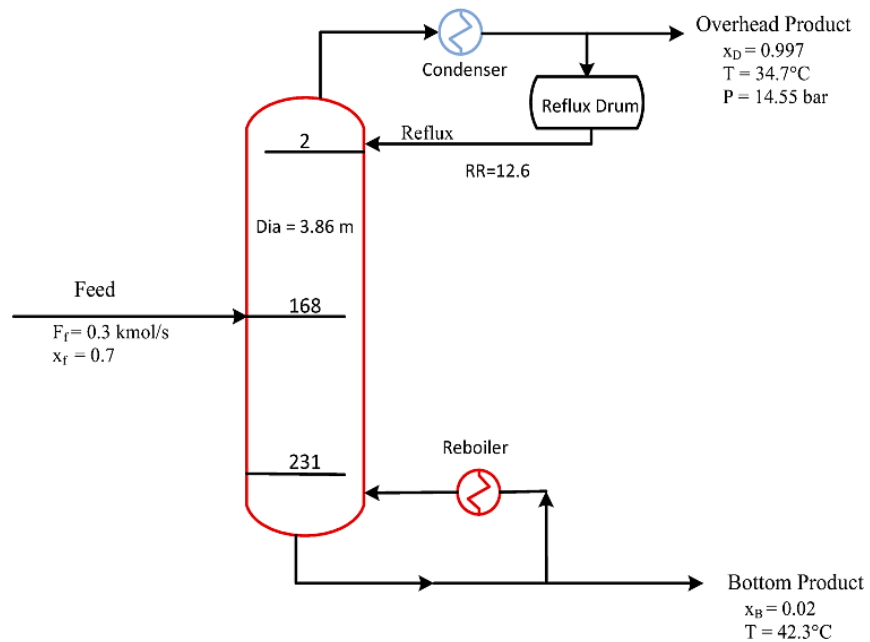


**Fig. 8.1** Existing distillation process described by Gokhale [15]

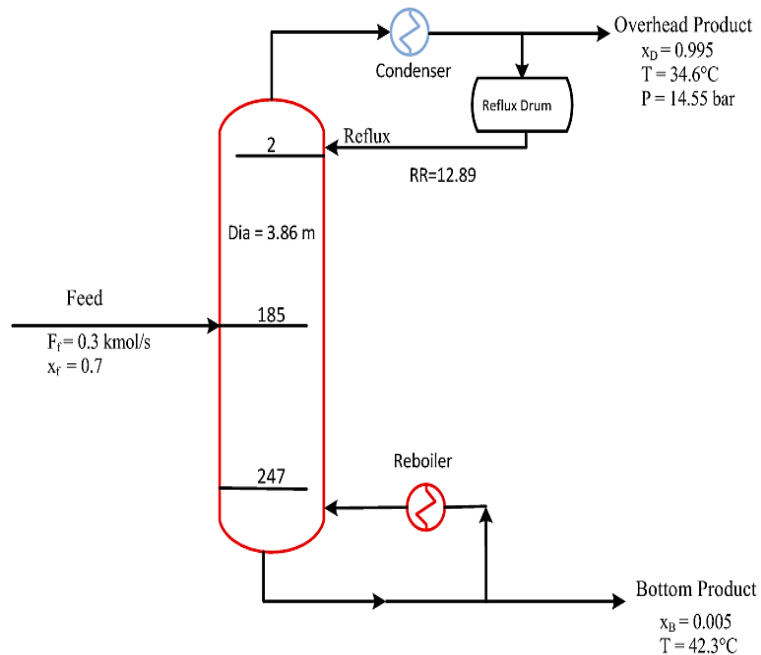


**Fig. 8.2** Optimal design of distillation process for propylene purity of 99.5%

**Table 8. 1** Costs of chemical plant common utilities

<b>Utility</b>	<b>Cost</b>
cooling water (20 °C)	0.35 \$/GJ
low pressure steam	8.00 \$/GJ
electrical power	0.06 \$/kWh

### **8.2.2 Module specification**

As the hollow fiber inner diameter becomes smaller, the inside pressure build-up becomes significant as it can be concluded from Eq. (3.28). This impact is expected to be further maximized as the flow rate or the fibers length increase. These observations are in good agreement with experiments conducted to measure pressure drop occurring in micro-tubes such as the one carried out by Li et al. [17]. This simply proves that the hollow fiber design influences the separation efficiency of the membrane module because of its direct impact on the permeation driving force. Therefore, the design parameters can be optimized for any specific application and under certain design considerations. Optimizing the membrane design is out of this study scope where the inner diameter and length of hollow fibers are fixed at 80 µm and 1.0 m.

In this study, the performance of membrane/distillation hybrid will be evaluated at different membrane separation parameters (permeance and selectivity) while considering the existing and yet to be discovered membranes. The high performance membranes for the separation of propylene/propane are listed in Table 6.1. Thus, the reasonable range for

permeance is from 10 to 100 GPU. Also, the membrane selectivity range over which the evaluation will be carried out is from 1.0 to 300.

### 8.3 Optimization method

The optimization problem is formulated to minimize the Total Annualized Cost (TAC) of the membrane/distillation hybrid configurations shown in Fig. 8.3. The optimization objective function is:

$$\text{Minimize } \mathbf{TAC} = (\mathbf{OPEX} + r\mathbf{CAPEX}) \quad (8.1)$$

The CAPEX of a hybrid configuration consists of two components; one accounts for the distillation unit and the other accounts for the membrane process. Therefore, it can be written as:

$$\mathbf{CAPEX} = \mathbf{CAPEX}_{dis} + \mathbf{CAPEX}_{Mem} \quad (8.2)$$

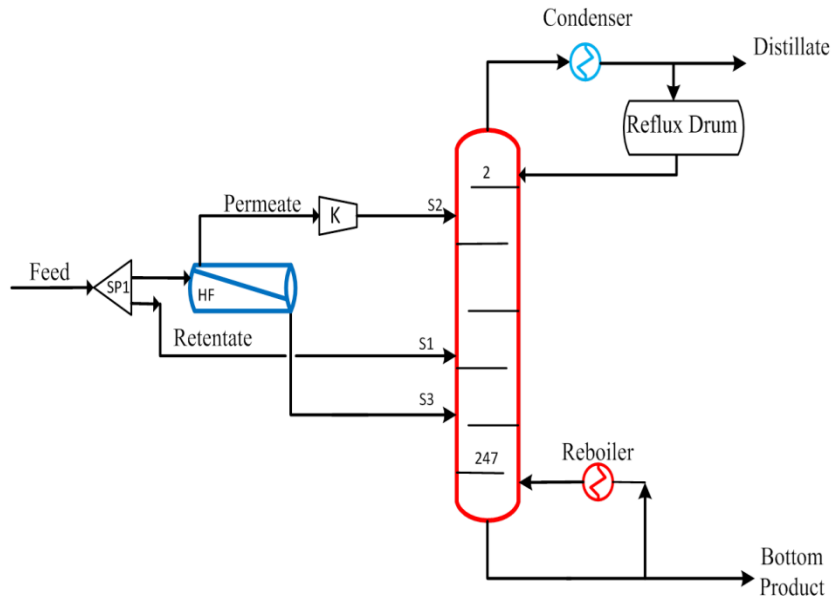
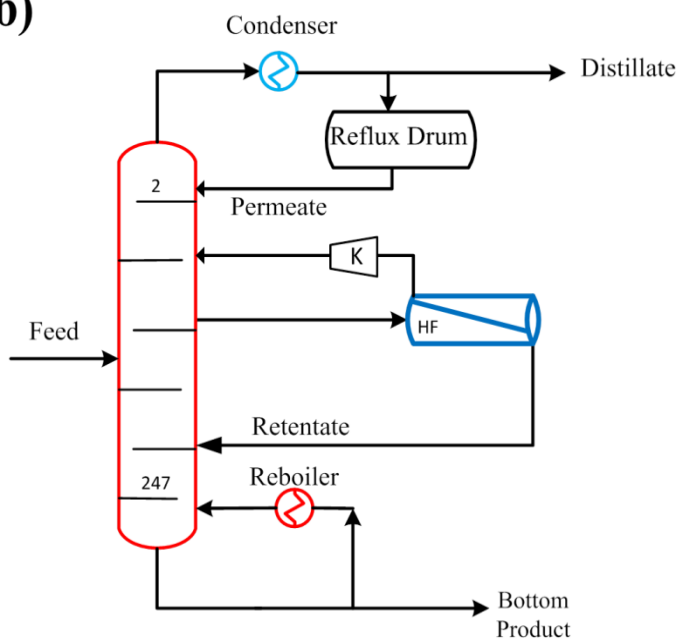
The distillation capital investment is fixed when only retrofitting is considered and it is variable in case of new installations. The total capital investment for the distillation units includes the cost of the column, column internals, condenser and reboiler. The column and internals costs are correlated to tray spacing, number of trays, column diameter, material of construction and operating pressure. The costs of condenser and reboiler are correlated to the heat transfer area, operating conditions and material of construction. In this study those capital cost of distillation column, column internals, condenser and reboiler are calculated using Guthrei [16] economic model. The membrane process capital investment includes the cost of membrane modules, compressors and heat exchangers (described earlier in chapter 6).

The operating expenditures (OPEX) are calculated based on equipment duties and the corresponding utility costs as given in Table 8.1 and are defined by Eq. (8.3) assuming a total operating time of 8000 hours annually.

$$\begin{aligned} OPEX &= OPEX_{reb} + OPEX_{con} + OPEX_{comp} + OPEX_{HX} \\ &= 8000[8.0D_{reb} + 0.354(D_{con} + D_{exch}) + 0.06 D_{comp}] \end{aligned} \quad (8.3)$$

Where,  $D_{reb}$ ,  $D_{con}$ ,  $D_{comp}$ , and  $D_{HX}$  are duties per hour (GJ/h) of reboiler, condenser, compressor, and heat exchanger, respectively.

The optimization constraints are set as the separation requirements in terms of the propylene concentration in the distillate product and its recovery ratio. Therefore, according to the considered case study, the distillate product should have a minimum propylene molar concentration ( $x_D$ ) of 99.5% and at the same time the propylene recovery ratio should be at least 99%. The optimization problem is completely formulated when the optimization variables are defined with their practical limits. The optimization variables are the membrane area, feed fraction to membrane unit, feed stage number, permeate and retentate return stages and reflux ratio. The same optimization variables apply to the parallel configuration but instead of the feed split ratio two variables should be considered which are the side-stream flow rate and its composition. The cost saving generated from retrofitting the distillation process can be estimated by subtracting the total annual cost (CAPEX and OPEX) of the introduced equipment from the reboiler operating cost. Therefore, the maximum expected cost saving is 70% which corresponds to the situation where the membrane module can meet the separation objectives with zero capital and operating cost.

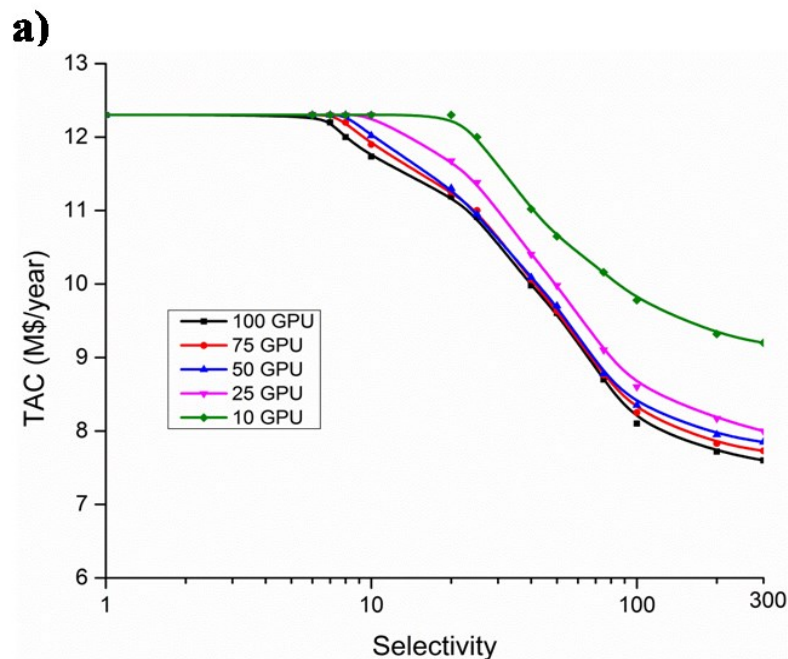
**a)****b)**

**Fig. 8. 3** Membrane/distillation hybrid configurations a) pre-distillation hybrid b) parallel or integrated hybrid.

## 8.4 Results and discussion

### 8.4.1 Membrane pre-distillation hybrid

The optimal cost of the pre-distillation hybrid configuration is plotted against the hypothetical membrane selectivity and permeance in Fig. 8.4a for a membrane module corresponding to a price of \$100/m<sup>2</sup> and an expected lifetime of 5 years. Under these assumptions, the membrane pre-distillation configuration is found to be more feasible than the conventional distillation process starting from a permeance higher than 10 GPU. As the membrane permeance increases, the minimum selectivity required for feasible hybrid configuration is significantly reduced. For example, as the membrane permeance increases from 10 to 20 GPU the minimum required selectivity is reduced from 20 to 12. The annualized cost of this hybrid configuration reaches a minimum of 7.6 M\$/year at the upper limits of the considered ranges of membrane selectivity and permeance.



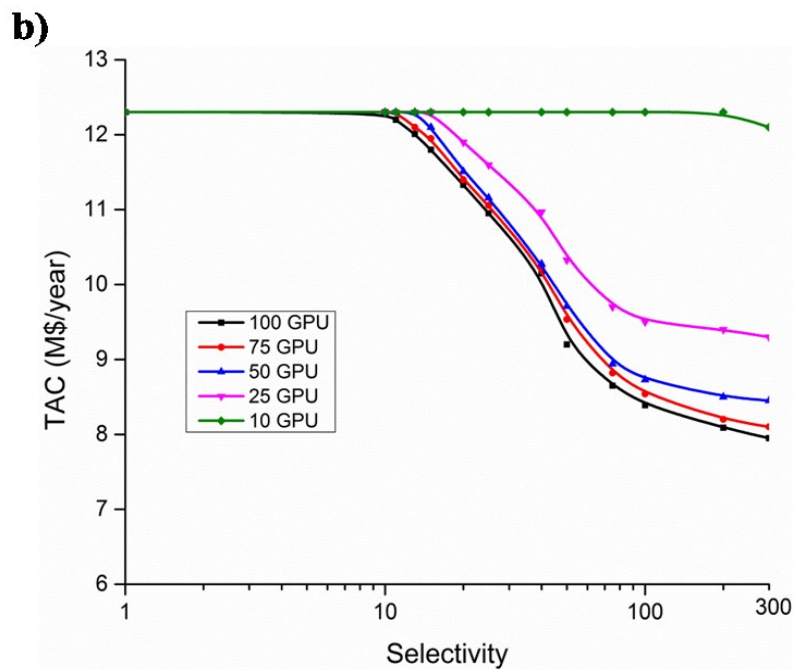


**Fig. 8.4** TAC of pre-distillation hybrid configuration at membrane cost of \$100/m<sup>2</sup> and lifetime of a) 5 years b) 2 years.

When membrane permeance is higher than 25, the increase in selectivity results in a sharp decrease of the optimal annual process cost till the selectivity reaches 100 where the cost still declines further but at a slower rate. In other words, the cost of this hybrid configuration, and at this cost per unit area and lifetime assumptions, is a strong function of both permeance and selectivity only at membrane permeance less than 25 GPU. Beyond this specific permeance the cost function becomes less dependent on permeance. This behavior can be attributed to the fact that at such low membrane cost and relatively high permeance the membrane capital and operating expenses are in a lower order of magnitude compared to the distillation part. Therefore, though the increase in membrane permeance reduces the required surface area, the cost reduction does not significantly improve the hybrid system economics. To generalize this finding, it can be stated that

based on the membrane selectivity and the conventional process economics, there is a critical permeance value after which the impact of permeance on the pre-distillation configuration cost becomes limited.

The annualized cost of the pre-distillation hybrid at a fixed selectivity of 40 and permeances of 50, 75 and 100 are 10.16, 10.11 and 10.07 M\$/year, respectively. On the other hand, as the membrane selectivity increases to 75 the annualized cost at the same permeances is reduced to about 8.76 M\$/year. At the optimal hybrid configuration and over the considered permeance and selectivity ranges, the membrane cost is found to be always lower than the permeate stream compression cost.

When the membrane lifetime is reduced to 2 years, the contribution of membrane cost to the TAC becomes 2.5 times its contribution when the membrane lifetime is 5 years. Therefore, it is expected that the optimal solution exists at lower membrane area with subsequent higher reflux ratio in the distillation column. The optimal cost of hybrid configuration is plotted against membrane selectivity and permeance in Fig. 8.4b. Table 8.2 compares the cost of the optimal hybrid designs for the two considered membrane lifetimes at membrane permeance of 50 GPU. The collected results showed that the permeance impact on the hybrid configuration cost becomes negligible compared to selectivity impact at membrane permeance higher than 50 GPU.

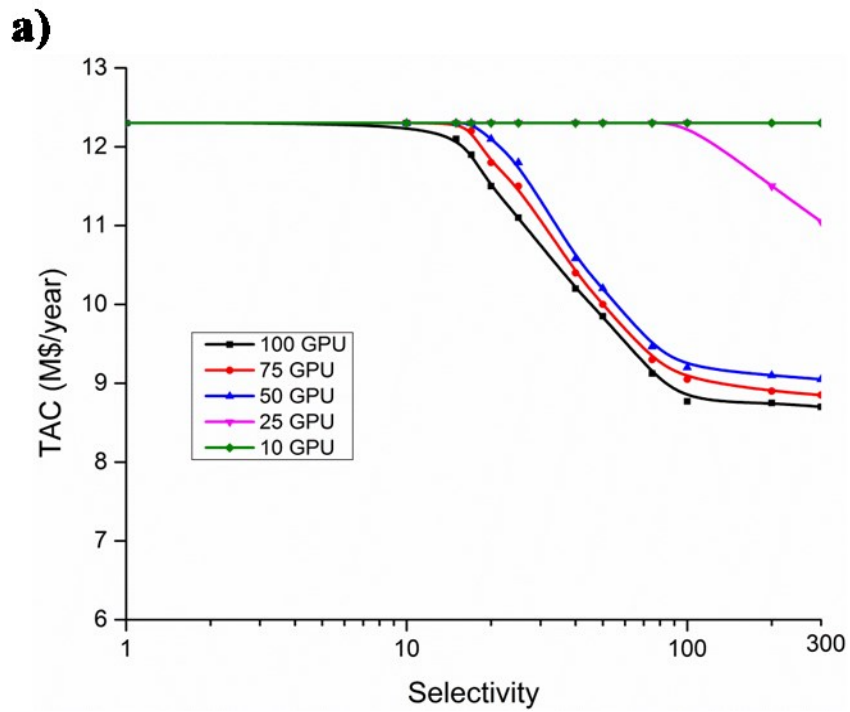
**Table 8.2** Reduction in TAC of the hybrid configuration at permeance of 50 GPU and membrane price of \$100/m<sup>2</sup>.

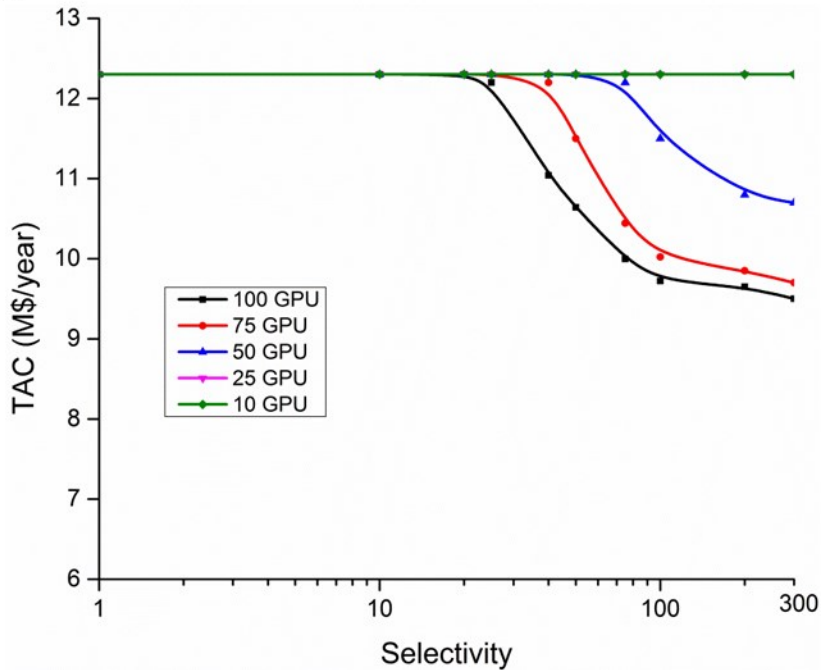
Selectivity	5 years		2 years	
	TAC (M\$)	Cost Saving %	TAC (M\$)	Cost Saving %
25	11.0	10.6	11.2	8.9
50	9.8	20.3	9.9	19.5
75	8.8	28.4	8.9	27.6
100	8.3	32.5	8.7	29.2
200	7.9	35.7	8.5	30.8

Considering a hypothetical membrane with cost of \$500/m<sup>2</sup>, the optimization results for the series configuration at such cost parameters of the membrane module are illustrated in Fig. 8.5a and b for lifetimes of 5 and 2 years, respectively. The optimal membrane area for this case is lower than those in cases 1. In addition, the optimal reflux ratio is higher, which indicates that the distillation process becomes more feasible than maximizing propylene recovery by the membrane module. When the membrane is durable for 5 years, the minimum permeance to make the hybrid configuration more feasible is 25 GPU with minimum selectivity of 75. On the other hand, the minimum required selectivity for feasible hybrid configuration is 40 with permeance of 100 GPU. The maximum cost reduction which occurs at the simulation upper limits of both separation parameters is 37.5%.

Reducing the membrane durability to 2 years is equivalent to increasing the membrane price by 2.5 compared to the 5 years lifetime. Therefore, the membrane process becomes

unfavorable to perform bulk separation, especially at low membrane selectivity where the two products are far from the required purity while the added cost is higher than what could be avoided by reducing the separation energy. The optimization results for this hybrid configuration at membrane cost of \$500/m<sup>2</sup> and lifetime of 2 years are illustrated in Fig. 8.5b. At these cost assumptions, the hybrid configuration shows feasibility only at a permeance higher than 75 GPU. This minimum permeance requires a selectivity of 75. As the membrane permeance increases to 100 GPU, the required selectivity decreases to 40 but with only 1% of cost saving. The maximum reduction in TAC is 28% which occurs at the upper limits of selectivity and permeance. Table 3 exemplifies the impact of the membrane durability on the cost of the optimal designs for this hybrid configuration at membrane permeance of 100 GPU.



**b)**

**Fig. 8.5** TAC of pre-distillation hybrid configuration at membrane cost of \$500/m<sup>2</sup> and lifetime of a) 5 years b) 2 years.

**Table 8.3** Reduction in TAC of the hybrid configuration at permeance of 100 GPU and Membrane price of \$500/m<sup>2</sup>.

Selectivity	5 years		2 years	
	TAC (M\$)	Cost Saving %	TAC (M\$)	Cost Saving %
25	11.66	5.2	12.3	0.0
50	9.92	19.3	10.64	13.5
75	9.12	25.8	10.00	18.7
100	8.52	30.7	9.72	21.0
200	7.68	37.6	8.85	28.1

Simulating the scenario where the membrane cost is \$1000/m<sup>2</sup>, the series hybrid configuration fails to perform the separation at lower cost than the only distillation setup, except at very high membrane performance. For membrane durability of 5 years, these exceptions are when the selectivity is higher than 75 for low permeable membranes or the permeance is higher than 75 GPU for low selective membranes. When the membrane lifetime is only 2 years, the minimum permeance to breakeven with distillation over the considered range of selectivity is 85 GPU. Considering a membrane with a permeance of 100 GPU, the hybrid process is found only feasible when selectivity is at least 20 and 100 for lifetimes of 5 and 2 years, respectively. This can be attributed to the fact that the reduction in the distillation process operating cost is less than the membrane separation cost at the two considered membrane lifetimes and permeance lower than the corresponding minimum value highlighted earlier. The relation noticed in all the earlier cases, regarding the reduction in the required selectivity for a break-even situation as permeance increases, holds here too. The maximum cost savings which take place at the upper bonds of permeance and selectivity are 32% and 8% for lifetime of 5 and 2 years, respectively. The optimization results for membrane module lifetime of 5 years are illustrated in Fig. 8.6.

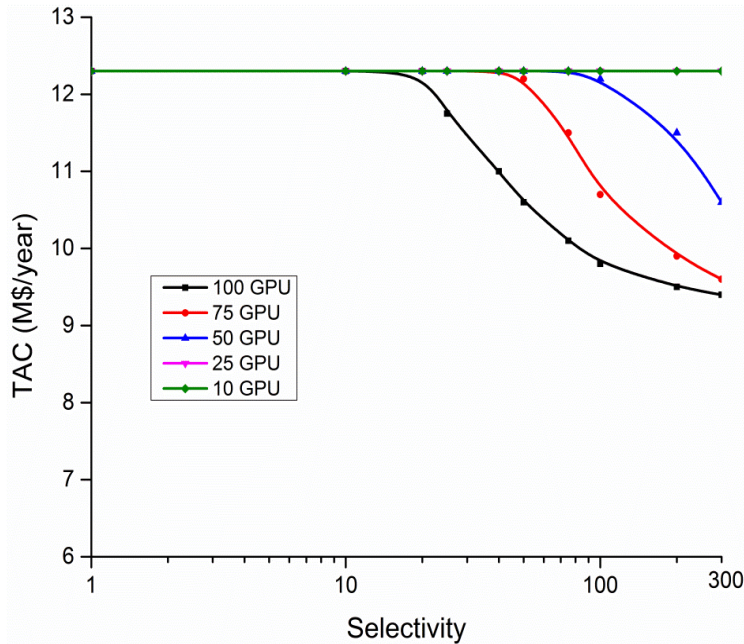
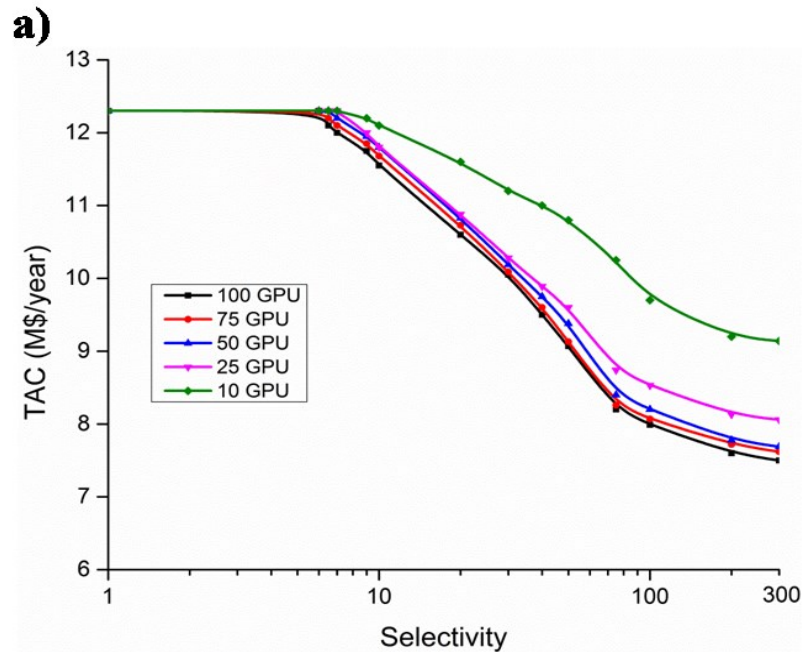


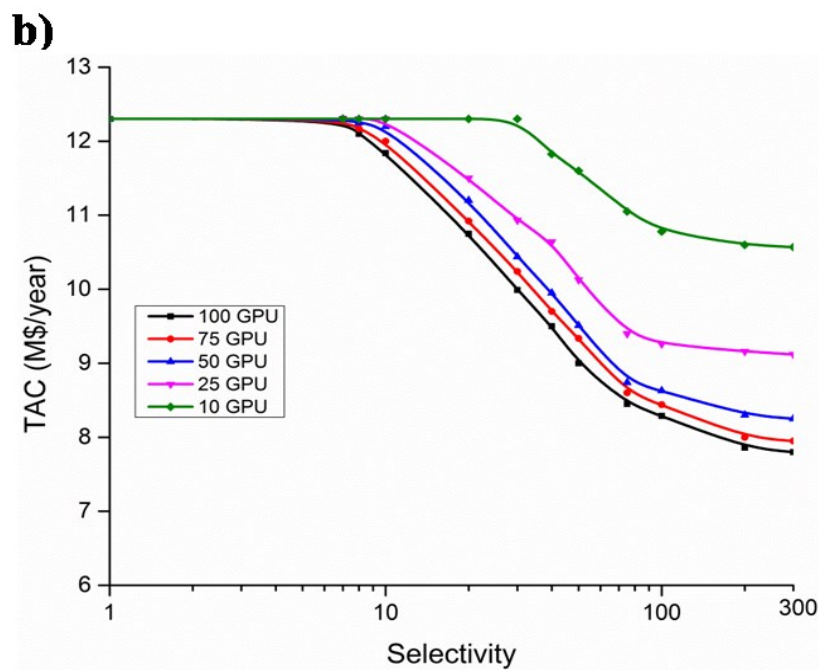
**Fig. 8. 6** TAC of the pre-distillation hybrid configuration at membrane cost of \$1000/m<sup>2</sup> and lifetime of 5 years.

#### 8.4.2 Integrated membrane/distillation hybrid

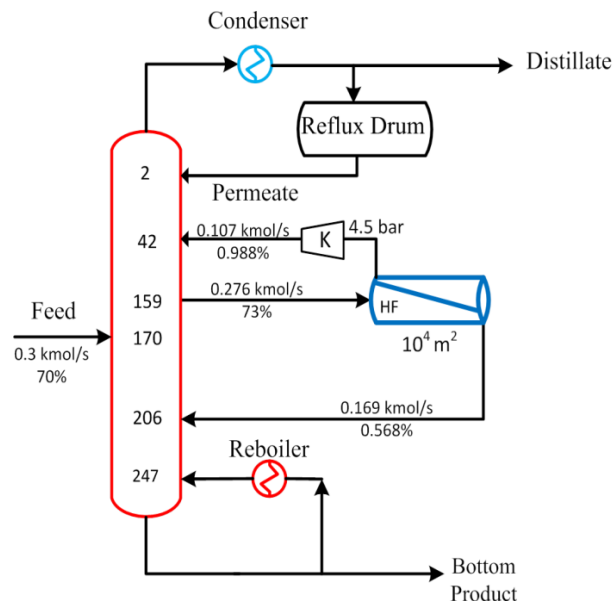
The optimal TAC of the integrated hybrid configuration is plotted against membrane selectivity for different membrane permeance in Fig. 8.7a and b. The illustrated data corresponds to membrane unit area price of \$100/m<sup>2</sup> and lifetimes of five and two years, respectively. At this relatively low membrane cost, the process TAC is not sensitive to the membrane lifetime except at very low membrane selectivity and permeance. When the membrane lifetime is 5 years, the hybrid configuration is found to be more feasible than the conventional distillation process starting from a permeance higher than 7 GPU but conditionally the selectivity should be higher than 200. When the lifetime is only 2 years, the minimum permeance is found to be 9 GPU when selectivity is at the upper bound of the considered range. Higher membrane permeance results in a lower membrane

area and hence lower membrane CAPEX. Therefore, the system requires lower selectivity to breakeven with the conventional distillation process. It is also noticed that the optimal side-stream flow rate is less than the distillation feed. As the membrane selectivity increases, the optimal side-stream concentration becomes closer but slightly higher than the feed concentration. The flexibility of adjusting the membrane feed flow rate and concentration makes this configuration perform the separation at lower TAC than the pre-distillation design. When the membrane cost per unit area is 100 or lower while its lifetime is 5 years, the hybrid system has relatively close annualized cost after a permeance of 50 is reached. This is because the membrane CAPEX after this critical permeance is at a lower order of magnitude than the accomplished saving. When the membrane lifetime is only 2 years, the critical permeance is identified to be 75 GPU. The optimal design of this hybrid configuration is illustrated in Fig. 8.8 for a membrane with selectivity of 40 and permeance of 50.



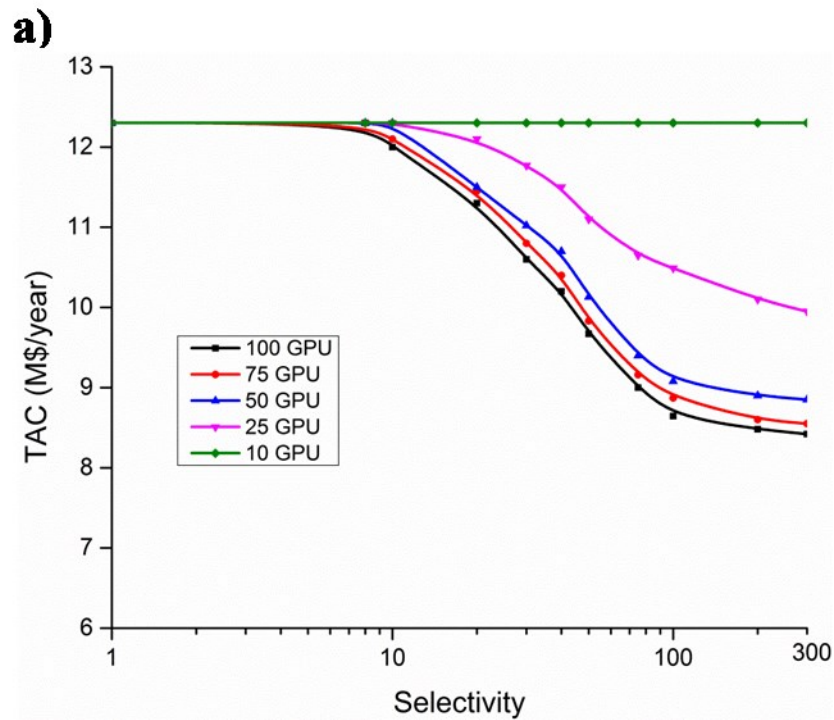


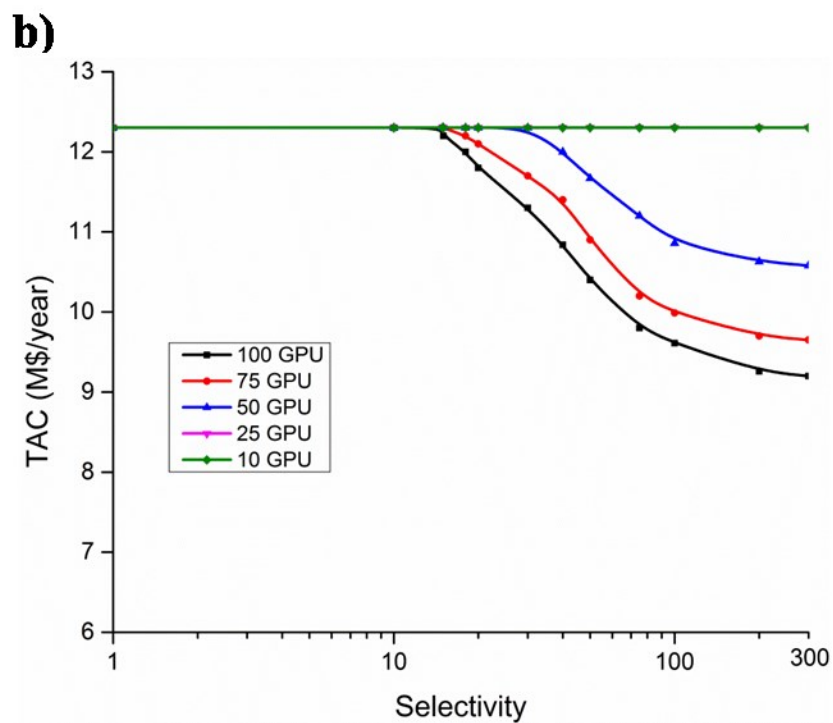
**Fig. 8.7** TAC of the membrane/distillation parallel configuration at membrane cost of \$100/m<sup>2</sup> and lifetime of a) 5 years b) 2 years.



**Fig. 8.8** The optimal design of the integrated hybrid configuration for a membrane with selectivity of 40 and permeance of 50.

When the membrane unit area price is set to \$500/m<sup>2</sup>, the lifetime impact becomes more significant as can be concluded by comparing the two studied lifetimes illustrated in Fig. 8.9. Hence, higher permeability is mandatory for the hybrid system to breakeven with the distillation process at lifetime of 2 years. A membrane with selectivity of 40 requires permeance of 40 GPU to start becoming feasible when its lifetime is 2 years while it only requires a permeance of 20 GPU when its lifetime is 5 years. As the membrane durability is reduced, the optimal TAC exists at higher pressure ratio to reduce the membrane area. This behavior did not appear when the membrane cost is \$100/m<sup>2</sup> since the cost of extra compression is higher than the expected saving from lower membrane CAPEX.

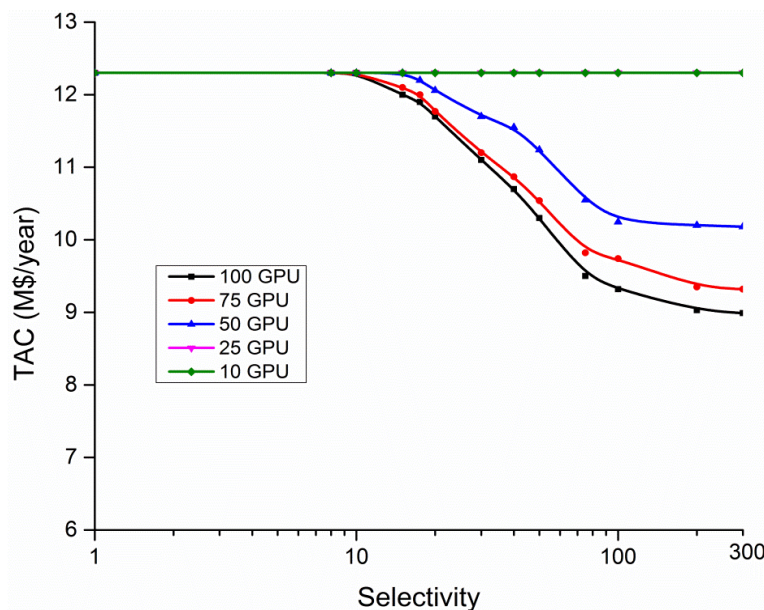




**Fig. 8.9** TAC of the membrane/distillation parallel configuration at membrane cost of \$500/m<sup>2</sup> and lifetime of a) 5 years b) 2 years.

Simulation of the integrated membrane distillation hybrid for a membrane cost of \$1000/m<sup>2</sup> showed more urgency for high durability to compete with distillation. Fig. 8.10 illustrates the system TAC against the membrane selectivity and permeances. When lifetime is 5 years, the behavior of the cost function against both selectivity and permeance is almost identical as the case when the membrane has a cost of \$500/m<sup>2</sup> and durability of 5 years. When the lifetime is 2 years, the hybrid system only feasible at permeance higher than 75 but conditionally the selectivity is higher than 50. When membrane permeance is increased to 100 GPU, the system showed a breakeven with the conventional distillation process at selectivity of 45. Therefore, at such membrane

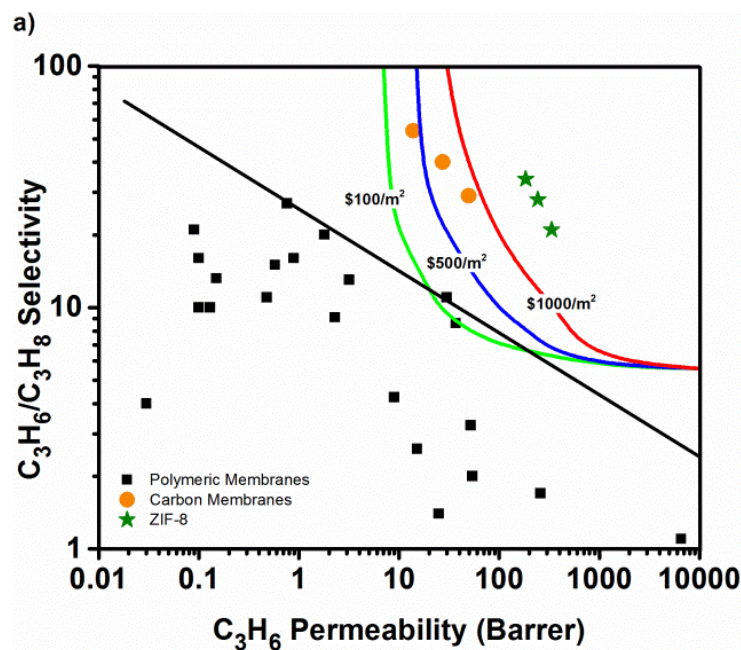
economic considerations, all the literature reported membranes failed to meet the minimum requirements for feasible hybrid system.



**Fig. 8.10** TAC of the membrane/distillation parallel configuration at membrane cost of 1000\$/m<sup>2</sup> and lifetime of 5 years.

Mapping the obtained breakeven membrane performance (permeability and selectivity) on Robeson trade-off curve for propylene/propane separation is absolutely of great importance to membrane technology research groups. In the previous discussions we considered permeance while Robeson plot is in terms of permeability, hence a conversion is need and therefore the membrane selective layer thickness is considered to be 1  $\mu\text{m}$ . Thus the permeance in GPU becomes equivalent to permeability in Barrer. Fig. 8.11a and b illustrate the feasible regions for the three studied membrane area unit prices (100, 500 and 1000 \$/m<sup>2</sup>) at membrane lifetime of 5 and 2 years, respectively. When the membrane durability is 5 years, some polymeric membrane has the potential if the commercialization cost is \$100/m<sup>2</sup> or less. Though some of the discovered polymeric

membranes are higher than the breakeven values, the return on investment is not economical. Hence, it is recommended to consider at least two folds of the breakeven identified values. As the prices reaches \$500/m<sup>2</sup>, the so far discovered polymeric are not sufficient, regardless of membrane durability. Membranes with performances such as those reported for carbon membranes or ZIF-8 with details in Table 2 can effectively reduce the separation cost even at membrane price higher than \$500/m<sup>2</sup> but conditionally along with durability of 5 years. At the same membrane unit area cost and durability of 2 years, only membranes with performance as ZIF-8 or better are attractive to hybridize with distillation. Finally, when the membrane unit area cost is \$1000/m<sup>2</sup> then only membranes with permeability higher than 30 GPU have the potential to reduce the separation cost when it is durable for 5 years. When the membrane durability is only 2 years, only membranes with permeance of at least 60 can make the hybrid system more feasible than the distillation process.



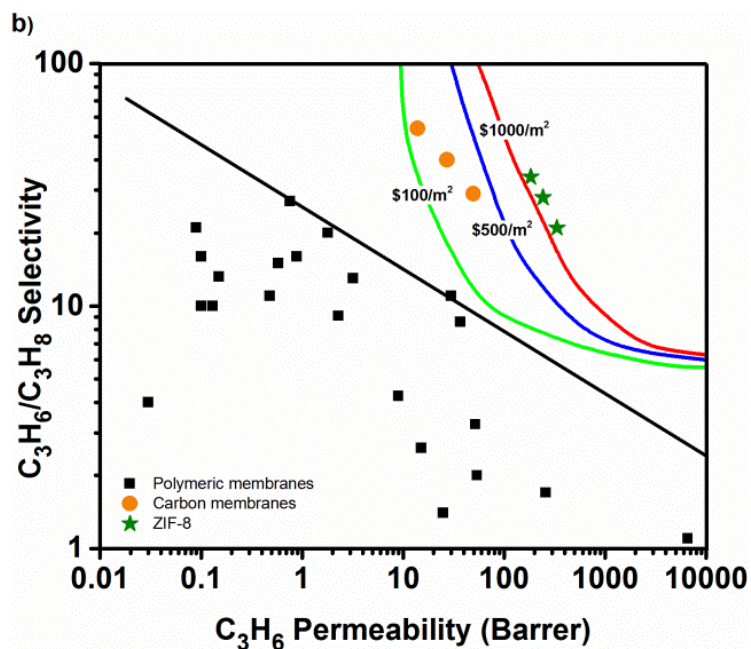


**Fig. 8. 11** The minimum membrane performance (selectivity and permeability) for feasible membrane/distillation hybrid process under membrane cost of 100, 500 and 1000 \$/m<sup>2</sup> and durability of a) 5-years b) 2-years.

## 8.5 Conclusion

In this chapter the economic feasibility of membrane/distillation hybrid configurations is thoroughly investigated for propylene/propane separation process. The analysis is carried out over wide ranges of membrane permeance and selectivity. Also, the economic evaluation is performed for different costs of membrane materials and under uncertainty of membrane lifetime. For all the simulated cases the parallel configuration outperforms the series configuration and this finding confirms the conclusions made in chapter 7.

At a certain membrane unit area cost, there is a minimum selectivity after which the hybrid system becomes more feasible than the conventional process. Higher membrane

durability and permeability reduces the minimum selectivity. Increasing selectivity away from this minimum will always reduce the separation cost. However; the cost reduction becomes insignificant at very high selectivity. At low membrane cost, high durability and high permeability, the minimum energy calculation can assess the membrane attractiveness. One the other hand, economic analysis is an essential tool to investigate the hybrid process potential as these parameters deviate. In general membranes with selectivity and permeance higher than 20 and 30, respectively, are attractive for propylene/propane separation but conditionally these membranes should be durable and has low cost per unit area.

## 8.6 References

- [1] T. Pettersen, K.M. Lien, Design of Hybrid Distillation and Vapor Permeation Processes, *J Membrane Sci*, 102 (1995) 21-30.
- [2] T.G. Pressly, K.M. Ng, A break-even analysis of distillation - membrane hybrids, *AIChE journal*, 44 (1998) 93-105.
- [3] J. Bausa, W. Marquardt, Shortcut design methods for hybrid membrane/distillation processes for the separation of nonideal multicomponent mixtures, *Industrial & Engineering Chemistry Research*, 39 (2000) 1658-1672.
- [4] Z. Szitkai, Z. Lelkes, E. Rev, Z. Fonyo, Optimization of hybrid ethanol dehydration systems, *Chem Eng Process*, 41 (2002) 631-646.
- [5] S. Steinigeweg, J. Gmehling, Transesterification processes by combination of reactive distillation and pervaporation, *Chem Eng Process*, 43 (2004) 447-456.
- [6] W. Marquardt, S. Kossack, K. Kraemer, A framework for the systematic design of hybrid separation processes, *Chinese J Chem Eng*, 16 (2008) 333-342.
- [7] J.A. Caballero, I.E. Grossmann, M. Keyvani, E.S. Lenz, Design of Hybrid Distillation-Vapor Membrane Separation Systems, *Industrial & Engineering Chemistry Research*, 48 (2009) 9151-9162.
- [8] A.M. Eliceche, M.C. Daviou, P.M. Hoch, I.O. Uribe, Optimisation of azeotropic distillation columns combined with pervaporation membranes, *Comput Chem Eng*, 26 (2002) 563-573.
- [9] I.K. Kookos, Optimal design of membrane/distillation column hybrid processes, *Industrial & Engineering Chemistry Research*, 42 (2003) 1731-1738.
- [10] A. Verhoef, J. Degreve, B. Huybrechs, H. van Veen, P. Pex, B. Van der Bruggen, Simulation of a hybrid pervaporation-distillation process, *Comput Chem Eng*, 32 (2008) 1135-1146.

- [11] R.A. Davis, Simple gas permeation and pervaporation membrane unit operation models for process simulators, *Chem Eng Technol*, 25 (2002) 717-722.
- [12] M.H.M. Chowdhury, X.S. Feng, P. Douglas, E. Croiset, A new numerical approach for a detailed multicomponent gas separation membrane model and AspenPlus simulation, *Chem Eng Technol*, 28 (2005) 773-782.
- [13] A. Hussain, M.B. Hagg, A feasibility study of CO<sub>2</sub> capture from flue gas by a facilitated transport membrane, *J Membrane Sci*, 359 (2010) 140-148.
- [14] F. Ahmad, K.K. Lau, A.M. Shariff, Removal of CO<sub>2</sub> from natural gas using membrane separation system: modeling and process design, *Journal of Applied Sciences*, 10 (2010) 1134-1139.
- [15] V. Gokhale, S. Hurowitz, J.B. Riggs, A Comparison of Advanced Distillation Control Techniques for a Propylene/Propane Splitter, *Industrial & Engineering Chemistry Research*, 34 (1995) 4413-4419.
- [16] J.M. Douglas, *Conceptual design of chemical processes*, McGraw-Hill, New York, 1988.
- [17] Z.-X. Li, D. Du, Z. Guo, Characteristics of frictional resistance for gas flow in microtubes, in: *Proceedings of symposium on energy engineering in the 21st Century*, DTIC Document, 2000, pp. 658-664.

## 9. Conclusions and Future Recommendations

### 9.1 General conclusions and contributions

The main objective of this work is to investigate the attainability, energy consumption and feasibility of membrane technology in a stand-alone setup or as part of a hybrid separation system. To undertake this objective, membrane simulations and optimization should be conducted on the selected case study process. Process simulation requires a full mathematic representation of all the involved unit operations and hence the urgency to incorporate the membrane module in one of the available process simulators raise since all unit operations except the membrane unit are pre-defined. The mathematical model for membrane separation in a counter-current flow pattern was corrected for the pressure change occurs inside the fiber lumen. The model was then solved and the solution was linked to a user-defined unit operation in ASPEN PLUS.

#### 9.1.1 Attainability of single-stage membrane

Using the complete well-mixed assumption, analytical solution is obtained for the separation of a binary gas mixture in a single-stage membrane process. The membrane selectivity and the pressure ratio are the only parameters defining the process attainability region to accomplish a certain separation task. Plotting these parameters against each other the attainability behavior of the membrane process is exemplified. The relationship between the selectivity and the pressure is monotonic. Hence, both parameters exhibit minimum thresholds that are independent of the value of any other parameters. By taking the limits of the governing relationship, formulas describing these thresholds were

obtained. The minimum pressure ratio was found to be independent of the membrane module design while the minimum selectivity was found strongly design dependent. Moreover, the importance of the non-recovered fraction ( $1-\eta$ ) of the high permeable component is recognized as it appears in the denominators of these formulas.

Plotting the simulated minimum selectivity in a hollow fiber module against the non-recovered fraction ( $1-\eta$ ), a power relationship was found to accurately fit all data points. The function intercept is equivalent to the separation factor while the power coefficient is a nonlinear function of product purity and feed composition. Using the minimum selectivity a relationship was obtained to produce the attainability behavior. Studying the attainability of membrane process for two case studies, accurate results were obtained.

### **9.1.2 Attainability and minimum energy of multiple-stage cascade membrane systems**

A single-stage membrane is theoretically capable to meet any product specification once it is made from material with sufficiently high selectivity and operated under appropriate transmembrane pressure ratio. Nonetheless, the existing membranes have much lower selectivity than what is needed especially when the separation task is to accomplish high enrichment and high recovery from a diluted feed mixture. Thus meeting the separation task can be only accomplished in the single-stage setup by high pressure operation resulting in high energy consumption. The alternative approaches to enhance the membrane process energy efficiency are using recycling or multiple-stages.

The energy consumption of multi-stage membrane systems was found primary determined by membrane selectivity. In general the higher the membrane selectivity, the lower is the energy consumption. Using a small recycle ratio will not change the energy consumption much, but can significantly reduce the required membrane selectivity. This indicates the benefit of using recycle streams in the membrane cascade designs. However, using a large recycle ratio will cause a big energy penalty, although it may further reduce the required membrane selectivity and pressure ratio and such benefit will become more and more marginal at larger recycle ratio. The minimum energy consumption at different membrane selectivity can be found by the energy envelope. This envelope curve can provide a simple way to find the minimum required membrane selectivity for multi-stage membrane designs in order to compete with conventional separation techniques from the energy point of view.

### **9.1.3 Systematic synthesis and optimization of membrane networks for gas separation**

A comprehensive systematic synthesis and optimization of a membrane network was proposed to investigate the attractiveness of membrane technology under uncertainty in membrane performance, price and lifetime for gas separation. Based on conceptual design knowledge gained from literature review, it was concluded that mass transfer between enriching and stripping stages should be only through the feed stage. Hence, a 5-stage membrane network superstructure was prepared using membrane modules, compressors, heat exchangers, mixers and splitters to cover all practical flowsheet configurations. Then an optimization formulation was developed using an objective function that minimizes the process Total Annualized Cost (TAC). The optimal

membrane network was found to consist of a feed stage, a single enriching stage and two stripping stages. This structure is valid for membrane selectivities lower than 50, above which only one stripping stage is optimal. The behavior of the network annual cost was illustrated as a function of permeance and selectivity at different membrane cost parameters. Results showed that at a specific membrane price and durability, there is a minimum sufficient permeance after which the membrane network economics is less sensitive to selectivity higher than 40.

#### **9.1.4 Minimum energy of single-stage membrane and membrane/distillation Hybrid processes**

Studies on the minimum practical separation energy of the membrane/distillation hybrid systems showed that the energy consumption is solely determined by the membrane selectivity and the applied transmembrane pressure ratio. At low selectivity, the membrane process is not competitive to the distillation process. Adding a membrane unit to the distillation tower will not help in reducing the energy. At medium selectivity, the membrane/distillation hybrid system will reduce the energy and the higher the membrane selectivity, the lower the energy. The pressure ratio will also significantly affect the energy. Increasing pressure ratio will further reduce the energy consumption. At high selectivity a single-stage membrane is able to achieve the separation tasks and significantly reduce the energy consumption once the applied pressure ratio is higher than the threshold limit. In general, the higher the selectivity, the lower the energy consumption is.

### **9.1.5 Optimization of membrane/distillation hybrid process for propylene/propane separation**

In order to study the impact of hybridizing a single-stage membrane unit to an existing distillation process, an economic analysis was conducted. The evaluation was carried out over wide ranges of selectivity and permeance. The analysis was also conducted under uncertainty in membrane price and lifetime. The integrated (parallel) setup is always outperforming the pre-distillation (series) setup due to the flexibility in adjusting the membrane feed flow rate and composition. In addition, it was found that membrane hybridization could notably improve the overall process economics. The importance of high durability and permeance was recognized at high membrane cost.

## **9.2 Suggestions for future work**

The following topics are identified as areas for future work based on the findings of this dissertation:

### **Studying the impact of module design on its attainability**

In this dissertation the membrane attainability is investigated for the counter-current hollow fiber membrane module. It would of great importance to generalize the discovered findings to cover the different flow patterns and also to the other membrane configurations and more specifically to the flat sheet module which is the mostly used design.

### **Enhancing the representation of the attainability chart**

The conducted economic analyses showed the influence of the membrane area on the feasibility of membrane systems. Therefore, modifying the attainability chart to illustrate the membrane area as a function of selectivity will make the attainability chart more informative. It will illustrate the selectivity impact on both the operating cost represented by the applied pressure ratio and the capital cost represented by the membrane area.

## Appendices

### Appendix A: Model derivation based on complete well-mixed

Assuming a binary gas mixed containing components A and B is fed into a membrane module as illustrated in Fig. A1. The feed stream has molar flow rate and concentration of F and  $x_A$ , respectively. The module is assumed to be operated under complete well-mixed. Therefore, the feed-side has a homogenous concentration equivalent to that of the retentate stream  $r_A$  and likewise the permeate side has a homogenous concentration equivalent to that of the final permeate stream  $y_A$ .

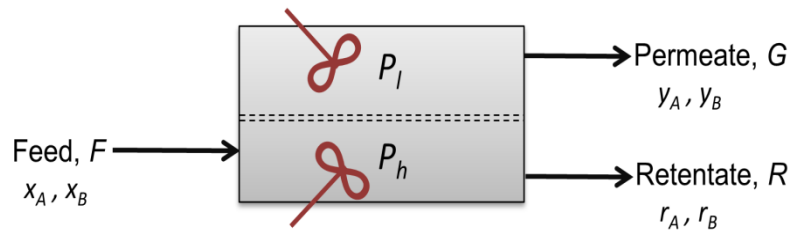


**Fig. A1:** Schematic representation of a single-stage membrane process.

Under these assumptions, the rate of permeation for component A can be written as:

$$y_A G = A \frac{\beta_A}{l} (P_h r_A - P_l y_A) \quad (\text{A1})$$

For component B, the permeation rate can be written as:

$$y_B G = A \frac{\beta_B}{l} (P_h r_B - P_l y_B) \quad (\text{A2})$$

Since:

$$y_B = 1 - y_A \quad (\text{A3})$$

$$r_B = 1 - r_A \quad (\text{A4})$$

Therefore, Eq. (A2) can be written as:

$$(1-y_A)G = A - \frac{\beta_B}{l}(P_h(1-r_A) - P_l(1-y_A)) \quad (\text{A5})$$

By dividing Eq. (A1) by Eq. (A5) the following relationship can be obtained:

$$\frac{y_A}{1-y_A} = S \frac{\gamma r_A - y_A}{\gamma(1-r_A) - (1-y_A)} \quad (\text{A6})$$

This relationship can be also written in terms of the dimensionless parameters as:

$$\frac{y_A}{1-y_A} = S \frac{\gamma r_A - y_A}{\gamma(1-r_A) - (1-y_A)} \quad (\text{A7})$$

## Appendix B: Model derivation for cascade membrane systems

### (1) Constant recycle ratio

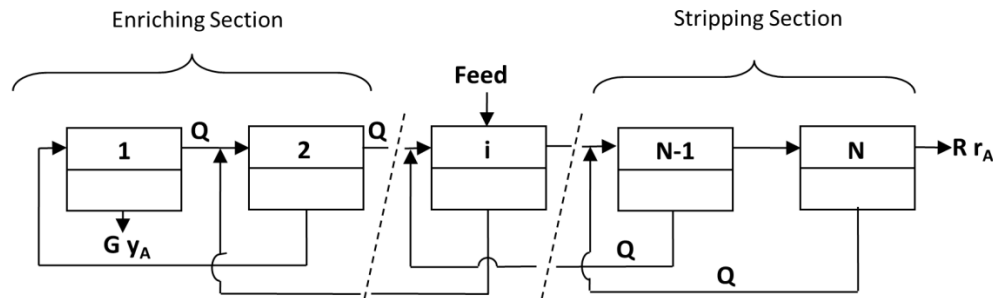


**Fig. B1** Schematic of N-stage membrane cascade with constant recycle ratio

By conducting an overall mass balance over the cascade system shown in Fig. B1, the following relations can be obtained regardless of the number of stages.

$$G = G_1 = \frac{\eta}{\varepsilon} F \quad (\text{B1})$$

$$y_A = y_{A_1} = \varepsilon x_A \quad (\text{B2})$$

$$R = R_N = \left[1 - \frac{\eta}{\varepsilon}\right] F \quad (\text{B3})$$

$$r_A = r_{AN} = \frac{\varepsilon x_A (1 - \eta)}{(\varepsilon - \eta)} \quad (\text{B4})$$

By definition of the constant recycle ratio, any retentate stream in the enriching stage has a constant flow rate of  $Q$  and the ratio of  $Q$  to the feed flow rate is fixed and equal  $\psi$ . Likewise the recycle stream in a stripping stage is the permeate stream and also has a flow rate and ratio to feed of  $Q$  and  $\psi$ , respectively. Therefore, mass balance is dependent on the stage location and can be described for stage  $i$  in a cascade of  $N$ -stages as:

Enriching section

$$G_i = Q + G \quad (\text{B5})$$

$$y_i = \frac{Q r_{i-1} + (Q + G)y_{i+1} - Qr_i}{Q + G} \quad (\text{B6})$$

$$R_i = Q \quad (\text{B7})$$

$$r_i = \frac{Q r_{i-1} + (Q + G)y_{i+1} - (Q + G)y_i}{Q} \quad (\text{B8})$$

Feed stage

$$G_i = Q + G \quad (\text{B9})$$

$$y_i = \frac{Q r_{i-1} + Fx_A + (Q)y_{i+1} - (Q + R)r_i}{Q + G} \quad (\text{B10})$$

$$R_i = Q + R \quad (\text{B11})$$

$$r_i = \frac{Q r_{i-1} + Fx_A + (Q + G) y_{i+1} - (Q + G) y_i}{Q + R} \quad (\text{B12})$$

Stripping section

$$G_i = Q \quad (\text{B13})$$

$$y_i = \frac{(Q + R) r_{i-1} + Q y_{i+1} - (Q + R) r_i}{Q} \quad (\text{B14})$$

$$R_i = Q + R \quad (\text{B15})$$

$$r_i = \frac{(Q + R) r_{i-1} + Q y_{i+1} - Q y_i}{Q + R} \quad (\text{B16})$$

Substituting these equations in the well mixed model will result in  $N$  equations with  $N+2$  unknowns (selectivity, pressure ratio, recycle ratio and  $N-1$  concentrations). Therefore, the attainability behavior is obtained by fixing the recycle ratio and solving the model equations over the pressure ratio range. Following are the obtained formulas for the two-stage enriching cascade:

$$S = \frac{(r_1\psi + x_A\eta)}{\left(\frac{\varepsilon\psi + \eta}{\varepsilon}\right)\left(1 - \frac{\varepsilon(r_1\psi + x_A\eta)}{\varepsilon\psi + \eta}\right)} \cdot \frac{\left[\gamma\left(1 - \frac{\varepsilon x_A(1 - \eta)}{\varepsilon - \eta}\right) + \frac{\varepsilon(r_1\psi + x_A\eta)}{\varepsilon\psi + \eta} - 1\right]}{\left[\gamma\left(\frac{\varepsilon x_A(1 - \eta)}{\varepsilon - \eta}\right) - \frac{\varepsilon(r_1\psi + x_A\eta)}{\varepsilon\psi + \eta}\right]} \quad (\text{B17})$$

$$S = \frac{\varepsilon x_A}{1 - \varepsilon x_A} \frac{[\gamma(1 - r_1) + \varepsilon x_A - 1]}{[\gamma r_1 - \varepsilon x_A]} \quad (\text{B18})$$

As recognized in our recent study about single-stage attainability, the minimum selectivity ( $S_{min}$ ) to accomplish a certain separation task at a given recycle ratio exists at infinite pressure ratio. Hence, taking the limits of Eq. (B17) and (B18) gives:

$$S_{min} = \frac{(\eta x_A + \psi r_1)(\varepsilon(1 + \eta x_A - x_A) - \eta)}{x_A(\varepsilon(\eta x_A + \psi(r_1 - 1)) - \eta)(\eta - 1)} \quad (B19)$$

Where,

$$r_1 = \frac{\varepsilon x_A}{S - S\varepsilon x_A + \varepsilon x_A} \quad (B20)$$

Substituting Eq. (B20) into Eq. (B19) and then taking the limit as recycle ratio goes to infinity, the absolute minimum selectivity to accomplish the separation task is:

$$S_{min} = \sqrt[2]{\frac{\varepsilon(1 - x_A)}{(1 - \varepsilon x_A)(1 - \eta)} - \frac{\eta}{1 - \eta}} \quad (B21)$$

To obtain the minimum pressure ratio at a given selectivity and recycle ratio both Eq. (B2) and (B3) are solved for pressure ratio and the limit is taken as selectivity goes to infinity. This gives the following relations:

$$\gamma_{min} = \frac{\eta^2 x_A - \eta x_A \varepsilon + \psi \eta r_1 - \psi \varepsilon r_1}{x_A(\eta^2 + \eta \psi \varepsilon - \eta - \psi \varepsilon x_A)} \quad (B22)$$

Where,

$$r_1 = \frac{x_A \varepsilon}{\gamma} \quad (B23)$$

Substituting Eq. (B23) into Eq. (B22) and then taking the limit as the recycle ratio goes to infinity, the absolute minimum pressure ratio to accomplish the separation task by this membrane configuration is:

$$\gamma_{min} = \sqrt[2]{\frac{\varepsilon - \eta}{1 - \eta}} \quad (B24)$$

To illustrate the systematic way followed to derive the relations in a three-stage cascade we choose the system consisting of two stripping stages and a single enriching stage shown in Fig. 3b. The complete well-mixed model can be written for the three stages as:

$$S = \frac{\varepsilon x_A}{1 - \varepsilon x_A} \frac{[\gamma(1 - r_1) + \varepsilon x_A - 1]}{[\gamma r_1 - \varepsilon x_A]} \quad (B25)$$

$$S = \frac{(r_1 \psi + x_A \eta)}{(\varepsilon \psi + \eta) - (r_1 \psi + x_A \eta)} \frac{\left[ \gamma \left( 1 - \frac{\varepsilon[x_A(1 - \eta) + \psi y_3]}{\varepsilon(\psi + 1) - \eta} \right) + \frac{\varepsilon(r_1 \psi + x_A \eta)}{(\varepsilon \psi + \eta)} - 1 \right]}{\left[ \gamma \left( \frac{\varepsilon[x_A(1 - \eta) + \psi y_3]}{\varepsilon(\psi + 1) - \eta} \right) - \frac{\varepsilon(r_1 \psi + x_A \eta)}{(\varepsilon \psi + \eta)} \right]} \quad (B26)$$

$$S = \frac{y_3}{1 - y_3} \frac{\left[ \gamma \left( 1 - \frac{\varepsilon x_A(1 - \eta)}{(\varepsilon - \eta)} \right) + y_3 - 1 \right]}{\left[ \gamma \frac{\varepsilon x_A(1 - \eta)}{(\varepsilon - \eta)} - y_3 \right]} \quad (B27)$$

Hence, the system is described by three nonlinear equations with five unknowns which are selectivity, pressure ratio, recycle ratio, stage-1 retentate stream concentration ( $r_1$ ) and stage-3 permeate stream concentration ( $y_3$ ). Therefore, the system can be solved by fixing the applied pressure ratio and recycle ratio.

In order to obtain a formula which describes the absolute minimum selectivity existing at infinite recycle ratio and pressure ratio then since the selectivity in all stages is

equal and hence the selectivity also equals the cubic root of the product of the right hand sides of Eq. (B25), (B26) and (B27).

$$S = \left[ \frac{\varepsilon x_A}{1 - \varepsilon x_A} \frac{[\gamma(1 - r_1) + \varepsilon x_A - 1]}{[\gamma r_1 - \varepsilon x_A]} \frac{y_3}{1 - y_3} \frac{\left[ \gamma(1 - \frac{\varepsilon x_A(1 - \eta)}{(\varepsilon - \eta)}) + y_3 - 1 \right]}{\left[ \gamma \frac{\varepsilon x_A(1 - \eta)}{(\varepsilon - \eta)} - y_3 \right]} \right]^{1/3} \quad (B28)$$

$$\frac{(r_1\psi + x_A\eta)}{(\varepsilon\psi + \eta) - (r_1\psi + x_A\eta)} \frac{\left[ \gamma \left( 1 - \frac{\varepsilon[x_A(1 - \eta) + \psi y_3]}{\varepsilon(\psi + 1) - \eta} \right) + \frac{\varepsilon(r_1\psi + x_A\eta)}{(\varepsilon\psi + \eta)} - 1 \right]}{\left[ \gamma \left( \frac{\varepsilon[x_A(1 - \eta) + \psi y_3]}{\varepsilon(\psi + 1) - \eta} \right) - \frac{\varepsilon(r_1\psi + x_A\eta)}{(\varepsilon\psi + \eta)} \right]}$$

By taking the limits of formula (B28) at infinite pressure ratio and recycle ratio, formula (B29) is obtained for the absolute minimum selectivity in the three-stage membrane system.

$$S_{min} = \sqrt[3]{\frac{\varepsilon(1 - x_A)}{(1 - \varepsilon x_A)(1 - \eta)} - \frac{\eta}{1 - \eta}} \quad (B29)$$

Solving Eq. (B25), (B26) and (B27) for the pressure ratio and then following the same solution methodology done for the selectivity, formula (B30) is obtained for the absolute minimum pressure ratio (exists at infinite selectivity and recycle ratio).

$$\gamma_{min} = \sqrt[3]{\frac{\varepsilon - \eta}{1 - \eta}} \quad (B30)$$

## (2) Constant stage-cut

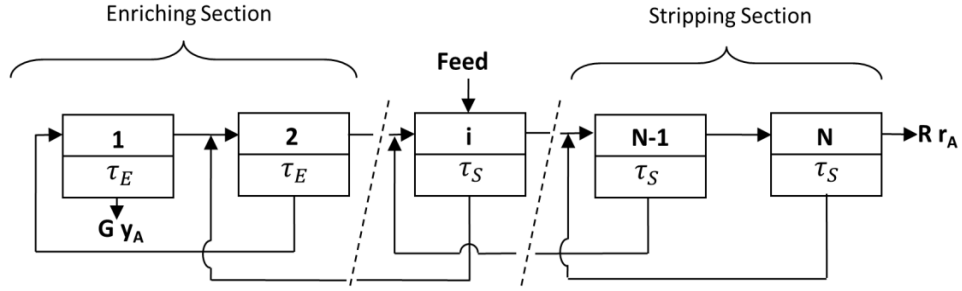


**Fig. B2:** Schematic of N-stage cascade system with constant stage-cut

The overall mass balance will also give the same formulas described earlier in Equations B1 to B4. In order to derive the general formulas describing the stage permeate and retentate concentration and flow rate based only on the stage-cut ( $\tau$ ), it is been assumed that the feed can enter to any stage in the cascade system with flow of  $F_i$ . Therefore, conducting mass balance over stage  $i$  in an  $n$ -stage cascade results in the following relations:

$$G_i = \tau_i [R_{i-1} + G_{i+1} + F_i] \quad (\text{B31})$$

$$y_i = \frac{R_{i-1} r_{i-1} + G_{i+1} y_{i+1} + F_i x_A - R_i r_i}{G_i} \quad (\text{B32})$$

$$R_i = (1 - \tau_i) [R_{i-1} + G_{i+1} + F_i] \quad (\text{B33})$$

$$r_i = \frac{R_{i-1} r_{i-1} + G_{i+1} y_{i+1} + F_i x_A - G_i y_i}{R_i} \quad (\text{B34})$$

Where,  $F_i = 0$  for all stages except the first stripping stage. Also,  $\tau_i = \tau_E$  for an enriching stage and  $\tau_S$  for a stripping stage. Substituting these equations in the well mixed model will result in  $n$  equations with  $N+2$  unknowns (selectivity, pressure ratio, enriching stage-

cut and  $N-I$  concentrations). Therefore, the attainability behavior is obtained by fixing the enriching stage-cut and solving the model equations over the pressure ratio range.

### (3) Minimum energy of cascade systems

The assumption of equal pressure ratio throughout all the cascade stages simplifies the system energy calculations. The minimum energy required to create the pressure ratio ( $\gamma$ ) in the cascade system equals to the sum of all permeate streams multiplied by the minimum compression specific energy.

Under the constant recycle ratio assumption, the permeate streams of the feed stage and enriching stages have identical flow rates and equal to  $Q+G$  while the stripping section permeate streams have identical flow rate of  $Q$ . Therefore, the sum of permeates flow rate for the cascade system illustrated in Fig. B1 with  $N$  total number of stage and feed entering to stage  $Z$  can be described by the following general formula:

$$\sum \text{Permeates Flow Rate} = ZF \left( \frac{\eta}{\varepsilon} + \psi \right) + (N - Z)F\psi \quad (\text{B35})$$

The minimum compression specific energy assuming isentropic work is given by:

$$E_{min}^S = C_p T \left( \gamma^{\frac{R}{C_p}} - 1 \right) \quad (\text{B36})$$

Hence, the minimum energy of separation for a cascade system of equal recycle ratio is:

$$E_{min} = \left( ZF \left( \frac{\eta}{\varepsilon} + \psi \right) + (N - Z)F\psi \right) C_p T \left( \gamma^{\frac{R}{C_p}} - 1 \right) \quad (\text{B37})$$